Investigation into the effect of wind power based embedded generators on distribution networks.

RIDA, I.M.A.

2000

INVESTIGATION INTO THE EFFECT OF WIND POWER BASED EMBEDDED GENERATORS ON DISTRIBUTION NETWORKS

THESIS

Submitted to

THE ROBERT GORDON UNIVERSITY

For the degree of

DOCTOR OF PHILOSOPHY

By

Ibrahim Moh'd Ali Rida

Collaborating establishments

National Wind Power **Scottish Power**

School of Electronic and Electrical Engineering

The Robert Gordon University, Aberdeen

July, 2000

ABSTRACT

Investigation into the effect of wind power based embedded generators on distribution networks

Wind turbine-generators are usually integrated into utilities' electrical networks at distribution voltage levels, and they are commonly known as "Embedded Generators (EGs)". Recently, it has been reported that the integration of wind power based embedded generators (WPBEGs) into distribution networks could cause mal-operation of automatic voltage control (AVC) relays. Further investigation is therefore required to improve the performance of AVC relays in the presence of EGs. On the other hand, the dynamic effects of WPBEGs on distribution networks (DNs) have been investigated for many years, but no attempt has been made to evaluate the effects of WPBEGs on the "Critical Clearing Time (CCT)" of faults on load feeders emanating from the substation where EGs are connected to the network.

Based on these findings, the work conducted and reported in this thesis covers two main aspects. The first aspect is related to the effect of EGs on the operation of AVC relays, including the compensation of voltage drop along distribution feeders. This is preceded by an introduction to the operating principles of conventional AVC relays. A new model of an AVC relay based on the application of Artificial Neural Networks (ANN) is then presented. The model is designed and trained to calculate the AVC voltage that is used to initiate the operation of the tap-changer of an appropriate transformer as conditions necessitate. In the process of the development of an ANN-based relay, a power flow program has been specially designed to generate training files using FORTRAN.

The second aspect reported in this thesis deals with the investigation of the effect of WPBEGs on the CCT of faults on load feeders. It has been concluded that CCT of faults, which is required to maintain the stability of WPBEGs can be several times less than that of the operating time of conventional protection schemes usually used on distribution feeders. The results obtained from the investigation related to both aspects are presented and discussed.

In summary, this thesis reports on the outcome of the investigation related to the design of an ANN based AVC relay capable of accommodating EGs and the effect of the dynamic behaviour of EGs on the CCT of faults on load feeders.

This work has resulted in the presentation of five technical papers at national and international conferences. One of these papers has been presented at the IASTED International Conference of Power Energy Systems. A further paper has been submitted for publication in one of the IEEE transactions, and is currently under consideration.

ACKNOWLEDGEMENTS

I would like to highly express my extreme thanks to Dr. S. K. Salman, project director and supervisor, for his priceless help, continuous guidance and encouragement throughout this project. I would also like to thank Dr. J. Watson, second supervisor of this project, for his valuable comments and proof reading of the thesis. I am sincerely grateful to Professor N. D. Deans, Head of School of Electronic and Electrical Engineering, for his constant support.

I am very grateful to the Robert Gordon University for the financial and administrative support throughout this project. I would also like to thank the Scottish Power plc and the National Wind Power, co-operative establishments of this project, for their helpful advice and useful information.

I would also like to express my thanks to Dr. David King, Daniel Aklil, and Anita Teo, the research team, for their co-operation and useful information.

Finally, I am sincerely grateful to my family for their encouragement and understanding.

Abbreviations

SYMBOL	DESCRIPTION
AC	Alternating current
ADALINE	Adaptive linear networks
ANN	Artificial neural network
ATP	Alternative transient program
ATR	Artificial transmission lines
AVC	Automatic voltage control
AVR	Automatic voltage regulator
BAM	Bi-directional associative memory
BP	Back-propagation
CB	Circuit breaker
CCT	Critical clearing time
CHP	Combined heat and power
DC	Direct current
DN	Distribution network
DTI	Department of trade and industry
EG	Embedded generator
EMTP	Electromagnetic transient program
FC	Fixed capacitor
GTO	Gate-Turn Off thyristor
IG	Induction generator
IGCC	Integrated gasification combined cycle
KN	Kohonen networks
MLP	Multilayer perceptron networks
NFFO	Non-fossil fuel obligations
OLTCT	On-load tap-changing transformer
PES	Public electricity supply
PURPA	Public regulatory policies act
PV	Photovoltaic
QF	Qualified facility
RBF	Radial basis function
REC	Regional electricity company
SC	Synchronous compensator
SG	Synchronous generator
SOM	Self organising maps
SVC	Static VAR compensator
TACS	Transient analysis of control systems
TCR	Thyristor controlled reactor
TNA	Transient network analyser
TSC	Thyristor switched capacitor
TSR	Thyristor switched reactor
UM	Universal machine
WF	Wind farm
WPBEG	Wind power based embedded generator

CONTENTS

CHAPTER 1

INTRODUCTION

1.1 General

The rapid increase of oil prices in the early 70's, has led to the development of high efficiency combined heat and power schemes [1] whereby the normally wasted heat is used to generate electric power. Such schemes are referred to as industrial co-generation [2]. In more recent times, as a result of economical and environmental factors, power system utilities have been encouraged to utilise power generation from what is called "Renewable energy sources" such as solar, tidal, wave and wind power [3]. The generation of electricity using wind power in particular has received considerable attention world wide, because of its negligible impact on the environment and low production cost [4]. It has been reported [5] that, during the 1980's more than 1400 MW of wind power generation has been installed in the USA, whereas the installed wind power in Europe reached 500 MW in 1991 [6]. A more recent report [7] has shown that the total installed capacity world-wide has increased from 6118 MW in 1996 to 7638 MW in 1997, representing a growth of 25% in a span of one year. Wind turbines that convert wind energy into mechanical energy can drive generators with capacities reaching 1500 kW [8]. In order to generate a significant amount of electricity using wind power, a number of wind power based generators are usually installed at one site constituting what is known as a wind farm. Generators which are used under both schemes, i.e. the industrial co-generation and the generation from renewable

energy sources, can be either synchronous or asynchronous types. When these generators are integrated into utilities' networks at distribution voltage levels [9] they are commonly known as "Embedded Generators (EGs)" [10].

Distribution networks (DNs) are designed as passive networks, and therefore are not tailored to collecting power from EGs. The integration of EGs with utilities' networks could create safety as well as technical problems [11-15]. Such problems include contribution to the fault currents, stability and reliability problems, introduction of harmonics, voltage fluctuation, and problems associated with automatic voltage control (AVC) of distribution networks.

Distribution networks are usually equipped with appropriate protective devices to ensure the quality of power supply to customers and to safeguard staff, public and equipment from the hazardous consequences of faults or any abnormal operating conditions. The design of protection schemes for DNs is usually based on two basic principles; they must ensure selectivity of a minimum amount of disconnected equipment to isolate a fault from the system and they must operate fast enough to minimise damage to system components [16]. The first principle is achieved by a proper co-ordination of the operating time of protective devices. This, however, may lead to operating times of protective devices at the up-stream of a distribution network being as high as 1.5s [9]. When EG is connected to a DN, the operating time of protective devices installed on load feeders may exceed the critical clearing time (CCT) limit of fault, which is required to maintain the stability of EG.

The voltage magnitude of a distribution network is usually maintained within statutory limits by using On Load Tap Changing Transformers (OLTCTs) [11], which are controlled by AVC relays. Conventional AVC relays usually have compounding settings to compensate

for the voltage drops along feeders of a distribution network. The use of compounding settings, particularly with negative reactance, is also recommended for the stable operation of parallel transformers [17-19]. Unfortunately, it has been reported [3,11] that the integration of EGs into utilities' distribution networks could affect the performance of these relays. It has been found that the voltage measured by a conventional AVC relay can vary with respect to the correct values depending on the power factor of EGs and system loads. Consequently, a proper voltage control of distribution network cannot be achieved. A solution to this problem is to use an AVC relay that has the capability of automatically adjusting its compounding setting to compensate for the offset in the measured voltage. An adaptive model of an AVC relay has been developed [17] for controlling these voltages. The study described in [17] was focused on the effects of wind power based embedded generators (WPBEGs) on the proper operation of parallel transformers. Nevertheless, further investigation is required to consider the effect of the voltage drop across load feeders on the voltage control of distribution networks that include EG.

1.2 Objectives

The research reported in this thesis has two main objectives. The first is related to the effect of EGs on the operation of AVC relays when compensation of voltage drop in distribution feeders is considered. The main objective behind this investigation is to design a new AVC relay, suitable for DNs with EGs that can accommodate the compensation of voltage drop in load feeders. A new AVC model is proposed based on the application of Artificial Neural Networks (ANN). A power flow program that can be used to generate training data for the ANN based AVC relay is also developed.

The second objective concentrates on an investigation into the effect of WPBEGs on the CCT due to faults on load feeders. In order to undertake this investigation, it is necessary to model a typical DN that includes WPBEGs. This modelling is conducted using the Electromagnetic Transient Program (EMTP). The dynamic behaviour of the WPBEGs is investigated following faults on load feeders. The CCT that is required to maintain stability of EGs is compared with the operating time of conventional protection schemes usually used on distribution feeders.

1.3 Outline of the Thesis

The structure of the thesis is organised, firstly, to introduce the reader to the main aspects of the subject under investigation. This includes an introduction to the different types of embedded generation with a particular focus on the wind power based type. An introduction to the methods and tools which have been implemented and developed throughout the study is also included. The investigation and analysis that has been carried out to satisfy the two main objectives of the project is then presented and discussed. The main findings and the developed models are also presented. Finally, a conclusion of the reported work with recommendations for possible future work is provided. The thesis comprises eight chapters and also includes a number of appendices.

Chapter 1 provides an outline of the project, including an introduction to the problems, which are expected from the integration of embedded generators into distribution networks, the objectives of the project, and a brief presentation of the project research.

Chapter 2 describes the current global potential of embedded generation, especially that based on renewable energy sources. Different types of renewable energy sources are briefly discussed. Wind power based embedded generation, which is the main thrust of this project, is then presented in some detail. A summary of the reported studies and investigations on the effects of embedded generation on distribution networks is also provided.

Chapter 3 describes the methods and tools of power system simulation that have been implemented in this work. These include the calculation of load-flow and losses, which are carried out to examine the steady-state operation of the investigated distribution network. Following a general introduction to power system transients and stability analysis, a specially dedicated computer program, which is known as EMTP [20], is described.

Chapter 4 outlines the general methods of voltage control of distribution networks. Because this project is mainly concerned with the effects of embedded generation on the voltage control using tap-changing transformers, the different types of tap-changers are briefly discussed with emphasis on their structure, advantages and disadvantages.

Chapter 5, an investigation into the dynamic behaviour of wind-power-based embedded generators is reported. Modelling of the investigated distribution network including embedded generators is described. The effect of embedded generators on the critical clearing time (CCT) of faults on distribution feeders has been a particular focus of the investigation. It has been revealed that induction (asynchronous) generators, which are commonly used for wind power based embedded generation, can have CCT much lower

than the time required for feeder's protection devices to operate and isolate the fault. A comparison between the behaviour of synchronous and asynchronous embedded generators is illustrated and discussed.

Chapter 6 introduces the conventional types of AVC relays, highlighting the problems that can be caused due to the integration of embedded generators into the DN. The principles of AVC relays with both the positive and the negative compounding setting arrangements are discussed. It is shown how the operation of these types of AVC relays can be affected by the integration of embedded generators into a distribution network.

Chapter 7 describes the development of an ANN based AVC relay that can be used for voltage control of distribution networks with embedded generators. The structure and principle of the proposed ANN based AVC relay is discussed. It can be established that the new model does not require compounding settings compared to conventional relays and thus avoids possible operational errors. The training data is obtained from a specially designed load flow program. The results of the training and testing of the proposed AVC relay model are illustrated and discussed.

Chapter 8 discusses the work and formulates the conclusions that can be drawn from it. Suggestions for future work are also explored.

CHAPTER 2

EMBEDDED GENERATION

2.1 Introduction

The first use of "embedded generation" could be referenced to the early days of electricity supply, when small-capacity generators were directly connected to distribution systems in order to supply local loads. For example, in 1919 there were about 570 separate electricity systems in the UK operating 430 generating stations [21]. Because those distribution systems were operated separately, a disturbance on one system had no effect on the operation of the others. Therefore, questions like high quality and reliability of power supply were not as vital as at the present time. With the increase in demand for electricity, power stations with much bigger generating capacities have been built all over the word, especially in USA and Europe. These power stations are not necessarily located close to the load centres, hence large public transmission systems have been built to allow the transmission of bulk power from remote power stations to the load centres. Consequently, these previously isolated distribution systems have gradually become interconnected through transmission systems. The small generating units became impractical to operate and they were abandoned.

Commonly, the majority of industrial plants purchase electric energy from utilities systems. However, due to the importance of maintaining a continuous power supply to critical loads, these plants are commonly equipped with standby emergency power generators that can be operated in case of failure of the public supply. This type of local generation can again be referred to as embedded generation. However, it is not designed to operate in parallel with the public electricity supply (PES) and is therefore, not expected to interfere with the operation of public networks.

Prior to the mid - 1970's, low cost energy was largely obtained from fossil fuel which in turn was used for the generation of electricity. As a result of the dramatic rise in energy costs since that time, industrial enterprises have been encouraged to utilise the energy of what was normally considered to be 'waste' heat to generate electric power [22,23]. This has led to the development of high efficiency combined heat and power (CHP) schemes [1]. Such schemes are referred to as industrial co-generation [2,24]. On the other hand, in recent years, as a result of economical and environmental considerations, power system utilities have been encouraged to utilise power generation from "Renewable energy sources" such as solar, tidal, wave and wind power [3]. Generators used under both schemes, i.e. the industrial co-generation and the generation from renewable energy sources, are usually integrated into utilities' networks at distribution voltage level, and they are also commonly known as "Embedded Generators" [9,10,25]. For this and other reasons, electric utilities are under increased customer demand for parallel operation of EGs with the utility's electric system.

In the United Kingdom, a combination of legislation and recommendation has been used to encourage and regulate the integration of different forms of EGs into utilities' distribution networks. The energy Act (1983) established a right for persons or companies to use the

public supply systems to transmit energy from one location to another or to third parties [9,21,25]. The Electricity Supply Industry requirements for the connection of parallel private generation are specified in Engineering Recommendation G.59 [9,10,25]. Although the G.59 was intended to apply to generation not exceeding 5 MW and 20 kV, it is commonly applied to large generating units as well [9]. The G75 [25] document is aimed at covering the requirements for generator connection to 33kV and 132kV networks.

2.2 Types of Embedded Generation

As mentioned above, embedded generation, which is commonly operated in parallel with the PES, can be divided into two main groups; the industrial co-generation and the renewable energy based EG. The latter group, particularly the wind energy based EG, is mainly addressed in the work reported in this thesis. Nevertheless, a short summary about the main aspects of industrial co-generation and other types of renewable sources is also provided.

2.2.1 Embedded Generation Based on Co-generation.

Most conventional power generation is based on burning a fuel to produce steam. It is then the pressure of the steam which turns turbines and generates power. The efficiency of such a method of power generation does not usually exceed 40% [26]. Co-generation plant in contrast, efficiently generates electric power accompanied with the production of steam, heat, mechanical, or other forms of useful energy [23,24]. As mentioned before, the focus on co-generation has dramatically increased after the oil crises during the first half of 70's. Industrial companies have been encouraged to produce electric power from the recovery of exhaust heat or the combustion of process wastes. In the USA, the Public Regulatory

Policies Act of 1978 (PURPA) opened the door for non-utilities to enter the wholesale market as small power producers or co-generators. When a co-generation facility is classified as a Qualified Facility (QF), it is given, under PURPA, the right to connect to the utilities grid and to sell excess power to the grid [24]. In the UK, following encouraging progress in the implementation of CHP schemes, the government set a target for CHP of 5,000 MW of installed capacity in the year 2000 [27]. By the end of year 1995, the installed capacity of CHP was approximately 3,500 MW, installed on around 1,300 sites, producing around 5% of the UK's electricity requirements.

Both synchronous and induction generators are used in co-generation, however the former is preferred. Unlike induction generators, synchronous generators are self-excited and can be operated connected to or independent from the utility's network at either leading or lagging power factor [26]. Voltage control of synchronous generators is achieved by using Automatic Voltage Regulators (AVRs). When connected to the distribution network, the network usually defines the voltage of generator terminals. The AVR in this case is adjusted to maintain the power factor of the power imported from the network close to unity.

2.2.2 Embedded Generation Based on Renewable Energy Sources

In the past, the combustion of coal and oil has been the predominant energy source for electricity generation. However, in the last two decades, two main factors were behind an increased search for other types of energy resources. The first is economical, which appeared following the sudden increase of oil prices as mentioned earlier. The second is environmental, due to the increased impact of combustion of coal and oil on the

environment. These factors have promoted the implementation of renewable energy sources for electricity generation. As an example, following the privatisation of the UK electricity supply industry in 1990, a number of orders known as 'non-fossil fuel obligations (NFFOs)' have been declared for England and Wales. NFFOs force regional electricity companies (RECs) to secure a minimum amount of their generated or purchased electrical energy from renewable energy sources [29,33]. The British Government has set a target of having 10% of UK's electricity supply generated by renewable energy sources by the year 2010 [32,33]. Until April 1999 only 2% (650 MW) had been achieved, the most common forms being renewable are geothermal, solar, hydro, biomass and wind energy.

Geothermal energy is the energy stored in the heat that comes from earth's core. It can be used to directly heat buildings but, for generation of electricity, hot water, at temperature of around 200° C [34], is brought from an underground reservoir to the surface through production wells. It is then flashed to steam to turn turbine engines and generate electricity. The main geothermal based electricity producers are in the USA, Philippines, Mexico and Italy [35]. In the USA, the geothermal based electric installed capacity is estimated to be in year 2000 around 3400 MW, whereas, the total forecast in all over the world for the same year is about 11000 MW [35].

Solar energy is another type of renewable energy source which can be used to provide heat, lighting, mechanical power and electricity. Heat from solar energy is normally obtained in a passive way through building elements such as walls, windows and roofs, where no additional equipment is used other than these elements. It is also obtained in an active way using glazed solar collectors to heat a heat transfer liquid, which is held in storage tanks. A heat exchange system is then used to distribute the heat inside buildings [36]. This form of obtaining solar energy is very popular all over the word, and even the legislation in a

number of countries, such as Egypt [35], requires solar heating systems to be an essential part of buildings. Solar energy is also converted to electricity using what is called "Photovoltaic (PV) cells". Using PV cells enables electricity generation directly from sunlight, without any mechanical motion or the production of harmful emissions to the atmosphere, making it the cleanest method of electricity generation. PV cells are made of semiconductor materials such as crystalline silicon [37]. Because of the low concentration of sunlight, a PV cell of 100 cm^2 can generate about half a volt of electricity. Therefore, higher voltages require large areas of bundled PV cells, which are called PV panels. PV electricity is widely used in telecommunications and for electricity supplies to isolated rural populations [37]. The global tendency is to promote the installation of PV panels for individual consumers without connection to utility networks, rather than building PV based power stations that may require connection to the network [35,39]. For example, the USA has set a programme for PV installation over one million roofs in the USA by the year 2010 [35].

Water is the largest practical energy source among the renewable energy sources on earth, and has been utilised for many years to generate electricity. Hydro turbine-generator units are usually installed between the upper and lower levels of dams and water falls. The kinetic energy of the falling water is converted to mechanical energy by the hydro turbine and hence to electrical energy [26]. Hydropower stations can be classified as small-scale stations [35,40] with generating capacities not exceeding 30 MW and large-scale stations with generating capacities reaching 10,000 MW [35]. Small-scale hydropower stations are usually integrated into power systems at distribution levels. Since 1990, the Department of Trade and Industry (DTI) in the UK has encouraged the development of small-scale hydropower schemes within the UK [40]. Five schemes have already been installed and commissioned by 1994, mainly in Scotland.

Biomass, such as forestry, crops, organic waste, domestic sewage, municipal solid and others [35], is a renewable energy source, which can be used to generate electricity by different ways [35,41], for example:

a) By direct combustion for steam production,

b) By gasification to provide a fuel gas for gas turbines,

c) By fast pyrolysis to provide a liquid fuel.

A well known method of gasification is called Landfill, whereby municipal waste and refuse is accumulated in specifically excavated holes in the land, where the bacteria and decomposing waste produce methane. The gas is then tapped and used to generate electricity [35]. The fast pyrolysis is a high temperature process in which biomass is rapidly heated in the absence of oxygen. Consequently, it decomposes generating vapours and aerosols. After cooling and condensation of the vapours, a dark brown liquid is formed, which has a heating value about half of that of conventional fuel oil [41]. The interest in biomass energy has been mainly in the USA, Brazil and European countries, especially utilising integrated gasification combined cycles (IGCC) [42].

2.3 Wind Power Based Embedded Generation

The discussion about wind energy is intentionally separated from the rest of other types of renewable energy sources because of its direct relevance to the reported work in this thesis. Wind energy is a substantial form of renewable energy on earth. It develops naturally from differential heating of the earth's surface by the sun [43]. This clean source of energy was initially used a long time ago. The first wind machines have been reported to exist more than 3500 years ago in Persia and Middle East [35,44]. They have mainly been used by Persians

and Arabs to grind seeds to produce flour. Wind turbines, which are also known as windmills, were made with vertical axes [45]. These machines remained unchanged until the 12th century, when horizontal axis mills with tilted wings or sails first appeared. Since then large-scale development of horizontal axis windmills started to spread in Western Europe to be used mostly for pumping water and for grinding. From the 19th century another type of windmill, known as the western wheels, became popular especially in the USA. By the end of 1930s, about eight million western wheels typed windmills had been installed [45].

Electricity generation from wind energy started in 1925 in the USA [44] and was followed by Germany in 1940 and Denmark in 1941 [45]. Wind turbines at that time were commonly made with horizontal axes and three aerodynamically formed blades. Although wind power based generators operated successfully, the lower-price of fossil fuels made wind energy technology economically uninteresting. However, the dramatic increase in the oil price in 1973 put wind energy back into focus again. Since then, the world has witnessed a rapid increase in the construction of wind farms. The total installed capacity of wind farms in the world exceeded 10000 MW in 1998 [46,47]. In the same year, the total in Germany was 2900 MW, whereas, in Denmark the total was about 1200 MW comprising 10% of the electricity consumption of that country.

In the UK, the situation of wind power has changed dramatically following the privatisation of the UK electricity supply industry in 1990. Before then, there were just a few isolated and experimental wind turbines scattered across England, Wales and Scotland [48]. By the beginning of the year 2000, the total number of the installed wind turbines has reached 786, generating about 350 MW [49].

2.4 Structure of Wind Turbine- Generator Units

Modern wind turbines for electricity generation have horizontal axes and fast-running rotors. Wind turbines with three blade rotors are the most popular, although turbines with two blades are also used. The most important components of a typical wind turbine-generator unit are the rotor blades, or wings, the mechanical drive unit, and the generator [44,45,50-53]. Fig. 2.1 depicts these main components. The blades, which are attached to a low speed, horizontal shaft through a hub, capture the kinetic energy of wind and convert it into rotational energy. The mechanical drive, which includes a gear box, transfers the energy, to a high speed shaft which is connected to the rotor of the generator to be converted into electrical energy.

The reason behind the choice of small number of blades can be explained from the energy conversion properties of wind turbines. The kinetic energy in the wind flowing through a wind turbine is given by [45]:

$$W_k = \frac{1}{2} A \rho v^3 \tag{2.1}$$

where A is the swept area of turbine's blades, ρ is density of the air and v is the wind speed.

Energy is extracted from the wind as it moves through the turbine's blades. Consequently, wind speed reduces after the passage through the blades. The more kinetic energy is extracted, the more wind speed will reduce as it leaves the blades. However, the whole energy from wind can not be converted, as this will require the wind speed leaving the blades to become zero. Hence, no energy can then be extracted at all. According to Betz' law [45, 53], a maximum of 59% of the kinetic energy in the wind, which is known as Betz limit, can only be converted into mechanical power. The remaining energy must remain in

the air passing the turbine. Bentz' law also states that, maximum energy conversion occurs, when the ratio between wind speed after the passage through the blades and that before the passage is about 33%. In other words, a wind turbine operating at maximum efficiency would slow the wind by 2/3 of its original speed. The ratio of the power absorbed by a wind turbine to that of the passing wind is referred to as the performance coefficient [45], or the power efficiency of the rotor [53], or power coefficient [51]. This coefficient is given as a function of the wind speed before and after passing the turbine (v_1, v_2) by:

$$C_p = \frac{1}{2}\left(1-\left(\frac{v_2}{v_1}\right)^2\right)\cdot\left(1+\left(\frac{v_2}{v_1}\right)\right) \tag{2.2}$$

where C_p is the performance coefficient of the rotor, v_1 is the wind speed before the turbine, and v_2 is the wind speed after the turbine.

Fig. 2.2 depicts C_p as a function of (v_2 / v_1) in a graphical form.

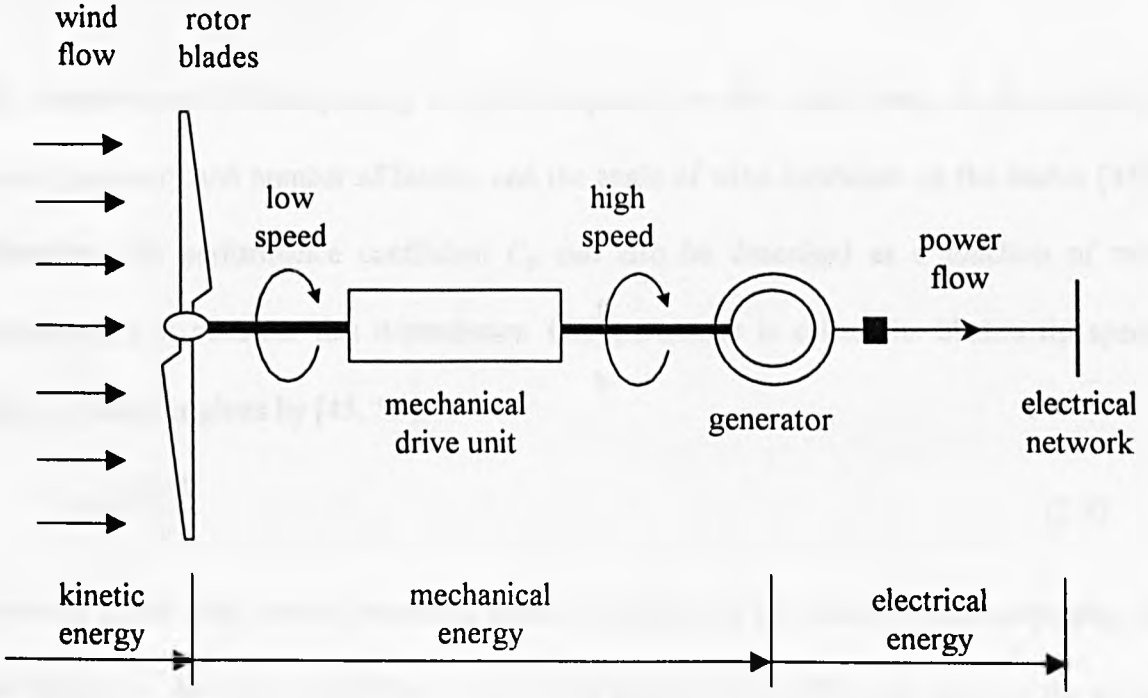

Fig. 2.1 Schematic diagram of a typical wind turbine-generator unit

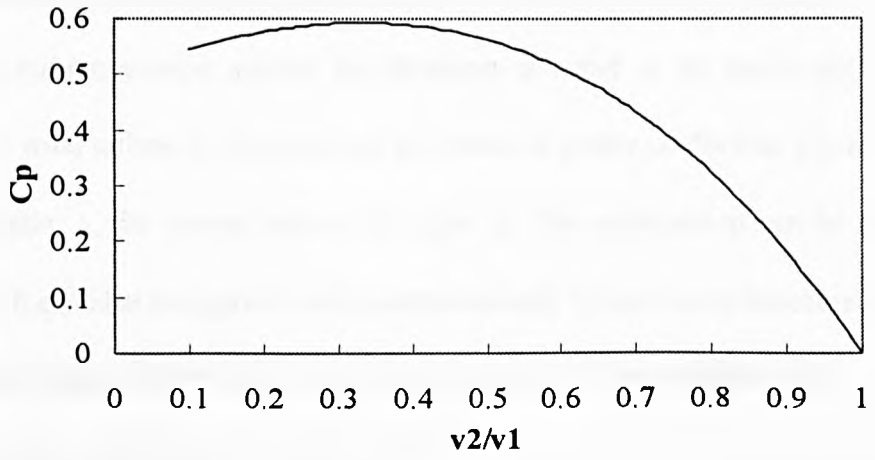

Fig. 2.2 Wind turbine's power coefficient, C_p , versus wind speed ratio, v_2/v_1.

Consequently, the amount of energy, which is actually converted by a wind turbine is:

$$W_c = \frac{1}{2} C_p \, A \, \rho \, v^3 \tag{2.3}$$

According to equation (2.3), if a wind turbine is always operated at a C_p as close to Betz limit as possible, then the power output of a wind turbine would be proportional to the cube of the wind speed, v^3.

The deceleration of wind passing a turbine depends, on the other hand, on the turbine's speed, geometry and number of blades, and the angle of wind incidence on the blades [45]. Therefore, the performance coefficient C_p can also be described as a function of two parameters that consider this dependency. One parameter is called the blade's tip speed ratio, λ, which is given by [45, 55]:

$$\lambda = \frac{\Omega \cdot R}{v} \tag{2.4}$$

where Ω is the wind turbine rotational speed in rad/s, R is the radius of the swept area of the blades, i.e. the length of blades; v is the wind speed, and (Ω R) is the speed of the tip of blades.

The other parameter is the angle of wind incidence on the blades, α. Variation of α can be either due to turbine yawing against the direction of wind or by blade pitch variation. Accordingly, a wind turbine is characterised by curves of power coefficient, C_p, as a function of tip speed ratio, λ, for various values of angle, α. This relationship can be obtained by measurement. It can also be approximated mathematically by non-linear functions. One of the functions, which is derived for pitch varied turbines has the following form [45]:

$$C_p = c_1\left(c_2 - c_3\alpha - c_4\alpha^x - c_5\right)e^{-c_6(\lambda,\alpha)} \qquad (2.5)$$

where c_1 to c_6 and x are constants.

Fig. 2.3 shows the relationship in equation (2.5) in a graphical form, whereby the following values of constants were used [45]:

$c_1 = 0.5$ $\quad c_2 = 116/\lambda_i$ $\quad c_3 = 0$

$c_4 = 0$ $\quad c_5 = 5$ $\quad c_6 = 21/\lambda_i$

and

$$\frac{1}{\lambda_i} = \frac{1}{\lambda + 0.08\,\alpha} - \frac{0.035}{\alpha^3 + 1}$$

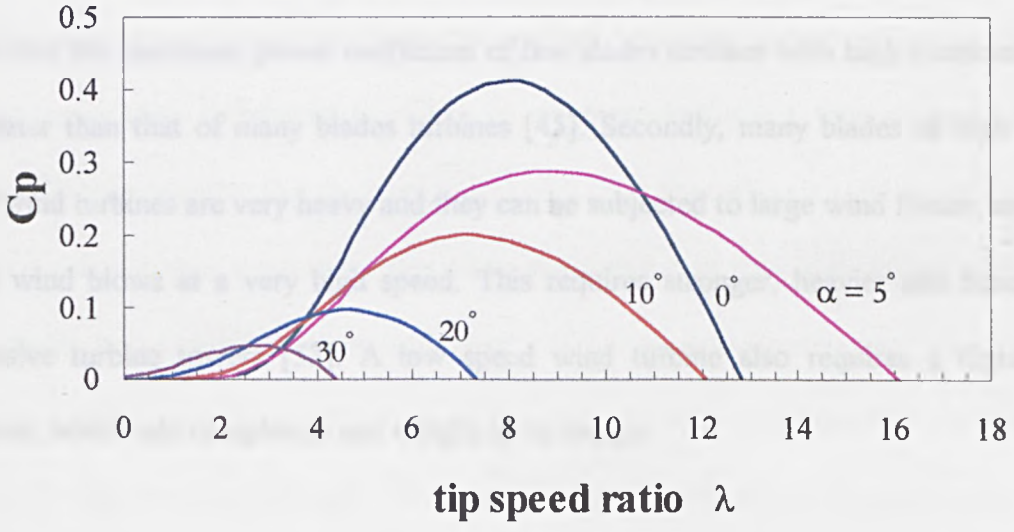

Fig. 2.3 The characteristic curves of a pitch controlled wind turbine.

As can be seen in Fig. 2.3, the performance coefficient of a wind turbine is highly affected by the tip speed ratio λ, which has a significant effect on the design and operation of wind turbines.

In general terms, the extraction of wind power from the wind can occur with any number of blades. However, recalling that the mechanical power output of a rotating mass is given as the product of the acting mechanical torque and rotational speed of the mass [54], e.g:

$$P_m = \omega T_m \tag{2.6}$$

where ω is the angular speed of the rotating mass and T_m is the mechanical torque acting on it.

It can be concluded that, either a slow rotation with a high torque, or a fast rotation with a lower torque can obtain the same amount of power. In a slow rotating wind turbine, high torque can be obtained using many blades, whereas, in a fast rotating turbine, lower torque can be obtained using fewer blades. For many reasons, the choice in the design of modern wind turbines was to the favour of fewer blades and higher speed types. Firstly, it has been found that the maximum power coefficient of few blades turbines with high rotational speed is greater than that of many blades turbines [45]. Secondly, many blades of high power-rated wind turbines are very heavy and they can be subjected to large wind forces, especially when wind blows at a very high speed. This requires stronger, heavier and hence more expensive turbine towers [53]. A low speed wind turbine also requires a higher ratio gearbox, which add complexity and weight to its design.

The least number of blades can be one. Wind turbines with one-blade do exist [53], but not very widespread. The reason is that these turbines are required to rotate at very high speed

to extract efficient power from the wind, which make them noisy. They also require a counterweight to be placed on the other side of the hub from the rotor blade to balance the rotor, which does not save much of weight compared to two-bladed design.

Two-bladed wind turbines have the advantage of saving the cost of blades, however, they require higher rotational speed to yield the same energy output, which is a disadvantage with respect to noise and visual intrusion [53]. They also require a complex hub and rotor design to overcome heavy shocks to the turbine, which may develop as the blades pass the tower.

Following many years of experience, the manufacturers of wind turbines have considered the three bladed turbines as the optimal design. Three bladed turbines overcome the disadvantages of the single and two bladed turbines and at the same time they do not suffer from the drawbacks of many blades [45,53].

Wind turbines are usually designed to normally operate at a rotor speed that gains a maximum power efficiency utilising the aerodynamics of the blades and the wind speed distribution at the expected site [51]. The optimal speed for maximum power efficiency usually occurs at tip speed ratio from 6 to 10, as shown in Fig. 2.3. Operating at maximum power efficiency requires that the wind will always be in the turbine's axial direction. This is achieved using a yaw mechanism that turns the turbine so that it faces the wind. Wind turbines are also provided with a method of controlling the power output from the rotor blades to maintain maximum efficiency and to protect wind turbine-generator units from the damaging effects of severe winds. There are two main methods of controlling the power output, the pitch control method and the stall control method [45, 50-53]. In the former method, the angle of the rotor blades is adjusted by a blade pitch mechanism, which is

activated by the turbine's control system. When the power output become too high, the pitch mechanism turns the blades out of the wind, as shown in Fig. 2.4, consequently, the extracted power from wind is reduced. Conversely, the blades are turned back into the wind as soon as wind drops again. Fig. 2.3 shows the effect of variation of the pitch angle on the power coefficient C_p, and hence on the turbine's power output.

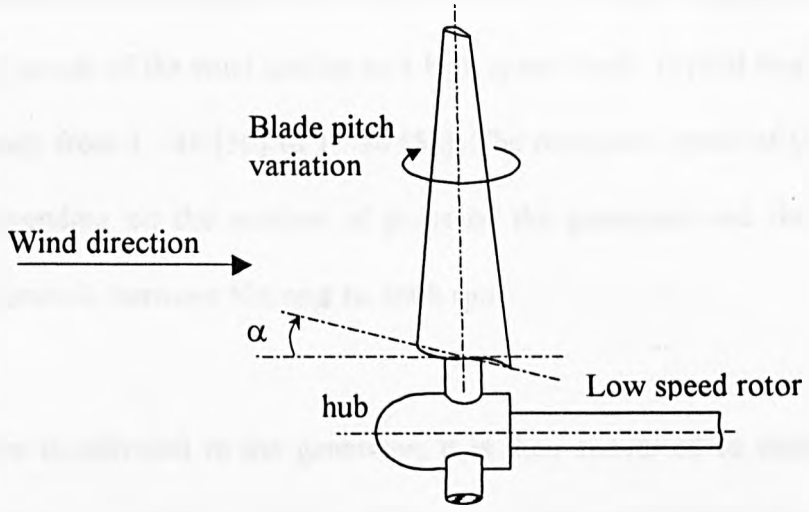

Fig. 2.4 Blade pitch control of wind turbines

Wind turbines utilising a stall control method, which is also known as passive control, have rotor blades attached to the hub at a fixed angle. However, the blades are aerodynamically designed in such a way to insure that turbulence occurs behind the blade whenever the wind speed becomes too high. The turbulence results in a phenomenon known as stall, whereby the lifting force of the rotor blade is prevented from acting on the rotor, and hence, the power output is reduced at high speeds. In order to ensure that the turbine stalls gradually rather than suddenly, the blades are twisted along their length. The main advantage of stall controlled wind turbines, that they do not have moving parts in the rotor blades. However, stall control requires a very complex aerodynamic blades design to avoid stall-induced vibrations.

As mentioned previously, the maximum power efficiency of wind turbines is typically achieved at a tip speed ratio of between 6 and 10 (see Fig. 2.3). Considering that the practical wind turbines are rated at wind speed around 15 m/s [44,45,53,56], it implies that the rotational speed of turbine's rotor will be much lower than the rotational speed of the rotor of typical power generators. Therefore, the mechanical drive unit, see Fig. 2.1, which is also known as the mechanical drive train [45,50], includes a gear box that converts the mechanical power of the wind turbine to a high speed shaft. Typical fixed gear ratios range approximately from 1 : 30 [50] to 1 : 50 [53]. The rotational speed of the high-speed shaft can be, depending on the number of poles of the generator and the frequency of the electrical network, between 500 rpm to 3600 rpm.

Once power is delivered to the generator, it is then converted to electrical power. Both synchronous and asynchronous (induction) generators are used for wind turbine-generator units. However, most of the wind turbine manufacturers use three-phase asynchronous generators, as they are very reliable and not expensive compared to synchronous generators. The investigation, which is reported in this thesis, mainly considers wind turbines with induction generators.

2.5 Connection of Wind Turbine-Generators to Utilities Network

Wind turbine-generator units are normally connected to the network either directly or indirectly [45]. In the direct connection method, the generator, whether synchronous or asynchronous, is connected directly to the AC network. A step-up unit transformer is used to transfer the generator voltage, for example 690 V for induction generators [53], to the network voltage, which is usually at distribution level [3,9,50]. In the case where a synchronous generator is used, the generator is synchronised with the network, hence the

angular speed of generator's rotor must remain constant to produce power at the network frequency. When integrated into a distribution network, a wind turbine-generator unit usually comprises a weak source compared to other main sources connected to the network. Therefore, voltage and frequency of the generated power are mainly dictated by the network, whereas, the generator's field voltage in case of synchronous generators provides control of the generated reactive power [29]. In the case of an asynchronous generator, the unit absorbs reactive power required to maintain the magnetic field in the generator from the network. The network controls the generator voltage and the rotational speed of the rotor, which is proportional to what is called the rotor slip, is dictated by the generated power. Fig. 2.1 illustrates the direct connection method.

In the indirect connection method, the wind turbine generator operates in its own mini AC system, as shown in Fig. 2.5. In this case, the frequency of the generated power can be variable. Hence, it is possible to run the rotor at a variable speed. Both synchronous and asynchronous generators can be used. Fig. 2.5 depicts a wind turbine with an asynchronous generator. The generator's AC current is rectified, i.e. converted into direct current (DC) using thyristors. The DC current is then converted back into an AC current using an inverter with the same frequency as the public electrical network.

The advantage of indirect connection is that it is possible to operate the wind turbine at variable speed, which allows running the rotor at higher speed during gusts, thus absorbing part of the wind energy until the gust is over. Another advantage is that it is possible to control the reactive power using the power electronics in the rectifier-inverter circuit [44,45]. The basic disadvantage of indirect connection is the cost of the additional power electronic components. Other disadvantages include the energy losses in the AC-DC-AC conversion circuit and the introduction of harmonics by the power electronic devices.

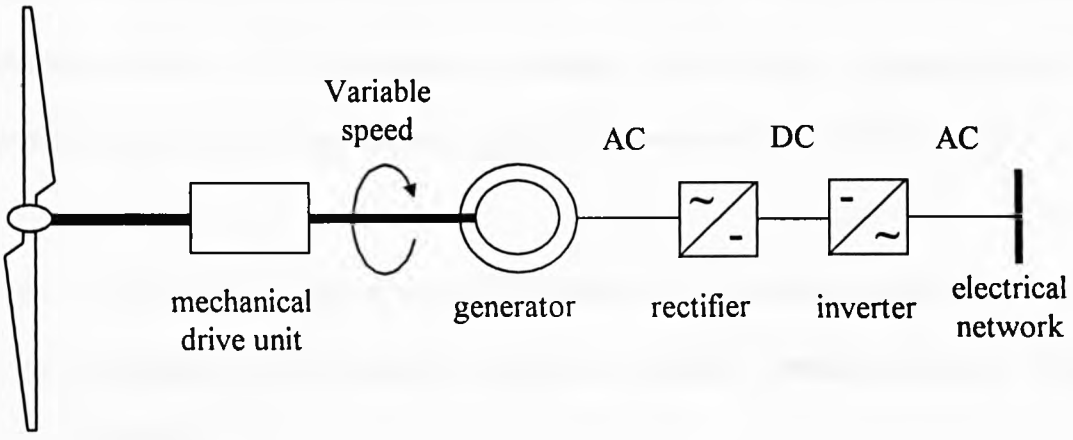

Fig. 2.5 Schematic diagram of the indirect connection method of wind turbine generator to the electrical network.

2.6 Effects of Embedded Generators on Distribution Systems

The operation of embedded generators including wind turbine generators in parallel with a utility's network has been widely investigated during the last two decades [3,9,10,11,15,17,25,30,55-75]. It has been reported that such integration could create safety as well as technical problems. These problems can be classified as follows:

a) Contribution from embedded generators into a fault current.

b) Stability and reliability problems.

c) The introduction of harmonics.

d) Voltage fluctuations.

e) Requirement for complicated protection schemes.

f) The effect of embedded generators on voltage regulation and losses in distribution networks.

In order to safeguard the quality of power supply, and to insure the safety of the public and distribution network, it is important to consider the following requirements for the integration of embedded generation into a distribution network [9,10,17,25,31,59]:

a) Maintenance of system voltage and frequency within statutory limits.

b) Operation of all equipment within the specified "make and break" fault ratings.

c) Adequate synchronising facilities in cases where synchronous generators are used.

d) Control of excessive circulating currents in neutral conductors or earth and harmonic or negative sequence currents.

e) Provision of protection to safeguard embedded generators, the system, and the public.

f) Provision of adaptive methods of voltage control of distribution networks.

2.6.1 Contribution to Fault Currents

The contribution of embedded generators to a fault current depends on the point of common coupling, type of generator (synchronous, induction, etc.), and type of fault (symmetrical or unsymmetrical). It also depends on the capacity of EGs compared to the capacity of utility's network. The contribution into a fault current from a relatively small generator, which is connected to the low voltage system is not usually a cause of concern. However, when a larger generator is connected to the medium or high voltage network it may increase the "make and break" duty levels of equipment [25,58,59]. Synchronous generators usually have an independent source of field current. Therefore, they can provide

a sustained contribution into a system fault until they are disconnected using an appropriate protection device. Induction generators, on the other hand, cannot make such contribution, as they do not have their own field current source. The fault contribution from induction generators decays very fast as the rotating magnetic field collapses [75]. However, for unsymmetrical faults, like single phase to ground faults, induction generators may feed a sustained fault current, being supplied by the field current through the healthy phases.

2.6.2 Stability Problems

The dynamic stability of an embedded generator is highly dependent upon the generator's main parameters [69], e.g. the rotor inertia, impedance of windings, and time constants. The generator inertia is proportional to the mass of the rotor, which is usually low for embedded generators, as such generators are usually small. The lower the generator inertia the less stable it will be during disturbances and vice versa. This can be demonstrated using the following acceleration equation [54, 76], which describes the motion of the rotor of a generator due to an unbalance between generator's input and output power:

$$\frac{d^2\delta_m}{dt^2} = \frac{1}{J\omega_m} P_a \qquad (2.7)$$

where the coefficient J is the total moment of inertia of the rotating masses, in kg-m^2, P_a is the accelerating power, which accounts for any unbalance between generator input and output power, and the left-hand side of equation (2.7) is the rotor acceleration due to the power unbalance.

The fault clearing time of protection devices associated with distribution networks can be rather high [9,69], especially when time graded over current relays are used. During this time generators may accelerate to the extent that it is unlikely they can maintain stability.

The effect of the generator reactance on stability can be shown using the power-angle equation, which is given by [26,69]:

$$P = \frac{EV}{Xd'} \sin \delta \qquad (2.8)$$

where E is the generator's induced electromagnetic force (EMF) corresponding to the current in the generator's field winding, V is the voltage of generator terminals, δ is the phase angle between E and V, and Xd' is the generator transient reactance.

As can be seen from equation (2.8), the output power, P, is proportional to the sine of angle δ. On the other hand, if E and V are maintained constant, it can also be seen that a bigger generator reactance would require a bigger angle δ to produce the same amount of power. A generator operating at large angle under steady-state conditions may not provide appreciable decelerating forces on its rotor following a transient disturbance [54]. Generator impedance is proportional to the reciprocal of generator rated power. Therefore, embedded generators commonly have high impedance compared to the high rated generators, which are used at main power stations. Then again, the stability margin of embedded generators is comparably low due to their high impedance.

Another factor that affects the stability of embedded generators is the impedance of the interfacing link between the generators and the point of their connection to the distribution network [69]. Embedded generators, especially those based on renewable energy sources, can be connected into a distribution network through long distribution lines that may have a considerable impedance. When the impedance of this link is added to the generator impedance, the stability margin of the embedded generators may reduce even more.

2.6.3 Impact on the Voltage Control

The voltage of 33kV and 11kV distribution networks is usually controlled using automatic voltage control (AVC) relays. These relays automatically control the position of the tap changer of main distribution network's transformers. Accordingly, the voltage of the low voltage terminals of these transformers is maintained within specified limits. In order to control the voltage at a certain point on the network, an AVC relay has compounding settings that can be in the form of a replica impedance (a resistance and either a positive reactance or a negative reactance). The relay then predicts the voltage of the remote bus by measuring the local voltage and the transformer current such that [31,63]:

$$V_m = V_L + I_T (R_{AVC} - j X_{AVC})$$

where V_m and V_L are the calculated relay voltage and the voltage at the local bus respectively, I_T is the current through the transformer and R_{AVC} and X_{AVC} are the resistance and reactance of the relay respectively.

When this voltage exceeds acceptable limits, the relay operates and changes the position of the tap changer in such a way to bring back the voltage within the limits. The integration of an embedded generator into a remote location on the network may change the direction of the active and reactive power flow through utilities' transformers leading to errors in the AVC relay measurement and operation [17,30,31,63,70].

CHAPTER 3

SIMULATION METHODS OF POWER SYSTEMS

3.1 Introduction

Generators, transformers, transmission lines, and loads are the main components that constitute a typical electrical power system. A power system is capable of generating, transmitting and distributing electrical energy over a large geographical area. Under normal operating conditions, an electrical power system is near equilibrium, with only minor deviations from true steady-state conditions caused by small, nearly continuous, changes in the loads. The main components of an electrical power system include inductive and/or capacitive elements that give them the capability to store energy that cannot be stored and released instantaneously. Therefore, following a disturbance on a power system, the latter experiences a transient period (or transient condition) when an exchange of energy occurs at different rates depending on the type of equipment involved and the nature and location of the disturbance.

In order to design, construct, and operate power systems, engineers need to investigate and understand the behaviour of individual system elements and also the behaviour of the whole system during both steady state and transient operating conditions. This process of investigation is referred to as power system analysis [76-79], which can be carried out utilising analogue models of power systems or computer based numerical simulation

methods and tools. Power system analysis includes, but not limited to, the following types of studies [16,26,76,77,79]:

a) Load flow and losses,

b) Short circuit analysis,

c) System protection,

d) Power system transients and stability analysis.

Power system analysis involves the modelling of the system by means of analogue and digital simulators. Prior to the development of digital computers, system analyses were made on analogue models [79], or what is called Analogue Model Power Systems [80]. A model used for transient analysis was also known as the Transient Network Analyser (TNA) [92]. These models comprise scaled single-phase replicas of actual system components, such as Artificial Transmission Lines (ATR) [81], and voltage sources [79]. These models typically use a voltage of 220 to 880 volts and they may include additional facilities for specific types of analysis. For example, in order to undertake system protection studies, analogue models provide adjustable current and/or voltage sources at the relaying point; they allow control of the duration and type of fault. They also provide a choice of the point-on-wave at which the fault is applied. Nevertheless, analogue models have a number of shortcomings:

1) The are usually large and expensive.
2) Setting up the connections, making adjustments, and reading the data is tedious and time consuming.
3) It may not be possible to scale all system components without ignoring some of component's properties.

Analogue simulation methods are still used for specific applications [82]. However, following the development of large digital computers in the 1940s [83], which was accompanied by a rapid growth of power systems, methods of power system analysis became based mainly on digital simulation. Digital simulation is about using mathematical models in software simulating programs that enables engineers to carry out rapid and accurate studies on large power systems. For instance, a load flow computer program may handle more than 1500 buses, 2500 lines and 500 transformers [79].

Some aspects of load-flow studies and stability studies will be provided in the following two sections respectively. This should serve as an introduction to the simulation methods that are used in this thesis to investigate the effects of integration of wind power based generators into distribution networks.

3.2 Load-Flow and Losses

A Load-flow study [26,78,79], which is also referred to as power flow study [16,83], is the basic type of analysis of power systems. It is carried out to examine the steady-state operation of electrical networks for network planning and optimisation. It is also used for identifying potential network problems in contingency analysis and for determining initial steady-state conditions prior to transient-stability calculations [76]. For distribution networks load-flow studies are necessary to determine the capability of a network under different system configurations and loading conditions [16].

The solution of a load flow study usually provides information about magnitudes and angles of bus-bar voltages, active and reactive power flows and losses in individual system

components. It also provides the reactive power injected or absorbed at any point on the network [78]. The basic concept of load flow is formulated using Kirchhoff laws and the interrelationships between branch currents, voltages, and power. Using the nodal analysis method for an interconnected electrical system, the node voltages and injected currents are related by the following nodal matrix equation [26,78,79]:

$$[\mathbf{I}] = [\mathbf{Y}][\mathbf{V}] \tag{3.1}$$

where **[V]** is node voltages, **[I]** the injected currents, and **[Y]** is the nodal admittance matrix.

The nodal matrix equation (3.1) is complex as **I, Y,** and **V** include real and imaginary components. Therefore, for n bus-bars system there will be n complex equations, which can be separated into real and imaginary parts to obtain 2n real equations. If the injected currents are known, the voltages can easily be obtained by solving these equations. However, for a real power system, the injected currents are not known at all buses. Some of the voltages are known and some of the currents are provided in terms of bus complex power, P + jQ. To alleviate the problem of solving these equations, bus-bars are divided into three different bus groups [78]:

a) Voltage controlled bus. The real power input to the network and the magnitude of the bus voltage are specified in advance. This corresponds to a typical case to which a synchronous generator, equipped with an automatic voltage regulator, is connected. The reactive power output of the generator and the phase angle of the bus voltage are unknown quantities.

b) Non-voltage control bus, also known as load-bus. The total injected power, P+jQ, is specified at this bus. Both P and Q are assumed to be unaffected by small variations in bus voltage. The unknown quantities for this type of buses are the magnitude of bus voltages and their phase angle.

c) Reference bus or slack bus. This is defined because in some circumstances the system losses are not known in advance of the load flow calculation. Therefore, the total injected power can not be specified at every bus. Instead, the power is left unspecified at one bus-bar, which can be used to supply the unknown power losses, and consequently, maintain a balance of power between generation from one side and load and losses from the other side. It is also used as phase reference for the whole system. For convenience, the phase angle at this bus is usually assumed zero.

The load flow problem does not usually have a unique solution. When a system comprises a couple of bus-bars (nodes), an exact solution for the load flow can be easily derived analytically. Conversely, a load flow solution for a system comprising a large number of nodes can be very tedious. To demonstrate this, consider the simple system shown in Fig. 3.1, where a load of (P+jQ) is supplied via a line of reactance x from a fixed voltage bus, which is taken as the slack bus. It is required to find magnitude and phase angle of the voltage at the load bus.

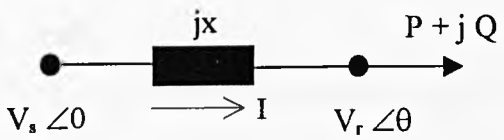

Fig. 3.1 Single-phase equivalent circuit of a simple system

The complex power $P + jQ$ is given by [3]:

$$P + jQ = V_r I^* \tag{3.2}$$

where I^* is the conjugate of current I in the line connecting the sending and receiving buses.

Current I can then be obtained as:

$$I = \frac{(P + jQ)^*}{V_r^*} \tag{3.3}$$

where V_r^* is the conjugate of voltage V_r and $(P + jQ)^*$ is the conjugate of the load complex power.

Voltage-drop in the line, $\Delta V = V_s - V_r$, is given by:

$$V_s - V_r = jx\left(\frac{P - jQ}{V_r^*}\right) \tag{3.4}$$

All terms in (3.4) are known except V_r. Equation (3.4) can be rearranged to:

$$(V_s - V_r \angle\theta)\, V_r \angle -\theta = jx\,(P - jQ)$$

Or

$$V_s V_r \angle -\theta \;\; - \;\; V_r^2 = jxP + xQ \tag{3.5}$$

Equating the real and imaginary parts on both sides of Equation (3.5) results in:

$$V_s V_r \cos\theta - V_r^2 = xQ$$

$$V_s V_r \sin\theta \;\; = \;\; -xP$$

Squaring and adding, yields:

$$V_s^2 V_r^2 (\cos^2\theta + \sin^2\theta) = (V_r^2 + Qx)^2 + (-Px)^2$$

From which the following equation is obtained:

$$V_r^4 + (2Qx - V_s^2) V_r^2 + x^2 (P^2 + Q^2) = 0 \tag{3.6}$$

This is a quadratic equation, which can be solved analytically for V_r to give four solutions. However, substituting typical values for $P + jQ$ and x, it can be shown that only one solution is practical.

As demonstrated above, analytical calculation of the receiving end voltages of the simple system, shown in Fig. 3.1, requires solving a quadratic equation, which would give four solutions. Hence, the calculation for systems with larger number of nodes and lines using analytical methods will obviously be tedious and impractical. The more practical approach to handle load-flow computation is to use digital computer based iterative methods. Some initial estimate values are usually made for the unknown voltages, and then adjusted using well established iterative algorithms [26,76,78,79,83] until satisfactory solutions are obtained. The most well known iterative methods are the Gauss - Seidel and the Newton - Raphson methods [26,78,79]. The latter method is more popular than the former, because it has much better reliability and faster convergence. Therefore, the Newton - Raphson method is implemented in this thesis to design a load flow program using FORTRAN programming software. More details about this program can be found in Chapter 6 and in Appendix A.

3.3 Power System Transient and Stability Analysis

Depending upon the time window involved, power system transient and dynamics can be divided into four groups defined as: wave, electromagnetic, electromechanical, and thermodynamic, shown in Fig. 3.2 [76]. This classification, however, is not distinct. As Fig. 3.2 shows, the boundaries of two or more groups may overlap. The fastest dynamics are related to the propagation of waves, or surges, which are caused by lightning strikes or switching operations in high-voltage transmission lines. The time frame of these dynamics

can be up to few milliseconds. Electromagnetic effect that take place in machine windings following a disturbance on the network are usually of a time frame from milliseconds to few seconds. An even slower group is the electromechanical dynamics, which result from the oscillation of the rotating masses of generating units and motors, which can last from around ten milliseconds to several seconds. The slowest dynamics are the thermodynamics changes, which are related, for example, to the boiler's control reaction in steam power plants. The time frame of these changes can be between tens of seconds and few hours. Only two groups of dynamics are of direct interest to the work in this thesis, those are the electromagnetic and electromechanical phenomena.

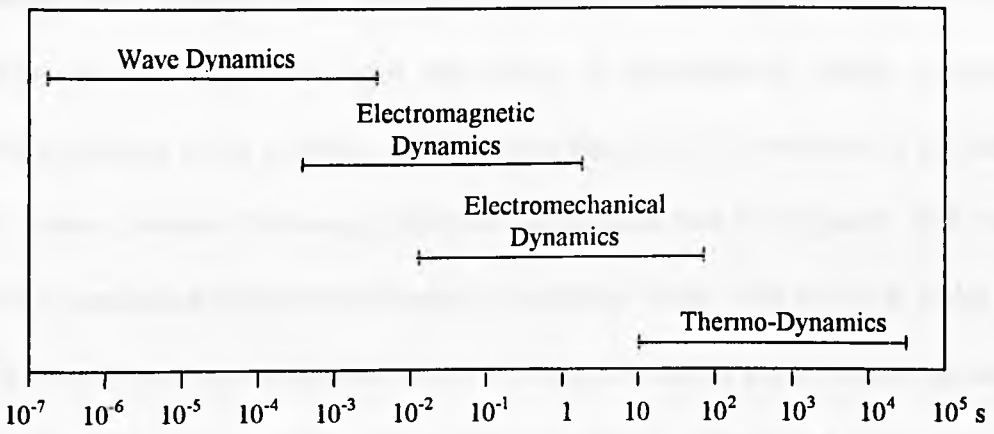

Fig. 3.2 Time frame of the basic power system dynamic groups

When a disturbance, such as a short circuit, occurs in a power distribution network, significant changes take place in the loading of some generators in the system. Changes on the electrical network are governed by the electromagnetic phenomena that occur within milliseconds, as shown in Fig. 3.2. On the other hand, the mechanical controls of generators, which fall in the electromechanical group, may take few seconds. Therefore, there is the possibility that one or more generators may encounter sufficient variations in rotational speed that they lose synchronisation with the power network. If a generator loses

synchronisation with the network, it should be taken off-line to avoid catastrophic problems. However, this will result in decrease of the available generator capacity and this will lead to another source of disruption, which will be injected into the power system. Cascading system failures can lead to widespread power outages, reduce the interconnected power grid to islands of power service, and even cause physical damage to generating equipment [77]. If a system returns to normal or stable operation after having been subjected to a major disturbance, then the system is said to be stable, otherwise, it is unstable.

Different types of transient and dynamic phenomena are usually investigated utilising digital computer based transient and dynamic simulation programs, and solutions are obtained in the time domain. Depending upon the period of investigation, system components are modelled utilising either algebraic or differential equations. For example, if the stability of a synchronous generator following a fault on the network was investigated, then the solution would be dominated by the time constant of generator rotor. This can be in order of 1 to 10 s [78]. In this case, the mechanical motion of the synchronous generator can be described by a couple of single-order differential equations. On the other hand, the response of the network and generator stator, which is largely determined by a much smaller time constant, can be described by a number of algebraic equations.

The number of equations required to solve the transient stability of an electrical network is usually large. In order to find the solution for systems of differential equations, different numerical methods are used, such as Trapezoidal method of integration [20,88], Rung-Kutta methods [78,83], and modified Eurler method [54]. The latter is also known as predictor-corrector method [78,83,88].

In this thesis, the dynamic behaviour of wind power based embedded generators following a fault on a load feeder of a distribution network is investigated utilising the electromagnetic transient program (EMTP). In this program, as explained in the section 3.4, the "Trapezoidal" rule of numerical integration is used for the simulation of transient problems. Therefore, the basic principle behind this particular method of integration is explained in Appendix B.

3.4 The Electromagnetic Transient Program (EMTP)

The ElectroMagnetic Transient Program (EMTP), is a computer program for simulating electromagnetic, electromechanical and control system transients on multiphase electrical power systems. The EMTP was developed in the late 1960's by Dr. Hermann Dommel [84], for the Bonneville Power Administration. In 1986, Dr. Scott Meyer [85] sponsored an independent version of the EMTP, which he called the Alternative Transient Program (ATP). The EMTP is designed to solve algebraic, ordinary and/or partial differential equations associated with a network. The latter can be modelled in the EMTP using a wide range of different system components that are provided in the program.

3.4.1 The Solution Method Used in the EMTP

Transient phenomena can only be simulated on digital computers at discrete intervals of time with a step size of Δt. It is assumed in the EMTP that the variable of interest is known at the previous time step ($t - \Delta t$) and that the solution must be found at the current instant of time (t) (e.g. a step by step numerical solution). This section presents basics of the solution method for simple components and electrical circuits under transient conditions.

More detailed information about modelling in EMTP can be found in references such as [20,84,87,88].

3.4.1.1 Representation of Basic Components

Consider an inductance, L, between two nodes as shown in Fig. 3.3. The voltage-current relationship for the element shown in Fig. 3.3 can be expressed as follows:

$$e_k - e_m = L\frac{di_{k,m}}{dt} \tag{3.7}$$

The integration of equation (3.7) from a previously defined state at time (t - Δt) to the current instant of time (t), is given by:

$$i_{k,m}(t) = i_{k,m}(t-\Delta t) + \frac{1}{L}\int_{t-\Delta t}^{t}(e_k - e_m)dt \tag{3.8}$$

Applying the trapezoidal rule of integration to equation (3.8) [88] yields the following:

$$i_{k,m}(t) = i_{k,m}(t-\Delta t) + \frac{\Delta t}{2L}[e_k(t) - e_m(t)] + \frac{\Delta t}{2L}[e_k(t-\Delta t) - e_m(t-\Delta t)] \tag{3.9}$$

Equation (3.9) can be rearranged as:

$$i_{k,m}(t) = \frac{\Delta t}{2L}[e_k(t) - e_m(t)] + I_{k,m}(t-\Delta t) \tag{3.10}$$

where:

$$I_{k,m}(t-\Delta t) = i_{k,m}(t-\Delta t) + \frac{\Delta t}{2L}[e_k(t-\Delta t) - e_m(t-\Delta t)] \tag{3.11}$$

The value of the equivalent current source, $I_{k,m}(t-\Delta t)$, is known from the past history. The equivalent impedance network corresponding to Equation (3.10) is shown in Fig. 3.4.

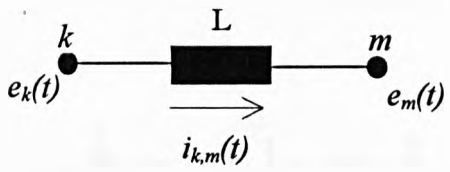

Fig. 3.3. Inductance between two nodes.

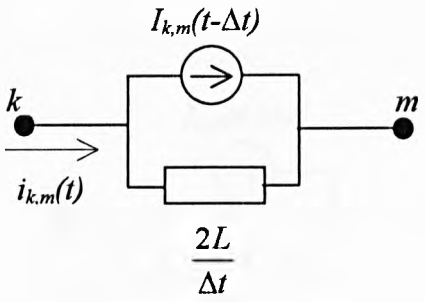

Fig. 3.4. Equivalent impedance network

The voltage-current relationship of a capacitance, C, between two nodes, shown in Fig.3.5, can be expressed as follows:

$$i_{k,m} = C\frac{d}{dt}(e_k - e_m) \tag{3.12}$$

Integrating both sides of Equation (3.12) from a pre-defined time (t - Δt) to the current instant of time (t), yields:

$$\int_{t-\Delta t}^{t} i_{k,m}(t)\,dt = C\left([e_k(t) - e_m(t)] - [e_k(t-\Delta t) - e_m(t-\Delta t)]\right) \tag{3.13}$$

or:

$$e_k(t) - e_m(t) = [\frac{1}{C}\int_{t-\Delta t}^{t} i_{k,m}(t)dt] + e_k(t-\Delta t) - e_m(t-\Delta t) \tag{3.14}$$

Using the trapezoidal rule for the integration of Equation (3.14) yields:

$$i_{k,m}(t) = \frac{2C}{\Delta t}[e_k(t) - e_m(t)] + I_{k,m}(t-\Delta t) \tag{3.15}$$

where:

$$I_{k,m}(t-\Delta t) = -i_{k,m}(t-\Delta t) - \frac{2C}{\Delta t}[e_k(t-\Delta t) - e_m(t-\Delta t)] \tag{3.16}$$

The value of the equivalent current source, $I_{k,m}(t-\Delta t)$, is known from the past history. The equivalent impedance network corresponding to Equation (3.15) is similar to that of an

inductor as shown in Fig. 3.6.

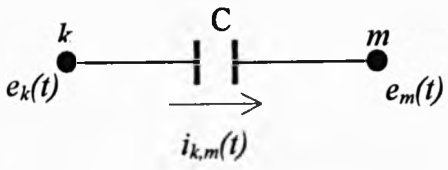

Fig. 3.5 Capacitance between two nodes

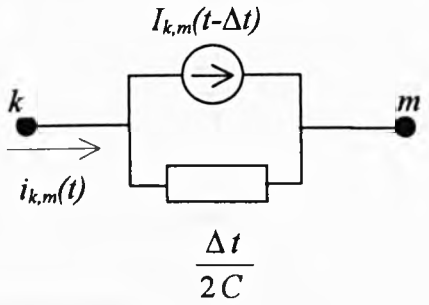

Fig. 3.6 Equivalent impedance network

The voltage-current relationship of a resistance between two nodes, shown in Fig. 3.7, can be directly expressed using Ohm's law as follows:

$$i_{k,m} = \frac{1}{R}[e_k(t) - e_m(t)] \tag{3.17}$$

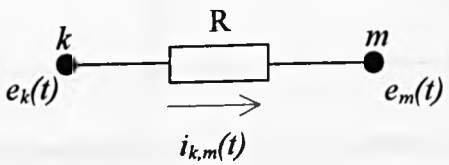

Fig. 3.7 A resistor between two nodes.

3.4.1.2 Representation of a Simple Electric Circuit

As illustrated above, the lumped R,L and C components can be represented by an equivalent circuit of a resistive branch and a current source. Then, an electrical circuit can also be represented using the combination of models of its individual components. As an example, the electric circuit shown in Fig. 3.8 can be represented by the equivalent circuit shown in Fig. 3.9.

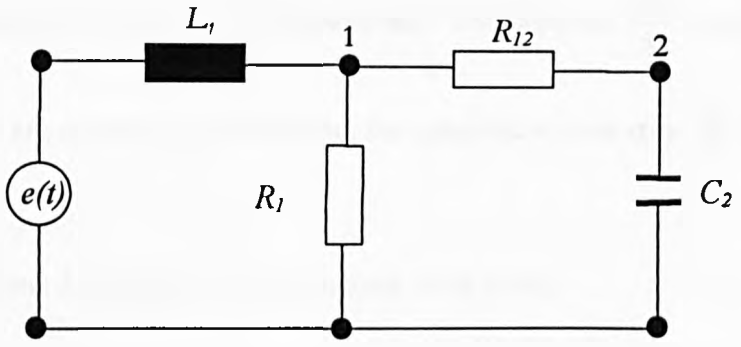

Fig. 3.8 Two node electrical circuit

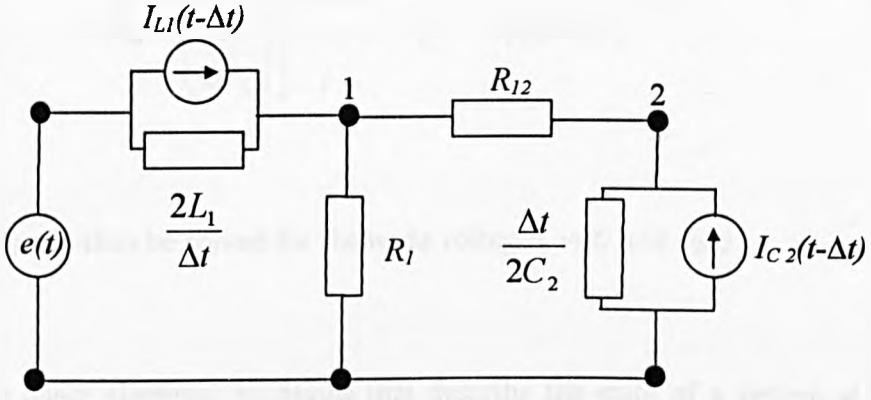

Fig. 3.9 Equivalent circuit of the two nodes circuit

The nodal equations for the equivalent circuit in Fig. 3.9 are:

$$\frac{[v_1(t)-e(t)]}{\left(\frac{2L_1}{\Delta t}\right)}+\frac{v_1(t)}{R_1}+\frac{[v_1(t)-v_2(t)]}{R_{12}}=I_{L1}(t-\Delta t) \tag{3.18}$$

$$\frac{[v_2(t)-v_1(t)]}{R_{12}}+\frac{v_2(t)}{\left(\frac{\Delta t}{2C_2}\right)}=I_{C2}(t-\Delta t) \tag{3.19}$$

Where $I_{L1}(t-\Delta t)$ and $I_{C1}(t-\Delta t)$ are the equivalent current sources that represent the history term from the previous step related to elements L and C respectively. $v_1(t)$ and $v_2(t)$ are the

instantaneous voltages of nodes 1 and 2 respectively. The resistors $\frac{2L_1}{\Delta t}$ and $\frac{\Delta t}{2C_2}$ are time-independent, which are constants provided that the calculation time step, Δt, is constant.

Rearranging Equations 3.18 and 3.19 into a matrix form yields:

$$\begin{bmatrix} \frac{1}{\left(\frac{2L_1}{\Delta t}\right)} + \frac{1}{R_1} + \frac{1}{R_{12}} & -\frac{1}{R_{12}} \\ -\frac{1}{R_{12}} & \frac{1}{R_{12}} + \frac{1}{\left(\frac{\Delta t}{2C_2}\right)} \end{bmatrix} \begin{bmatrix} v_1(t) \\ v_2(t) \end{bmatrix} = \begin{bmatrix} I_{L1}(t-\Delta t) + \frac{e(t)}{\left(\frac{2L_1}{\Delta t}\right)} \\ I_{C2}(t-\Delta t) \end{bmatrix} \tag{3.20}$$

Equation (3.20) can then be solved for the node voltages $v_1(t)$ and $v_2(t)$.

In general, the linear algebraic equations that describe the state of a system at time t are given by [20]:

$$[\,Y\,]\,[\,v(t)\,] = [\,i(t)\,] - [\,I\,] \tag{3.21}$$

where

$[\,Y\,]$ is the nodal conductance matrix,

$[\,v(t)\,]$ is the column vector of the node voltages at time t,

$[\,i(t)\,]$ is the column vector of injected currents at time t,

$[\,I\,]$ is the column vector equivalent current sources, which are known at time $(t-\Delta t)$.

The solution of Equation 3.21 for the node voltages is given by:

$$[\, v(t) \,] = [\, Y \,]^{-1} [\, i(t) \,] - [\, Y \,]^{-1} [\, I \,] \tag{3.22}$$

As can be seen, the transient calculations can be accomplished by solving a system of linear equations at each time step. During the transient calculation, the coefficient matrix **[*Y*]** remains constant unless the configuration of the network is changed, due to for example, switching operations.

3.4.2. Simulation of System Components in the EMTP.

Electrical systems are described in the EMTP by nodes, branches, switches and sources as follows [86]:

- Each node is identified in EMTP by a 6-character alphanumeric name, except ground, which identified by a blank.
- Branches (lines, cables, transformers or any other linear or non-linear element) are identified by their data and the names of nodes to which they are connected. Branch data are arranged in what is called "branch cards."
- Switches, which are considered as special branches, are also described by the names of nodes to which they are connected within the switch data cards.
- Sources usually have two terminals, and one of these must be ground. The ungrounded terminal is identified by a 6-character name in the specified field. Most sources are described using a single data card format.

A branch can be a lumped R-L-C series element, a transmission line, a cable line, or a transformer. Different models that are used to simulate transmission lines and cables

include:

- Lumped - parameter coupled π equivalent model
- Constant - parameter model, where a line is represented by incremental sections at steady- state power frequency.
- Double - Circuit Distributed Line Model with Zero-sequence coupling.
- Rigorous, frequency - dependant model (Jose Marti) which accounts for the frequency dependence of transmission line parameters over the wide range of frequencies that are present in the signals during transient conditions [89].
- Second order, recursive - convolution model (Semlyen model) [90].

Transformers are represented in the EMTP program using one of the following three models:

- Lumped R-L-C series connected circuit
- Transformers as coupled impedance
- Saturable Transformer Component Model. This model is suitable for the transient analysis of inrush currents, ferroresonance and similar phenomena.

Saturation and magnetising-current effects of transformers are required for the transient analysis of inrush currents, ferroresonance and similar phenomena. The "Saturable Transformer Component" model is designed in such a way that these effects are internally modelled as a pseudo-nonlinear reactor, which has two or more segments. It uses what is referred to as "the star-circuit representation" [20] as shown in Fig. 3.10. The primary winding is modelled as an uncoupled R-L branch connected between Bus1 and star point S, R_1 and L_1 in Fig. 3.10. Each of the other windings, from the second to the N^{th}, is modelled as a two-winding transformer, which comprises a cascade connection of an ideal transformer that represents the transformation ratio, and an R-L branch. Saturation and magnetising effects are represented as a single non-linear reactor, L_m, in the primary winding circuit. Core losses are modelled as a linear resistance, R_m, which is assumed in parallel

with the saturation branch.

The data required to model saturation is generated from the saturation curve corresponding to the transformer to be modelled.

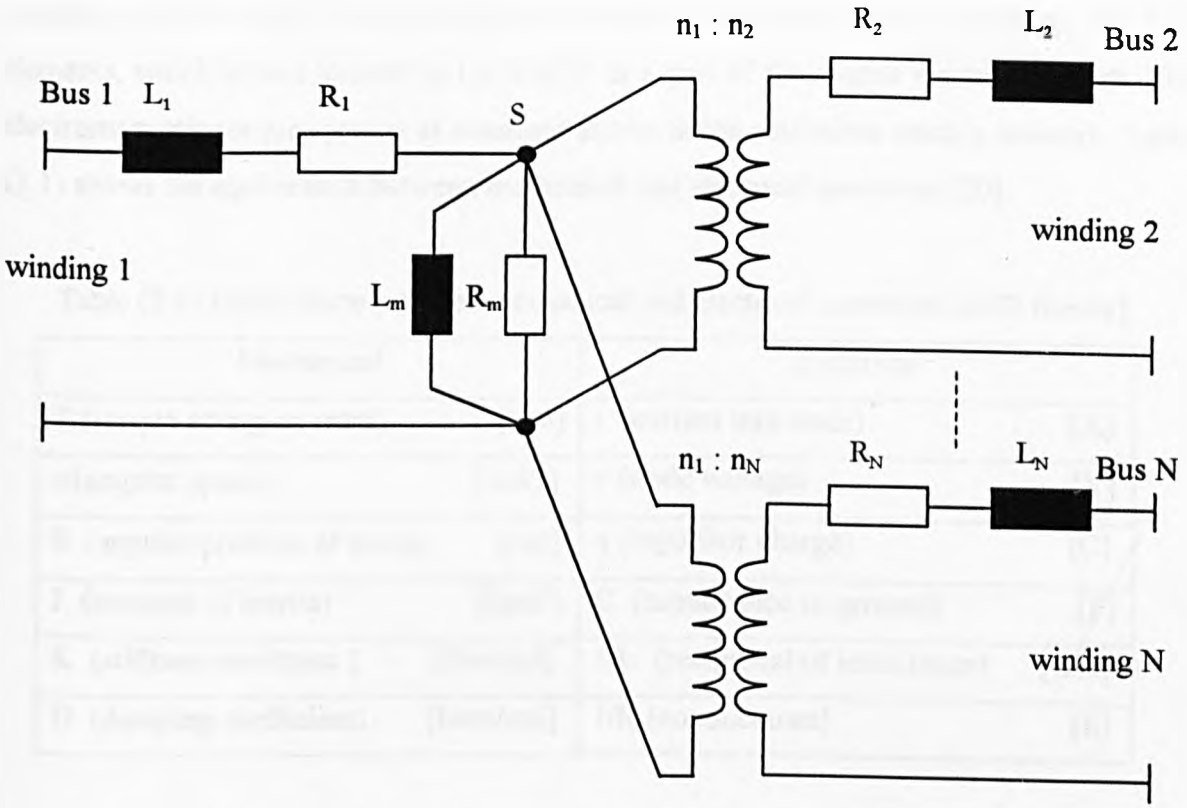

Fig. 3.10 Star-circuit representation of N-winding transformers

Induction generators are simulated using one of the EMTP models called the Universal Machine (UM) model, which has been proposed by Lauw and Meyer [91] in 1982. The UM model is an electromechanical energy conversion device, which can be connected to an electrical network and a mechanical system. It can be used to represent 12 major types of electric machines, e.g. single-phase, two-phase and three-phase synchronous or induction machines and dc machines of different types [20]. Generally, any electric machine has two types of windings: one is referred to as armature windings and the other called the field structure windings. In induction and synchronous machines, armature windings are commonly stationary on the stator, whereas, in DC machines, they are on rotor. Field structure windings in synchronous machines are usually on the rotor, while in DC machines, they are on the stator. In induction machines, they are on the rotor, either in the form of a

short-circuited copper or aluminium bars, which known as squirrel-cage, or in the form of a wound rotor with slip-ring connections to the outside. The UM theory is based on a generalised machine model where the two groups of machine windings, i.e. armature and field windings, are represented by equivalent electrical coils, which are assumed on the direct, quadrature, and zero-sequence axes. A UM model may include up to three armature windings and any number of windings on the field structure. The mechanical side of a machine can be included in the model by an equivalent electric network with lumped R,L,C elements, which is then treated by the EMTP as a part of the overall electric network. The electromagnetic torque appears as a current source in the equivalent electric network. Table (3.1) shows the equivalence between mechanical and electrical quantities [20].

Table (3.1) Equivalence between mechanical and electrical quantities [ATP theory].

Mechanical		Electrical	
T (torque acting on mass)	[Nm]	i (current into node)	[A]
ω(angular speed)	[rad/s]	v (node voltage)	[V]
θ (angular position of mass)	[rad]	q (capacitor charge)	[C]
J (moment of inertia)	[kgm^2]	C (capacitance to ground)	[F]
K (stiffness coeficiant)	[Nm/rad]	1/L (reciprocal of inductance)	[1/H]
D (damping coefficient)	[Nms/rad]	1/R (conductance)	[S]

Each mass on the shaft system is represented by a capacitor. If there is damping proportional to speed on this mass, a resistor is put in parallel with the capacitor. The flexibility in this model enables the modelling of induction generators in detail and allows changes in the input torque to be considered.

A Synchronous generator (SG) can also be simulated in the EMTP using the UM model, however, another machine model which is known as Type59 is found more suitable for this work. It is a three-phase dynamic synchronous machine model, which represents the details of the electrical part of a generator as well as the mechanical part of the generator and its associated turbine [86]. The Type59 model allows the dynamics of the prime mover (e.g. governor and turbine) to be included in the simulation. This is achieved using the Transient

Analysis of Control Systems (TACS), which is specially developed in the EMTP, and can easily be interfaced with the control circuitry of the SG Type95 model. The voltage applied to the field winding can also be controlled using TACS. Another advantage of the Type59 model is that the required control machine variables (e.g. rotor speed and field voltage) are obtained directly.

CHAPTER 4

VOLTAGE CONTROL OF DISTRIBUTION SYSTEMS

4.1 Introduction

One of the main objectives in the design and operation of a distribution system is to achieve an acceptable level of quality of electricity supply [16]. The power quality issue is concerned with all voltage deviations and disturbances, such as sustained under-voltages and over-voltages, harmonics, voltage flicker, voltage sags and sustained interruptions. It is also concerned with deviations of system frequency. There are number of standards and regulations which bind electricity suppliers to maintain power quality indices within acceptable limits [93-95]. During the normal operation of a power system, the deviation of voltage is caused by voltage drop in distribution lines and transformers. In order to prevent the development of sustained under-voltages or over-voltages that may affect the normal operation of consumer's equipment, electricity supply authorities are required to use a means of voltage regulation that maintains voltages within the statutory limits. According to the IEC recommendations 60038 [93] and the British Standard BS EN 50160 [94], a nominal voltage of 230/400 V should operate until 1 January 2003 with a permitted voltage tolerance range of +10/-6 %. After January 2003, the permitted voltage tolerance will be amended to the range of $\pm$10%. Voltage levels above 1kV and not exceeding 35kV have to be maintained to within $\pm$10% from the nominal voltage of the system [93]. Two main

methods of voltage regulation are commonly used [17,26,76,96], these are:

1) Injection of reactive power

2) Change the voltage-ratios of transformers.

Voltage regulation based on the former method is achieved indirectly by adjusting the reactive power flow through a regulated point on the network. The basic idea behind voltage regulation using reactive power injection and the main methods of reactive power injection are summarised in Appendix (C). More details about these methods can be found in the literature, such as [26, 76, 97, 98].

The latter method of voltage regulation is achieved directly by changing the voltage ratio of transformers in the network. The reported work in this thesis is mainly concerned with the effects of integration of embedded generation on the voltage control of distribution systems when this method of regulation is used. Particularly, the effects of embedded generation on the operation of the AVC relays, which control the operation of on-load tap changers, are investigated.

4.2 Voltage Control Using Tap-Changing Transformers.

Transformers are mainly used to link those parts of a power system that operate at different voltage levels. In addition to that, transformers are also used for voltage control. Since the voltage ratio of a transformer is directly proportional to its turns-ratio, voltage control is achieved by adjusting the latter by changing the number of turns of one or more of transformer's winding(s). For this purpose, a tap- changing device is used to switch the

required number of turns into the circuit until the output voltage falls within statutory limits, as shown in Fig. 4.1. This method constitutes the most popular and widespread form of voltage control at all voltage levels [26].

Transformers with tap changing devices fall into two main categories [99,100]:

a) Off-load Tap-Changing Transformers, and

b) On-load Tap-Changing Transformers (OLTCTs).

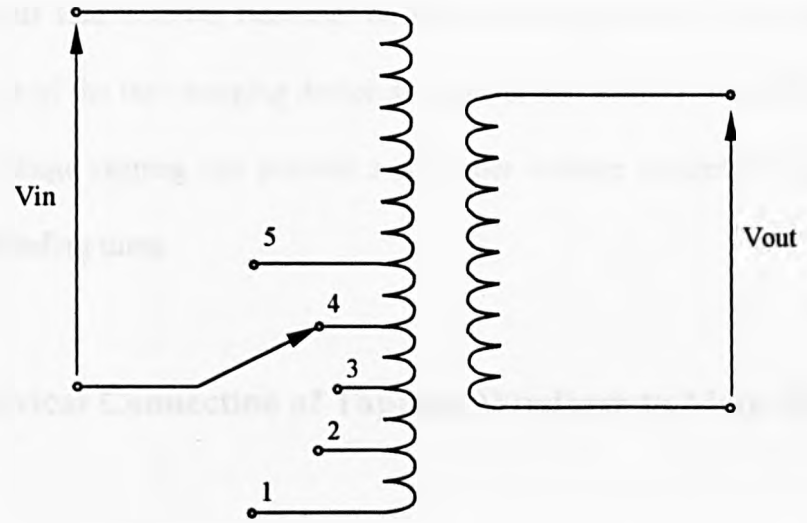

Fig. 4.1 The principle of tap-changer transformer.

Tap changing using an Off-load tap-changing device can only be carried out when the transformer is not energised. The simplest and cheapest arrangement of this type is that where transformer tapping is terminated just below the oil level in transformer's tank and tap changer is operated manually by an internal handle [100]. The drawback to this arrangement is that it requires removing the transformer tank cover each time tap changing is required. A more convenient arrangement is commonly used where taps inside the tank are connected to an internal selector which is operated by an external handle. Because of the simple structure of transformers with Off-load tap-changers, they are widely used in distribution systems

with nominal voltages ranging from11kV to 33kV. The commonly used range of tapping is ±5% of the nominal voltage in 2.5% or 5% steps [16,100].

On the other hand, OLTCTs are used to provide voltage control of high-voltage distribution systems under varying load conditions. Therefore, the structure of this type of tap changing devices is more complicated when compared to that of the Off-load tap-changer. An On-load tap changer can be situated in the same tank as the main winding or in a separate tank. The taps are usually on the high voltage side of the transformer, because transformer current on this side is lower than that on the low voltage side, consequently, the current carrying parts of the tap-changing device are smaller and simpler. In addition, a transformer with high voltage tapping can provide a smoother voltage control because of the greater number of winding turns.

4.2.1 Electrical Connection of Tapping Windings to Main Winding

Taps of star-connected windings are usually closer to the neutral end of the winding [99], as shown in Fig. 4.2. Consequently, the voltage of the tap terminals with respect to the ground is smallest, which is preferable from the insulation viewpoint.

When tapping is applied to delta-connected windings, the tapped turns are located either at the line-end or in the middle of the main winding [99], as shown in Fig. 4.3 and Fig. 4.4 respectively. The line-end connection requires that tappings be properly isolated against dielectric stresses. On the other hand, the mid-winding arrangement reduces the dielectric stresses but it alters other parameters such as transformer impedance and winding insulation integrity.

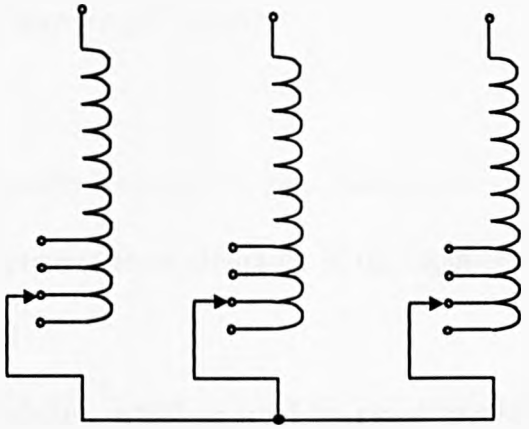

Fig. 4.2 Tapping of Star-connected windings at the neutral end.

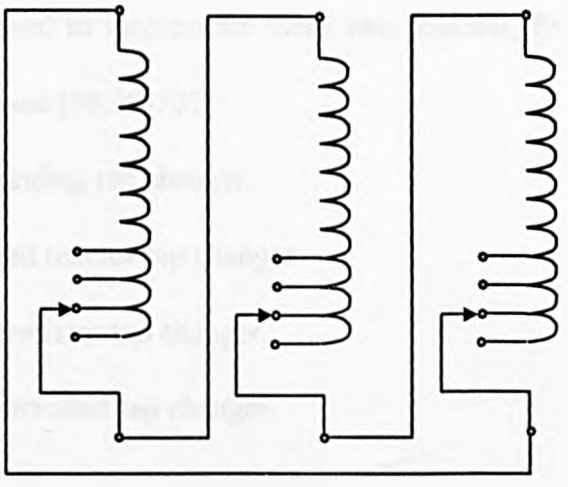

Fig. 4.3 Line-end tapping arrangement in Delta-connected windings.

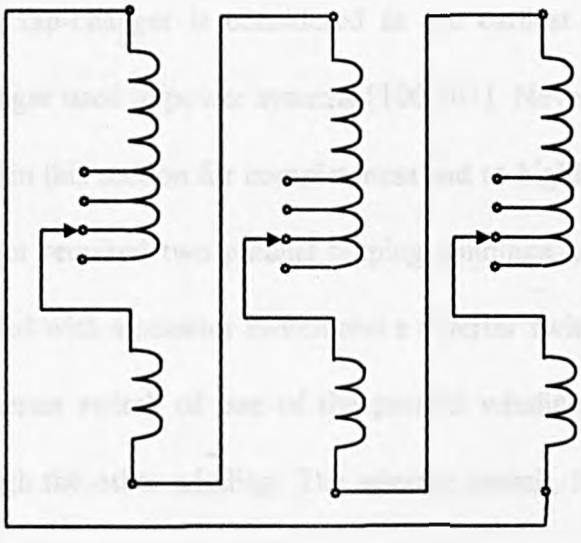

Fig. 4.4 Mid-winding arrangement of tapping in Delta-connected windings.

4.2.2 On-load Tap Changing Circuits

The circuit of OLTCTs usually includes two important features [96,99-101]:

a) A facility to prevent short circuiting of the tapping section during tap changing, and

b) A duplicate circuit, which is used to avoid breaking the circuit by providing an alternative path to carry the load current while tapping the other circuit.

Based on the method used to incorporate these two features, four types of tap changing circuits are commonly used [96,99-101]:

a) Duplicate winding tap changer.

b) Centre-tapped reactor tap changer.

c) High-speed resistor tap changer.

d) Thyristor controlled tap changer.

4.2.2.1 Duplicate Winding Tap Changer.

The duplicate winding tap-changer is considered as the earliest design of on-load tap-changer and it is no longer used in power systems [100,101]. Nevertheless, the principle of this design is discussed in this section for completeness and to highlight its main drawbacks. This type of tap changer required two parallel tapping windings, as illustrated in Fig. 4.5. Each winding is provided with a selector switch and a diverter switch. To change from one tap to another the diverter switch of one of the parallel windings, say S_1, is opened to transfer the load through the other winding. The selector switch, S_3, is then moved to the new position. After that, S_1 is closed. At this stage circulating current flows in the parallel

windings due to the difference in tap positions. The same procedure is applied to the second winding until the two windings are set at the same tap position. A disadvantage of this method is that the parallel windings need to be designed to carry the full load current in turn during the tap changing process, which increases the size of the transformer. Using two parallel windings also makes the transformer more expensive. Another disadvantage is that the leakage reactance of the windings must be suitable to maintain the circulating current within reasonable limits.

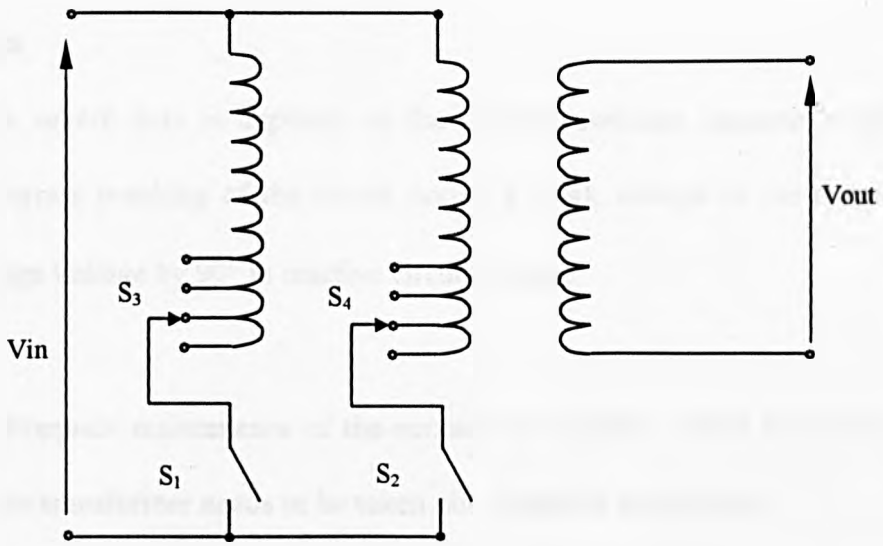

Fig. 4.5 Principle of Duplicate Winding Tap Changer

4.2.2.2 Centre-Tapped Reactor Tap Changer

The arrangement for this method is shown in Fig. 4.6 [96,100]. As can be seen in this figure, two selector switches and two diverter switches are used in this arrangement to avoid breaking the load current and the mid-point tapped reactor L is used to prevent short circuiting of the tapping section during tap changing. Suppose it is required to change from tap 1 to tap 2; First, diverter switch S_1 is opened, consequently load current will only flow

through the second circuit. The selector switch S_3 is then changed to position 2. S_1 is then closed. This condition will cause a circulating current to flow through the reactor because of the difference in the voltages between terminals S_3 and S_4. The voltage of the reactor's mid-point will be approximately intermediate between the voltage at tap 1 and tap 2. By designing the reactance to maintain the circulating current within acceptable limits, this intermediate position is utilised to double the number of tappings. Changing the position of the second circuit follows the same sequence as for the first circuit utilising diverter switch S_2 and selector switch S_4. The centre-tapped reactor tap-changer however has the following disadvantages:

a) A severe duty is imposed on the diverter switches because a zero current breaking of the circuit occurs at peak voltage as the current lags voltage by 90° in reactive circuits, hence,

b) Frequent maintenance of the contacts is required, which means that the transformer needs to be taken out of service more often.

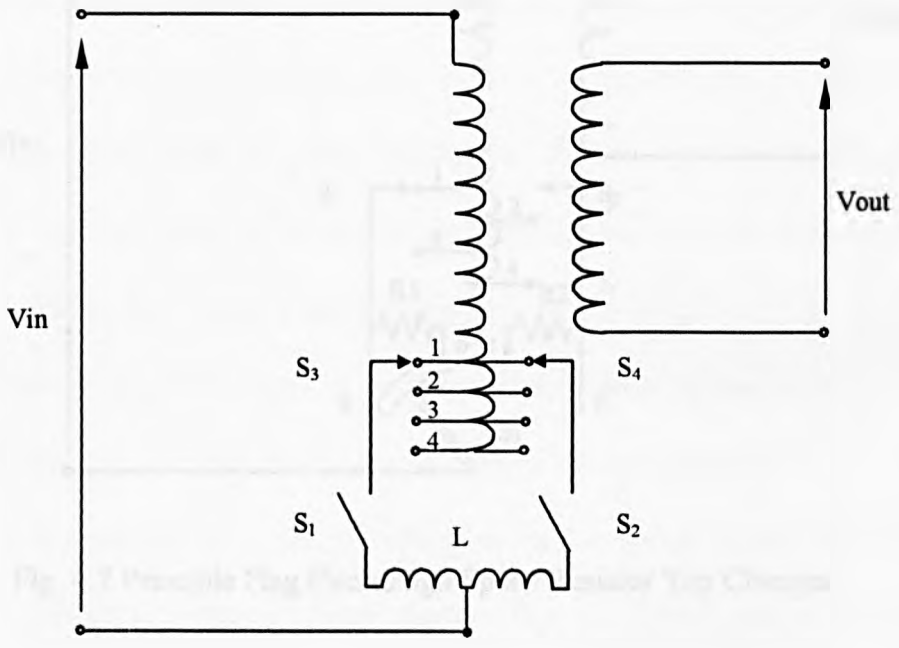

Fig. 4.6 Principle of Centre-Tapped Reactor Tap Changer

4.2.2.3 High-Speed Resistor Tap-Changer

As the name implies, in high-speed resistor tap-changers a resistor is used to limit the circulating current during the tapping operation. The different arrangements of high-speed resistor tap-changers [96,99-101] can be divided into two main types: the Pennant Cycle type and the Flag Cycle type. In the former type a single resistor is used to reduce circulating currents, whereas two resistors are used in the latter. The principle of a flag cycle high-speed resistor tap-changer is depicted in Fig. 4.7. This type of tap changer comprises two selector switches, S1, which is used to select the odd taps, and S2, which is used to select the even ones. It also comprises a diverter switch, S3, with two shunt resistors, R1 and R2.

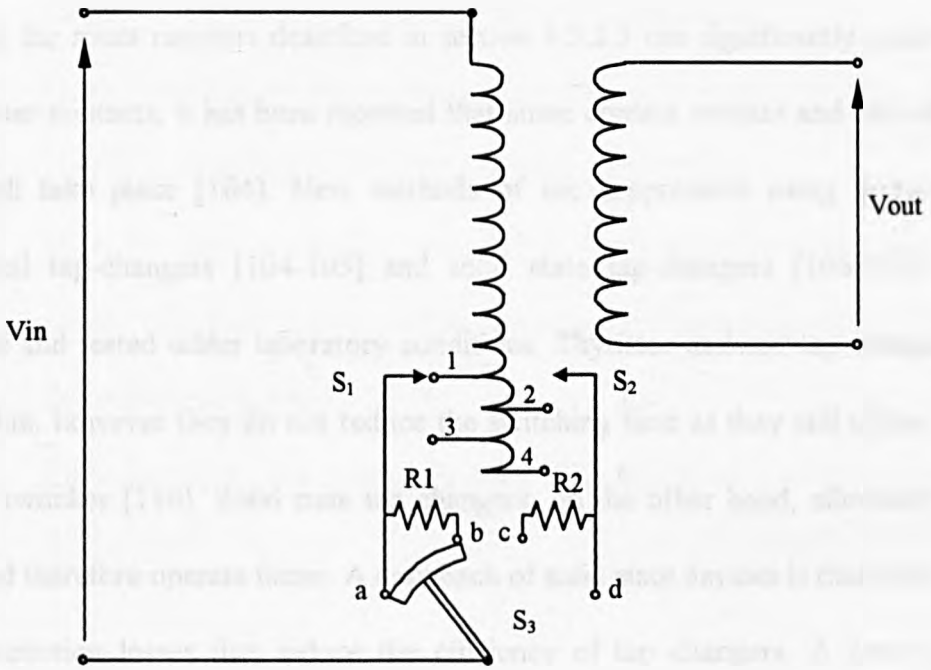

Fig. 4.7 Principle Flag Cycle High Speed Resistor Tap Changer

In order to change from position 1 to position 2, switch S_2 is firstly moved to position 2. Then, switch S_3 moves from its position short-circuiting a and b to the position short-circuiting b and c, and finally to the position short-circuiting c and d. The resistors R1 and R2 carry the load current in turn during the tap change and they limit the circulating current. Consequently, it is important to operate the tap changer as fast as possible to avoid overheating the resistors. Unlike the case with reactor tap changers, high- speed resistor tap changers operate at near zero current and near zero voltage as the current through a resistor is in phase with the voltage. This advantage helps in reducing arcing that may appear at the diverter contacts. Therefore, a contact life of 250,000 operations is common for this type compared to 10,000-20,000 for reactor tap-changers [104].

4.2.2.4 Thyristor Controlled Tap Changer

Although the shunt resistors described in section 4.3.2.3 can significantly reduce arcing at the diverter contacts, it has been reported that some contact erosion and oil contamination could still take place [104]. New methods of arc suppression using thyristor assisted mechanical tap-changers [104-105] and solid state tap-changers [106-109] have been proposed and tested under laboratory conditions. Thyristor assisted tap-changers increase contact life, however they do not reduce the switching time as they still utilise mechanical diverter switches [110]. Solid state tap changers, on the other hand, eliminate mechanical parts, and therefore operate faster. A drawback of solid state devices is that they suffer from high conduction losses that reduce the efficiency of tap changers. A new type of tap-changer has been described [110,112] which uses a fast acting vacuum switch selector and Gate-Turn-Off (GTO)/vacuum switch diverter. Fig. 4.8 depicts this tap changer scheme [110,112]. The diverter comprises two solid-state GTO based AC switches A and B, and

two vacuum switches V_1 and V_2 connected in parallel with A and B respectively, as shown in Fig. 4.8. For the selector switches (S_1 - S_4 or more) vacuum switches are used to obtain a faster response. Tap changing is performed using the AC switches A and B, which transfer load current from one tap to the next on a current zero using an improved snubber in the GTO circuit [111]. The vacuum switches do not therefore make or break the load current. The configuration of each AC switch, which comprises four diodes and one GTO, is shown in Fig. 4.9 [111]. The four diodes are required since the GTO cannot block high reverse voltages [112,113]. The auxiliary current diverter transfers load current from vacuum switches V_1 or V_2, to the parallel switches B or A, respectively, allowing V1 or V2 to be opened under no-load conditions. As an operational example, assume initially that S1 and V_1 are closed and it is required to change the tap to the second position, which is connected to S_2. The following sequence is then applied [112]:

a) Close S_2. No current pass through S_2 as V_2 is still open,

b) On the next current zero crossing, turn on switch A and divert the current from switch V_1 to switch A using the auxiliary current diverter.

c) Open V_1. Since current flows through A, V_1 does not break any current.

d) On the next current zero, turn off switch A and turn on switch B. Current now flows through S_2 and B.

e) Close switch V_2 and then using the auxiliary diverter, transfer the current flow to switch V_2.

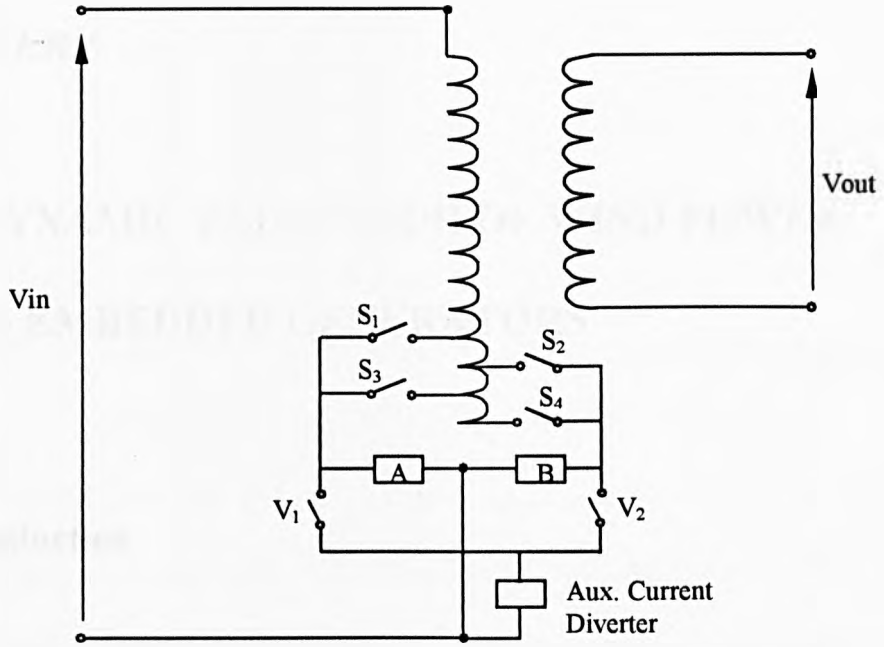

Fig. 4.8 Principle of GTO/Vacuum Switch Diverter Tap Changer

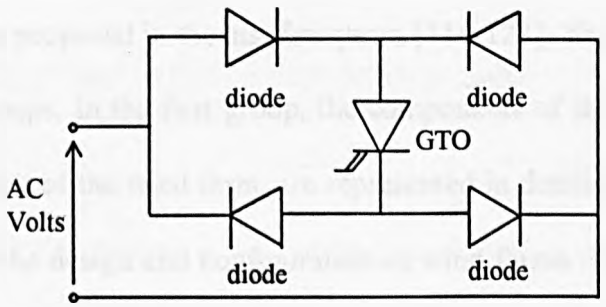

Fig. 4.9 AC switch arrangement

CHAPTER 5

THE DYNAMIC BEHAVIOUR OF WIND POWER BASED EMBEDDED GENERATORS

5.1 Introduction

The development of an accurate model of a wind farm connected to a distribution system is a crucial stage that should be considered prior to investigating the impact of wind power based embedded generators on distribution systems. Different system operating conditions require different modelling and simulation strategies. A number of wind turbine-generator models have been proposed in the last few years [114-123]. These models can be classified into two main groups. In the first group, the components of the turbine-generator units, as well as components of the wind farm, are represented in detail [114-118]. Such models are suitable to assist the design and configuration of wind farms. The second group comprises simplified models, which are able to simulate the dynamics of the wind farm with respect to the system [119-123] with reasonable accuracy. An approach based on a simplified model of wind turbines is used in this project.

5.2 Modelling of Wind Turbine - Generator Units using the EMTP

In order to produce significant amount of power, a wind farm usually comprises several wind turbine-generator units. A wind turbine-generator unit includes blades, a mechanical

drive unit, or drive train and a generator, see Fig. 2.1. The generator, which is commonly of the asynchronous type, is represented in the EMTP using the UM model. This model is found particularly attractive [124-126] because the mechanical side of the machine can be conveniently represented using an equivalent electric network consisting of lumped RLC elements, which is then solved as part of the whole electric network. The blade torque developed by wind speed is transmitted to the generator via the drive train [115]. In order to simplify the analysis, it is assumed that the mechanical torque on the turbine's shaft follows the same pattern as that of wind speed [115]. Hence, the driving force of the wind is simulated by the mechanical torque applied on the shaft, which is in turn represented using the EMTP by an equivalent current source. The inertia of the rotating components of the wind turbine is included within the inertia of the generator rotor. Therefore the rotating mass of the wind turbine-generator unit in total is represented by a capacitor connected to the generator model, as described earlier in section 3.4.2.

5.3 Description of the Distribution System under Consideration

A "typical" distribution system is used within this project to investigate the effects of the dynamic behaviour of wind power based embedded generators. The distribution system consists of the Grid, a wind farm and a substation. The substation is represented by a 20MVA, 132/33kV transformer with an impedance of 10%. The wind farm is assumed to have sixteen wind-turbine-generator units each rated at 600kW and 690V (see Fig. 5.1). In order to simplify the simulation of the wind farm, and at the same time maintain the flexibility of varying the injected power, the generating units are represented using three wind turbine-generator blocks. The first block, as can be seen in Fig. 5.1, represents two 600 kW units, while the second block represents four 600kW units and the third block represents ten 600kW units. All units are assumed connected at the same bus (No. 4). A

10MVA, 690V/33kV step-up transformer with an impedance of 10% is assumed between buses 3 and 4. A 33kV feeder of 10km is assumed connecting the wind farm with the main substation. A 20km feeder is assumed connecting the main substation to two groups of loads. One group connected at the middle of the feeder, at bus 5, and the second group connected at the remote end, at bus 6.

A similar distribution system was used with a gas turbine EG in order to compare its behaviour with that of wind based plant. This time the wind farm is replaced by a gas-turbine synchronous generator (SG) unit. It is assumed that the SG is rated at 10MVA and 11kV. It is also assumed that the generator is interfaced with the 33kV system through a 10MVA, 11kV/33kV step-up transformer with an impedance of 10%. The rest of the system is assumed similar to first one. Fig. 5.2 shows a schematic diagram of the considered system with synchronous embedded generation.

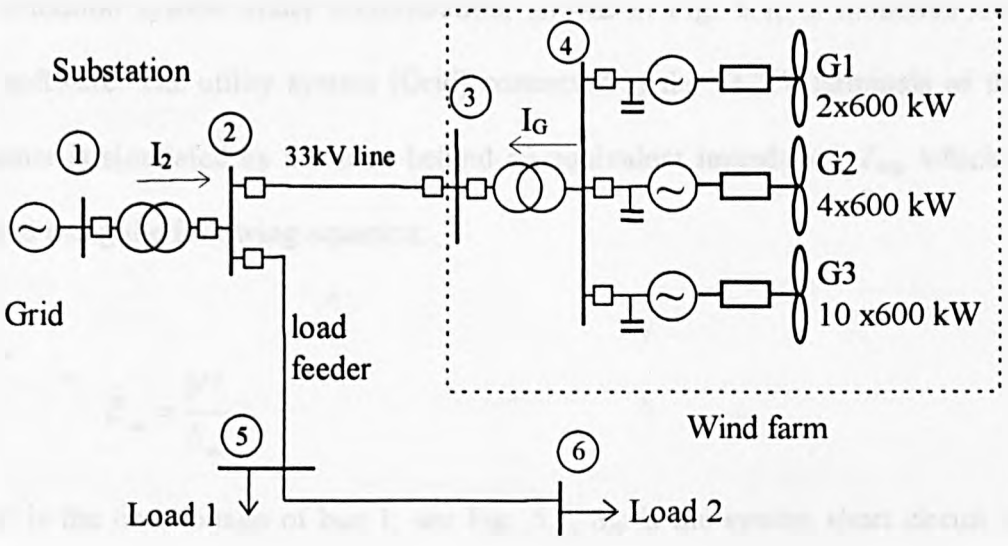

Fig. 5.1 Schematic diagram of the considered distribution system that includes a wind farm.

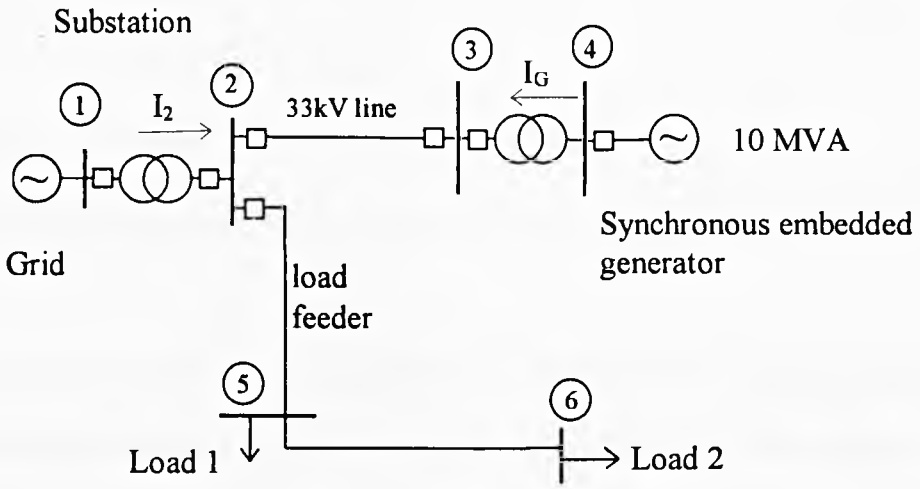

Fig. 5.2 Schematic diagram of the considered distribution system that includes a synchronous generator.

5.4 Modelling of the Distribution System in the EMTP

The distribution system under consideration, shown in Fig. 5.1, is modelled using the EMTP software. The utility system (Grid) connected at the 132kV terminals of the main transformer is simulated by a source behind an equivalent impedance, Z_{eq}, which can be calculated using the following equation:

$$Z_{eq} = \frac{V^2}{S_{sc}}$$

where V is the line voltage of bus 1, see Fig. 5.1, S_{sc} is the system short circuit level at bus1.

The resistive, R_{eq}, and reactive, X_{eq}, components of the equivalent impedance are found as follows:

$$R_{eq} = Z_{eq} \cdot \cos(\tan^{-1}(X/R))$$

$$X_{eq} = Z_{eq} \cdot \sin(\tan^{-1}(X/R))$$

where *X/R* is the ratio of equivalent impedance of the system at bus 1.

The short circuit level at bus 1 is assumed to be 1800 MVA at maximum generation and 1000 MVA at the minimum. It is also assumed that the X/R ratio of the system is equal to 10. Based on these assumptions, the equivalent impedance is calculated for the maximum and minimum generation conditions. For maximum generation:

$$Z_{eq}^{\max} = \frac{132^2}{1800} = 9.68\ ohm$$

$$R_{eq}^{\max} = 9.68 \cdot \cos(\tan^{-1} 10) = 0.9632\ ohm$$

$$X_{eq}^{\max} = 9.68 \cdot \sin(\tan^{-1} 10) = 9.632\ ohm$$

For minimum generation:

$$Z_{eq}^{\min} = \frac{132^2}{1000} = 17.424\ ohm$$

$$R_{eq}^{\min} = 17.424 \cdot \cos(\tan^{-1} 10) = 1.734\ ohm$$

$$X_{eq}^{\min} = 17.424 \cdot \sin(\tan^{-1} 10) = 17.34\ ohm$$

Transformers are represented using the "Saturable Transformer" model. As mentioned in chapter 3, this model considers both the connection group and the saturation phenomena of transformers. However, in this study, saturation is not included in the simulation and the magnetising current of the transformers is neglected; copper losses and core losses are also

neglected. The per unit value of the reactance of a transformer is converted to ohms as follows:

$$X_{T,ohm} = X_{T,pu} \cdot \frac{V_{base}^2}{S_{rating}} \quad ohm$$

where $X_{T,\,ohm}$ is the winding reactance in Ohms, $X_{T,\,pu}$ is the winding reactance in per unit, V_{base} is the voltage of transformer terminals, and S_{rating} is the transformer rating.

The inductance of the transformer is then calculated by:

$$L_T = \frac{X_{T,ohm}}{2\pi f} \quad Henry$$

where f is the system frequency.

The reactance of individual transformer windings is usually not available. However, the total reactance in per unit values, which is defined based on transformer's rating, is usually provided by the manufacturer. Therefore the total reactance is assumed equally divided between the primary winding, X_1, and the secondary winding, X_2 [20]. This approach is used to calculate the winding reactances of the three considered transformers. The winding reactance of the 20MVA transformer at the main substation are given by:

$$X_1 = 0.5 \text{ x } 0.1 \text{ x } \frac{132^2}{20} = 43.56 \quad ohm$$

and

$$X_2 = 0.5 \text{ x } 0.1 \text{ x } \frac{33^2}{20} = 2.7225 \quad ohm$$

The inductance of the windings of the 20MVA transformer:

$$L_1 = \frac{43.56}{2 \text{ x } 50 \text{ x } \pi} = 0.138 \quad Henry$$

and

$$L_2 = \frac{2.7225}{2 \text{ x } 50 \text{ x } \pi} = 0.00867 \quad Henry$$

Similarly, the reactance and inductance of the windings of the 10MVA transformer at the wind farm respectively are:

$$X_1 = 5.445 \quad ohm$$

$$X_2 = 0.0024 \quad ohm$$

and

$$L_1 = 0.0173 \quad Henry$$

$$L_2 = 7.6 * 10^{-6} \quad Henry$$

Similarly, the reactance and inductance of the windings of the 10MVA transformer for the synchronous EG respectively are:

$$X_1 = 5.445 \quad ohm$$

$$X_2 = 0.605 \quad ohm$$

and

$$L_1 = 0.0173 \quad Henry$$

$$L_2 = 0.00193 \quad Henry$$

The distribution lines used in the system of Figs. 5.1 and 5.2 can be classified as short lines as their lengths are less than 80km. Consequently, their shunt capacitance is so small as to be neglected without affecting the accuracy of simulation [79]. Based on this fact, the 33kV feeders are represented in the EMTP using lump RLC models that include the resistance, R, and the reactance, X, of the line only, with typical values of 0.185 ohm/km and 0.324 ohm/km, respectively.

As mentioned before, induction generators at the wind farm are represented using the UM model. Typical data for the equivalent circuit of a 600 kW induction generator, shown in Table 5.1, are used in the simulation. Data for the groups of two and five generators are calculated by a linear scaling [127] of the data related to a single generator. In order to account for the required power factor correction, a 138kVAr, shunt capacitor bank is assumed connected at the terminals of each generator.

The Synchronous generator in the second system is represented using the Type59 model, as described in chapter 3. The dynamics of the gas turbine and its associated governor control is included in the simulation using TACS. In order to control the field voltage of the generator, an excitation control scheme is also included in the simulation using TACS. The required control interface with the machine variables (e.g. rotor speed and field voltage) is also included.

Table 5.1. Data for a 600 kW induction generator

Item	Explanation of symbols used under "Item" column	1 gen.	2 gens(*)	5 gens(*)	Units
P_n	Nominal power of the generator	600	1200	3000	kW
U_n	Nominal voltage of the generator	690	690	690	V
PF	Power factor at full load	0.9	0.9	0.9	-
Q_{cap}	Nominal power factor correction	138	276	690	kVAr
J	Moment of inertia	10.5	21	52.5	kgm^2
H	Inertia constant (MVAsec/ MVA)	3.7(**)	3.7	3.7	-
R_1	Stator resistance at nominal duty	0.0073	.00365	.00146	ohm
X_1	Stator reactance at nominal duty	0.0750	.0375	0.015	ohm
R_2	Rotor resistance at nominal duty	0.0065	.00325	0.0013	ohm
X_2	Rotor reactance at nominal duty	0.09	0.045	0.018	ohm
R_m	Loss resistance at normal duty	0.08	0.04	0.016	ohm
X_m	Magnetising reactance at normal duty	3.25	1.625	0.65	ohm

(*)scaled values from the values for one machine, (**) Total inertia for the turbine-generator unit including blades, hub, shaft, gearbox converted to the high speed and the generator inertia.

5.5 Effects of Embedded Generation on the Critical Clearing Time of faults

5.5.1 Introduction

Prior to the introduction of embedded generation into distribution systems such systems are considered passive, i.e. their role is confined to transferring the electrical energy received from the transmission system to consumers. The design and protection of these systems are based on this description. For example, protection schemes of distribution feeders are usually designed based on the following two basic principles [16]:

a) They must insure minimum disruption of supply, i. e., the removal of a fault from the system should be achieved with minimum tripping of equipment.

b) They must be fast enough to minimise damage to system components.

The first principle is achieved by an appropriate protection co-ordination. This however, may require the operation time of protective devices at the up-stream of a distribution network to be as high as 1.5s [9]. On the other hand, the CCT limit required to maintain the stability of EG, such as a wind farm, can be much lower than the operating time of the above mentioned protective devices. This will be investigated in this chapter, but before proceeding with the investigation, it is important to explain the meaning of CCT with respect to synchronous generators and induction generators.

5.5.2 The Concept of Critical Clearing Time of Faults

5.5.2.1 CCT of Faults in Case of Synchronous Generators

During normal operating condition, a synchronous generator (SG) embedded into a distribution network usually runs at synchronous speed with a rotor angle of δ_0 corresponding to an electrical output power, P_e, and mechanical input power, P_m. The output power, P_e, which is transferred from the generator to the system, is approximately proportional to the square of the terminal voltage of the generator [54]. When a fault occurs on the network, P_e suddenly reduces due to the sudden change in network voltage. This leads to the acceleration of SG to account for the difference between P_m and P_e according to the well known swing equation [54]:

$$\frac{d^2\delta}{dt^2}=\frac{\omega_s}{2H}(P_m-P_e) \tag{5.1}$$

Where ω_s is the synchronous angular speed of rotor in electrical radians, t is the time, H is the inertia constant of the rotating mass and δ is the rotor angle.

This in turn causes the SG to gain kinetic energy, which is normally stored in its associated rotating mass. When this happens, the rotor angle increases. For example, when a three-phase fault occurs at the terminals of the generator, P_e reduces to zero and consequently, the rotor angle increases with time according to the following equation [79]:

$$\delta=\frac{\omega_s P_m}{4H}t^2+\delta_0 \tag{5.2}$$

When the fault is cleared at time t_c, which corresponds to a rotor angle δ_c, the power demand by the system re-establishes and the generator finds itself generating power greater

than P_e due to the new rotor angle position. If the input mechanical power remains unchanged, the extra power is supplied from the kinetic energy of the rotating mass. However, the rotor angle continues to increase due to the moment of inertia, but because the input power this time is less than the output power, the generator begins to decelerate passing its synchronous speed. The oscillation of the speed (and consequently the rotor angle δ) continues for a while, but eventually settle down to a new steady-state condition and the system is considered stable. Alternatively, δ continues to increase and the generator eventually loses synchronism with the network. The system in this case is considered unstable. There is a maximum rotor angle, below which the SG can retain a stable operation. This position is known as critical clearing angle. The corresponding maximum clearing time is known as the critical clearing time (CCT) for synchronous generators.

5.5.2.2 CCT of Faults in Case of Induction Generators

Unlike SGs, induction generators (IGs), which are commonly used in wind turbine-generator units, do not have field windings to develop the required electro-magnetic field in air-gap inside the machine. Therefore, they cannot work without an external power supply. The electro-magnetic torque (T_e) developed inside an induction machine at any given speed is proportional to the square of the terminal voltage as follows [128]:

$$T_e = K\, s\, V^2 \tag{5.3}$$

where K is a constant value and depends on the parameters of the machine, s is the machine slip.

It can be seen from (5.3) that T_e is bound to reduce following a fault condition. On the other hand, the dynamic behaviour of the rotor is governed by the swing equation given

below [54,91]:

$$J\frac{d\omega}{dt}=T_m-T_e \tag{5.4}$$

where J is the moment of inertia of the rotating mass, T_m is the mechanical torque applied to the rotor of the associated wind turbine and ω is the rotor speed.

It can be concluded from equation (5.4) that if the mechanical torque is maintained constant, then any reduction in the electro-magnetic torque, for instance due to a fault condition, causes the rotor to accelerate. This in turn leads to an increase in the kinetic energy of the rotating mass. When the fault is cleared and system voltage recovers, the magnetic field inside the air-gap of the machine starts to build up. This causes a flow of high current from the network into the machine. This current in turn causes a voltage drop across the interfacing link between the induction generator (in this case the wind farm) and the substation, leading to a reduction in the voltage at the generator (wind farm) terminals. The resulting electro-magnetic torque acts on the rotor in a direction opposite to that of mechanical torque applied by wind turbine(s). If the electromagnetic torque resulting from the newly established rotating magnetic field becomes higher than that of the mechanical torque acting on the rotating mass, the rotor speed is forced to reduce. The generator eventually retains its normal operating condition following a few oscillations, otherwise, its speed continues to increase until it is tripped by appropriate protection devices. When this happens the generator terminals usually experience a sustained voltage dip. Investigation into this phenomenon [124-126] has revealed that there is a maximum time during which the fault needs to be cleared, otherwise the induction generator loses its stability. Such time will thereafter be referred to as the CCT for induction generators.

5.5.3 Effects of WPBEGs on the CCT of Faults

The dynamic effects of the integration of WPBEGs into distribution networks have been investigated for many years. A summary of the reported effects of such integration has been given in chapter 2. However, no attempt has been made to examine the performance of an induction generator following a fault condition on a load feeder. Consider the system shown in Fig. 5.3, whereby a three-phase fault is assumed on the load feeder at point F.

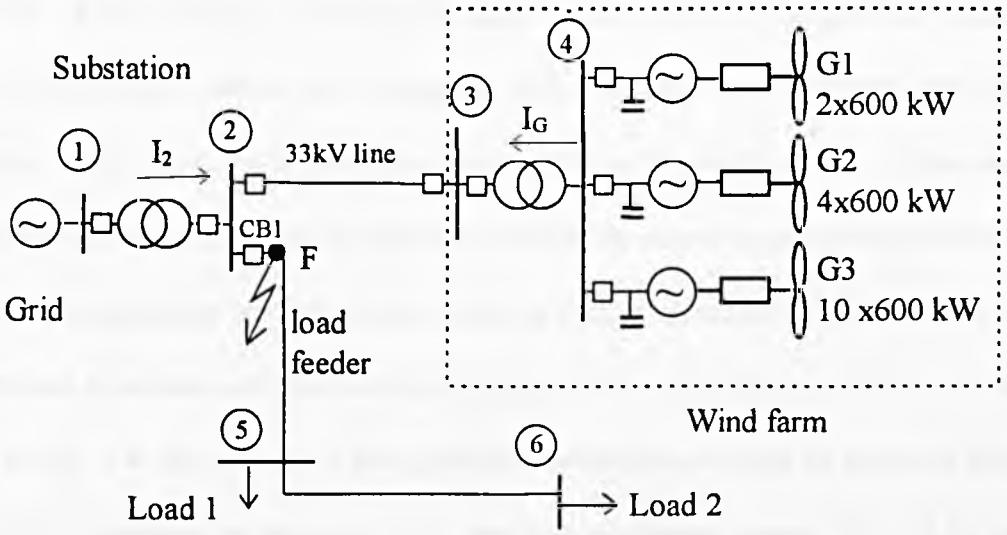

Fig. 5.3 A three-phase fault at point F on the load feeder of the network that includes a wind farm.

As previously explained in section 5.5.1, according to the basic principles of protection schemes of distribution feeders [16], the fault should be isolated by disconnecting only the faulted feeder. In other words, the fault described above should not cause the disconnection of other equipment from the network, including the wind farm. Therefore, protection relays upstream of the faulted feeder should initiate a trip signal that opens the circuit breaker CB1 and isolates the fault from the rest of the network before other equipment is tripped unnecessarily. However the operating time of these relays is usually co-ordinated with the operating time of other down stream relays on the feeder. As mentioned previously this can

make the tripping time to isolate the fault as high as 1.5s [9]. Such an operating time may exceed the CCT for an induction generator at the wind farm (see section 5.5.2.2), with the consequences described in the preceding section.

To further investigate this scenario, a three-phase fault with 180ms duration is assumed on the load feeder at location F. Fig.5.4 shows the variation of voltage of the terminals of induction generators at the wind farm, i.e. at the 690V bus-bar shown in Fig. 5.3, following the described fault condition. It can be seen from Fig.5.4 that, at the instance of fault, the magnitude of the voltage is dropped to approximately 25% of its pre-fault value. This value is simply the voltage drop along the link between the wind farm and the main substation, which is caused by the contribution of IGs to the fault current. As the voltage at the terminals of an IG drops at the instance of fault, the electro-magnetic field stored in the air-gap of the generator starts to reduce, causing further reduction of the terminal voltage. This process continues until the voltage becomes zero or the fault is cleared. In the case shown in Fig. 5.4, the voltage of the generator terminals continues to decrease during the fault until it becomes, at the time when the fault is cleared, about 10% of its pre-fault value. As the fault is cleared, the terminal voltage increases, but not to the pre-fault value. The reason for this is due to the high current drawn from the network by IGs in order to recover the electro-magnetic torque, causing a voltage drop along the link between bus 2 and bus 4. However it can be seen that in this case the voltage recovers to its pre-fault value approximately 1.5s after the isolation of the fault.

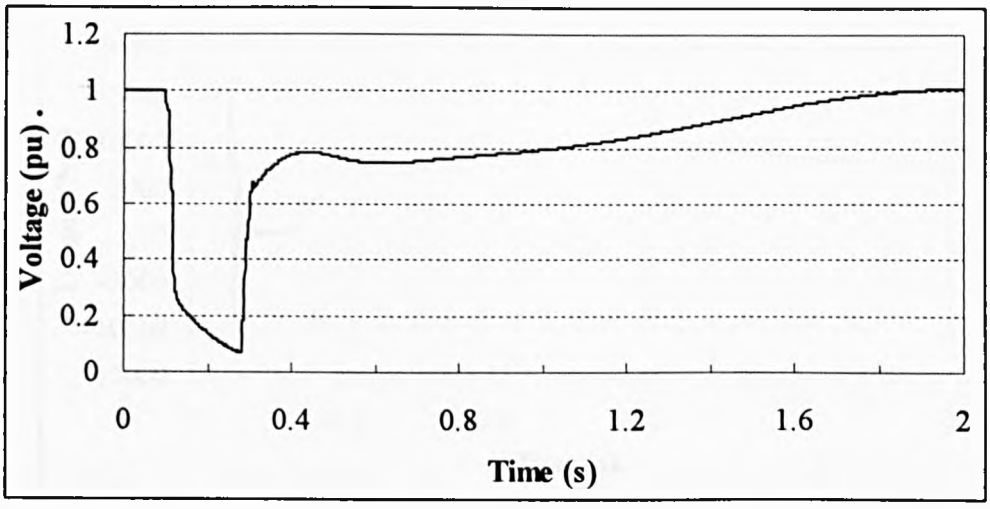

Fig. 5.4 Variation of terminal voltage of IGs at the wind farm due to a three-phase on the network with duration of 180ms.

According to Equation (5.3), the electromagnetic torque (T_e) developed inside an induction machine is proportional to the square of the terminal voltage; hence, T_e also reduces during the fault. However, when the fault is cleared and the voltage at the generator terminals recovers, the electromagnetic torque also recovers to its pre-fault value, provided that the machine remains stable (see section 5.5.2.2). Fig. 5.5 shows the variation of the electromagnetic torque inside the air gap of the 2x600 kW induction generators following the above fault condition. Based on Equation (5.4), such variation of torque leads to a variation in the rotor speed of the generator, as illustrated in Fig. 5.6. On the other hand, the recovery of the electromagnetic torque after the clearance of the fault normally requires a high current to be drawn from the network and Fig. 5.7 shows the variation of the total current of the wind farm during and following the fault under consideration. As can be seen in Fig. 5.7, following the removal of fault, the total current drawn from the network can be as much as twice the pre-fault steady state current. However, the pre-fault current is recovered approximately after 1.5s from the isolation of the fault. It can also be concluded from this investigation that the 180ms clearing time is less than the CCT of faults for the considered distribution network that ensures the stability of the connected wind farm.

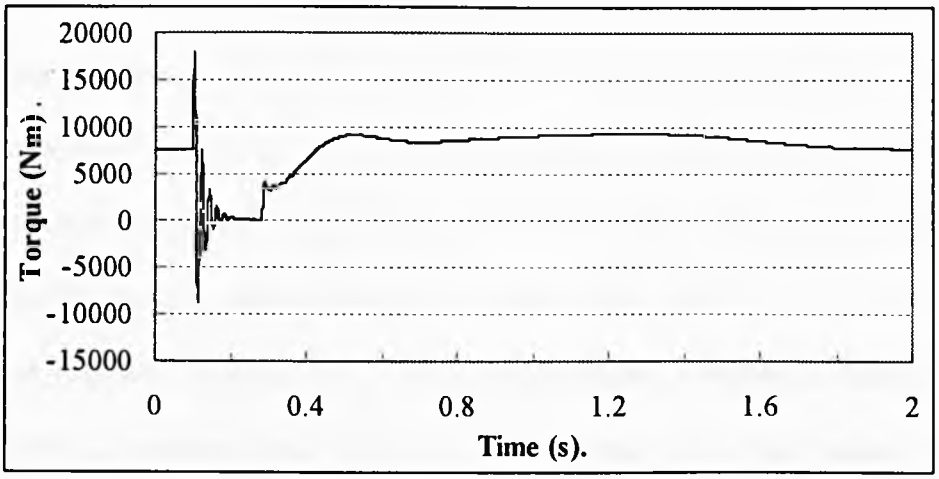

Fig. 5.5 Variation of electromagnetic torque inside the air gap of 2x600 kW IG due to a three-phase fault on the network with duration of 180ms.

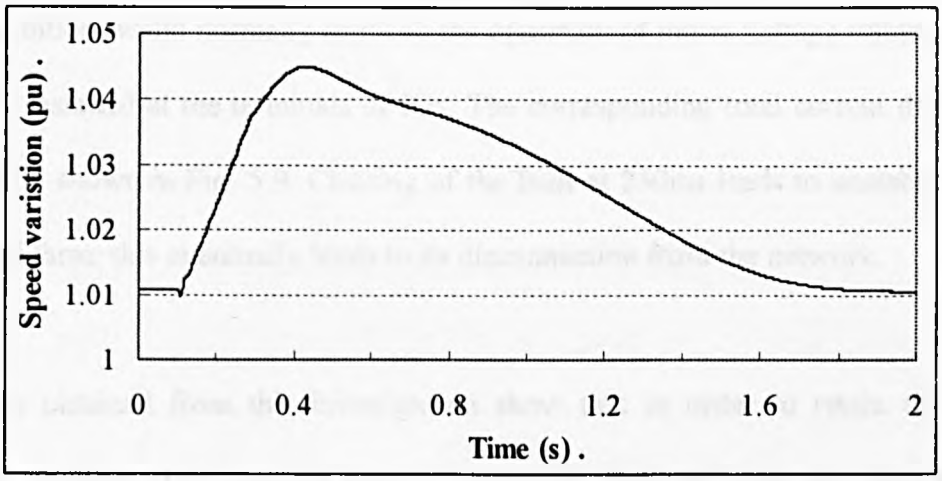

Fig. 5.6 Variation of rotor speed of the 2 x 600 kW IG due to a three-phase fault on the network with duration of 180ms.

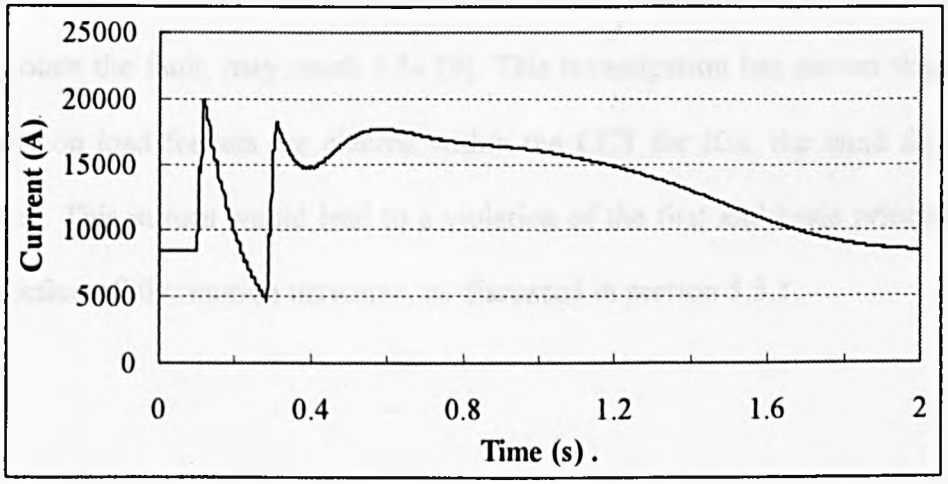

Fig. 5.7 Variation of the total current of the wind farm due to a three-phase fault on the network with duration of 180ms.

This investigation was repeated for different values of fault clearing time on the load feeder. It has been found that, for the system under consideration, IGs cannot retain their pre-fault operating conditions when the clearing time exceeds 200ms. Consequently, this time is considered as the CCT of the fault under consideration. This investigation has also shown that if the fault is cleared after a time greater than the CCT, the speed of the IGs continues to increase. Consequently, induction generators continue to draw high inrush currents from the network until they are disconnected. This high current can cause sustained voltage sag at the generator terminals. Fig. 5.8 shows the variation of such voltage due to a three-phase fault with duration of 250 ms. The terminal voltage of IGs does not regain its pre-fault value and remains below 0.8 pu (80%) of its nominal value. Such a condition would normally result in the operation of under voltage relays, which are commonly installed at the terminals of IGs. The corresponding total current drawn by the wind farm is shown in Fig. 5.9. Clearing of the fault at 250ms leads to unstable operation of the wind farm; this eventually leads to its disconnection from the network.

The results obtained from this investigation show that in order to retain the pre-fault operating conditions of the wind farm; it is vitally important that the fault should be isolated within 200ms. However, as has previously been explained, the operating time of protection relays at the source of the load feeder, which are expected to initiate a tripping signal to isolate the fault, may reach 1.5s [9]. This investigation has shown therefore that unless faults on load feeders are cleared within the CCT for IGs, the wind farm will be disconnected. This in turn would lead to a violation of the first and basic principle related to the protection of distribution networks, as discussed in section 5.5.1.

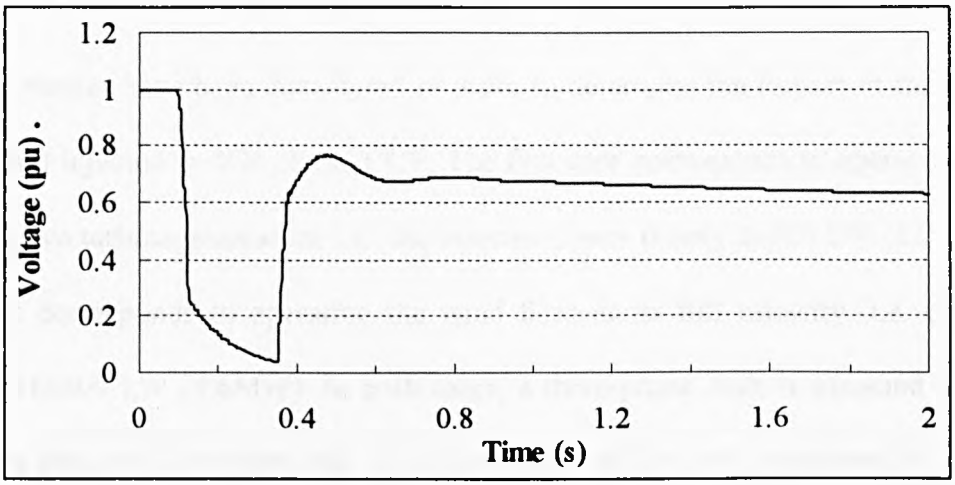

Fig. 5.8. Variation of terminal voltages of IGs at wind farm due to a three-phase fault on the network with duration of 250ms.

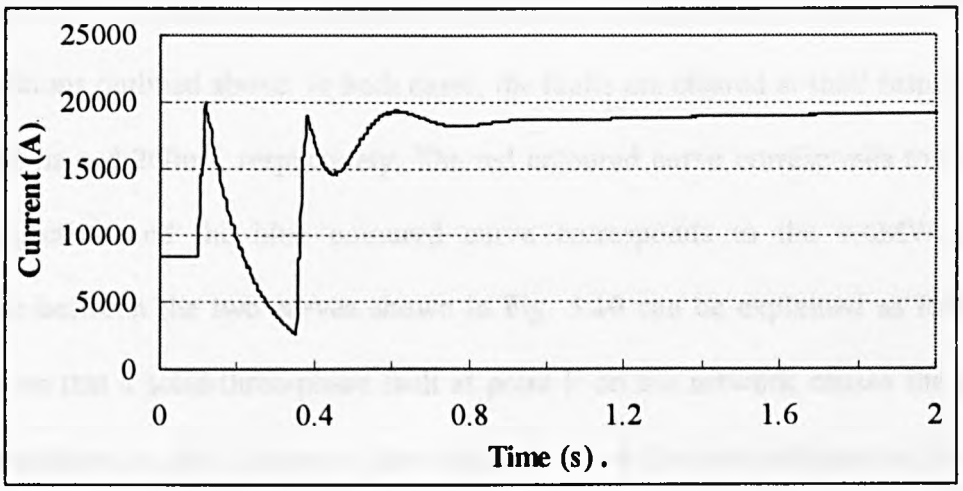

Fig. 5.9. Variation of the total current of wind farm due to a three-phase fault on the network with duration of 250ms.

5.5.4 The Impact of the Magnitude of Injected Power by IGs on the CCT

Two case studies have been considered in order to determine the impact of the magnitude of the power injected by IGs on the CCT. The first case corresponds to operating the wind farm with two turbine-generators, i.e., the injected power is only 2x600 kW (1.2 MW). The other case corresponds to operating the wind farm at its full capacity, i.e. the injected power is 16x600 kW (9.6MW). In both cases, a three-phase fault is assumed to occur at point F on the load feeder (see Fig. 5.3). Simulation of the fault is repeated in both cases for different clearing times of fault until the CCT for each case is obtained. It was found that the CCT for the first case was 580ms, whereas that for the second case was found to be 200ms. Fig. 5.10 shows the variation of post-fault voltage at bus 4 corresponding to the two conditions outlined above. In both cases, the faults are cleared at their respective CCT, i.e. at 580ms and 200ms, respectively. The red coloured curve corresponds to the 1.2MW power injection and the blue coloured curve corresponds to the 9.6MW case. The difference between the two curves shown in Fig. 5.10 can be explained as follows: It is well known that a solid-three-phase fault at point F on the network causes the voltage of bus 2 to collapse to zero. However, the voltage at bus 4 does not collapse to zero, because of the voltage drop along the link between bus 2 and bus 4, which is proportional to the current contribution by the wind farm during the fault condition which is in turn proportional to the machine size. For the case of 1.2MW IGs, the voltage of bus 4 falls to a value near to zero at the instance of fault. After that, it continues to reduce to zero during the fault. When the fault occurs in the case of 9.6MW IGs, the voltage drop along the link is high during the fault condition and consequently the voltage of bus 4 falls only to approximately 25% at the instant of fault.

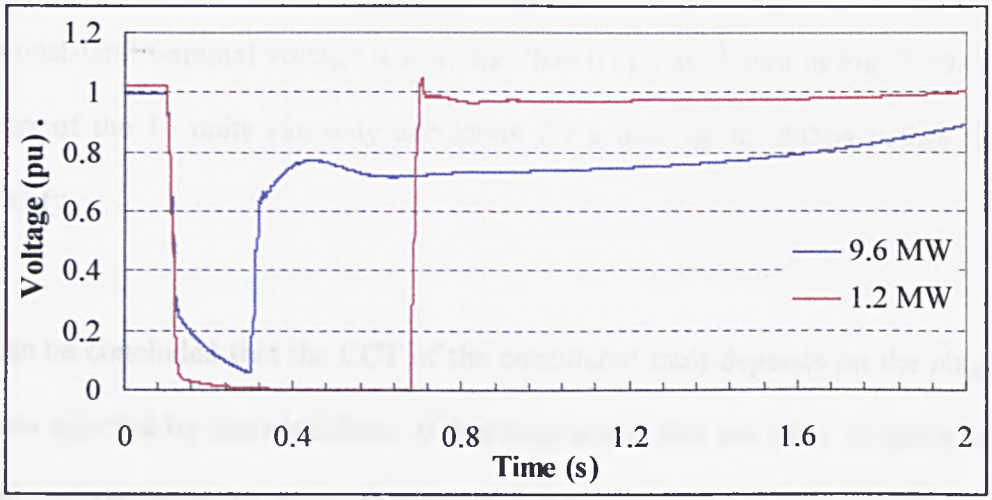

Fig. 5.10 The effect of power injected by wind farm on the CCT.

The difference in the CCT in the two cases is due two main factors. The first factor is that following the fault the rotating masses of IGs start to accelerate and additional kinetic energy is stored in its rotating mass, which appears in a form of mechanical torque on the rotating masses. The larger the number of wind turbine-generator units operating at the instance of the fault, the higher the stored total kinetic energy. To regain the pre-fault conditions, it is required to overcome the stored kinetic energy by an opposing electromagnetic energy in a form of electromagnetic torque acting on the rotating masses in such a way to decelerate them. The second factor has been briefly explained above, i.e. when the fault is cleared and the terminal voltages recover, IGs start to draw a high current from the network to re-establish the electromagnetic torque. However, the high current causes a voltage drop along the link between the main substation and the wind farm, consequently affecting the magnitude of the re-established electromagnetic torque. Therefore, in the case of 1.2MW, because the post fault voltage is high, the newly re-established electromagnetic torque is proportionally high. Hence, the rotors of the two units in this case are allowed to accelerate for a time up to 580ms, and yet the re-established electromagnetic torque is able overcome the mechanical torque due to the

stored kinetic energy and maintain their stability. On the other hand, in the case of 9.6MW, the post-fault terminal voltage is low, less than 0.8pu as shown in Fig. 7.10. Therefore, the rotors of the 16 units can only accelerate for a time up to 200ms before they lose their stability.

It can be concluded that the CCT of the considered fault depends on the magnitude of the power injected by the wind farm. It has been found that the CCT of faults with only two wind turbine-generator units are connected is 580ms, whereas that for all the sixteen units are assumed connected is 200ms. Therefore, for the wind farm under consideration, the corresponding CCT is expected to be between 200ms and 580ms depending on the number of IGs in service. This range is obviously below the previously mentioned time that is required for time graded protection relays to isolate the fault (1.5s). Consequently the likelihood of a wind farm losing its stability due to a three-phase fault on the load feeder is still high, regardless of the magnitude of the power injected.

5.5.5 Effect of the location of faults on the CCT

The distribution network shown in Fig. 5.3 is considered again in order to determine the effect of fault location on the CCT. A three-phase to ground fault is assumed to occur at three different locations on the load feeder. These are, at point F, i.e. 0km from bus 2, at half the distance between bus 2 and bus 5, which is 5km from bus 2, and at bus 5, which is 10km from bus 2. For each of these locations, the study is repeated for different values of power injection from the wind farm. It is observed that the corresponding CCTs are greatly affected by the location of fault on the load feeder. Fig. 5.11 summarises the results obtained from this investigation. This figure illustrates that as the distance of fault from the main substation increases, the CCT of the fault increases. For example, consider the

condition whereby the injected power by the wind farm is 1.2 MW. Fig. 5.11 shows that the CCT due to fault locations at 0km, 5km and 10km from bus 2 are 580ms, 700ms and 870ms, respectively. This means that the further the fault location from bus 2 is, the greater the CCT. This can be explained as follows: the further the fault from bus 2, the greater the impedance of the fault current path. Thus, the further the fault from bus 2, the greater the voltage at the terminals of IGs at the wind farm due to the high voltage drop in the circuit between fault location and the wind farm. This in turn leads to progressively higher electromagnetic torque as the fault location moves away from the wind farm, which helps in preventing the rotor of IGs from experiencing rapid acceleration. This obviously enables IGs to remain stable for longer during fault conditions, i.e. longer CCTs.

It is also observed from this study that the magnitude of the injected power by the wind farm has greater effect on the CCT when the fault occurs at a greater distance from the main substation. For example, for a fault at bus 2, the difference between the CCT in case of 1.2MW injection and that for the case of 9.6MW injection is 380ms (see Fig. 5.11). However, when the fault is assumed at bus 5, i.e. 10km away from bus 2, the difference between the CCT due to both cases is found 500ms.

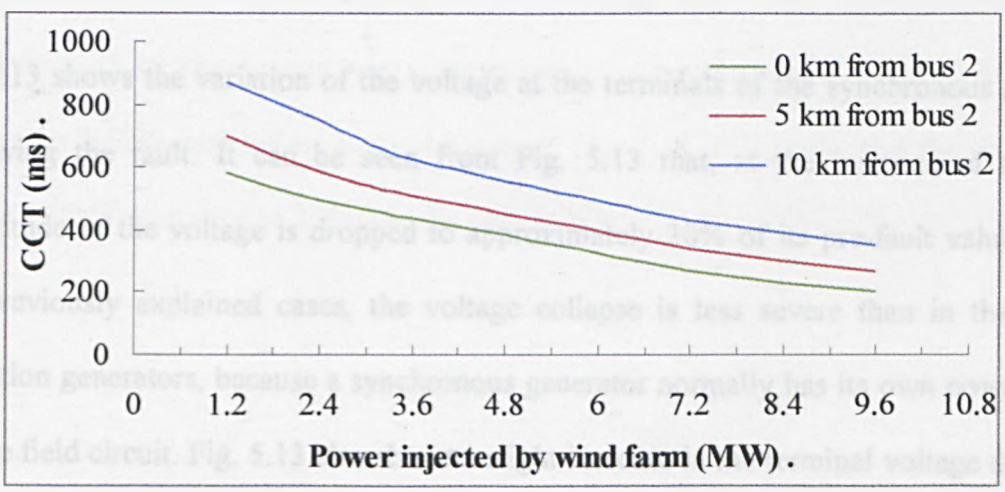

Fig. 5.11 The effect of location of fault on the CCT.

5.5.6 Effects of Embedded Synchronous Generators on the CCT

The idea behind this investigation is to compare the CCT of faults due to WPBEGs with that related to an embedded gas-turbine driven synchronous generator (SG). The network shown in Fig. 5.12 is similar to that shown in Fig. 5.3, except that the wind farm is replaced by a gas turbine-generator unit with power rating equal to the total ratings of the WPBEGs. To investigate the CCT of faults in this case, a three-phase to ground fault with 200ms duration is assumed on the load feeder at location F, as can be seen in Fig. 5.12.

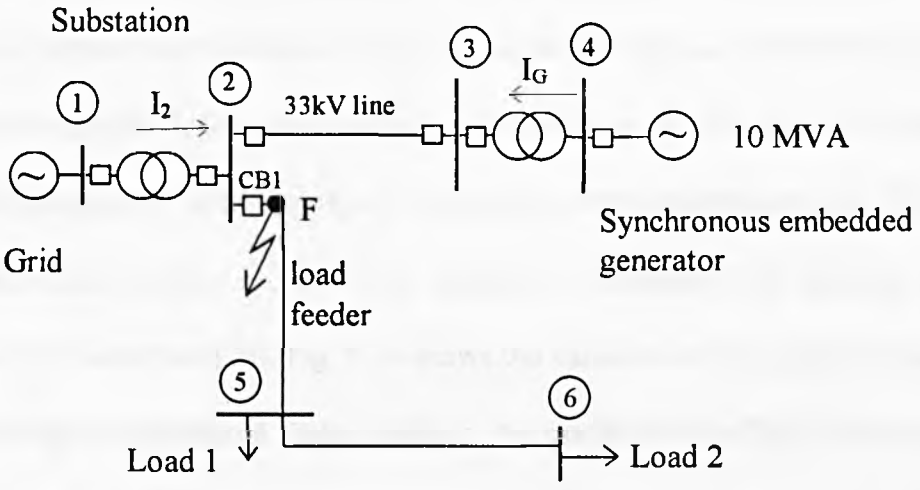

Fig. 5.12 A three-phase fault at point F on the load feeder of the network that includes a synchronous generator.

Fig.5.13 shows the variation of the voltage at the terminals of the synchronous generator following the fault. It can be seen from Fig. 5.13 that, at the instance of fault, the magnitude of the voltage is dropped to approximately 30% of its pre-fault value. Unlike the previously explained cases, the voltage collapse is less severe than in the case of induction generators, because a synchronous generator normally has its own power supply for the field circuit. Fig. 5.13 also shows a slight increase in the terminal voltage during the fault. This is due to the action of the excitation control circuit, which controls the voltage magnitude at the generator terminals. In this case, the excitation control increases the field

current to increase the voltage at the terminals of the generator.

After the fault is cleared, the voltage at the generator terminals recovers. However, its magnitude overshoots its pre-fault value due to the action of excitation control. The voltage then decays to the pre-fault value after a period of oscillation. As previously explained in section 5.5.2.1, one of the parameters used when investigating the performance of SG is the angular position, δ, of the rotor with respect to the Grid voltage. According to Equation (5.1), when a fault occurs on the network, the rotor of the SG starts accelerating and the angular position of the rotor with respect to the Grid reference voltage starts to change. The variation of δ versus time following a fault can be used to indicate whether the SG remains stable or not after the clearance of the fault. This variation can be obtained by solving the differential equation (5.1) for the angle δ. In the case under investigation, the SG retains its stability after the isolation of fault. The solution of Equation (5.1) leads to sinusoidal oscillations of δ with time [79]. Fig. 5.14 shows the variation of the angular position of the rotor following the considered fault condition. As can be seen in Fig. 5.14, the pre-fault value of δ is 40°. This value starts to increase following the application of the fault. However δ continues to increase even after the fault is cleared due to the surplus kinetic energy, which the rotor gains during the fault, until δ reaches 50°. After that, the angle δ oscillates with an exponentially decaying envelope versus time until it regains its pre-fault or another steady-state value, as can be seen in Fig. 5.14. It is found that the CCT in this case is 360ms compared to 200ms in the case of IGs.

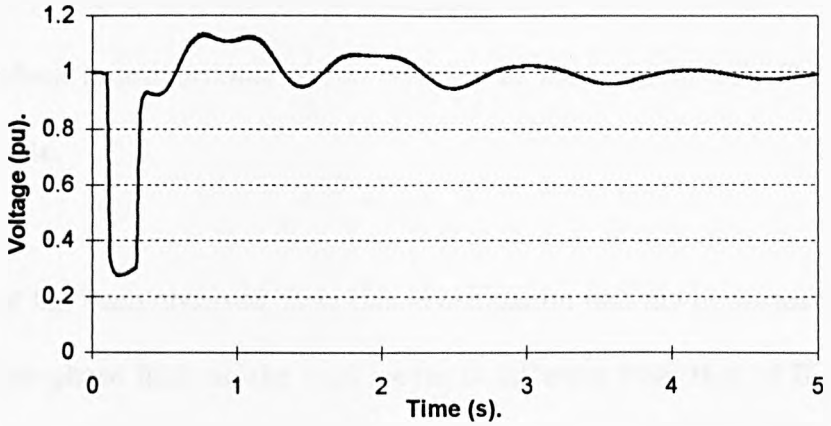

Fig.5.13 Variation of the terminal voltage of synchronous generator following a three-phase, 200ms duration fault on the network.

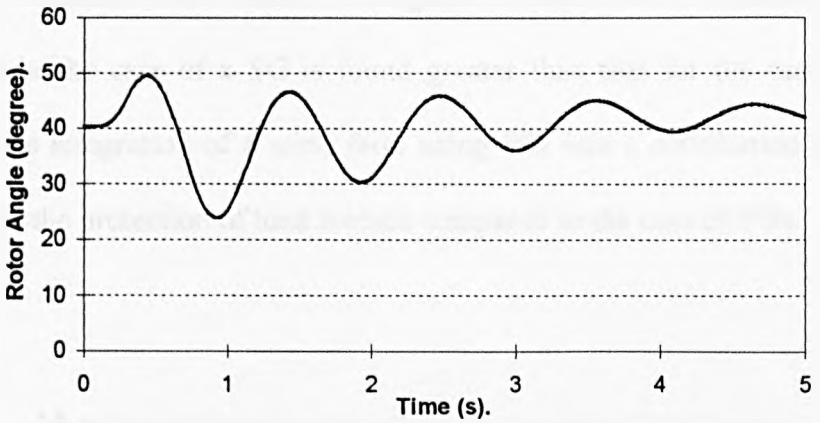

Fig.5.14 Variation of rotor angle of synchronous generator following a three-phase, 200ms duration fault on the network.

This investigation was repeated for different values of fault clearing time. It has been observed that for the considered fault condition, the SG cannot maintain its stability when the clearing time becomes slightly greater than 360ms. Thus, this time is considered as the CCT of the fault under consideration. It has also been found that if the fault is cleared at time greater than the CCT, the speed of the SG continues to increase and consequently, the angular position of the rotor with respect to the network continues to increase and the SG eventually loses synchronism with the network. Fig. 5.15 and 5.16 show the variation of the terminal voltage of the generator and its corresponding rotor angle following a three-phase fault with duration of 400ms. It can be seen from Fig. 5.16 that the rotor angle continues to increase. The oscillation of the terminal voltage during post fault period that

can be observed in Fig. 5.15 is due to the oscillation of the power transfer between SG and the network, which is proportional to the position of the rotor of SG. This condition is obviously unstable.

In conclusion, it has been observed from this investigation that the performance of the SG, following a three-phase fault on the load feeder is different from that of IGs at the wind farm, discussed in the previous section. It has also been found that the CCT of faults in this case is mainly decided by the variation of the rotor angle, whereas, that related to IGs is decided by the variation of the terminal voltages of the IGs. The CCT for the investigated fault condition in the case of a SG is found greater than that for the case of IGs. This indicates that the integration of a wind farm using IGs into a distribution network has a greater effect on the protection of load feeders compared to the case of SGs.

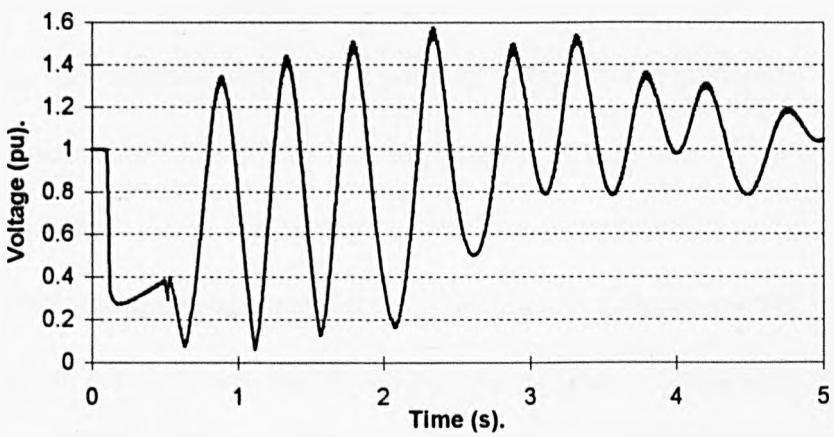

Fig.5.15 Variation of terminal voltages of SG following a three-phase, 400ms duration fault on the network.

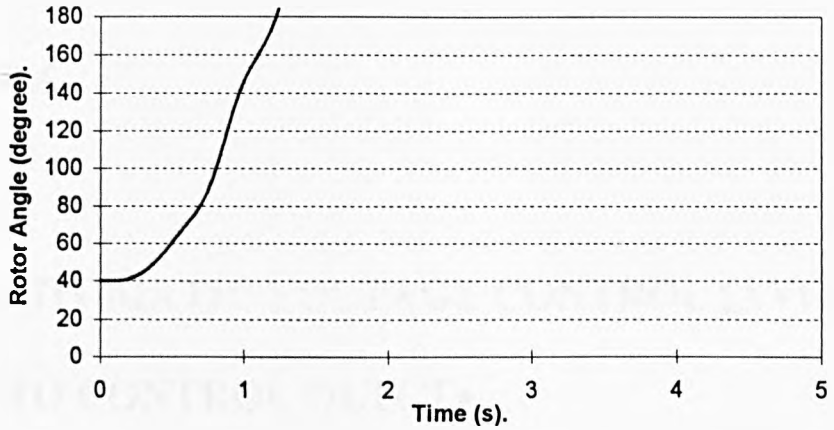

Fig.5.16. Variation of rotor angle of SG following a three-phase, 400ms duration fault on the network.

CHAPTER 6

USE OF AUTOMATIC VOLTAGE CONTROL (AVC) RELAYS TO CONTROL OLTCTs

6.1 Introduction

An explained previously in chapter 4, voltage regulation of distribution networks can be achieved either by the injection of reactive power or by changing voltage-ratios of transformers. The second method is the most popular and widespread form of voltage regulation, whereby voltage control is achieved directly using tap-changing devices that switch in or out the required number of winding turns of a transformer to regulate the voltage. Automatic voltage control (AVC) without the interruption of the power supply is usually achieved using AVC relays that automatically control the operation of the tap changer of on-load-tap-changing transformers (OLTCT). In order to control the voltage of a certain point on the network, conventional AVC relays have compounding settings, which can be in a form of impedance (a resistance and either a positive reactance or a negative reactance). The compounding is used to compensate for the voltage drop in the distribution lines that link the transformer terminals to the remote points on the network [16,100]. In the case of two or more transformers operated in parallel, compounding with negative reactance is recommended to ensure stable operation of the tap-changers [19]. AVC relays with a compounding setting operate properly for passive distribution networks, i.e. when power flows only in one direction from the grid to consumer's loads. However, when embedded

generators are integrated into a distribution network, the power flow through the main distribution transformers can be either from the grid to a distribution network, or in the opposite direction, and AVC relays therefore may not operate correctly and may affect the proper operation of the tap-changers of parallel transformers [3, 17]. This is because conventional AVC relays with compounding settings are sensitive to the direction of power flow in the controlled transformers. In order to overcome the problems related to the operation of parallel transformers, an adaptive AVC relay was developed by Fan Jiang [17]. This relay was not designed to compensate for the voltage drop in load feeders however and in the work reported in this thesis, an attempt is made to design an AVC relay based on the application of artificial neural networks (ANN) which will compensate for the voltage drop along load feeders. In this chapter, the behaviour of conventional AVC relays as applied to a network with embedded generators is discussed. Then, in chapter 7, the proposed ANN based AVC relays is presented and discussed.

6.2 Voltage Control of single OLTCTs Using AVC Relays

6.2.1 The Principle of Conventional AVC Relays

An AVC relay is usually connected to the low voltage side of a main distribution transformer, and arranged to operate the tap changer, which is commonly installed at the high voltage side of the transformer as mentioned in Chapter 4. The operating principle of an AVC relay is illustrated by the schematic diagram shown in Fig. 6.1 [16,19,100]. The AVC relay is capable of maintaining system voltage within a bandwidth around a target voltage, V_{target}, for any load condition.

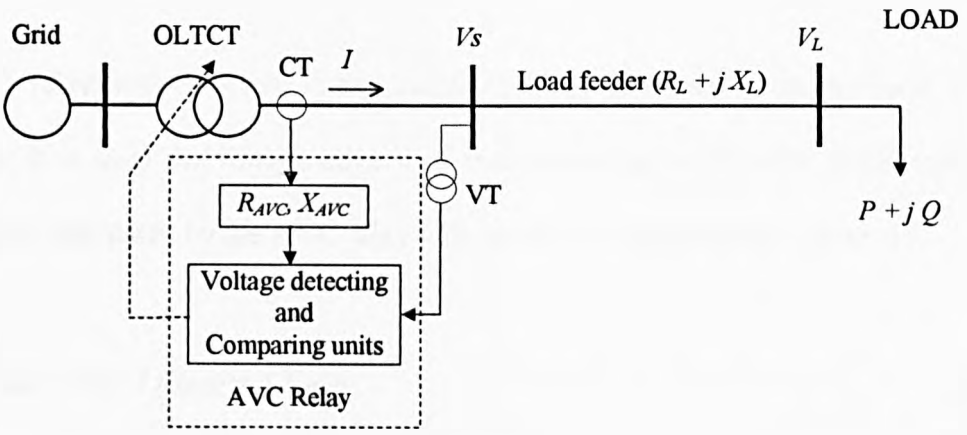

Fig. 6.1 Schematic diagram of an AVC relay

As can be seen in Fig. 6.1, the AVC relay is supplied by the secondary side voltage of the transformer using a measuring voltage transformer (VT). It is also supplied by the current at the secondary side of the transformer using a current transformer, CT. A voltage-detecting unit then calculates the controlled voltage of the AVC relay using the following equation:

$$V_{AVC} = V_s - I\,(R_{AVC} \pm j\,X_{AVC}) \tag{6.1}$$

where V_{AVC} is the voltage determined by the AVC relay, i.e. the AVC relay voltage, V_s is the secondary side voltage of the transformer, I is the current at the secondary side of the transformer, and $R_{AVC} \pm j\,X_{AVC}$ is the relay compounding setting, which consists of a positive resistance, R_{AVC}, and either a positive reactance or a negative reactance, X_{AVC}.

The AVC relay voltage is compared with the upper and lower limits of a control bandwidth. Whenever the voltage falls outside these limits for a time longer than a pre-set time delay, the relay initiates a signal to operate the tap changer of the transformer to correct the voltage to be within the specified limits.

6.2.2 AVC Relays Using Positive Compounding Settings

An AVC relay with positive compounding settings employs a resistor and a positive reactance. It is used for voltage control of distribution networks with single transformers. The voltage calculated by the AVC relay with positive compounding is given by:

$$V_{AVC} = V_s - I\,(R_{AVC} + j\,X_{AVC}) \tag{6.2}$$

The term subtracted from V_s on the right hand side of Equation (6.2) is used for the compensation of the voltage drop across the load feeder (see Fig. 6.1). This is achieved by settings R_{AVC} and X_{AVC} equal to the values R_L *and* X_L, respectively. In this case, the controlled voltage V_{AVC} will be equal to the voltage of the load busbar, V_L, as demonstrated in the phasor diagrams of Fig. 6.2.

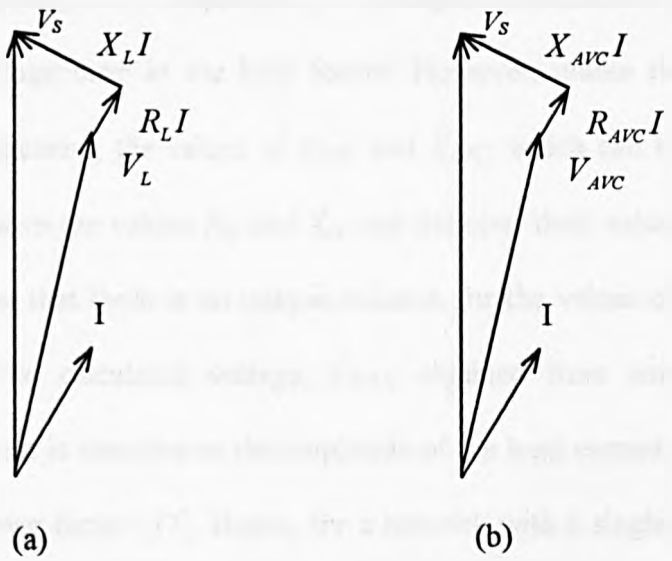

Fig. 6.2 (a) Phasor diagrams of the network in Fig. 6.1
(b) Phasor diagram of AVC relay with positive compounding settings

The advantages of this arrangement are that the compounding settings are very easy to choose, the calculated voltage directly accounts for the voltage drop across the load feeder, and the control is not affected by the power factor of the load. However, this arrangement is not suitable for parallel transformers, as the calculated voltage in this case is affected by circulating currents that may exist [3].

6.2.3 AVC Relays Using Negative Compounding Settings

An AVC relay with negative compounding settings employs a resistor and a negative reactance. The voltage determined by the AVC relay is given by:

$$V_{AVC} = V_s - I\,(R_{AVC} - j\,X_{AVC}) \tag{6.3}$$

The phasor diagram of Fig. 6.3 depicts the vectors of V_{AVC} using the negative compounding settings. As can be seen in Fig. 6.3, compounding with negative reactance can also be used to compensate for the voltage drop in the load feeder. However, unlike the case with the positive reactance arrangement, the values of R_{AVC} and X_{AVC}, which can be used to obtain $V_{AVC} = V_L$, are not equal to the values R_L *and* X_L, and defining their values involves some difficulty. It is also clear that there is no unique solution for the values of R_{AVC} and X_{AVC}, which can be used. The calculated voltage, V_{AVC}, obtained from using the negative compounding arrangement is sensitive to the amplitude of the load current, I [19], it is also sensitive to the load power factor [17]. Hence, for a network with a single transformer, the negative compounding arrangement offers no advantage over the positive compounding arrangement in compensating voltage drop in lines. However, it will be shown later that the negative compounding arrangement offers one of the cheapest solutions for having a stable operation of parallel transformers.

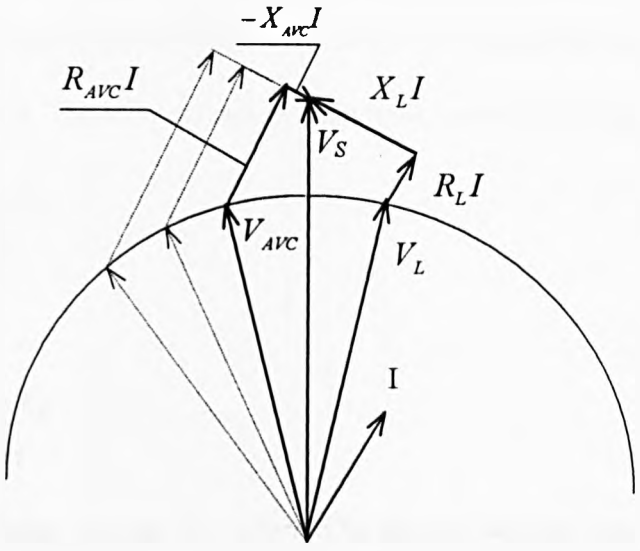

Fig. 6.3 Phasor diagrams of the network in Fig. 6.1 and AVC relay with negative compounding settings

6.3 Voltage Control of Parallel OLTCTs Using AVC Relays

6.3.1 Circulating Currents induced in Parallel OLTCTs

When two or more transformers are considered to operate in parallel, particular attention must be paid to ensure that the transformers have the same p.u. impedance as expressed based on their ratings [100]. This should ensure that transformers share the total load proportional to their ratings. They also need to have equal transformation ratios. This requirement is very important to avoid undesirable circulating currents between transformers. Unfortunately this is not always possible to achieve in practice. The reason is that transformers may have different numbers of taps resulting in different transformation ratios. Even when the number of taps is equal, there are conditions when parallel transformers operate at different tap positions, resulting in different transformation ratios.

Consequently, circulating currents are set up between transformers. Consider the case of two transformers operating in parallel and assume that a circulating current flows between them, as shown in Fig. 6.4. The total current of each transformer under this condition is given by:

$$I_{T1} = \frac{E_1 - V_S}{Z_{T1}} \tag{6.4}$$

and

$$I_{T2} = \frac{E_2 - V_S}{Z_{T2}} \tag{6.5}$$

where E_1 is the busbar voltage V_H referred to the low voltage side using the transformation ratios of OLTCT 1 and Z_{T1} is the impedance of OLTCT 1. E_2 and Z_{T2} are the corresponding values for OLTCT 2.

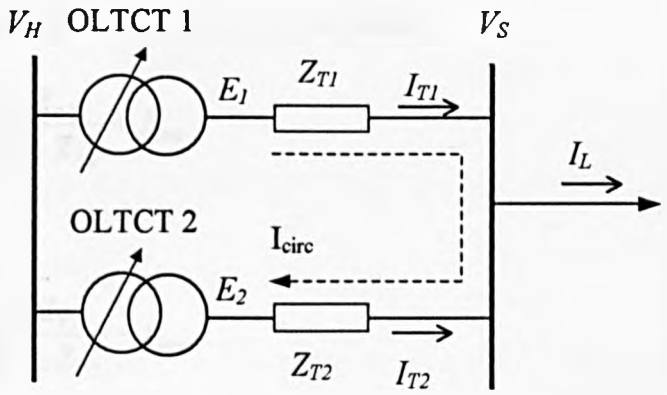

Fig. 6.4 Current distribution in two parallel transformers

Applying the superposition theorem, currents I_{T1} and I_{T2} can be decomposed into two components, i.e. a load current component and a circulating current component. The load current component is the portion of the total load current I_L that flows though each transformer which is decided by the impedances of the transformers. The circulating current component is proportional to the voltage difference between the secondary voltages of the

two transformers. This in turn depends on the difference between the transformation ratios of the two transformers. Assume the ratio of OLTCT1 is lower than that of OLTCT2. This results in E_1 becoming greater than E_2, which causes a circulating current flowing from OLTCT1 to OLTCT2 as shown in Fig. 6.4. As can be seen in this figure, the circulating current through OLTCT1 flows in the same direction as the load current component, whereas, in OLTCT2 it flows in the opposite direction of its own load current component. Thus, currents in the parallel transformers can be written as:

$$I_{T1} = \frac{I_L Z_{T2}}{Z_{T1} + Z_{T2}} + I_{circ} \tag{6.6}$$

and

$$I_{T2} = \frac{I_L Z_{T1}}{Z_{T1} + Z_{T2}} - I_{circ} \tag{6.7}$$

Substituting (6.4) in (6.6) and (6.5) in (6.7), we obtain:

$$\frac{E_1 - V_S}{Z_{T1}} = \frac{I_L Z_{T2}}{Z_{T1} + Z_{T2}} + I_{circ} \tag{6.8}$$

and

$$\frac{E_2 - V_S}{Z_{T2}} = \frac{I_L Z_{T1}}{Z_{T1} + Z_{T2}} - I_{circ} \tag{6.9}$$

From (6.8) and (6.9), the circulation current can be given as:

$$I_{circ} = \frac{E_1 - E_2}{Z_{T1} + Z_{T2}}$$

or

$$I_{circ} = \frac{V_H \left(\frac{1}{a_{t1}} - \frac{1}{a_{t2}} \right)}{Z_{T1} + Z_{T2}} \tag{6.10}$$

where a_{t1} and a_{t2} are the transformation ratios of OLTCT1 and OLTCT2, respectively.

It is worth noting that because the reactance of each of the two transformers is much larger than its resistance, the circulating current lags behind the voltage V_H by approximately 90°. Fig. 6.5 depicts the phase relation between the currents and voltages of the circuit shown in Fig. 6.4. The circulating current I_{circ} has a significant effect on the behaviour of AVC relays, as will be explained in the next sections.

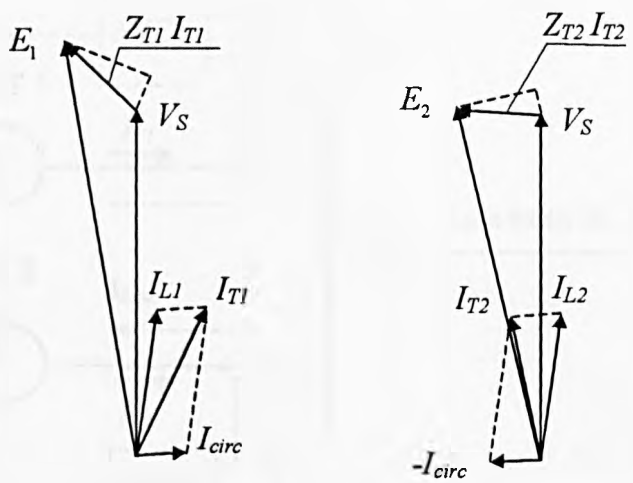

Fig. 6.5 Phasor diagrams of circulating currents in parallel transformers

6.3.2 AVC Relays with Positive Compounding Settings for Parallel Transformers

Fig. 6.6 shows an example of a substation represented by two parallel transformers and a feeder connecting the substation to a variable load. Let us assume that both transformers have the same rating, and both are at the k^{th} tap position. Assume also that both transformers are equipped with an AVC relay with positive compounding, which is set to compensate for the voltage drop along the feeder. The measured voltages of these relays are expressed as follows:

$$V_{AVC1} = V_S - \frac{I_L}{2} Z_{AVC}$$

and

$$V_{AVC2} = V_S - \frac{I_L}{2} Z_{AVC}$$

where $Z_{AVC} = R_{AVC} + \mathrm{j}\, X_{AVC}$ and $R_{AVC} = R_L$ and $X_{AVC} = X_L$.

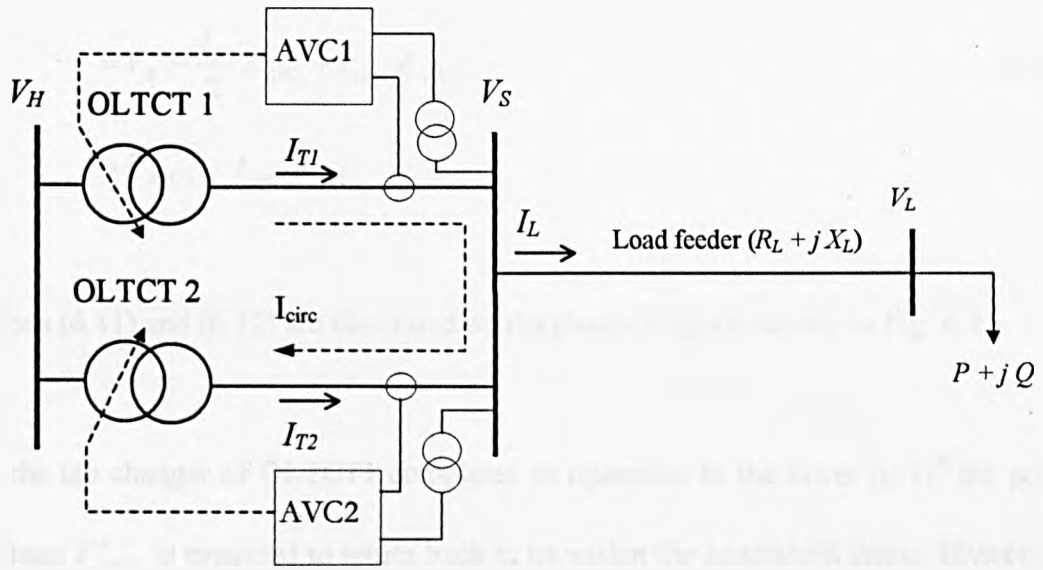

Figure 6.6 Schematic diagram of a distribution network with two parallel transformers

Consider the situation when the measured voltages of the two AVC relays fall below the lower limit of the control bandwidth. Owing to equipment tolerances, one of the transformers may operate to step down its tap changer to a new tap position before the other. Stepping down the tap changer reduces the number of turns of transformer's primary winding, and consequently reduces its transformation ratio (see Appendix D for more details). Let us assume that OLTCT1 operates first, then circulating current flows in the direction shown in Fig. 6.6. The measured voltages of the AVC relays following the operation of the tap changer of OLTCT1 are given by:

$$V_{AVC1}^{k-1} = V_S - \left(\frac{I_L}{2} + I_{circ}\right) Z_{AVC}$$

$$= V_S - \frac{I_L}{2} Z_{AVC} - I_{circ}\, Z_{AVC} \qquad (6.11)$$

$$= V_{AVC1} - I_{circ}\, Z_{AVC}$$

and

$$V_{AVC2}^{k} = V_S - \left(\frac{I_L}{2} - I_{circ}\right) Z_{AVC}$$

$$= V_S - \frac{I_L}{2} Z_{AVC} + I_{circ}\, Z_{AVC} \qquad (6.12)$$

$$= V_{AVC2} + I_{circ}\, Z_{AVC}$$

Equations (6.11) and (6.12) are illustrated by the phasor diagram shown in Fig. 6.7.

When the tap changer of OLTCT1 completes its operation to the lower (k-1)th tap position, the voltage V_{AVC1}^{k-1} is expected to return back to be within the bandwidth limits. However, due to the effect of circulating current, this voltage decreases further down, as can be seen in Fig. 6.7. At the same time, the other voltage V_{AVC2}^{k} increases to a value beyond the upper limit of the controlled bandwidth. In the situation just described, one tap changer continues tapping down towards the lowest tap position, whereas, the other tap changer continues tapping towards the highest tap position. In other words, the tap changers of the two transformers are diverting instead of converging and consequently, proper voltage control can not be achieved.

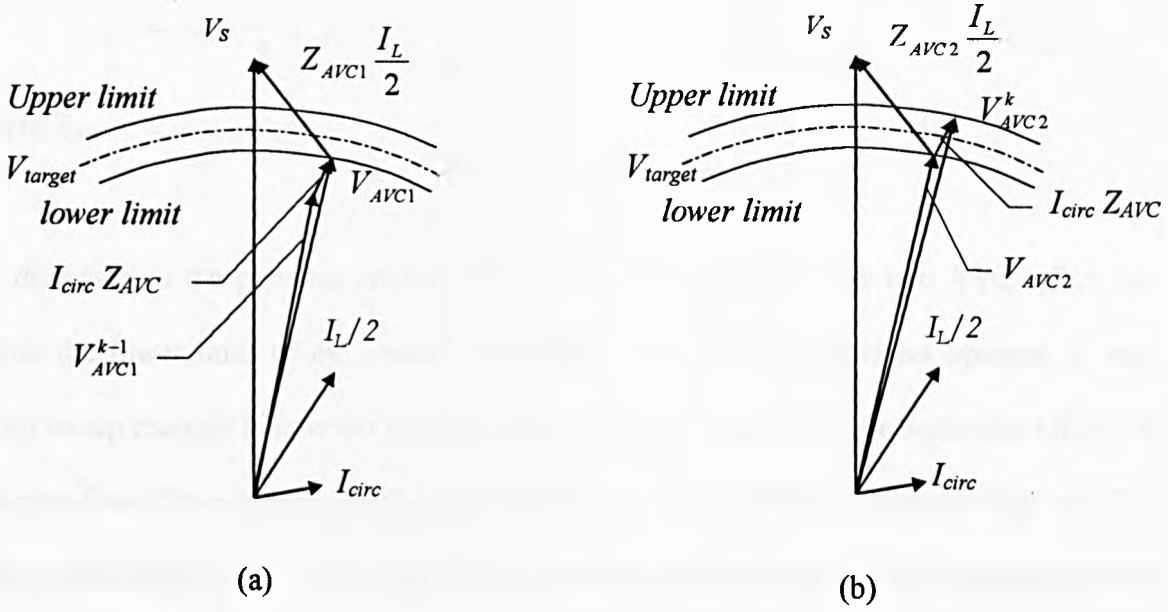

Fig. 6.7 Voltage control of two parallel transformers using positive compounding setting
(a) Phasor diagrams of AVC relay 1 (first to operate)
(b) Phasor diagram of AVC relay 2 (second to operate)

6.3.3 AVC Relays with Negative Compounding Settings for Parallel Transformers

A practical and economical solution to the problem of tap changer divergence of parallel transformers can be achieved using AVC relays with negative compounding settings. Consider the network depicted in Fig. 6.6 again. This time however let us assume that each transformer is equipped with an AVC relay with negative compounding setting to compensate for the voltage drop along the line. The measured voltages of these relays are then expressed as follows:

$$V_{AVC1} = V_S - \frac{I_L}{2} Z_{AVC} \tag{6.13}$$

and

$$V_{AVC2} = V_S - \frac{I_L}{2} Z_{AVC} \tag{6.14}$$

where $Z_{AVC} = R_{AVC} - j X_{AVC}$

As discussed in the previous section, if the measured voltages of the two AVC relays fall below the lower limit of the control bandwidth, one of the transformers operates to step down its tap changer to new tap position before the other. Let us assume again that OLTCT1 operates first. The resulting circulating current flows in the direction shown in Fig. 6.6. The measured voltage of the AVC relays of the two transformers following the operation of the tap changer of OLTCT1 are given by:

$$V_{AVC1}^{k-1} = V_S - \left(\frac{I_L}{2} + I_{circ} \right) Z_{AVC} \tag{6.15}$$

$$= V_{AVC1} - I_{circ} Z_{AVC}$$

and

$$V_{AVC2}^{k} = V_S - \left(\frac{I_L}{2} - I_{circ} \right) Z_{AVC} \tag{6.16}$$

$$= V_{AVC2} + I_{circ} Z_{AVC}$$

where $Z_{AVC} = R_{AVC} - j X_{AVC}$

The phasor diagrams shown in Fig. 6.8 illustrate the effect of circulating current on the calculated control voltages of both relays.

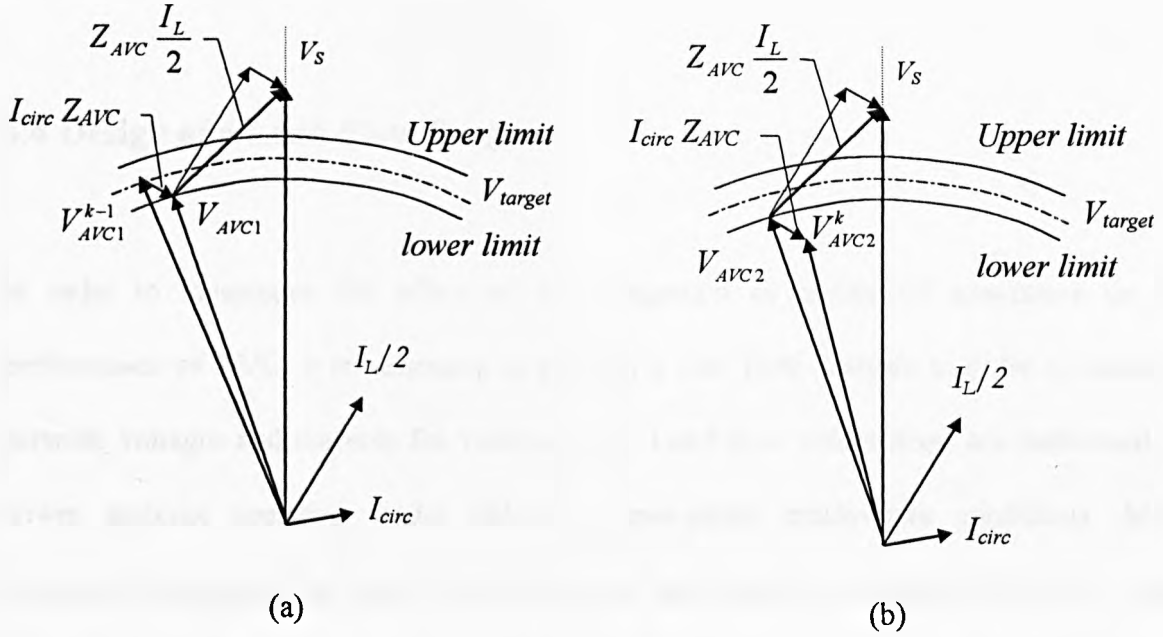

Fig. 6.8 Voltage control of two parallel transformers using negative compounding settings
(a) Phasor diagrams of AVC relay 1 (first to operate)
(b) Phasor diagram of AVC relay 2 (second to operate)

When the tap changer of OLTCT1 operates to the $(k\text{-}1)^{th}$ tap position, the relay 1 voltage V_{AVC1}^{k-1} increases due to effect of circulating current, as can be seen in Fig. 6.8. At the same time, it can be seen from the same figure that the voltage of the other relay, V_{AVC2}^{k}, decreases and consequently, the tap changer of OLTCT 2 is also forced to step down to a correct position. Thus the two transformers follow each other, resulting in a stable voltage control operation. Compounding with negative reactance therefore has two functions; firstly to compensate for the voltage drop along the distribution lines, and secondly, to compensate for the effects of circulating currents in parallel transformers. However, as mentioned before, the negative compounding arrangement is sensitive to the magnitude and phase angle of the measured currents. Therefore, when this arrangement is implemented, it is assumed that the load power factor does not change appreciably. The relay settings are therefore commonly set to small values to minimise the error that can be induced due to the variation of the

measured currents [18,19]. Consequently, a complete compensation for voltage drop in feeders may not always be achieved.

6.4 Design of a Load Flow Program

In order to investigate the effect of the integration of embedded generators on the performance of AVC, it is necessary to perform a load flow analysis in order to calculate network voltages and currents for various loads. Load flow calculations are performed on power systems operating under balanced three-phase steady-state conditions. Many commercial programs for load flow calculation are available nowadays. However, these programs perform the calculation under fixed system loading conditions. To investigate the operation of an AVC relay, it is necessary to have a program which can automatically perform load flow calculation for various loading conditions. It is also necessary to have a program to which the models representing AVC relays can be linked, thus allowing appropriate tap-changing of OLTCTs to be achieved as the system load changes. In this project, a load flow program is written in FORTRAN 77 using the Newton-Raphson method. The basic formulation of this method is described in Appendix (A). The program is designed to calculate bus-bar voltages and branch currents, as well as power flows and power losses in the network branches. The program is linked with AVC relay models that can be implemented for any OLTCT in the network. The tap-changing process of the OLTCT is represented in the load flow program as an equivalent circuit, whose parameters are dependent on the transformation ratio of the OLTCT under consideration. The details of the representation of an OLTCT in the load flow program are given in Appendix (D). Input data, including the network topology, bus data, branch data, and AVC relays settings are presented to the load flow program during the execution of the program. Such data is obtained from a separate input-data file, which can easily be prepared using a file editor. System loads are

represented in the program by their real and reactive power values P and Q respectively, both of which are variable. The following operations are executed every time the load changes:

a) Steady-state currents and voltages of the network are calculated using the Newton-Raphson algorithm.

b) Whenever the voltage of the AVC relays exceed the limits of a specified bandwidth, the transformation ratio of the involved transformer is adjusted to represent the tap-changing operation.

c) Results of calculations are saved in different output files. One of the files provides data for graphical presentation of the results. Another file stores the result in a table form to be used as inputs for the training of the neural network based AVC relay, as will be explained later in Chapter 7.

Table 6.1 shows an example of the content of the input data file for a network with seven buses and six branches.

Table 6.1 A list of a load flow input data file

C----------

C---------- Load flow data file ----------

C Base MVA

100.00

C number of buses, branches, and voltage controlled buses

7 6 0

C Bus data

C PV buses

C No	P (MW)	Q (MVAR)	Q_{max} (MVAR)	Q_{min} (MVAR)	$V_{nominal}$ (kV)
1	2.0000	1.0000	1.000	0.0000	33.0000

C PQ buses

C No	P (MW)	Q(MVAR)	G_{shunt} (pu)	B_{shunt} (pu)	$V_{nominal}$ (kV)
2	.0000	.0000	0.0	0.0	33.0000
3	.0000	.000	0.0	0.0	11.0000
4	.0001	.000	0.0	0.0	11.0000
5	.0001	.000	0.0	0.0	0.6900
6	.0000	.000	0.0	0.0	11.0000
7	.0001	.000	0.0	0.0	0.4000

C Branch data

C	from	to	R(pu)	X(pu)	B(pu)	(0.0 for lines, per unit ratio for transformers)
1	1	2	.0218	0.2212	.0000	.000
2	2	3	.0000	1.000	.0000	1.00
3	3	4	1.5290	2.6780	.0000	.000
4	4	5	.0000	1.0000	.0000	1.00
5	3	6	0.7645	1.339	.0000	.000
6	6	7	.0000	1.0000	.0000	0.97

C Relay compounding settings

(R_{AVC}, X_{AVC})

(2.0, -1.0)

C Voltage control limits

C Upper, Lower

1.02, 0.98

C incremental load used to change the load at any desired busbar

C ΔP (MW), ΔQ (MVAR)

0.0005, 0.00024216

6.5 The effect of Integration of Wind Power Based Embedded Generators on the Performance of AVC relays

Consider the distribution network shown in Figure 6.9. It comprises a substation, which is represented by two parallel OLTCTs, and two distribution feeders. One of the feeders is connecting a load busbar to the substation while the other is connecting the substation to a wind farm. Busbars are identified by a number from one to seven, as shown in Fig. 6.9. The nominal voltage of each busbar is also shown in brackets beside each bus number. Therefore, busbars will be referred to in future discussions by their numbers. The voltage of each bus will also be referred to by its number. For example, the voltage of bus 1 will be referred to as V(1), and so on. The tap-changers of the two OLTCTs at the substation are controlled by individual AVC relays, AVC1 and AVC2. In order to maintain the network voltages within the statutory limits, it is assumed that the voltage of bus 6 is required to be controlled within a bandwidth of $\pm 2\%$ of its nominal value.

The performance of the AVC relays is investigated using the previously described load flow program for cases when the wind farm is either connected or disconnected from the network. For the purpose of this investigation, the power factor of the variable load at busbar 7 is assumed constant and equals to 0.95 (lagging). Each of the AVC relays is assumed equipped with negative compounding to compensate for the voltage drop along the load feeder connecting buses 3 and 6.

In the first step of this investigation, the wind farm is assumed disconnected from the network by opening circuit breaker (CB) A (see Fig. 6.9). The load flow program is then run allowing the load at bus 7 to change from zero to its rated power and back again to zero. Fig. 6.10 shows the voltage profile of bus 6, V(6), and the AVC1 relay, V_{AVC1}. The latter voltage

is determined using Equation (6.1). Fig. 6.10 shows the variation of each of these voltages verses the power of the load at bus 7 in a form of loop. The lower part of each of these curves corresponds to the load increase from zero to its maximum value, whereas, the upper part corresponds to the decrease of the load back to zero again. The two arrows seen in Fig. 6.10 show the direction of the variation of the above voltages in response to the load variation. As can be seen in Fig. 6.10, when the load at bus 7 increases from zero to maximum, the voltage at bus 6 decreases. This is obviously due to voltage drop along the load feeder. At the same time, the AVC1 relay Voltage, V_{AVC1}, also decreases as expected from Equation (6.1). However, as V_{AVC1} reaches the lower control limit, i.e. 0.98pu represented by the lower dashed line shown in Fig. 6.10, AVC1 relay initiates a signal to operate the tap-changer of OLTCT1 in such a way to boost the voltage. It has been observed that AVC2 behaves similarly to that of AVC1. Fig. 6.10 shows that the operation of tap-changers of OLTCT1 and OLTCT2 occurs at approximately 1.2MW, 2.4MW and 3,5MW.

When the load decreases from its maximum value back to zero, both voltages, V(6) and V_{AVC1}, increase. Again, whenever V_{AVC1} reaches the upper control limit, shown by the upper dashed line in Fig. 6.10, AVC1 relay initiates a signal to operate the tap-changer of OLTCT1 in such a way to prevent V(6) exceeding the upper limit. Fig. 6.10 shows that this action occurs twice at approximately 2.2MW and 1.0MW. Comparing V(6) with V_{AVC1} in Fig. 6.10, it can be concluded that AVC1 relay at the substation has properly calculated the voltage of the remote bus 6, hence a proper voltage control of the controlled bus is achieved over the whole range of load variation.

The general behaviour of the system and AVC relay voltages that will be presented in the reminder of this chapter and in chapter 7, will be similar to those described above. Therefore, the curves depicted on such illustrations will not be explained in such detail, to avoid

unnecessary repetition.

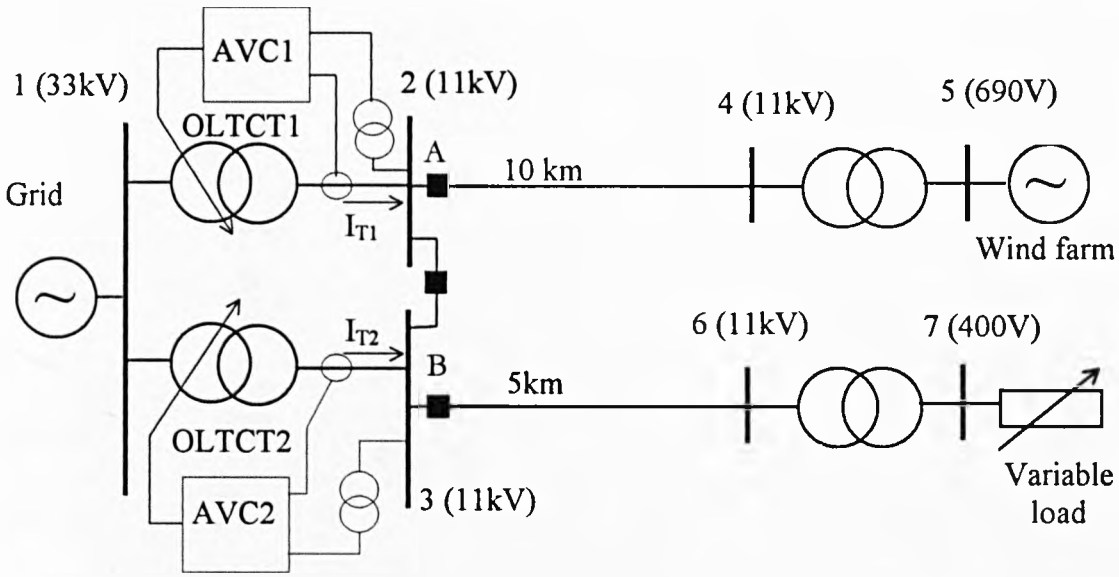

Fig. 6.9 Schematic diagram of a distribution network with embedded generators

The second step of this investigation involves the connection of the wind farm to the network by closing CB A. As previously mentioned in chapter 2, wind power based EG commonly employ induction (asynchronous) generators, which normally operate at a leading power factor. This means an EG of this type injects active power into the network but absorbs reactive power from the network. Thus, it is assumed that the wind farm provides the network with 4 MW total generation at leading power factor of 0.95. The performance of the AVC relays in this case is depicted in Fig. 6.11.

As demonstrated in Fig. 6.11, the integration of a wind power based EG with a leading power factor into the network causes an offset to the voltage measured by AVC relays. As can be seen in Fig. 6.11, while the measured voltage falls within the control limits, 0.98pu and 1.02pu, the controlled voltage, V(6), remains outside the limits of the control bandwidth in the range from 0.915pu to 0.96pu. The voltage difference between V_{AVC1} and V(6) at all

load conditions is fixed and approximately equal to 0.06pu, which means that the calculated voltage is always higher than the voltage of the controlled busbar. It has also been found that the voltage of AVC2 behaves similarly to that of AVC1. The reason for this difference is due to the contribution of the power injected by the wind farm into the power demand of the load, which results in the measured complex current through the OLTCTs differing from actual complex current in the load feeder. Hence, the voltage drop along the load feeder is wrongly calculated by the AVC relays [17]. Consequently, the network voltages fall outside the specified limits and the AVC relay cannot detect this error or make the necessary correction. It can then be concluded that AVC with negative compounding cannot perform properly when an EG is integrated into the network.

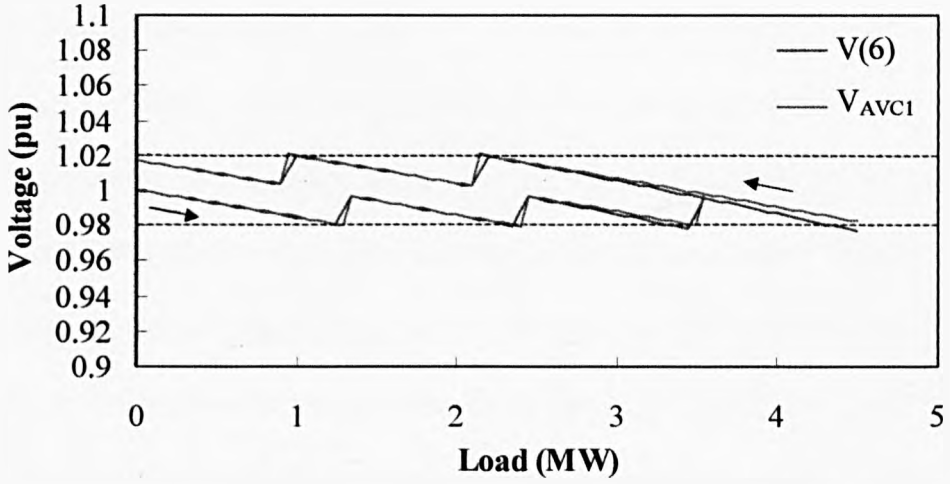

Fig. 6.10 Voltage control of network without the wind farm using AVC relays with negative compounding settings

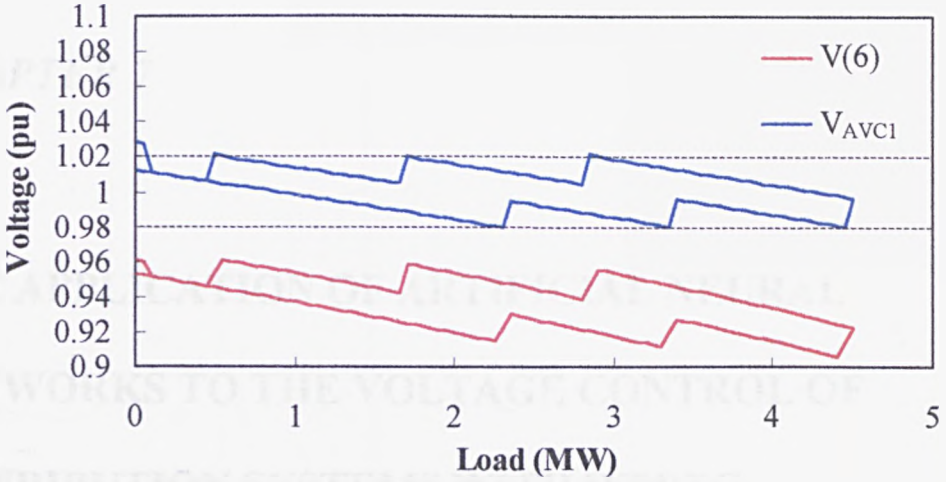

Fig. 6.11 The effect of the wind power based EG on the performance of AVC relays with negative compounding settings

CHAPTER 7

THE APPLICATION OF ARTIFICIAL NEURAL NETWORKS TO THE VOLTAGE CONTROL OF DISTRIBUTION SYSTEMS WITH WPBEG

7.1 Introduction

As previously mentioned in chapter 6, the integration of wind power based embedded generators (WPBEG) into a distribution network may cause problems to the operation of AVC relays. One such problem is the error introduced in calculating the magnitude of the voltage of AVC relays, resulting in malfunctioning of these relays. This may be explained due to the non-linear relationship between the compounding settings of the relays, which are required to compensate for voltage drop along distribution lines, and the power factor of the load of OLTCTs. In order to solve these problems, an attempt is made in this work to design an AVC relay based on the application of an artificial neural network (ANN).

The term "artificial neural network" has emerged following many years of research to understand and mimic the behaviour of human brain. The first attempts were reported in the early 1940's [129-131]. Since then, different algorithms and types of artificial neural networks have been proposed [129-134]. However, the interest in ANN has dramatically increased following the invention of the Multilayer Perceptron (MLP) Networks by Parker in 1982 and Rumelhart in 1985 [131,138]. A MLP network requires training before it can be

implemented to perform a useful task. One of the popular methods commonly used for the training of MLP networks is referred to as the "Back-Propagation (BP)" algorithm [129-138]. A MLP network based on the BP training algorithm is commonly known as Multilayer Back-Propagation Network. This type of ANN has been particularly attractive for applications in power systems, being used for more than 80% of such applications [137]. More details about the MLP networks and the other types of ANN can be found elsewhere [129-138].

In order to design an automatic voltage control (AVC) relay based on the application of ANN, a Multilayer BP network has been implemented [139,140]. The ANN based AVC relay has been designed utilising a specially dedicated neural network design tool called the "NeuralWorks". Further details about this tool can be found in reference 134.

In the following section, some of the reported applications of ANN in power systems are summarised. An AVC relay based on the application of ANN is then presented and discussed. The performance of the relay is tested for different configurations of the distribution network previously investigated. The results are demonstrated and discussed. Hereafter, WPBEGs will simply be referred to as embedded generators (EGs).

7.2 Application of ANN in Power Systems

The application of ANN in power systems has grown widely during the last few years [130]. ANNs have proved to be robust and have tremendous capabilities to learn complex nonlinear relationships that can effectively be used in solving problems which are otherwise difficult to solve. ANNs has been found to be useful for different types of power systems applications, such as load forecasting [141], fault classification and protection [142-149], power system

dynamic and stability studies [150-151], and control of power and voltage of electrical networks [152,153]. Some of the proposed techniques have already been constructed and installed on real systems to evaluate their performance under service conditions [142].

The short-term load forecasting technique proposed in [141] made use of ANN proceeded with a Fuzzy-based classifier, which was implemented to pre-classify training data. Classification of data was based on weather conditions, seasons in a year, days, and time. Data of every class was then utilised for training a separate MLP network; i.e. a number of ANNs was used in parallel for the load forecasting. The training of the ANN was achieved off-line to predict the short-term load forecast using historical data, which were obtained from a local utility. A performance test of the proposed ANN has shown that the error, which is referred to as "mean absolute percentage error (MAPE)" [141], between actual load measurement and that predicted by the ANN model did not exceed 2%.

The work proposed in [142-147] has demonstrated the effectiveness of ANN for fault classification and protection applications. For example, in [142] an ANN is proposed to overcome problems that occur when a distance relay detects a fault on a transmission system, which is composed of an overhead line (OHL) and a cable. The difference in the properties of OHLs and cables may cause the distance relay to over-reach or under-reach, whereas, a properly trained ANN can accurately predict the location of fault. Data for training and testing of the proposed ANN [142] is obtained by fault simulation utilising the EMTP program. Under-reach of distance relays due to fault arc resistance is the problem addressed in the work proposed in [143]. An ANN based distance relay that can properly operate for a fault with arc resistance is proposed. Training data, which includes the measured impedance of the faulted line at the relay location, is obtained by fault simulation. The performance of the proposed ANN based distance relay was found to be very good. Problems that face

conventional phase comparison relays, which are used in combination with distance relays, are reduced using ANN [144,145]. An ANN based on a phase comparison device has the ability to operate properly without having the serious effect caused by variations of source impedance. It has also been shown that an ANN based distance relay can operate properly when the voltage and current signals contain DC offsets [146] and when these signals are affected by the mutual coupling between parallel transmission lines [147]. It is worth noting that the MLP network that is based on the BP training algorithm is implemented in the reported works in [141-147].

In order to improve the performance of ANN based fault classification and protection devices, training methods, based on Genetic Algorithm (GA) techniques, are proposed in [148,149]. In these reports, the weights of MLP networks are calculated and updated using GA until the output error is minimised.

With regard to the application of ANN to power system stability and dynamic studies, research has been focused on the development of ANN based tools that can accurately provide an advanced and fast warning on the likelihood of unstable operation conditions [150,151]. On-line assessment of power system stability is difficult to achieve using different numerical techniques, because such techniques usually require relatively long computational time. In contrast to this, the ANN based techniques, which can be off-line trained, have the ability to evaluate system stability, when implemented on-line, much faster than conventional methods. Having fast and on-line assessment of system stability helps power system operators undertake proper preventive actions fast enough to safeguard the stability of the system. The proposed ANN specially developed for security assessment reported in both references [150,151] is also of the MLP type with BP training algorithm.

The application of ANN for voltage control of power systems and voltage stability problems is also reported in the literature [152,153]. In order to co-ordinate the switching of shunt capacitors and on-load-tap-changing devices, a combined ANN and fuzzy dynamic approach has been proposed in [152]. The model has been designed to provide a 24 hour power/voltage control strategy. This approach is therefore similar to the load forecasting technique described in [141] in the sense that it merely provides the operator an assessment on the future demand of reactive power of power system. Hence it is not designed to initiate operation of tap-changing devices or switching on or off shunt capacitors. H Schmidt has implemented the ANN to assess voltage stability problem in electrical power systems [153]. Firstly, he has studied the dynamics of the voltage stability problem. This was achieved by producing a dynamic model for a power system, which enabled him to run a dynamic simulation in the time-domain. The results of the dynamic simulation were then used to train a MLP network, which is used to assess the possibility of the occurrence of voltage collapse on the system.

7.3 First Attempt of Designing ANN based AVC relay

Voltage control using an AVC relay is achieved using two main steps. The first step involves the calculation of the voltage of AVC relay, V_{AVC}, using equation (6.1), from measured values of currents and terminal voltages of the associated OLTCT. In the second step, the calculated relay voltage is compared with a reference voltage (V_{target}). If the deviation of the relay voltage from a reference voltage exceeds a specified bandwidth, say $\pm 2\%$, the relay initiates a signal to operate the tap-changing device of the transformer in such a way as to ensure that the controlled voltage is brought back within the bandwidth. The bandwidth is usually chosen so that its value should be greater than that due to a single step change of the tappings of the controlled OLTCT.

The idea behind an ANN based AVC relay is to design an ANN that can perform the calculation related to the first step mentioned above, i.e. design an ANN that can process input signals and calculate the relay voltage, V_{AVC}. Hence the problem from the viewpoint of neural computation is a prediction problem. The ANN is expected to learn the nonlinear relationship between the power factor of transformer load current and the AVC relay compounding settings that would result in a proper voltage control of the distribution network with integrated embedded generators. The design of an ANN that performs such a task can be accomplished in three stages, e.g. determination of the structure, or topology of the ANN, training of the ANN, and testing its performance. An ANN based AVC relay is required to process the measured system parameters, such as the magnitude and phase angle of busbar voltages and transformer currents and the active and reactive power required for calculating the AVC relay voltage, V_{AVC}. Consequently the structure of the ANN must include an input layer to be used as a buffer for the inputs, at least one hidden layer, because of the non-linearity of the problem, and an output layer with a single neuron for holding the relay voltage, V_{AVC}. Therefore, a three-layer network, similar to that shown in Fig. 7.1, was implemented. The meaning of symbols used in this figure are explained below.

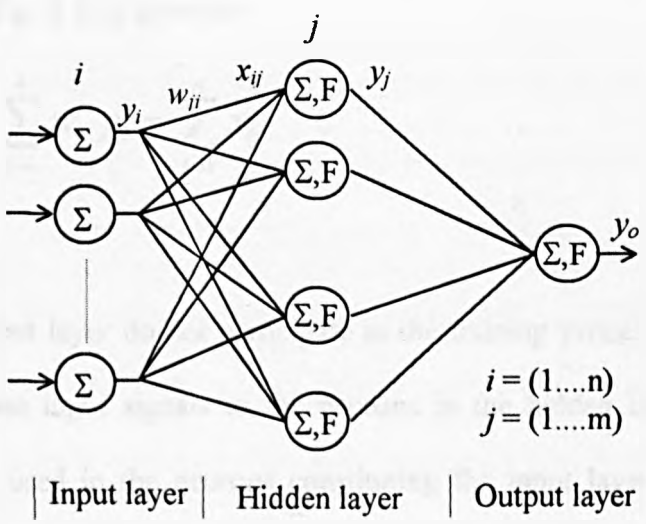

Fig. 7.1 A three-layer BP network

y_i is the output of the i^{th} neuron in the input layer,

w_{ij} is the weight of connection between the i^{th} neuron in the input layer and the j^{th} neuron in the hidden layer,

x_{ij} is the input into the j^{th} neuron in the hidden layer, where $x_{ij} = y_i w_{ij}$,

y_j is the output of the j^{th} neuron in the hidden layer,

y_o is the final output of the ANN.

F is a nonlinear function, for example a logistic or a hyperbolic tangent function,

n and m are the number of neurons in the input and hidden layers, respectively.

The following logistic function is used to process the input signals in the neurons of the hidden and output layers [129-134]:

$$y = \frac{1}{(1+e^{-sum})} \tag{7.1}$$

where *sum* is sum of the input signals into a neuron in the hidden or output layers, and y is the output of that neuron. For example, the sum of input signals into the j^{th} neuron in the hidden layer, see Fig. 7.1, is given by:

$$sum_j = \sum_{i=1}^{n} w_{ij} y_i = \sum_{i=1}^{n} x_{ij} \tag{7.2}$$

Neurons in the input layer do not participate in the training process [129-132]. Neurons in this layer only pass input signals to the neurons in the hidden layer. Therefore, transfer functions are not used in the neurons constituting the input layer. The number of input signals into the ANN dictates the number of neurons in the input layer. It has been found in this work [139, 140] that an input layer with three neurons is sufficient for the required ANN. The number of neurons in the hidden layer needs to be chosen carefully and can be

decided during the training process of the ANN, whereby an optimal number can be found that would provide the best training and performance of the ANN. When the number of neurons in the hidden layer is not sufficient, proper training can not be achieved, and when the number is too big, the training process may lead the ANN to memorise the training patterns rather than having the ability to adopt the relationships among them [129, 130]. A facility in the NeuralWorks software, which is called "save best" [134], optimises the number of neurons in the hidden layer by automatically training the ANN with a different number of hidden neurons. It then saves the network that provides minimum error as the best network. The optimal number of hidden neurons for this investigation is found equal to ten [139,140]. A three-layer ANN is constructed using the NeuralWorks software, as illustrated in the screen dump of the graphical interface of the NeuralWorks, which is shown in Fig. 7.2. As can be seen in the lower left part of Fig. 7.2, the ANN comprises an input layer with three neurons, a hidden layer with ten neurons, and an output layer with a single neuron. A bias neuron is also employed to add more flexibility to the ANN. The other features of the ANN shown in Fig. 7.2 will be explained later in section 7.5 when the training of the ANN is discussed.

As mentioned previously, the BP algorithm has been used for training of the proposed ANN. This algorithm is one of the known supervised training algorithms [129-134]. In order to train an ANN using the BP algorithm, it is usually fed with data, which consists of an input vector of patterns and the corresponding vector of desired outputs patterns. As far as the ANN presented in this work, the vector of input patterns includes network parameters, which can be measured at the low voltage side of the involved OLTCT. The corresponding vector of outputs of the ANN includes the desired values of the AVC relay voltage, V_{AVC}. The training data files are prepared by simulating voltage control of the considered distribution network using conventional AVC relays. Several cases have been considered, whereby in

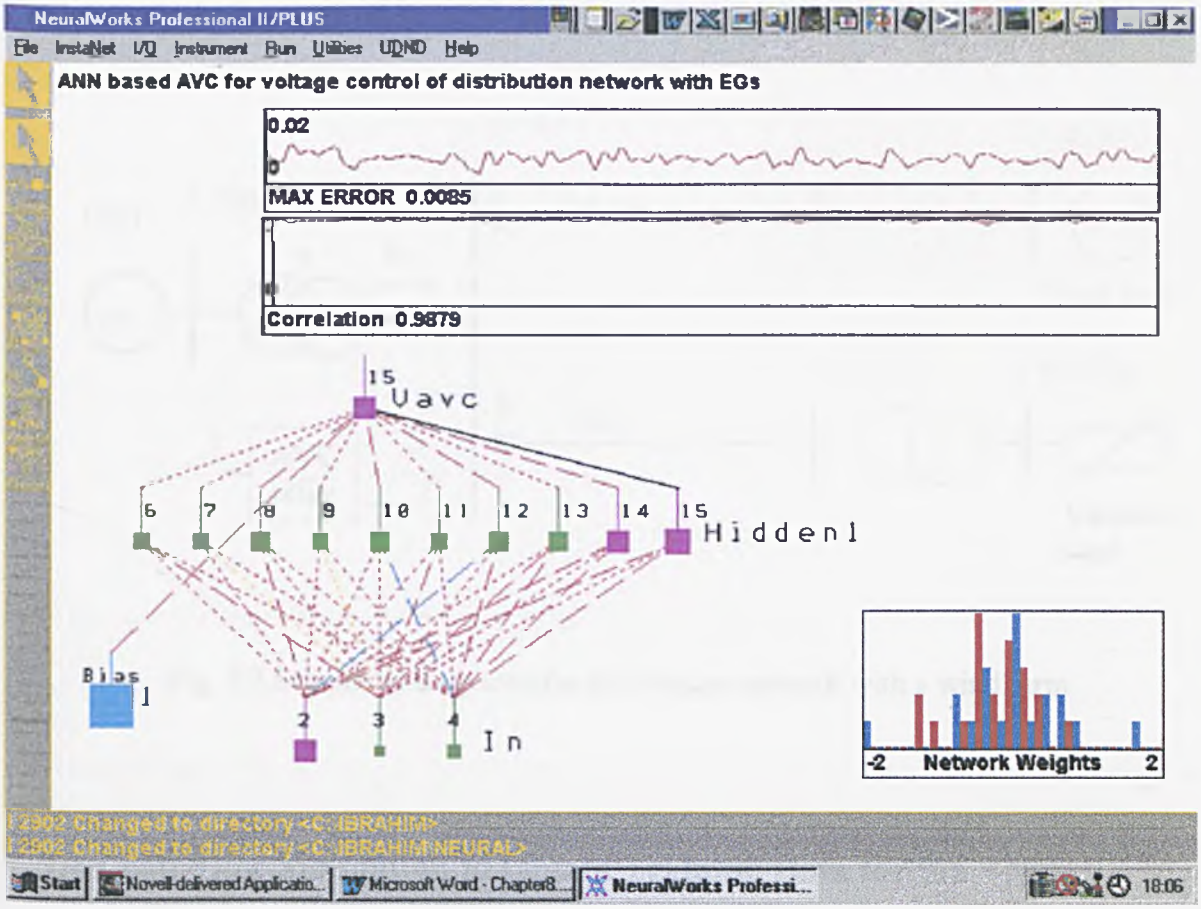

Fig. 7.2 Design of ANN based AVC relay using NeuralWorks software

some of them a wind farm is assumed connected to the network; while in other cases, the wind farm is assumed disconnected. The load flow program, which has been described in chapter 6, is used for this purpose. To demonstrate the procedure of designing and training the ANN based AVC relay, consider the simple distribution network shown in Fig. 7.3. It comprises a substation, which is represented by a 33kV/11kV OLTCT, a variable load, and a wind farm with a capacity of 4MW. A load feeder and an 11kV/415V transformer are used to connect the variable load with the substation, while another feeder is used to connect the wind farm with the substation. In this system it is assumed that the OLTCT is controlled by a conventional AVC relay with positive compounding arrangement. Bus-bar voltages shown in brackets in Fig 7.3 correspond to bus-bar nominal voltages.

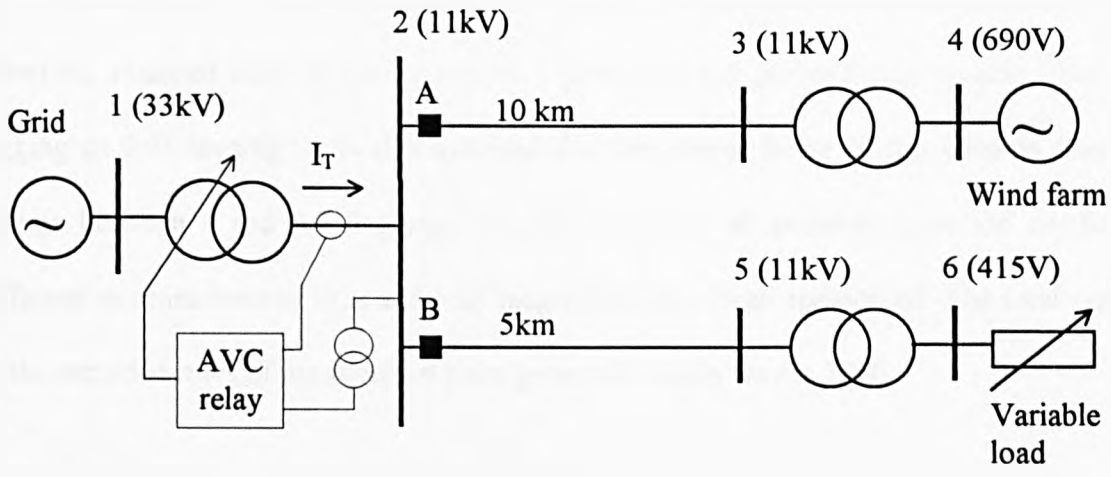

Fig. 7.3 Schematic diagram of a distribution network with a wind farm

7.4 Load Flow Simulation to Obtain Training Data for the ANN

Voltage control of the network shown in Fig. 7.3 is simulated using the load flow program specifically developed for this purpose using FORTRAN (see section 6.4). Several cases have been considered. A summary of these cases is shown in Table 7.1. In each of these cases, the load is allowed to incrementally change from zero to 4.5MW and back again to zero. Following each incremental change of the load a load flow calculation is executed and the results are recorded in data files, each of which constitute sets of rows of input and output patterns. These results include input signals that can normally be measured in a real network at the transformer low-voltage side. Such signals include the magnitude of busbar voltages, the transformer currents, the phase angle between the busbar voltage and the transformer current and active and reactive power flows in the transformer. The measured current and its phase angle with respect to the measured voltage are used to convert it into real and imaginary components. The AVC relay compounding settings are adjusted in each case study so that a proper voltage control is ensured whether the wind farm is connected or not. Wind farms commonly operate at a leading power factor as asynchronous (induction)

generators are usually employed in wind turbine-generator units, nevertheless, conditions when synchronous generators operating at lagging power factor are also considered. It is therefore, assumed that the wind farms may operate at any power factor ranging from 0.95 lagging to 0.95 leading. It is also assumed that the power factor of the variable load can change between 1 and 0.9 (lagging). In order to cover all possible operation conditions, different combinations of EGs and load magnitude have been considered. The total number of the recorded rows of input/output pairs generated in this way is 2500.

It has been found that not all the recorded signals are simultaneously required for the training of the ANN under consideration [139,140]. It has also been found that the results can be separated into two groups of inputs, each comprising three signals, which are sufficient to achieve good training of the ANN. The signals used in the first group include the amplitude of voltage, the real and imaginary components of transformer current, while the signals used in the second group consist of the voltage, which is the same as that used in the first group, and the measured real and reactive power though the transformer. These two groups are therefore saved with the corresponding AVC relay voltage in two separate data files.

As mentioned earlier, the training of an ANN should give it the ability to adopt the common relationships among input and output patterns, and not memorising them. In order to achieve this requirement, pairs of the generated input/output patterns are randomly separated into two groups and saved in two separate files. The first file, which contains 70% of the simulation results, is used for the training process of the proposed ANN based AVC relay, while the second file, which contains the remaining 30% is used for the testing stage of the ANN.

Table 7.1 Load flow conditions of the distribution network including embedded generation and variable loads, used to create a training file for an ANN model.

Case	Embedded Generation		Variable Load		Comp. Impedance		V_{target},
No	P(MW)	PF	Max.	PF	Ravc	Xavc	PU
1	0	-	4.5	1.0	0.4	0.8	1.0 ± 2%
2	0	-	4.5	0.95	0.4	0.8	1.0 ± 2%
3	0	-	4.5	0.9	0.4	0.8	1.0 ± 2%
4	4	0.95 lead	4.5	1.0	0.2	0.8	1.0 ± 2%
5	4	0.95 lead	4.5	0.95	0.2	0.8	1.0 ± 2%
6	4	0.95 lead	4.5	0.9	0.2	0.8	1.0 ± 2%
7	4	1	4.5	1.0	0.2	1.0	1.0 ± 2%
8	4	1	4.5	0.95	0.2	1.0	1.0 ± 2%
9	4	1	4.5	0.9	0.2	1.0	1.0 ± 2%
13	4	0.95 lag	4.5	1.0	0.0	1.4	1.0 ± 2%
14	4	0.95 lag	4.5	0.95	0.0	1.4	1.0 ± 2%
15	4	0.95 lag	4.5	0.9	0.0	1.4	1.0 ± 2%

7.5 Training and Testing of the ANN based AVC Relay

Before presenting the training data to the ANN, they should be first normalised to avoid saturation of the calculated outputs [134]. Normalisation of input patterns is performed in the NeuralWorks software using the following equation [134]:

$$x_{i,\,norm} = \frac{\left(x_i\,(R_{\max} - R_{\min}) + (R_{\min} x_{i,\max} - R_{\max} x_{i,\min})\right)}{x_{i,\max} - x_{i,\min}}$$

where:

$x_{i,\,norm}$ is the normalised input to neuron i in the input layer,

$x_{i,\,max}$ is the maximum value of input i in the training/testing data set,

$x_{i,\,min}$ is the minimum value of input i in the training/testing data set,

R_{max} is the upper limit of the implemented transfer function,

R_{max} = 1 for the logistic or hyperbolic tangent functions,

R_{min} is the lower limit of the implemented transfer function,

R_{min} = -1 for the logistic or hyperbolic tangent functions.

The training is performed using the normalised values. In the implementation stage, the relay voltages calculated using the ANN based AVC relay are then de-normalised to their corresponding real values using the following equation [134]:

$$y_{j,real} = \frac{\left(y_j\,(y_{j,\max} - y_{j,\min}) + (D_{\max} y_{j,\min} - D_{\min} y_{j,\max})\right)}{D_{\max} - D_{\min}}$$

where:

$y_{i,\,real}$ is the de-normalised output of neuron j in the output layer,

$y_{i,\,max}$ is the maximum value of desired output j in the training/testing data set,

$y_{i,\,min}$ is the minimum value of desired output j in the training/testing data set,

D_{max} is the upper limit of the implemented transfer function in the output neurons,

D_{max} = 1 for the logistic or hyperbolic tangent functions,

D_{min} is the lower limit of the implemented transfer function in the output neurons,

D_{min} = 0 for the logistic function and D_{min} = -1 for the hyperbolic tangent functions.

As mentioned above, the BP training method is employed in this work, whereby the delta rule of learning is applied to minimise the root mean square (RMS) error between the predicted and desired controlled voltages of the AVC relay. The training of the ANN based AVC relay was achieved by presenting it with randomly selected pairs of patterns from the training data file 80000 times. Presenting the training patterns for this number has resulted in a maximum RMS error not exceeding 2%. After the training process, the performance of the ANN is examined by presenting it with the data patterns from the test file. A snap shot of the

graphical interface of the NeuralWorks software has been previously shown in Fig. 7.2. As mentioned above, Fig. 7.2 depicts the three-layer ANN whereby the input layer is shown at the bottom, then the hidden layer, and finally the output layer. Fig. 7.2 also shows a number of graphical instruments, which are available in the NeuralWorks software that has been used in this work to monitor the process of the training of the ANN. The rectangular window at the top of Fig. 7.2 is one of these instruments that illustrates the error between the predicted (calculated) and desired outputs. This window shows the RMS error corresponding to 100 input patterns, which have been successively presented to the ANN. The same instrument also indicates that the maximum error, which has been reached when the patterns in the test file were presented to the ANN, was 0.0085. The next instrument located below the previous one illustrates the correlation between the general relationships which the ANN has learned in the training process and those relationships found in individual input patterns. This indicator is usually very low when training has just started. However, when the ANN begins to visualise the general properties in the training data, the correlation index starts to increase. If the correlation remains close to one in the test mode, this indicates that the ANN has successfully generalised the learned relationships over the space from which the input patterns of the training data file are obtained. It can be seen in Fig. 7.2 that the correlation among the training patterns for the considered ANN is always close to one, which provides evidence that the ANN has been properly trained. Another instrument, which is known as "network weights", shows the distribution of values of network weights in a graphical form, as depicted in the window which is located at the bottom right-hand corner of Fig. 7.2. The horizontal axis in this window shows the range of weight values extending from –2 to 2, which is divided into equal intervals. On the top of each interval, there is a graphic bar, which has a width equals to the width of the interval. The height of each bar equals to the number of connections in the ANN, which have a weight value falling within the corresponding interval. All the bars in the graph are automatically scaled by the

NeuralWorks program according to the value of the highest bar. As can be seen here, some connections have positive weight values, while other connections have negative weight values.

Fig. 7.4 depicts a comparison between the desired values of the voltage of the AVC relay and those calculated by the ANN for 100 input patterns which have been presented to the ANN from the test data file. As can be seen in Fig. 7.4, the predicted values of V_{AVC} match the desired values very well.

As a result of the training process of the ANN, a final set of weights, which correspond to the connections between neurons in successive layers, is produced. After the training and testing, the set of weights is saved into a text file in a form of a table.

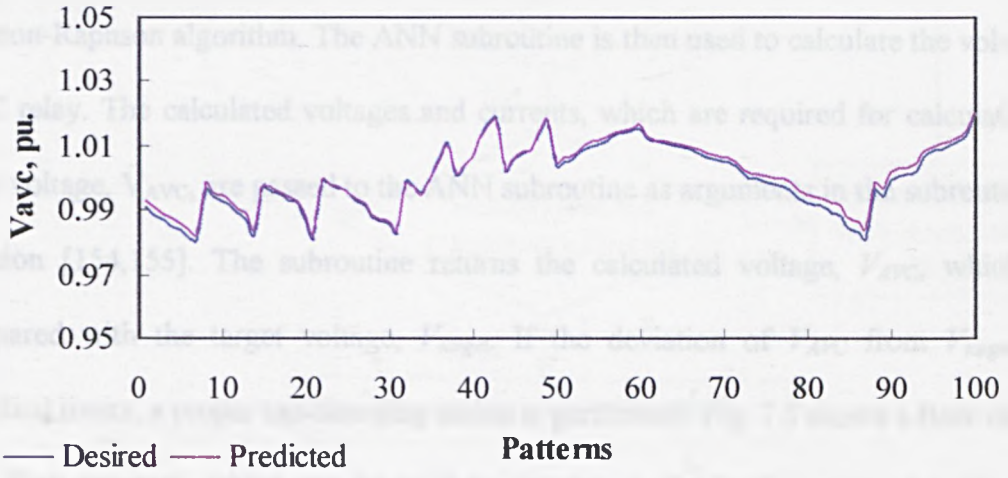

Fig. 7.4 A comparison between desired values of AVC relay's controlled voltage and those predicted by an ANN based relay

7.6 Integration of the ANN based AVC Relay into the Load Flow Program

After designing, training and testing the ANN-based AVC relay using the NeuralWorks program, it is included in the load flow program to further investigate its performance. As mentioned above, the final values of weights of the ANN are saved in a separate data file. On the other hand, the simulation of a conventional AVC relay used in the specifically developed FORTRAN load flow program is replaced by the ANN based AVC relay. Thus, the ANN computation is included in the program in a form of a subroutine. The load flow program is modified in such a way that when it is executed, weights are loaded from the data file into the memory of the computer and assigned to their corresponding connections in the ANN based AVC relay. When the load is incrementally changed during voltage control simulation, network voltages and currents are calculated, as previously explained, using the Newton-Raphson algorithm. The ANN subroutine is then used to calculate the voltage of the AVC relay. The calculated voltages and currents, which are required for calculation of the relay voltage, V_{AVC}, are passed to the ANN subroutine as arguments in the subroutine calling function [154,155]. The subroutine returns the calculated voltage, V_{AVC}, which is then compared with the target voltage, V_{target}. If the deviation of V_{AVC} from V_{target} exceeds specified limits, a proper tap-changing action is performed. Fig. 7.5 shows a flow chart of the load flow program, which can be used to simulate a distribution network with the ANN based voltage control.

Thus, the modified load flow program can be used as a tool to investigate the performance of the ANN based AVC relay as the variable load connected to the network (see Fig. 7.3) is changed from zero to its maximum value. It also allows the testing of whether a proper voltage control can be achieved using the ANN based AVC relay or not.

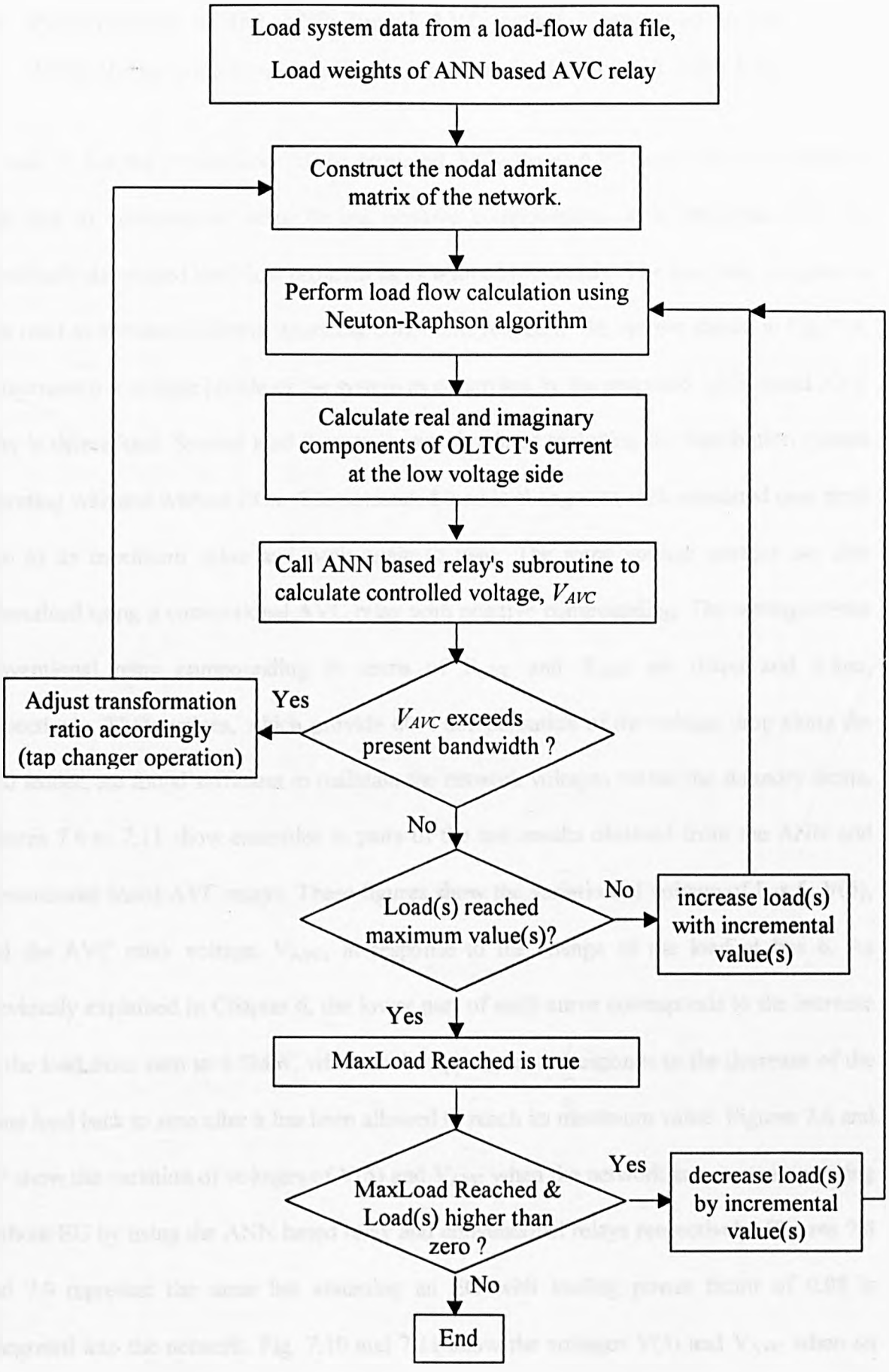

Fig. 7.5 Flow chart of the load flow program to simulate voltage control using ANN based AVC relays

7.6 Performance of the ANN based AVC Relay Compared to an AVC Relay with Positive Compounding in a Network with EG

In order to test the performance of the proposed ANN based AVC relay and to compare it with that of conventional relay having positive compounding, it is integrated into the specifically developed load flow program as mentioned previously. The load flow program is then used to simulate different operating conditions related to the system shown in Fig. 7.3. Consequently a voltage profile of the system as controlled by the proposed ANN based AVC relay is determined. Several load flow cases are simulated including the distribution system operating with and without EGs. The connected load is changed in each simulated case from zero to its maximum value and back again to zero. The same voltage profiles are also determined using a conventional AVC relay with positive compounding. The settings of the conventional relay compounding in terms of R_{AVC} and X_{AVC} are 0.4pu and 0.8pu, respectively. These values, which provide 60% compensation of the voltage drop along the load feeder, are found sufficient to maintain the network voltages within the statutory limits. Figures 7.6 to 7.11 show examples in pairs of the test results obtained from the ANN and conventional based AVC relays. These figures show the variation of voltage of bus 5, V(5), and the AVC relay voltage, V_{AVC}, in response to the change of the load at bus 6. As previously explained in Chapter 6, the lower part of each curve corresponds to the increase of the load from zero to 4.5MW, whereas the upper part corresponds to the decrease of the same load back to zero after it has been allowed to reach its maximum value. Figures 7.6 and 7.7 show the variation of voltages of V(5) and V_{AVC} when the network is assumed operating without EG by using the ANN based relay and conventional relays respectively. Figures 7.8 and 7.9 represent the same but assuming an EG with leading power factor of 0.98 is integrated into the network. Fig. 7.10 and 7.11 show the voltages V(5) and V_{AVC} when an EG with a lagging PF of 0.98 is assumed connected to the network. In all these cases, the variable load is assumed to have a constant lagging PF of 0.97.

Fig. 7.6 represents the behaviour of the ANN based AVC relay, whereas, Fig. 7.7 represents the behaviour of a conventional relay. By comparing these two figures, it can be observed that the performance of the ANN based relay in this case is similar to that of the conventional one. The relay voltage, V_{AVC}, of both the ANN-based and conventional relays vary within the upper and lower control limits of the bandwidth, which are shown by horizontal dashed lines in Figs 7.6 and 7.7. By comparing Fig. 7.6 and 7.7 it can also be seen that the profile of the voltage of bus 5, V(5), is the same for both cases and it is also well controlled. The same figures show that the voltage V(5) is maintained within the range of 0.96pu and 1.02pu.

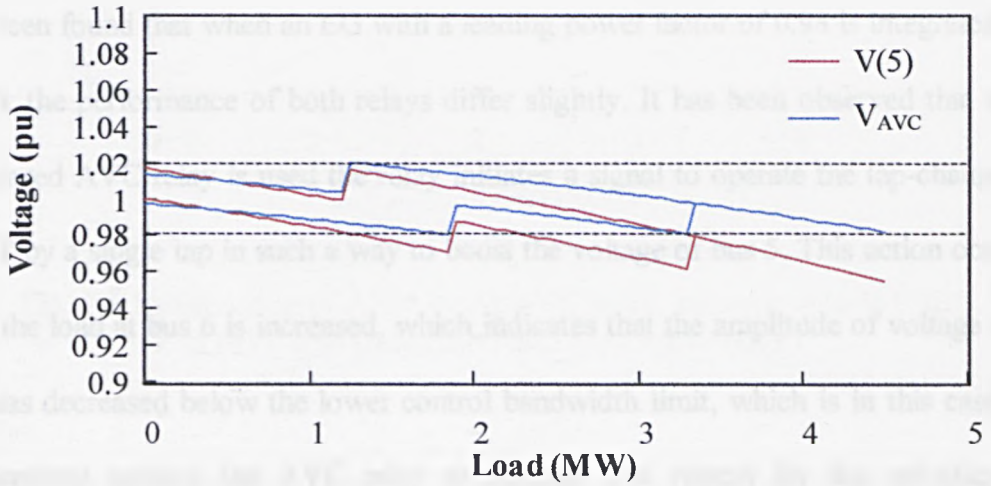

Fig. 7.6 Performance of ANN based AVC relay, network without EG and PF of load = 0.97 (Lag.)

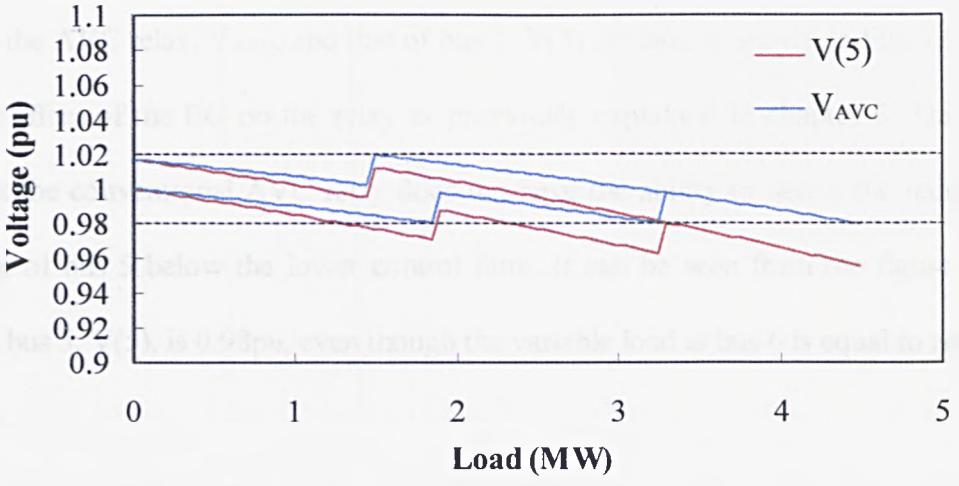

Fig. 7.7 Performance of conventional AVC relay with positive compounding, network without EG and PF of load = 0.97 (Lag.), $R_{AVC} = 0.4$ and $X_{AVC} = 0.8$

It has been found that when an EG with a leading power factor of 0.98 is integrated into the network the performance of both relays differ slightly. It has been observed that when the ANN based AVC relay is used the relay initiates a signal to operate the tap-changer of the OLTCT by a single tap in such a way to boost the voltage of bus 5. This action occurs even before the load at bus 6 is increased, which indicates that the amplitude of voltage of bus 5, V(5), has decreased below the lower control bandwidth limit, which is in this case 0.98pu, and therefore causing the AVC relay to operate. The reason for the reduction of the amplitude of V(5) is due to a voltage drop in the OLTCT, which results from the flow of power through the OLTCT when the EG is connected to the network. Consequently, the voltage of buse 2, and hence, bus 5 decreases. Fig. 7.8 shows the profile of the AVC relay voltage, V_{AVC}, and the voltage of bus 5, V(5), when the ANN based relay is used. As can be seen in this figure, the initial values of these voltages, i.e. when the load at bus 6 is zero, is about 1pu. By comparing the voltage profiles in Fig. 7.6 with those shown in Fig. 7.8, it can be seen that the performance of the ANN based AVC relay is not affected by the integration of EG.

On the other hand, it has been observed that when the conventional AVC relay is used, the voltage of the AVC relay, V_{AVC}, and that of bus 5, V(5) deviate, as shown in Fig. 7.9. This is due to the effect of the EG on the relay as previously explained in chapter 6. This simply means that the conventional AVC relay does not have the ability to detect the reduction of the voltage of bus 5 below the lower control limit. It can be seen from the figure that the voltage of bus 5, V(5), is 0.98pu, even though the variable load at bus 6 is equal to zero.

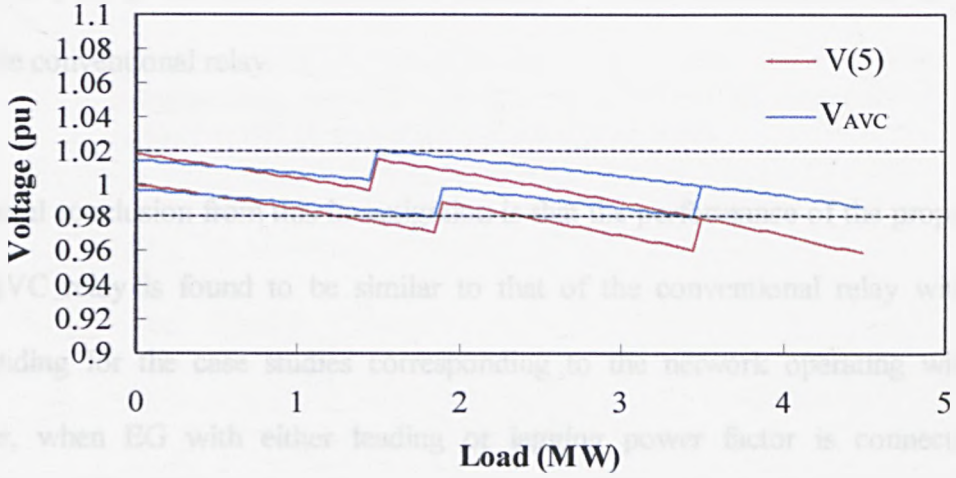

Fig. 7.8 Performance of ANN based AVC relay, network with WPBEG. PF of EG = 0.98 (lead) and PF of load = 0.97 (Lag.)

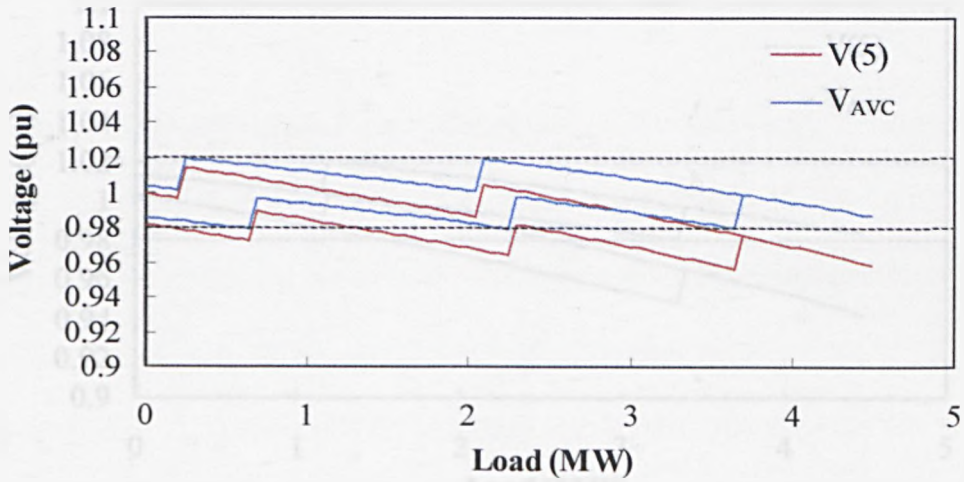

Fig.7.9 Performance of conventional AVC relay with positive compounding, network with WPBEG. PF of EG = 0.98 (lead) and PF of load = 0.97 (Lag.), R_{AVC} = 0.4 and X_{AVC} = 0.8

Fig. 7.10 and 7.11 show the performance of the ANN based and the conventional AVC relays when an EG with a lagging power factor of 0.98 is integrated into the network. It can be seen that the behaviour of the ANN based AVC relay is similar to the case that corresponds to the integration of an EG with a leading power factor, which is explained above. The AVC in this case also initiates a single step operation of the tap-changer to adjust the voltage of bus 5 to 1pu when the load value is still zero as can be seen from the voltage profile of V(5) in Fig. 7.10. The conventional AVC does not react in the same way. Consequently the performance of the ANN based AVC relay is considered to be better than that of the conventional relay.

The general conclusion from this investigation is that the performance of the proposed ANN based AVC relay is found to be similar to that of the conventional relay with positive compounding for the case studies corresponding to the network operating without EG. However, when EG with either leading or lagging power factor is connected to the investigated network, the proposed ANN based relay exhibits better performance than that of the conventional relay.

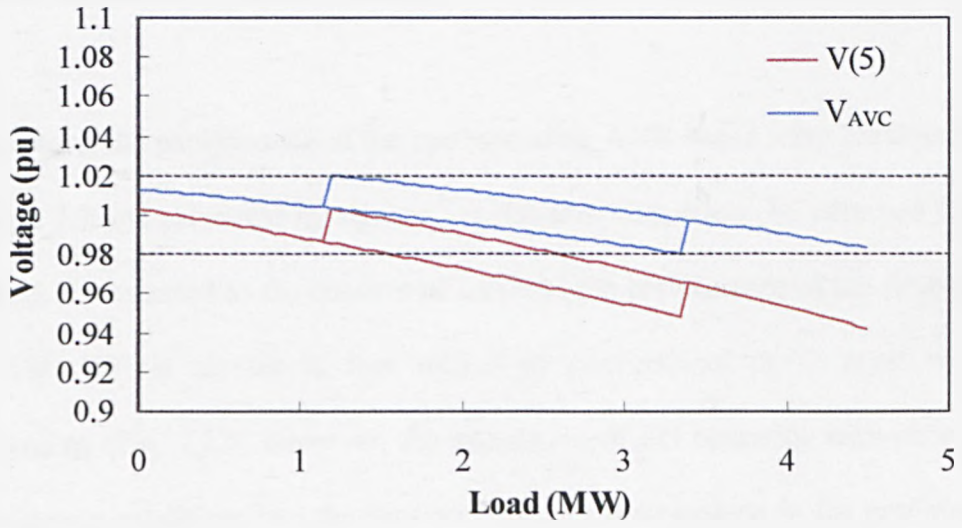

Fig. 7.10 Performance of ANN based AVC relay, network with EG. PF of EG = 0.98 (Lag.) and PF of load = 0.97 (Lag.)

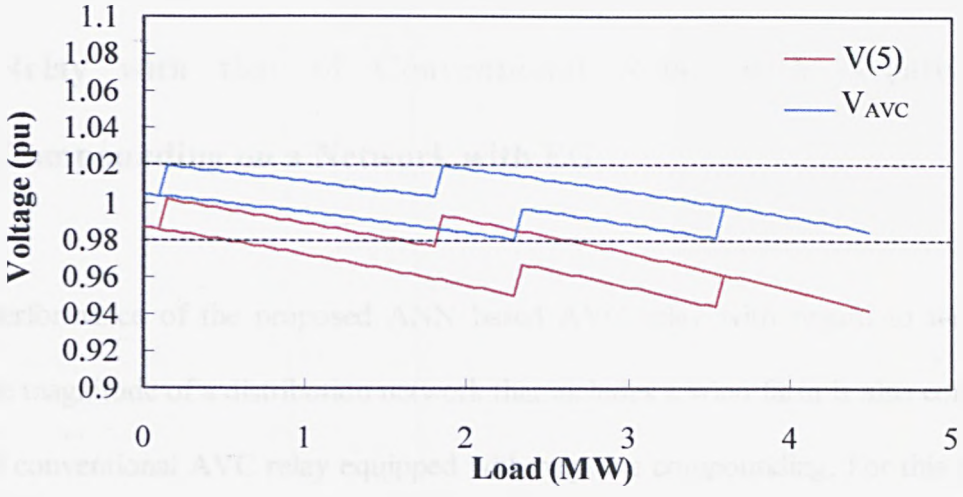

Fig.7.11 Performance of conventional AVC relay with positive compounding, network with EG. PF of EG = 0.98 (Lag.) and PF of load = 0.97 (Lag.), R_{AVC} = 0.4 and X_{AVC} = 0.8

7.8 Comparison between the Performance of ANN based AVC Relay with that of Conventional Relay with Negative Compounding on a Network with EG

The performance of the proposed ANN based AVC relay with regard to the control of voltage magnitude of a distribution network that includes a wind farm is also compared with that of conventional AVC relay equipped with negative compounding. For this purpose, the distribution system shown in Fig. 7.3 is considered again, assuming this time that a conventional AVC relay with negative compounding is used. Practically, this situation represents the case when two transformers are initially operated in parallel, but one of them is temporarily switched out of service. Case studies similar to those described in the previous section were repeated, whereby, the load at bus 6 is allowed to change from zero to its maximum value and back again to zero. Figures 7.12 to 7.14 show examples of the results obtained from the simulation. Fig. 7.12 shows the corresponding voltages of bus 5, V(5) and the voltage of the AVC relay, V_{AVC}, for the case when the network is operated without the EGs. Whereas, Fig. 7.13 corresponds to an EG with a leading power factor (PF) of 0.98 integrated into the network, whereas Fig. 7.14 represents an EG with a lagging PF of 0.98.

By comparing the performance of the corresponding ANN-based relay previously discussed in section 7.7 and presented by figures 7.6, 7.8 and 7.10, it can be observed that when no wind farm is connected to the considered network, the performance of the ANN based AVC relay (Fig. 7.6) is similar to that related to conventional AVC relay with negative compounding (Fig. 7.12). However, the integration of EG operating with either leading or lagging power conditions into the network, causes a deterioration in the performance of the conventional relay, as can be seen in Figures 7.13 and 7.14, respectively. For example, the voltage of bus 5, V(5) in both figures is always below the lower control limit set at 0.98pu.

On the other hand, it can be seen that the performance of the ANN based relay for the same cases has not been affected by the integration of the wind farm into the network and remains capable of properly controlling the voltage of the network, as shown in figures 7.8 and 7.10, respectively. The reason of the such high-quality performance exhibited by the ANN-based relay is because the training of the ANN is made using training patterns that are obtained from load flow case studies corresponding to the network operating with and without EG. As previously explained in section 7.4, the training patterns are generated using a conventional AVC relay to simulate the voltage control of the investigated network, whereby its compounding settings are continuously adjusted to account for the connection or disconnection of EGs. Thus, the ANN based AVC relay has been trained to properly control network voltage, whether EG is connected to the network or not.

From these results, it can be concluded that an ANN based AVC relay can perform better than a conventional relay with negative compounding arrangement when EG is connected to the distribution network.

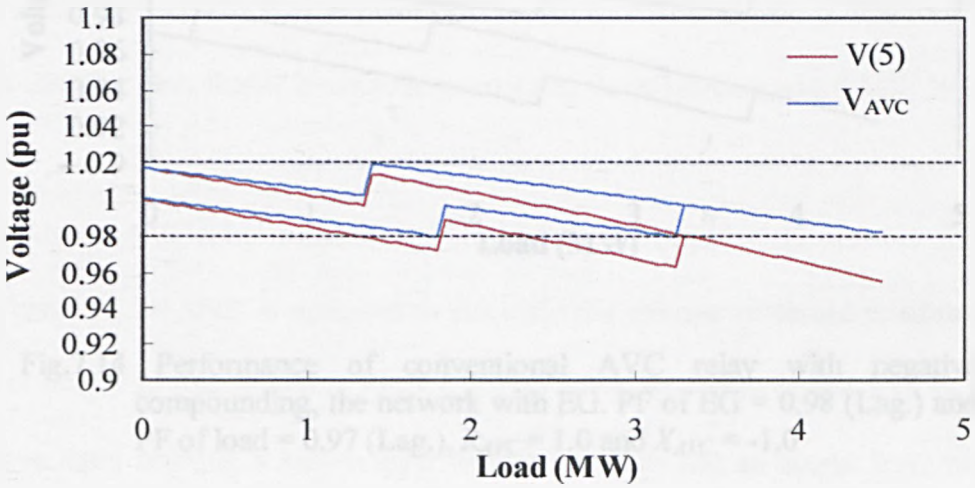

Fig.7.12 Performance of conventional AVC relay with negative compounding, the network without EG. PF of load = 0.97 (Lag.), R_{AVC} = 1.0 and X_{AVC} = -1.0

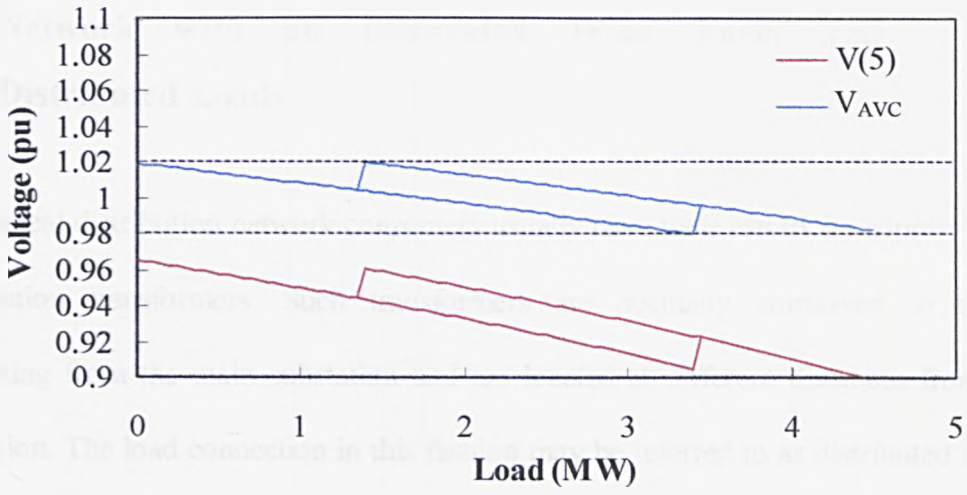

Fig.7.13 Performance of conventional AVC relay with negative compounding, the network with EG. PF of EG = 0.98 (lead) and PF of load = 0.97 (Lag.), R_{AVC} = 1.0 and X_{AVC} = -1.0

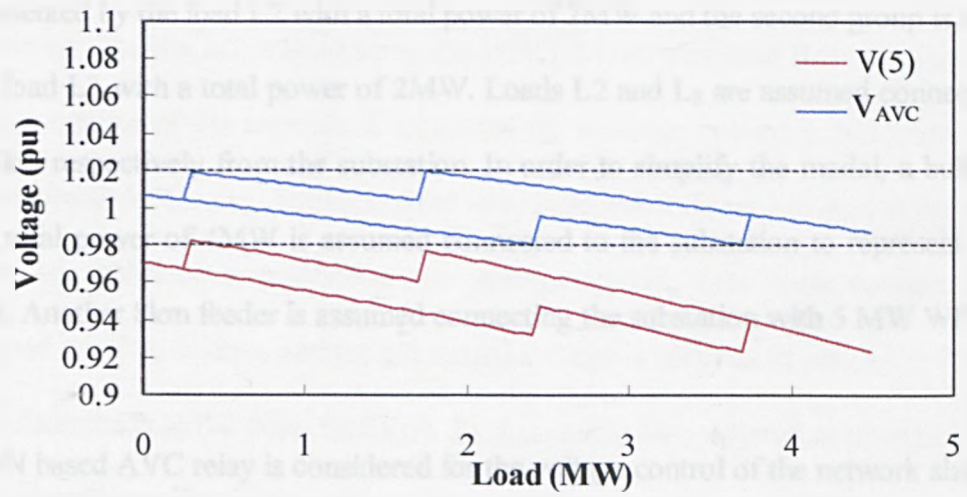

Fig.7.14 Performance of conventional AVC relay with negative compounding, the network with EG. PF of EG = 0.98 (Lag.) and PF of load = 0.97 (Lag.), R_{AVC} = 1.0 and X_{AVC} = -1.0

7.9 Performance of an ANN based AVC Relay on a Network with an Integrated Wind Farm and Distributed Loads

In a typical distribution network consumers usually have their electricity supply via MV/LV distribution transformers. Such transformers are normally connected to the feeders emanating from the main substation and are located at different distances from the main substation. The load connection in this fashion may be referred to as distributed load. Loads of such networks may change independently. Consequently voltage drops along load feeders cannot be guaranteed to be identical. For this reason, the voltage control of a distribution network with an integrated wind farm and distributed loads is investigated. The network is shown in Fig. 7.15. This figure shows that the network comprises a 33kV/11kV substation, which is represented by a 20MVA OLTCT, a radial load feeder connected with two groups of variable loads via MV/LV transformers with voltage ratio of 11kV/0.415 kV. One group is represented by the load L2 with a total power of 2MW and the second group is represented by the load L3 with a total power of 2MW. Loads L2 and L_3 are assumed connected at 8km and 13km respectively from the substation. In order to simplify the model, a bulk load, L1, with a total power of 4MW is assumed connected to the substation to represent other load feeders. Another 8km feeder is assumed connecting the substation with 5 MW WPBEGs.

An ANN based AVC relay is considered for the voltage control of the network shown in Fig. 7.15. Therefore, an ANN is designed to calculate the voltage of the AVC relay. The ANN model is similar to that shown in Fig.7.1, it also comprises three layers, e.g. an input layer with three input neurons, a hidden layer with ten neurons and an output layer with a single neuron.

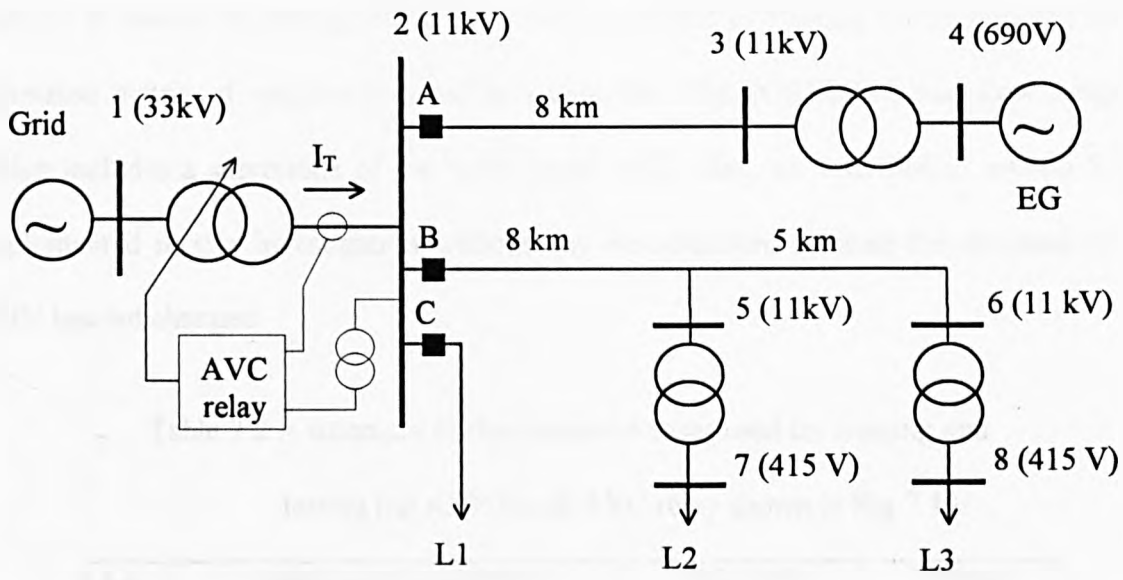

Fig. 7.15 Schematic diagram of a distribution network with distributed loads and embedded generators

A training data file is obtained using the FORTRAN-based load flow program whereby the voltage control of the network is simulated for different operating conditions employing a conventional AVC relay. Settings of the relay compounding are adjusted in each case in such a way to continuously provide proper voltage control. The target voltage for control is assumed equal to 0.98pu, and the calculated voltage is allowed to vary by $\pm$ 2%. During the simulation loads at the three locations, L_1, L_2, and L_3, are allowed to change in incremental steps simultaneously from zero to their maximum values and back again to zero. The calculated results at every step are saved in a training data file. The input patterns for the ANN based AVC relay are derived from the voltage of bus 2, V(2) and the real and imaginary components of the transformer current, I_T. The output is the calculated AVC relay voltage, V_{AVC}. Table 7.2 shows a summary of the simulated cases. For the reason explained previously in section 7.5, the training file is divided into two separate files by randomly

selecting pairs of input and output patterns for each file. A data file containing 50% of the patterns is used in the training process, whereas another file containing the remaining 50% of patterns is used in the testing mode. Following a satisfactory training and testing, the finally generated matrix of weights is saved in a data file. The FORTRAN load flow program, which includes a subroutine of the ANN based AVC relay, as described in section 7.6, is implemented in this investigation without any modification, because the structure of the ANN has not changed.

Table 7.2 A summary of the simulated cases used for training and testing the ANN based AVC relay shown in Fig 7.13.

Case No	Maximum Load, MW Load power factor, PF (lagging)				EG, MW PF (leading)		Voltage setting and control bandwidth
	L1	L2	L3	PF		PF	
1	2	2	2	.95	0	-	0.98 ± 2 %
2	2	0	2	.95	0	-	0.98 ± 2 %
3	0	0	2	.95	0	-	0.98 ± 2 %
4	4	0	2	.95	0	-	0.98 ± 2 %
5	4	2	2	.95	0	-	0.98 ± 2 %
6	2	2	2	.95	0	.98	0.98 ± 2 %
7	2	0	2	.95	5	.98	0.98 ± 2 %
8	0	0	2	.95	5	.98	0.98 ± 2 %
9	4	0	2	.95	5	.98	0.98 ± 2 %
10	4	2	2	1	5	.98	0.98 ± 2 %
11	2	2	2	1	0	-	0.98 ± 2 %
12	2	0	2	1	0	-	0.98 ± 2 %
13	0	0	2	1	0	-	0.98 ± 2 %
14	4	0	2	1	0	-	0.98 ± 2 %
15	4	2	2	1	0	-	0.98 ± 2 %
16	2	2	2	1	0	.98	0.98 ± 2 %
17	2	0	2	1	5	.98	0.98 ± 2 %
18	0	0	2	1	5	.98	0.98 ± 2 %
19	4	0	2	1	5	.98	0.98 ± 2 %
20	4	2	2	1	5	.98	0.98 ± 2 %

The performance of the proposed ANN based AVC relay is first tested by running the ANN model in the NeuralWorks program in the test mode. An example of the test results is illustrated in Fig. 7.16, from which a comparison between the desired voltage of the AVC

relay and that predicted by the ANN model can be made. For this case, the maximum power of L_1, L_2, and L_3 are assumed equal to 3 MW, 0 MW, and 2 MW, respectively. The power factor of the three loads is assumed the same and equals to 0.98 (lag). As can be seen in Fig. 7.16, the two curves match very well, indicating that a very good training of the ANN-based relay is achieved.

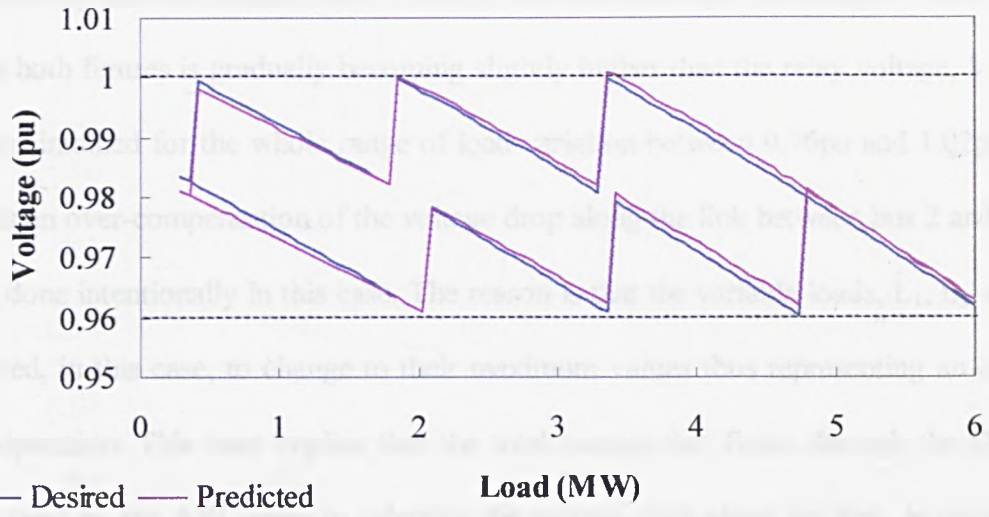

Fig. 7.16 A comparison between desired values of controlled voltage of AVC relay and those predicted by an ANN based relay.

The performance of the ANN based AVC relay is further investigated using the FORTRAN load flow program. Several case studies are simulated, including the wind farm either connected to or disconnected from the network. Figures 7.17 to 7.20 show two examples in pairs of the test results obtained from the ANN and its conventional counterpart. These figures show the variation of voltage of bus 6, V(6), and the AVC relay voltage, V_{AVC}, in response to the change of the loads L_1, L_2, and L_3. Figures 7.17 and 7.18 shows the results of the case when the loads L_1, L_2, and L_3 are assumed to have a maximum of 4 MW, 2 MW, and 2 MW, respectively, and all have the same power factor of 0.98 (lag). As previously explained in Chapter 6, the lower part of each curve corresponds to the increase of the total load from zero to its maximum of 8MW, whereas the upper part corresponds to the decrease

of the same back to zero after being allowed reaching its maximum value. Fig. 7.17 and 7.18 show the voltage of AVC relay, V_{AVC}, and the voltage of bus 6, V(6), for the case when the network is operated without EGs, and with control from the ANN based and conventional relays, respectively. As can be seen in Figs 7.17 and 7.18 the voltage of the both AVC relays has the same profile. For example both are confined between the upper and lower control limits shown by the two dashed lines. It can be seen that although the voltage of bus 6, V(6), shown in both figures is gradually becoming slightly higher than the relay voltage, V_{AVC}, its value is maintained for the whole range of load variation between 0.96pu and 1.02pu. This represents an over-compensation of the voltage drop along the link between bus 2 and bus 6, which is done intentionally in this case. The reason is that the variable loads, L_1, L_2, and L_3, are allowed, in this case, to change to their maximum values thus representing an extreme case of operation. This case implies that the total current that flows through the OLTCT, which is used by the AVC relay to calculate the voltage drop along the link, is equal to its maximum expected value. It is found that by allowing some degree of over-compensation leads to preventing large under-compensation when the operational condition is reduced to the other extreme case; e.g. when only the minimum load, say L_2 or L_3, is connected to the network. In other words, due to the nature of distributed loads whereby each load may vary independently, the controlled voltage may be subjected to a small offset either above or below the voltage of bus 6. The error between the voltage of the AVC relay and the voltage of the controlled bus, V(6), is difficult to avoid because it is difficult to calculate the voltage drop along a load feeder correctly when the loads are distributed at different locations. If the load currents through individual feeders or at least through the feeder which connects the substation with the controlled remote bus, is provided to the AVC relay, this problem might be alleviated. However this may require additional equipment to be installed in the substation; such equipment may include current transformers, additional control circuitry, etc. and such action may not be economically justified. Nevertheless, it is found that in

general, even with the above-described offset, the profile of voltages of the considered network is continuously maintained within the statutory limits.

Comparing Fig. 7.17 with Fig. 7.18 shows that the performance of the ANN based AVC relay in the considered case is similar to that of the conventional relay and that the voltage of bus 5 is properly controlled using either relays.

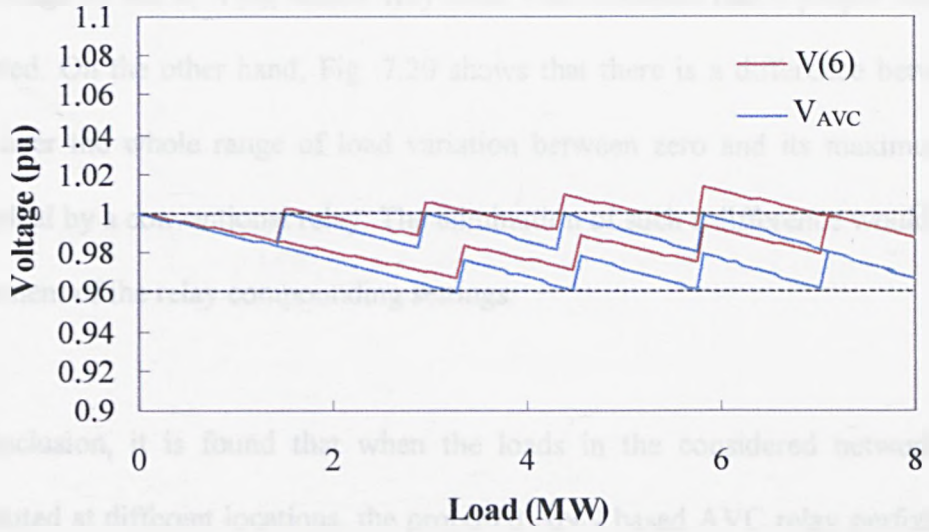

Fig.7.17 Performance of ANN based AVC relay, network without EG. $L_1 = 4$ MW, $L_2 = L_3 = 2$ MW, PF of load = 0.98 (Lag.).

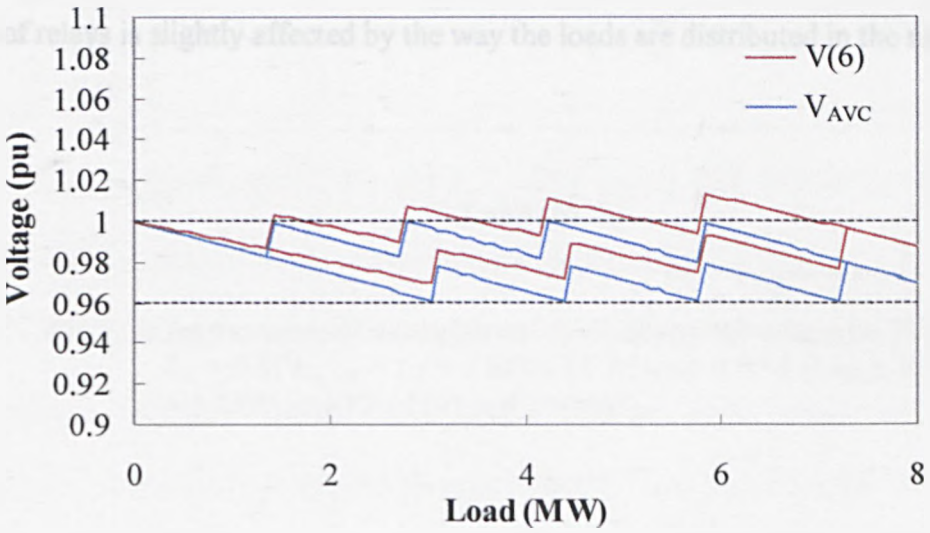

Fig.7.18 Performance of conventional AVC relay; network without EG. $L_1 = 4$ MW, $L_2 = L_3 = 2$ MW, PF of load = 0.98 (Lad.).

As in the previous case, Fig. 7.19 and Fig. 7.20 show the profile of V_{AVC} and V(6) due to the voltage control of the network with an integrated wind farm using the proposed ANN based and conventional relays respectively. It is assumed that the wind farm is injecting into the network a total power of 5 MW at a leading power factor of 0.98. The maximum loads of L_1 and L_3 are assumed the same and equal to 2 MW with a lagging power factor of 0.98, whereas load L2 is set to zero. As can be seen in Fig. 7.19, the AVC relay voltage, V_{AVC}, and the voltage of bus 6, V(6), match very well. This indicates that a proper voltage control is achieved. On the other hand, Fig. 7.20 shows that there is a difference between V_{AVC} and V(6) over the whole range of load variation between zero and its maximum value when controlled by a conventional relay. The elimination of such a difference would require the re-adjustment of the relay compounding settings.

In conclusion, it is found that when the loads in the considered network are assumed distributed at different locations, the proposed ANN based AVC relay performs the voltage control of the network properly irrespective whether an EG is connected to the network or not. Such performance, in many cases, is similar to that of the conventional relay and in other cases, it is even better. It is also observed that the calculated AVC relay voltage using both types of relays is slightly affected by the way the loads are distributed in the network.

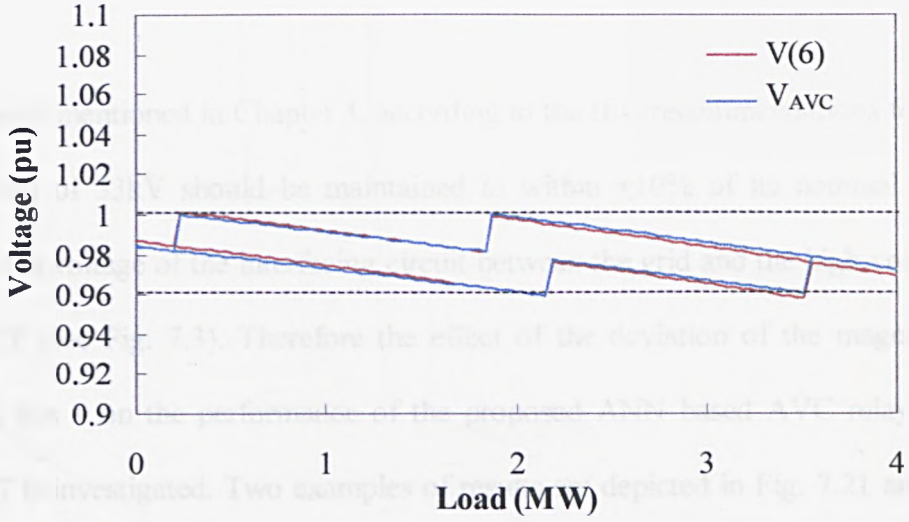

Fig.7.19 Performance of ANN based AVC relay, network with EG. $L_2 = 0$ MW, $L_1 = L_3 = 2$ MW, PF of load = 0.98 (Lag.), EG = 5 MW, and PF of EG = 0.98 (lead).

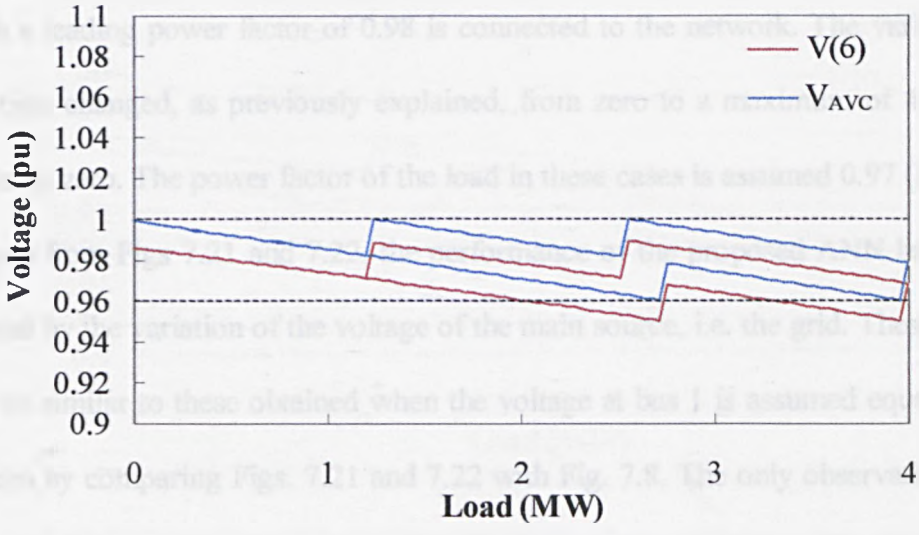

Fig.7.20 Performance of conventional AVC relay; network with EG. $L_2 = 0$ MW, $L_1 = L_3 = 2$ MW, PF of load = 0.98 (Lag.), EG = 5 MW, and PF of EG = 0.98 (lead).

7.10 The Effect of Voltage Source on the Performance of the ANN based AVC relay

As previously mentioned in Chapter 4, according to the IEC recommendations 60038 [93], a voltage level of 33kV should be maintained to within ±10% of its nominal value. This applies to the voltage of the interfacing circuit between the grid and the high voltage side of the OLTCT (see Fig. 7.3). Therefore the effect of the deviation of the magnitude of the voltage at bus 1 on the performance of the proposed ANN based AVC relay covered in section 7.7 is investigated. Two examples of results are depicted in Fig. 7.21 and Fig. 7.22. The former shows the process of voltage control of the considered network using the ANN based AVC relay assuming the voltage at bus 1 equals 90% of its nominal value, i.e. 90% of 33kV. Whereas, the latter shows the same but this time assuming the voltage magnitude of bus 1 is fixed at 110% of the nominal value. In both cases, it is assumed that a 4MW wind farm with a leading power factor of 0.98 is connected to the network. The variable load at bus 6 is then changed, as previously explained, from zero to a maximum of 4.5 MW and back again to zero. The power factor of the load in these cases is assumed 0.97 (lagging). As can be seen from Figs 7.21 and 7.22, the performance of the proposed ANN based relay is not affected by the variation of the voltage of the main source, i.e. the grid. These results are found to be similar to these obtained when the voltage at bus 1 is assumed equal to 1pu, as can be seen by comparing Figs. 7.21 and 7.22 with Fig. 7.8. The only observation is that in the process of simulation of the above-described operating conditions, the proposed AVC relay initiates tap-changing action(s) in such a way to compensate for the variation of the source voltage. This action is not shown on Figs. 7.21, 7.22 because it occurs before the variable loads in the network start to change. This indicates that the proposed ANN based AVC relay is capable of adapting itself to the variation of the source voltage, and hence managing to properly maintain the voltage of the network.

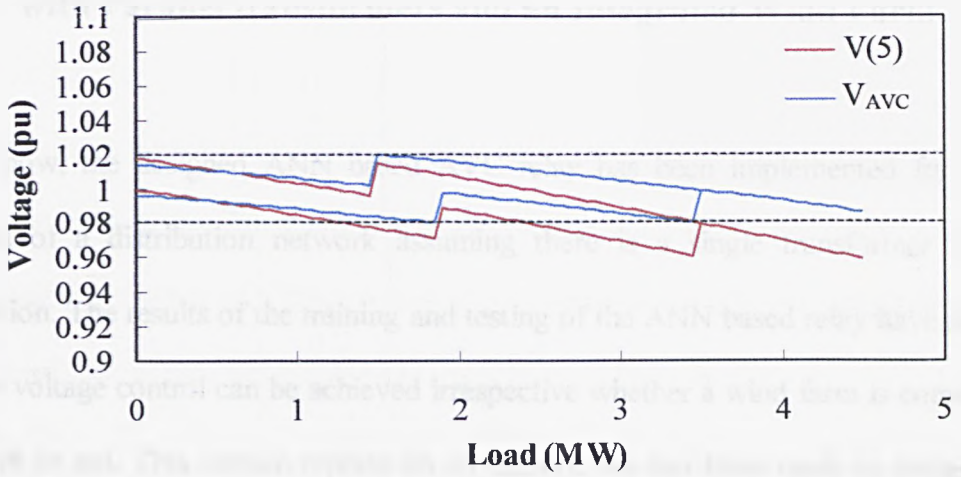

Fig. 7.21 Performance of ANN based AVC relay, network with EG and voltage of bus 1 equals 90% of the nominal. PF of EG = 0.98 (lead) and PF of load = 0.97 (Lag.)

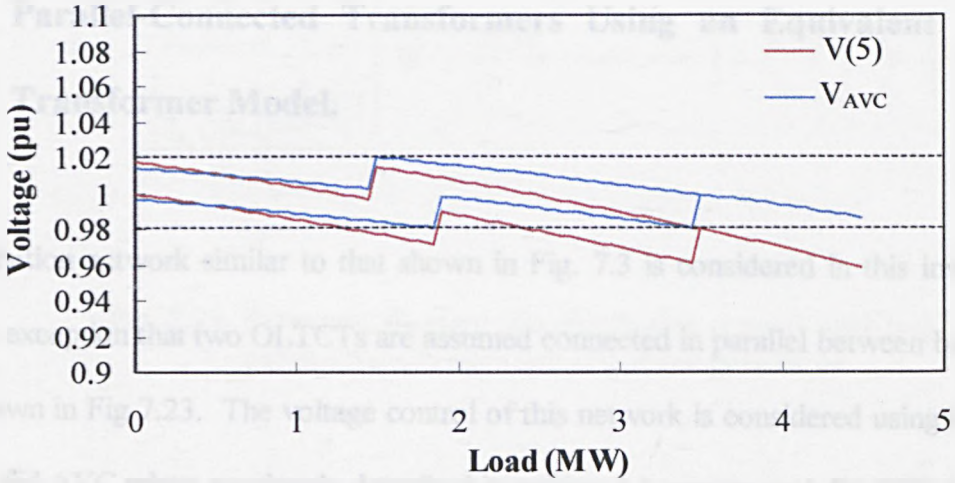

Fig. 7.22 Performance of ANN based AVC relay, network with EG and voltage of bus 1 equals 110% of the nominal. PF of EG = 0.98 (lead) and PF of load = 0.97 (Lag.)

7.11 Performance of the ANN Based AVC Relay on a Network with Parallel transformers and an Integrated Wind Farm

Until now, the designed ANN based AVC relay has been implemented for the voltage control of a distribution network assuming there is a single transformer in the main substation. The results of the training and testing of the ANN based relay have shown that a proper voltage control can be achieved irrespective whether a wind farm is connected to the network or not. This section reports on an attempt that has been made to design an ANN-based AVC relay suitable for the voltage control of a distribution network that includes a wind farm and parallel-connected transformers is reported.

7.11.1 The Training of ANN-Based AVC Relays for Two Parallel-Connected Transformers Using an Equivalent Transformer Model.

A distribution network similar to that shown in Fig. 7.3 is considered in this investigation with the exception that two OLTCTs are assumed connected in parallel between buses 1 and 2, as shown in Fig 7.23. The voltage control of this network is considered using two of the ANN based AVC relays previously described in section 7.3, one on each OLTCT. In order to prepare data for the training of the ANN based AVC relays, the two parallel OLTCTs are represented in a FORTRAN load flow program using a model based on replacing the two transformers by one equivalent transformer. For this purpose, it is assumed that both transformers have identical power ratings and identical tap positions. It is also assumed that both AVC relays initialise the operation of the corresponding tap changer simultaneously. The equivalent impedance of the two parallel OLTCTs is simply calculated as half the impedance of one transformer. It is also assumed that identical transformers at similar tap

positions equally share the total load current. Based on these assumptions, the network shown in Fig. 7.23 is used to prepare the training data for ANN based AVC relays, AVC1 and AVC2. For this purpose, the FORTRAN load flow program is modified to calculate the current through each OLTCT following each incremental change of load. Several load flow cases have been simulated including cases where the wind farm is assumed connected or disconnected. Based on a random selection of patterns the data file containing the results of the simulation is then equally divided into a training and test files.

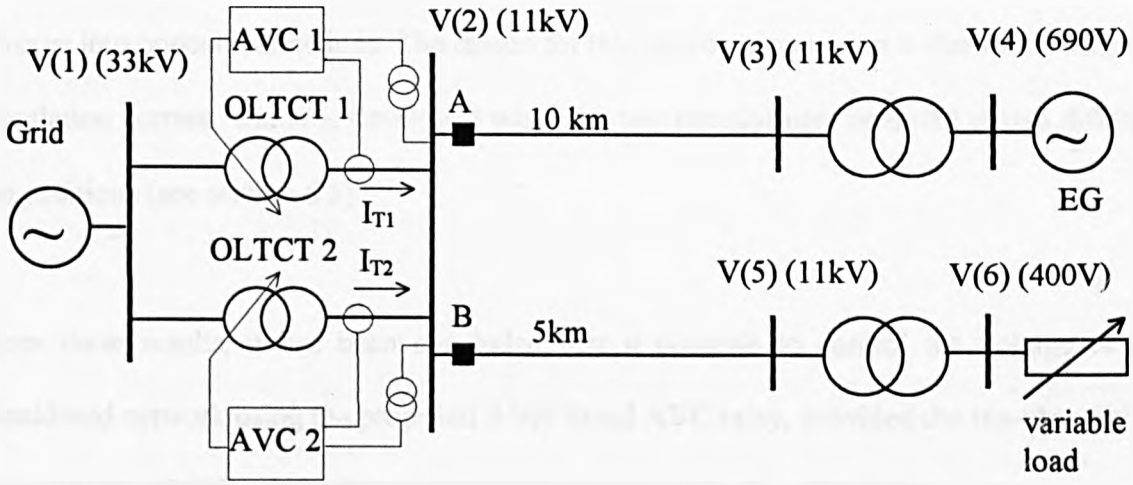

Fig. 7.23 Schematic diagram of a distribution network with two parallel transformers and embedded generators

The ANN, which has been previously described in section 7.3 is then trained and tested using the NeuralWorks software. Results of the training and testing are found to be almost the same as those obtained from the ANN based AVC relay that was trained for a network with a single transformer, as described in section 7.5.

The load flow program, originally developed with a provision of a single ANN based AVC relay, is modified to include two AVC relays which are accommodated using one ANN

subroutine. This modified program is then used to investigate the performance of the two ANN based AVC relays, AVC1 and AVC2. Two cases have been examined. In the first case, it is assumed that the two AVC relays initiate the operation of the tap-changing devices of both transformers simultaneously. The results have shown that the behaviour of the ANN based AVC relays for the two parallel OLTCTs is similar to that obtained for the single transformer previously discussed in section 7.7. In the second case, it is assumed that the operation of the tap-changing device of one transformer occurs after a time delay from that of the other. It is found in this case that the behaviour of the ANN based AVC model is not as it should be, because the operation of the tap-changing devices of the two transformers diverge into opposite directions. The reason for this improper operation is due to the effect of circulation current, which is developed when the two transformers operated at two different tap positions (see section 6.3).

From these results, it has been concluded that it possible to control the voltage of the considered network using the proposed ANN based AVC relay, provided the tap-changers of both parallel OLTCTs are initiated simultaneously by the proposed relays.

7.11.2 Consideration of the Inclusion of Circulating Current in the Training Data File

It has been shown in the previous section that the proposed ANN based AVC relay can properly control the voltage of a distribution network, including a wind farm and two parallel transformers, provided that tap changing occurs in both transformers simultaneously. However, in practice, owing to equipment tolerances, one of the transformers may operate to change its tap position before the other; resulting in circulating current flowing through the two transformers, as explained previously in chapter 6. In order to consider the effect of circulating currents in the design of an ANN based AVC relay, they are added to the input patterns in the training data file. This has been achieved by making the following modifications to the FORTRAN, load flow program:

(a) The program calculates the circulating currents in parallel transformers based on the tap ratio and impedance of transformers using equation 6.10. The real and imaginary components of these currents are then calculated.

(b) Each of the two parallel transformers is controlled using a separate AVC relay.

(c) The voltage of AVC relays is not calculated using the conventional relay, instead it is simply assigned the value of the calculated voltage of a remote busbar, for example the voltage of bus 5 in Fig. 7.23.

(d) The measured transformer voltages, currents (including the circulating currents) and the voltage of a remote bus are saved in a data file, as explained previously. As in the previous studies, the load is allowed to change from zero to its maximum value and back again to zero in incremental steps.

The voltage control of the network shown in Fig. 7.23 is then used to simulate several case studies that represent different operating conditions of the network. These case studies can be classified into three groups as shown in Table 7.3. The target voltage magnitude is assumed to be 0.99pu and a bandwidth of ± 2% of the nominal voltage is assumed. It is worth noting that during the simulation two sets of pairs of input/output patterns are saved successively in a data file following each incremental change of load. One set comprises the voltage magnitude of bus 2, real and imaginary components of the current through OLTCT1, the real and imaginary components of the circulating current and the voltage magnitude of bus 5. The second set of patterns includes the same signals, except that the real and imaginary components through OLTCT1 are replaced by the currents in OLTCT2, as shown in Table 7.4. For example, row 1 in Table 7.4 corresponds to OLTCT1 and row 2 corresponds to OLTCT2. Rows 5 and 6 correspond to the OLTCT1 and OLTCT2, respectively assuming that OLTCT2 operates before OLTCT1. Hence, as can be seen in Table 7.4, the circulating currents in both transformers are in opposite directions. It is therefore important that measurements related to both transformers are presented to the ANN for the cases when either of the OLTCTs is operated first, and hence included in the training data file.

Table 7.3 Simulated load flow cases to generate training data files for ANN.

Group	Case	Embedded gen.		Maximum load at bus 7.		Voltage limits
		MW	PF	MW	PF	
A	1	0	-	4.5	1.0	0.99 ± 2%
	2	0	-	4.5	0.95 (Lag.)	0.99 ± 2%
	3	0	-	4.5	0.9 (Lag.)	0.99 ± 2%
B	4	4	0.95 (lead)	4.5	1.0	0.99 ± 2%
	5	4	0.95 (lead)	4.5	0.95 (Lag.)	0.99 ± 2%
	6	4	0.95 (lead)	4.5	0.9 (Lag.)	0.99 ± 2%
C	7	4	1.0	4.5	1.0	0.99 ± 2%
	8	4	1.0	4.5	0.95 (Lag.)	0.99 ± 2%
	9	4	1.0	4.5	0.9 (Lag.)	0.99 ± 2%

Table 7.4 An example of an output data file for ANN training.

	V_2	I_{real}	I_{imag}	$I_{circul,\ real}$	$I_{circul,imaginary}$	$V_{avc\ desired}$
1	.99057	.01151	-.00609	.00000	.00000	.97031
2	.99057	.01152	-.00610	.00000	.00000	.97031
3	.99032	.01177	-.00626	.00000	.00000	.96957
4	.99031	.01178	-.00626	.00000	.00000	.96957
5	.99855	.01183	.00209	-.00416	-.83209	.97753
6	.99856	.01204	-.01483	.00416	.83209	.97753
7	.99839	.01209	.00199	-.00425	-.83204	.97689
8	.99839	.01230	-.01493	.00425	.83204	.97689
9	.99812	.01235	.00182	-.00434	-.83197	.97615
10	.99813	.01257	-.01510	.00434	.83197	.97615
11	.99787	.01261	.00165	-.00443	-.83189	.97541
12	.99787	.01283	-.01526	.00443	.83189	.97541
13	.99762	.01287	.00150	-.00452	-.83182	.97468

In practice, the operation of tap-changers of parallel OLTCTs can occur either simultaneously or with some time delay. In order to cater for these two possibilities, the case studies described in Table 7.3 are simulated for the two different conditions. Figures 7.24, 7.25, 7.26 depict the desired voltage of the AVC1 relay, V_{AVC1}, and the voltage of bus 5, V(5), corresponding to cases 3, 6, and 9 listed in Table 7.3, respectively. As can be seen in all these figures, the curves representing the profile of the voltage at bus 5 and the AVC1 relay voltage, V_{AVC1}, over lap and they therefore appear as a single curve. This behaviour is obvious as the relay voltage, V_{AVC1}, and similarly V_{AVC2}, are simply assigned the corresponding value of the voltage of bus 5, V(5), instead of using Equation (6.1) to calculate them.

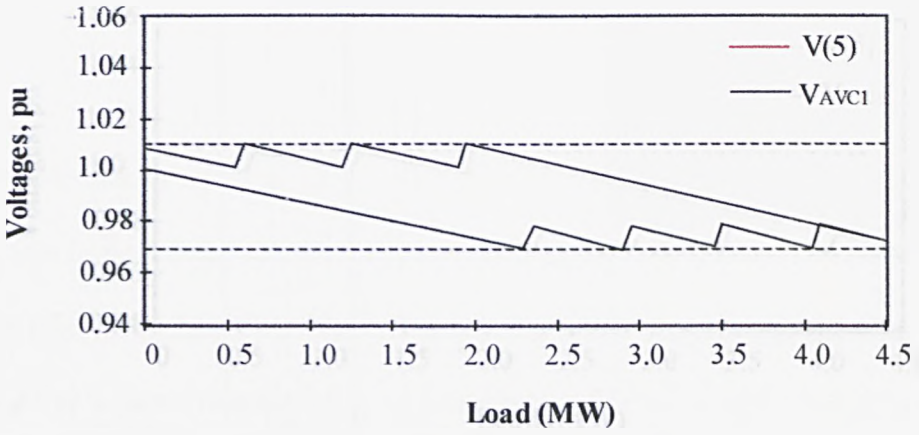

Fig. 7.24 Voltage control of the network shown in Fig. 7.23 corresponding to case 3 in Table 7.3, when the voltages, V_{AVC1} and V_{AVC2} are assumed equal to the voltage of bus 5.

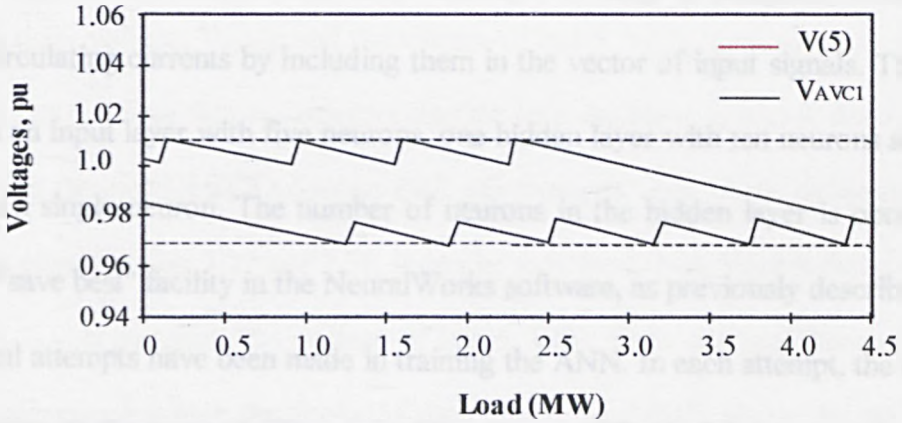

Fig. 7.25 Voltage control of the network shown in Fig. 7.23 corresponding to case 6 in Table 7.3, when the voltages, V_{AVC1} and V_{AVC2} are assumed equal to the voltage of bus 5.

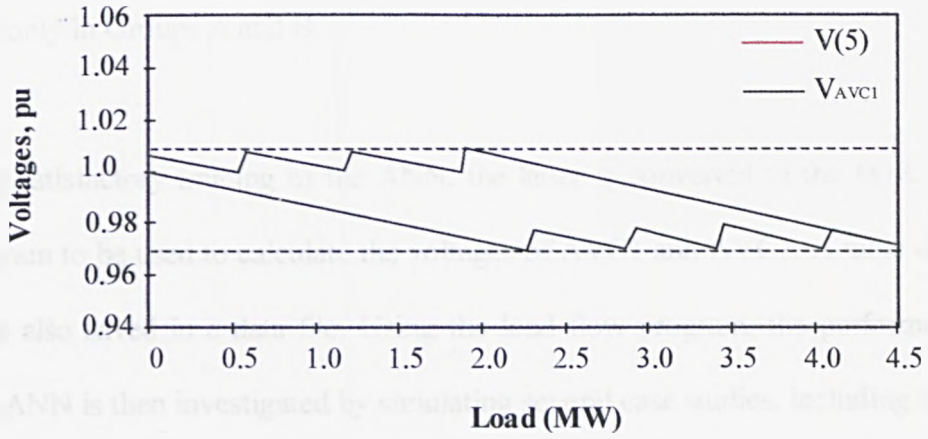

Fig. 7.26 Voltage control of the network shown in Fig. 7.23 corresponding to case 9 in Table 7.3, when the voltages, V_{AVC1} and V_{AVC2} are assumed equal to the voltage of bus 5.

Based on the above results a new ANN based AVC relay is designed, which takes into account circulating currents by including them in the vector of input signals. The new ANN comprises an input layer with five neurons, one hidden layer with ten neurons and an output layer with a single neuron. The number of neurons in the hidden layer is optimised to ten using the "save best" facility in the NeuralWorks software, as previously described in section 7.3. Several attempts have been made in training the ANN. In each attempt, the training data corresponding to the cases of either one of the groups of Table 7.3 or a combination of two or more groups is used. It has been found that the training, which is based on using individual groups, is very successful. The same has been observed when the training of the ANN is based on combined data related to Groups A and B. However, the training of the ANN based on using a combination of data related to Group C and those related to either A or B has not been successful. It seems that the general relationships among the training patterns in Group C are not coherent with those in Groups A and/or B, leading to the ANN being unable to generalise the relationships of the three groups combined together.

Therefore, the training of the ANN based AVC relay is performed using the training patterns contained only in Groups A and B.

Following satisfactory training of the ANN, the latter is converted to the FORTRAN load flow program to be used to calculate the voltages of AVC1 and AVC2. A table of the ANN weights is also saved in a data file. Using the load flow program, the performance of the proposed ANN is then investigated by simulating several case studies, including the network operating with or without the wind farm being connected to the network. In each of these cases, the variable load at bus 6 is changed from zero to maximum and back again to zero. The performance test has been conducted assuming simultaneous tap-changing operation of OLTCT1 and OLTCT2 as well as with a time delay. Examples of the results of the investigation are depicted in Figures 7.27, 7.28, and 7.29. These figures show the variation of the AVC1 relay voltage, V_{AVC1}, and the voltage of bus 5, V(5), in response to the change of the load at bus 6. These figures correspond to the case studies 3, 6, and 9, described in Table 7.3 assuming the two OLTCTs operate their tap-changers with a time delay between them. Let us first consider Figs 7.27 and 7.28. It can be seen from these figures that the AVC relay voltage, V_{AVC1}, is matching the voltage of bus 5, V(5). Thus, the amplitude of the latter is properly maintained within the limits of the control bandwidth shown by the two dashed lines in Figs. 7.27 and 7.28. A similar performance has also been observed regarding the AVC2 relay. The tap-changers of the parallel OLTCTs are allowed to operate at two different times, hence circulating current is induced each time the tap positions of the two transformers are different from each other, as previously explained in chapter 6. Nevertheless, it is observed that both tap-changers have successfully operated to the same tap position without being affected by the existence of circulating current.

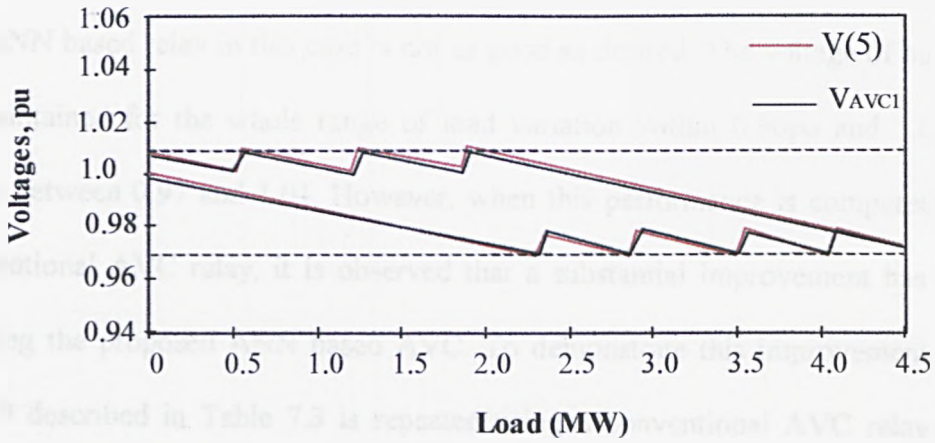

Fig. 7.27 Voltage control of the network using an ANN based AVC relay corresponding to the operation conditions of case 3 in Table 7.3

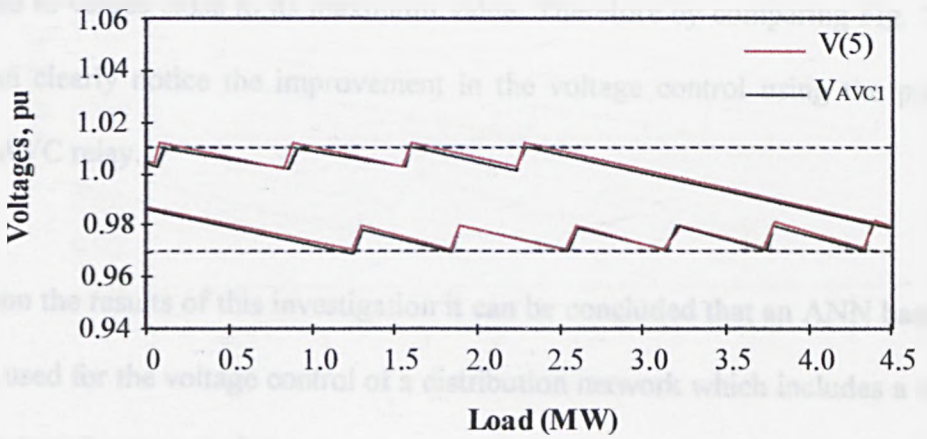

Fig. 7.28 Voltage control of the network using an ANN based AVC relay corresponding to the operation conditions of case 6 in Table 7.3

Fig. 7.29 corresponds, as mentioned above, to the network conditions described in case 9 in Table 7.3. In this case it is assumed that a 4MW of EG with unity power factor is connected to the network. This case belongs to group C which, as previously explained, has not been used for the training of the proposed ANN based AVC relay. As can be seen in Fig. 7.29 there is an error of approximately 0.008pu between the AVC1 relay voltage and the voltage

of bus 5 over the considered load variation. As can be seen in Fig. 7.29 the performance of the ANN based relay in this case is not as good as desired. The voltage of bus 5 in this case is maintained for the whole range of load variation within 0.96pu and 1.01pu instead of being between 0.97 and 1.01. However, when this performance is compared with that of a conventional AVC relay, it is observed that a substantial improvement has been achieved utilising the proposed ANN based AVC. To demonstrate this improvement, simulation of case 9 described in Table 7.3 is repeated using a conventional AVC relay with negative compounding. The result of this simulation is depicted in Fig. 7.30. It can be seen in Fig. 7.30 that the error between the AVC1 relay voltage and that of bus 5 is approximately 0.05pu resulting in the voltage of bus 5 being well below the lower limit of the control bandwidth to the degree that it becomes outside the specified statutory limits when the load at bus 6 is changed to values close to its maximum value. Therefore by comparing Fig. 7.29 with 7.30 one can clearly notice the improvement in the voltage control using the proposed ANN-based AVC relay.

Based on the results of this investigation it can be concluded that an ANN based AVC relay can be used for the voltage control of a distribution network which includes a wind farm and parallel transformers at the main substation. To achieve this, it is required to provide the ANN based relay with five signals comprising the magnitude of voltage of transformer terminals, the real and imaginary components of transformer current, and real and imaginary components of the circulating current flowing through the parallel transformers.

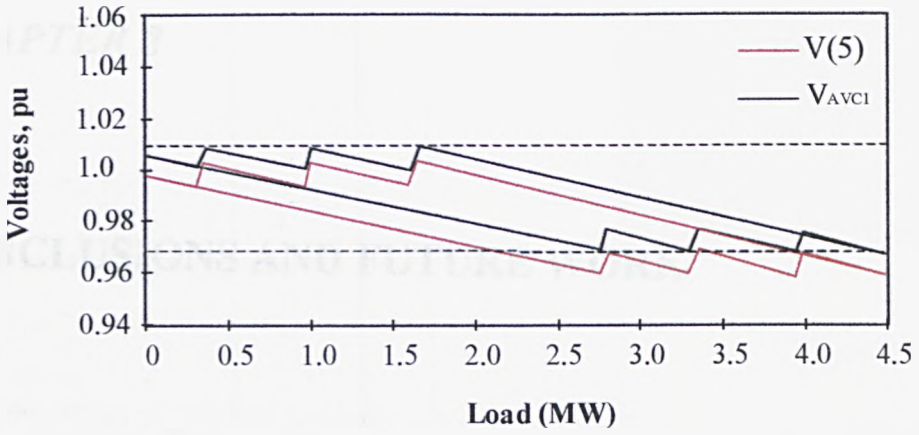

Fig. 7.29 Voltage control of the network using an ANN based AVC relay corresponding to the operation conditions of case 9 in Table 7.3

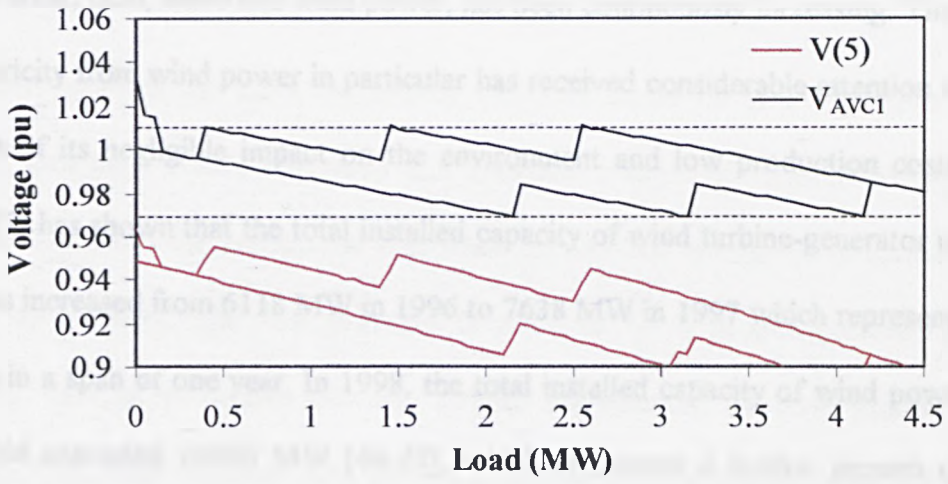

Fig. 7.30 Voltage control of the network using conventional AVC relay with negative compounding corresponding to the operation conditions of case 9 in Table 7.3

CHAPTER 8

CONCLUSIONS AND FUTURE WORK

8.1 Conclusions

Since the early 70's, electrical power generation derived from renewable energy sources, such as solar, tidal, wave and wind power, has been continuously increasing. The generation of electricity from wind power in particular has received considerable attention world-wide, because of its negligible impact on the environment and low production costs. A recent report [7] has shown that the total installed capacity of wind turbine-generator units world-wide has increased from 6118 MW in 1996 to 7638 MW in 1997 which represents a growth of 25% in a span of one year. In 1998, the total installed capacity of wind power plants in the world exceeded 10000 MW [46,47], which represents a further growth of 25%. In order to generate a significant amount of electricity using wind power, a number of wind power based generators are usually installed at one site constituting what is known as a wind farm. Generators, which are used to generate electricity from renewable energy sources, are usually integrated into utilities' networks at distribution voltage levels and they are commonly referred to as "Embedded Generators (EGs)".

Utilities' distribution networks (DNs) however, may not be properly designed to receive power from EGs. It has been reported that the integration of EGs into a DN could create safety as well as technical problems. Such problems include contribution to the fault

currents, stability and reliability problems, introduction of harmonics, voltage fluctuation, and problems with the automatic voltage control (AVC) of DNs.

In this work two main aspects related to the integration of wind power based embedded generators (WPBEGs) into a distribution network have been investigated:

(a) The effect of WPBEGs on the critical clearing time (CCT) of faults on load feeders and,

(b) The effect of WPBEGs on the operation of AVC relays, including compensation for the voltage drops along distribution feeders.

Protection schemes for DNs are usually designed based on two basic principles [16]. Namely, they must ensure selectivity of a minimum amount of disconnected equipment to isolate a fault from the system and they must operate fast enough to minimise damage to system components. The first principle is achieved by a proper co-ordination of the operating time of protective devices, usually implemented by time graded protection schemes. This, however, may lead to having operating times for the protective devices at the up-stream of a distribution feeder as high as 1.5 s [9]. When a wind farm is integrated into a DN the critical clearing time (CCT) of a fault on a load feeder is dictated, as explained in this thesis, by the stability of IGs at the wind farm. This CCT may, in many cases, become shorter than the time required for protective devices installed on the feeder to isolate the fault.

To investigate this problem it was necessary to be familiar with different types of embedded generation; particular emphasis being placed on the wind power based generators. Similarly, familiarity with the appropriate methods and tools that are commonly used in power system

studies was essential. The electromagnetic magnetic transient program (EMTP) has been employed to model a typical distribution network, which includes a wind farm. A model in EMTP, called the "Universal Machine (UM)" model, has been used to simulate the IGs at wind farms. The EMTP also allows representation of the mechanical side of a wind turbine-generator unit by an equivalent electrical circuit.

In order to compare the behaviour of EGs, which employ IGs, with that of EGs using synchronous generators (SGs), a distribution network that includes a gas turbine-generator unit has also been modelled using the EMTP program. A gas-turbine-SG unit has been simulated using a model in EMTP called the "Type95" model. This model allows the inclusion of the gas turbine, its associated governor and excitation controls in the simulation using a facility in EMTP called "Transient Analysis of Control Systems (TACS)".

The concept of CCT of faults for the cases when either embedded SGs or embedded IGs are integrated into a distribution network has been extensively discussed. It is well known that the CCT of faults in the case of embedded SGs is defined by the maximum rotor angle, above which SGs are considered unstable. In the case of embedded IGs, the concept of CCT is different from that related to SG. In this work, it is defined as the time below which the IG retains its pre-fault voltage after the removal of the fault. This however requires the setting of a minimum electromagnetic torque in the machine, which can overcome the external mechanical torque applied by wind on the machine rotor when the fault is isolated. When the CCT is not exceeded, the electromagnetic torque developed in the air-gap of the IG will be sufficient to retain its normal operation. This, in turn, does not cause a sustained voltage dip at the terminals of the machine. Otherwise, a sustained voltage dip occurs at the terminals of the IG and the latter is eventually isolated from the network by a trip signal

initiated from an associated protection device, such as under voltage, over current, or frequency relays.

The results of investigating the effects of WPBEGs on the CCT of a fault on a load feeder have revealed that there are conditions at which such a fault would lead to the disconnection of the IGs at the wind farm. Furthermore, the network would also be subjected to a voltage dip with amplitude lower than the statutory limits. It has been revealed that the CCT of faults, especially three phase faults, on a load feeder can be as low as 200ms for the system under consideration.

On the other hand, it has been found that the amount of injected power from a wind farm has a considerable effect on the CCT. The smaller the injected power is, the higher the CCT, and vice versa. The location of a fault on a load feeder has also an effect on the CCT. The CCT increases when a fault occurs at a greater distance from the substation. However, the highest CCT value found in this investigation is approximately 900ms. This value corresponds to a three phase to ground fault on a load feeder at a distance of 10 km from the substation and a minimum injected power of 1.2MW by the wind farm.

A comparison between the effect of embedded SGs and embedded IGs of the same capacity on the CCT has revealed that the former gives rise a greater CCT than that of the latter. For example, a three phase to ground fault on a load feeder close to the substation resulted a CCT for embedded SGs of 360 ms and 200ms for embedded IGs.

As mentioned previously, the second aspect of the investigation reported in this thesis has focused on the effects of the integration of WPBEGs on the operation of AVC relays, when compensation for the voltage drop across load feeders is considered. Consideration of the

latter is important, especially when load feeders are long enough to cause a substantial voltage drop. According to the IEC60038 [93], the statutory voltage limits for 33kV and 11kV distribution networks is ± 10% of the nominal voltage. When a 33kV/11kV substation is considered to supply electricity to a distribution network, the voltage at the 33kV side of transformers at the substation is allowed to vary within the statutory limits. Thus, if voltage control using the AVC relays at the substation do not consider the voltage drop across the 11kV load feeders, a substantial decrease of voltage at remote buses could be experienced. In this thesis the effect of WPBEGs on the performance of AVC relays, when a voltage drop in the load feeders is considered, has been investigated. The performance of conventional AVC relays, which can be based on positive and negative compounding settings, has been analysed. Prior to this, an overview of the main methods of voltage control of distribution networks has been provided. According to the basic principles, voltage control of a distribution network is usually achieved either indirectly, by injection of reactive power to the network, or directly, by adjusting the transformation ratio of transformers at distribution substations. The latter is commonly adopted in distribution networks using an on-load tap-changing transformer (OLTCT), whereby AVC relays are employed to automatically initiate the operation of the tap-changer of the OLTCT.

It has been demonstrated that the integration of WPBEGs may cause an error in the calculation of AVC relay voltages when compensation for voltage drop along load feeders is taken into account. This error is more likely to occur when negative compounding is used, as is normally the case for parallel connected transformers.

After identifying the problem, a new AVC relay based on the application of artificial neural networks (ANN) has been proposed. The design of an ANN based AVC relay has been achieved through the following steps:

(a) Generate a training data file using a specifically developed FORTRAN load flow program.

(b) Design, train and test the proposed ANN using the NeuralWorks software.

(c) Convert the trained ANN into FORTRAN code to act as an AVC relay

(d) Integrate the converted ANN code into the FORTRAN load flow program.

(e) Test the performance of the proposed ANN based AVC relay to control the voltage magnitude of a DN, which may or may not include a wind farm.

As mentioned above, in order for an ANN based AVC relay to operate properly, it must be properly trained. The proposed ANN based AVC relay is based on off-line training. Hence training data files have been prepared utilising a specifically developed load flow program using FORTRAN software. Using this program, voltage control of a distribution network that includes WPBEGs has been simulated. For this purpose, a model of a conventional AVC relay has been included in the load flow program to adjust the transformer tap ratio whenever the controlled voltage exceeds specified statutory limits due to the variation of loads. In order to properly control the voltage of the considered network, the relay compounding setting has been adjusted for the condition of connecting or disconnecting a wind farm.

An ANN has been designed for the voltage control of a DN, which includes a single transformer at a main substation and a wind farm connected to the substation through a feeder. The proposed AVC relay is based on "Multilayer Back-Propagation" ANN comprising an input layer with three input neurons, a hidden layer and an output layer with a single neuron to provide the voltage of the relay. It has been designed utilising special software called "NeuralWorks". The training of the ANN has been achieved by presenting it

with the training data files generated by the load flow program. Testing of the ANN has revealed satisfactory results. It has been found that it is sufficient to present the ANN with input signals, which are commonly used as inputs to conventional AVC relays, and yet obtain a good performance. Such signals include the magnitude of the transformer terminal voltage at the low voltage side and either the real and imaginary components of the transformer current or the transformer real and reactive powers.

After the ANN based AVC relay has been trained it is converted into a FORTRAN code and integrated into the specifically developed load flow program. The performance of the proposed AVC relay has been investigated by simulating voltage control of the considered network for the cases when a wind farm is connected or disconnected. The results from this simulation have shown that the ANN based AVC relay can provide a better performance compared with that of conventional AVC relays whether equipped with positive or negative compounding. One of the main advantages of the proposed ANN based AVC relay is that it does not include compounding settings similar to the conventional relay consequently removing the necessity of readjustment every time a wind farm is connected or disconnected from the network.

An ANN based AVC relay has also been developed for the voltage control of a distribution network that includes a wind farm as well as two parallel transformers at the main substation. It has been found that the same ANN based AVC relay used for a single transformer can also be trained and used for the voltage control of a network with two parallel transformers. However, this requires that the tap changing device of both transformers operate simultaneously. It has been found that such relay cannot work appropriately when one of the transformers operates before the other due to the effect of generated circulating current.

This problem is solved by modifying the ANN based AVC relay whereby the circulating current in parallel transformers has also been taken into account by including it as an input to the ANN. After the training of the modified ANN, its performance has been investigated by considering two parallel transformers controlled using two independent modified ANN based relays. It has been found that a stable operation of the two parallel transformers has been achieved. However, the voltage calculated by such an ANN based relay is found not always to be as accurate as desired. Nevertheless, the relay managed to properly control the voltage of the investigated network whether a wind farm was connected or not.

In summary, the dynamic effect of WPBEGs on the CCT of faults on load feeders has been investigated. An ANN based AVC relay has been designed which compensates for voltage drop across load feeders. Such a relay is characterised by not having compounding settings and therefore removes the necessity for readjustment (as the case with a conventional relay) and can at the same time be used when a wind farm is connected or disconnected to a distribution network.

Based on the obtained results, five technical papers have been presented at national and international conferences. One paper has been submitted for publication in one of the IEEE transactions, and is currently under consideration. Appendix (E) contains a list and copies of the published papers.

8.2 Future work

Regarding the investigation of the effects of integration of wind farms into a distribution network on the CCT of faults that may occur on load feeders, the problems that may rise due to such integration have been illustrated in this thesis. The following points are suggested for consideration in any future work:

(a) To simulate wind turbine-generator units utilising more detailed models. For example, it may worth considering modelling the mechanical components of a wind turbine using separate masses. There may be advantage by considering torsional and damping effects in the simulation.

(b) To find solutions to the problems highlighted in this thesis aiming at either eliminating or at least reducing their effects. For example an investigation may be suggested to address the implementation of dynamic reactive compensation techniques, such as SVC and STATCOM devices, and also the application of adjustable speed machines in wind turbine-generator units.

An ANN based AVC relay has been proposed for the voltage control of a distribution network with WPBEGs when the voltage drop along load feeders is examined. In any future work in this direction, the following may be suggested for consideration:

(a) Development of a more general ANN-based AVC relay model for the voltage control of DN that includes parallel transformers. For this purpose, it is suggested that the application of other types of artificial intelligent techniques is considered. This may provide the benefit of combining such as the "Fuzzy logic network" and ANN. This may help in the pre-processing of input signals or the automatic adjustment of weights

of an ANN in such a way to suit various operating conditions of the DN, i.e. whether EGs are connected or disconnected. Consequently, an improved performance of the ANN based AVC may be achieved.

(b) The proposed ANN based AVC relay has been developed, trained and tested in off-line mode utilising the specially obtained program "NeuralWorks". Its performance has been investigated using a specifically developed load flow program. The structure of the proposed ANN based relay has been identified, and a final table of weights has been obtained. It is therefore suggested for future work that the proposed ANN, and its table of weights is downloaded into a microprocessor. Then laboratory and field tests could be performed to confirm its performance.

References

[1] N Nichols, "The electrical considerations in cogeneration," IEEE Transaction on Industrial Applications, IA-21, 1985, pp 754-761.

[2] A R Mollah and S K Salman, "Fault location on an industrial co-generator - public electric supply interface," Proceedings of the 24th Universities Power Engineering Conference, UPEC'89, September 1989, UK, pp. 157 - 160.

[3] S K Salman and F Jiang, "Effects of wind power generation on the voltage control of utility distribution networks," Renewable Energy, Conference Publication No. 385, November 1993, pp. 196 - 201.

[4] R M G Castro, et al, "A wind park reduced-order model using singular perturbations theory," IEEE Transaction on Energy Conversion, Vol.11, No. 4, Dec. 1994.

[5] EPRI - Report No G5-6256, 1989, "Assessment of Wind Power Station Performance and Reliability," USA.

[6] L Freris, 1992, IEE Review, 38, pp. 155 - 1159.

[7] K Dodman, "Public opinion warms to wind power," International power generation, October 1998, pp. 16-17.

[8] P Gardner, et al, "Network connection of large wind turbines," Wind Energy Conversion, 17th BWEA wind energy conference, July 1995.

[9] W J S Rogers, "The parallel operation of generating plant within a regional electricity company's distribution network," IEE Colloquium on The Parallel Operation of Generating Plant Within A Public Electricity Supply Network, February 1991, pp. 1/1 - 1/9.

[10] Engineering Recommendation G.59/1, "Recommendations for the Connection of Embedded Generating Plant to the Regional Electricity Companies Distribution System," UK, 1991.

[11] S K Salman, F Jiang and W J S Rogers, "The effect of private generators on the voltage control of 11 kV networks and on the operation of certain protective relays," Proceedings of IEEE/NTUA Athens International Conference on Modern Power Systems, Athens, September 1993, pp 591-595.

[12] P A Nobile, "Power system studies for cogeneration: What's really needed?," IEEE Transaction on Industrial Applications, Vol. IA-23, 1987, pp 777-85.

[13] Y Pourcin, J Fourgous and B Battalia, "Technical and economic aspects of the connection of small generating plant to public MV and LV distribution networks operated by Electricite de France", ibid, Paper No a.02.

[14] H Kirkham and R Das, "Effect of voltage control in utility interactive dispersed storage and generation systems," IEEE Transaction on Power Apparatus & Systems, Vol. PAS-103, 1984, pp 2277-82.

[15] S K Salman, "Optimising system losses by effective communication between embedded generators and distribution networks," International conference and exhibition on Protecting electrical networks and quality of supply, ERA, London, January 1997.

[16] E Lakervi, E J Holmes, "Electricity distribution network design," IEE Power Engineering series 21, Peter Peregrinus Ltd., on behalf of the IEE, London, UK, 1995.

[17] F Jiang, "Voltage control of a distribution network with embedded generation," Thesis submitted to the Robert Gordon University for the degree of PhD, 1995.

[18] MANWEB Headquarters Engineering, "Voltage control of 33 kV transformers," Memorandum No. 108, August 1961.

[19] M Rahim, et al, "Application negative reactance compounding for automatic voltage control at multi-transformer substations," Proceedings of the 32nd Universities Power Engineering Conference, UPEC'97, Vol. 2, Manchester, UMIST, UK, September 1997, pp. 967 - 970.

[20] H W Dommel, "Electromagnetic transient program reference manual (EMTP theory book)," Bonneville Power Administration, Portland, USA, 1986.

[21] N Jenkins, "Embedded generation," IEE Power Engineering Journal, UK, June 1995, pp. 145 - 150.

[22] S Russell, "Combined heat and power in Britain," The combined generation of heat and power in Great Britain and the Netherlands (Stockholm: NUTEK, 1994), report R1994:29, [WWW] http://www.uow.edu.au/arts/sts/srussell/ReportMH4-93.html, 1996.

[23] J W Pope, "Parallel operation of customer generation," IEEE Transaction on Industrial Applications, Vol. IA-19, No. 1, January 1983, pp 32-36.

[24] T Kenneth, "EUN/APEM training series: Laying down the law" Energy Management Training Series, Energy User News, USA, August 1999, [WWW] http://www.energyusernews.com/0899test.htm.

[25] W J S Rogers, "Overview of embedded generators in public electricity networks," IEE Colloquium on The Effective Response of A Public Electricity network to Independent Generators, April 1993, pp. 1/1 - 1/5.

[26] B M Weedy, "Electric power systems, third edition" Published by John Willey and Sons Ltd, UK, December 1987.

[27] M A Pierce "A UK Strategy for combined heat and power," The Combined Heat and Power Association, London, UK, July 1996, [WWW] http://www.energy.rochester.edu/uk/chpstrategy.htm.

[28] A R Wallace and S A Stepleton, "Renewable energy generation schemes embedded in rural grid systems," 30th Universities Power Engineering Conference, UPEC'95, UK, September 1995, pp 609 - 612.

[29] "Information on the Non-Fossil Obligation for Generators of Electricity from Renewable Energy Sources," Fifth Round of Bidding - NFFO-5, Renewable Energy Bulletin No. 7, Department of Trade and Industry, November 1997.

[30] S K Salman and A R Mollah, "Factors influencing the interconnection between private generators and public network," Proceedings of the 24th Universities Power Engineering Conference, UPEC'89, 1989, pp. 69 - 72.

[31] S K Salman and W J S Rogers, "The impact of integrating embedded generation into utilities' distribution networks," ERA Technology Conference on Protecting Electrical Networks and quality of Supply in a De-regulated Industry, February 1995, pp. 9.5.1 - 9.5.8.

[32] "Power UK : Renewables," Published by the Financial Times Business Ltd, Issue No. 62, 29 April 1999, UK, p. 10 - 13.

[33] D Elliott, "Prospects for renewable energy and green energy markets in the UK," Renewable Energy, Vol. 16, Issues 1-4, 4 January 1999, pp 1268-1271.

[34] U Desideri and Francesco Di Maria, "Simulation code for design and off design performance prediction of geothermal power plants," Energy Conversion and Management, Vol. 41, Issue 1, January 2000, pp. 61-76.

[35] A Sayigh, "Renewable energy - the way forward, " Applied Energy, Vol. 64, Issues 1-4, September 1999, pp. 15-30.

[36] Y Diab and G Achard, "Energy concepts for utilisation of solar energy in small and medium cities: the case of Chambéry," Energy Conversion and Management, Vol. 40, Issue 14, September 1999, pp. 1555-1568.

[37] P Menanteau, "Learning from variety and competition between technological options for generating photovoltaic electricity," Technological Forecasting and Social Change, Vol. 63, Issue 1, January 2000, pp. 63-80.

[38] J C Hollick, "Solar co-generation panels, " Renewable Energy, Vol. 15, Issues 1-4, September 1998, pp. 195-200.

[39] M Oliver and T Jackson, "The market for solar photovoltaics, " Energy Policy, Vol. 27, Issue 7, July 1999, pp. 371-385.

[40] T Price and D Probert, "Harnessing hydropower: a practical guide," Journal of Applied Energy, Vol. 57, No. 2/3, June 1997, pp.175-251.

[41] A V Bridgwater, et al, "An overview of fast pyrolysis of biomass," Journal of Organic Geochemistry, Vol. 30, No. 12, December 1999, pp. 1479-1493.

[42] K Maniatis and E Millich, "Energy from biomass and waste: the contribution of utility scale biomass gasification plants, " Journal of Biomass and Bioenergy, Vol. 15, No. 3, September 1998, pp 195-200.

[43] V Valtchev, et al, "Autonomous renewable energy conversion system," Renewable Energy, Vol. 19, Issues 1-2, January 2000, pp. 259-275.

[44] G Bellarmine and J Urquhart, "Wind energy for the 1990s and beyond," Energy Conversion and Management, Vol. 37, Issue12, December 1996, Pages 1741-1752.

[45] S Heier, "Wind energy conversion systems," Published by John Wiley and Sons Ltd, Chichester, UK, 1998.

[46] P Gipe, "Overview of worldwide wind generation," [WWW] http://rotor.fb12.tu-berlin.de/overview.html.

[47] S Krohn, "Danish wind energy 4th quarter 1998," Wind Power Note, [WWW] http://www.windpower.dk/publ/index.htm.

[48] Cranfield University, "Current wind technology: Developments in the UK, " Wind energy pages. [WWW] http://www.cranfield.ac.uk/sme/ppa/wind/lectuknow.htm.

[49] The British Wind Energy Association, " New in 2000 projects commissioned," BWEA Winfarms of the UK: New projects in 2000. [WWW] http://www.bwea.com/map/2000.html.

[50] N Jenkins, "Engineering wind farms," Power energy journal, April 1993, pp. 53-60.

[51] D Richardson and G McNerney, "Wind energy systems," Proceedings of the IEEE, Vol.81, No.3, 1993, pp.378-389.

[52] The British Wind Energy Association, "Wind energy technology," December 1999, [WWW] http://www.bwea.com/ref/tech.htm.

[53] Danish Wind Power Association, "Guided Tour on Wind Energy," February 2000, [WWW] http://www.windpower.dk/tour/index.htm.

[54] P M Anderson and A. A. Fouad, 'Power System Control and stability,' Iowa University Press, 1977.

[55] C Johnson and R Smith, "Dynamics of wind generators on electric utility networks," IEEE Transaction on Aerospace and Electronic Systems, Vol. AES-12, No. 4, July 1976, pp. 483 - 493.

[56] T Wakui, et al, "Effect of operating methods of wind turbine generator system on net power extraction under wind velocity fluctuations in fields," Renewable Energy, Vol. 16, Issues 1-4, January 1999, pp. 843-846.

[57] E Hinrichsen and P Nolan, "Dynamic and stability of wind turbine generators," IEEE transactions on Power Apparatus and Systems, Vol. PAS-101, No. 8, August 1982, pp. 2640 - 2648.

[58] J Patton and D Curtice, "Analysis of utility protection problems associated with small wind interconnections," IEEE Transactions on Power Apparatus and Systems, Vol. PAS-101, No. 10, October 1982, pp. 3957 - 3966.

[59] R Dugan and D Rizy, "Electric distribution protection problems associated with the interconnection of small, dispersed generation devices," IEEE Transactions on Power Apparatus and Systems, Vol. PAS-103, No. 6, June 1984, pp. 1121-1127.

[60] H Kirkham and R Das, "Effects of voltage control in utility interactive dispersed storage and generation systems," IEEE Transactions on Power Apparatus and Systems, Vol. PAS-103, No. 8, August 1984, pp. 2277-2282.

[61] J Herrera, et al, "Harmonics generated by two variable speed wind generating systems," IEEE Transactions on Energy Conversion, Vol. 3, No. 2, June 1988, pp. 267-273.

[62] K Jensen, "Connection of wind turbines and wind farms to a distribution system," proceedings of the 10th International Conference on Electricity Distribution, CIRED 1989, May 1989, pp. 446 - 449.

[63] S K Salman, et al, "The impact of addition of private generator(s) on voltage control of 11kv network," Proceedings of the 27th Universities Power Engineering Conference, UPEC'92, September 1992, pp. 530 - 533.

[64] S K Salman and F Jiang, "Comparison between the effects of embedded synchronous and induction generators on the voltage control of a distribution network," Proceedings of the 28th Universities Power Engineering Conference, UPEC'93, UK, September 1992, pp. 401 - 404.

[65] S K Salman, et al, "Investigation of using remotely connected embedded generators to regulate local voltage network," Proceedings of the 29th Universities Power Engineering Conference, UPEC'94, UK, September 1994, pp. 90 - 93.

[66] L M Craig and N Jenkins, "Impact of a medium sized wind turbine on a weak rural network," Proceedings of the 17th BWEA Wind Energy Conference, UK, July 1995, pp. 333 - 338.

[67] N Jenkins, "Some aspects of the electrical integration of wind turbines," Proceedings of the 17th BWEA Wind Energy Conference, UK, July 1995, pp. 149 - 154.

[68] T Davies, et al, "Integration of wind turbines into low voltage networks," Proceedings of the 30th Universities Power Engineering Conference, UPEC'95, September 1995, pp. 567 - 570.

[69] M Checksfield and M Redfern, "Assessment of embedded generator stability when connected to a HV utility distribution system," Proceedings of the 30th Universities Power Engineering Conference, UPEC'95, UK, September 1995, pp. 219-222.

[70] S K Salman, et al, "Investigation of the effect of AVC relay settings on the power losses of distribution networks with embedded generation," Proceedings of the 30th Universities Power Engineering Conference, UPEC'95, UK, September 1995, pp. 199-202.

[71] N Jenkins and G Strbac, "Effects of small embedded generation on power quality," IEE Colloquium on "Issues on Power Quality", Warwick, UK, November 1995, pp. 6/1 - 6/4.

[72] M Bruntt, et al, "Incorporation of wind power in the East Danish power system," Proceedings of the IEEE Power Tech.'99 Conference, Budapest, Hungary, August/September 1999, pp.

[73] T Ackermann, et al, "Embedded wind generation in weak grids, economic optimisation and power quality simulation," Renewable Energy, Vol. 18, Issue 2, October 1999, pp. 205-221.

[74] J O G Tande, "Exploitation of wind-energy resources in proximity to weak electric grids, " Applied Energy, Vol. 65, Issues 1-4, April 2000, pp. 395-401.

[75] D Kinh and P Pham, "Cogeneration application: interconnection of induction generators with public electric utility," 35th Annual Rural electric power conference, April 1991, pp. d4/1 - D4/7.

[76] J Machowski, et al., "Power system dynamic and stability," Published by John Wiley & Sons Ltd, Chichester, UK, 1997.

[77] A R Bergen, "Power systems analysis," Prentice-Hall series in electrical and computer engineering, Prentice-Hall, London, 1986.

[78] J Arrillaga, et al., "Computer modelling of electrical power systems," Published by John Wiley & Sons Ltd, Chichester, UK, 1983.

[79] W D Stevenson, "Elements of power system analysis," International Student Edition, Published by McGraw-Hill international book company, 1982.

[80] N C Smith, P A Crossley, "Network equivalent for the transient simulation of power system sources," Proceedings of the 26th Universities Power Engineering Conference, UPEC'91, Brighton, UK, September 1991, pp. 706 - 709.

[81] L P Cavero, "Computed Aided/Evaluation and Application of Distance Relays," Proceedings of the 5th International Conference on Developments in Power System Protection (Conf. Publ. No. 368), IEE, London, 1993, pp. 199-202.

[82] E A Leonidaki, et al, "A physical laboratory model of a thyristor controlled series capacitor," Proceedings of the 33rd Universities Power Engineering Conference, UPEC'98, Edinburgh, UK, September 1998, Vol. 1, pp. 138 - 141.

[83] G T Heydt, "Computer analysis methods for power systems," Published by Macmillan publishing Company, USA, 1986.

[84] H W Dommel, "Digital computer solution of electromagnetic transients in single and multiphase networks," IEEE Transaction on Power Apparatus and Systems, Vol. PAS-88, April 1969, pp. 388-399.

[85] DCG/EPRI EMTP User Support and Maintenance Centre, "EMTP historical notes," Ontario Hydro Services Company, Canada, [WWW] http://www.emtp96.com/history.htm.

[86] K U Leuven EMTP Centre, "Alternative Transient Program (ATP) Rule Book," Belgium, July 1987.

[87] L Dude, "Users guide to MODELS in ATP," DEI, Oregon, USA, April 1996.

[88] E Kreyszig, "Advanced engineering mathematics," Published by John Wiley and Sons Ltd., Singapore, 1993.

[89] J R Marti, "Accurate modelling of frequency-dependant transmission lines in electromagnetic transient simulation," IEEE Transaction on Power Apparatus and Systems, Vol. PAS - 101, No. 1, 1982, pp. 147 - 155.

[90] A Semlyen and A Dabuleanu, "Fast and accurate switching transient calculations on transmission lines with ground return using recursive convolutions," IEEE Trans. on Power Apparatus and Systems, Vol. PAS-94, March 1975, pp. 561 - 571.

[91] H K Lauw and W S Meyer, "Universal machine modelling for the representation of rotating electric machinery in an electromagnetic transients program," IEEE Trans. on Power Apparatus and Systems, Vol. PAS-101, June 1982, pp. 1342 - 1351.

[92] R K Aggarwal, et al, "Computer modelling of series-compensated EHV transmission systems," IEE Proceedings, Vol. 131, Pt C, No. 5, September 1984, pp. 188 - 196.

[93] IEC Publication 60038, "IEC standard voltage", Switzerland, 1983.

[94] British Standard, "Voltage characteristics of electricity supplied by public distribution systems," BS EN 50160, 1995.

[95] Engineering recommendation G5/3, "Limits for harmonics in the UK electricity supply system," Engineering Association, UK, 1976.

[96] H Cotton and H Barber, "The transmission and distribution of electrical energy," Published by Hodder and Stoughton, London, UK, 1970.

[97] R J Stephen, "Capacitor control applications," IEEE Transaction on Industry Applications, Vol. IA-20, No. 1, January 1984, pp. 131- 136.

[98] B Adkins and R G Harley, "The general theory of alternating current machines," Published by Chapman and Hall Ltd, UK, 1979.

[99] C Bayliss, "Transmission and Distribution Electrical Engineering," Published by Butterwotrh-Heinemann, UK, 1996.

[100] A C Franklin and D P Franklin, " The J&P Transformer Book," 11th Edition, Published by Butterworth & Co. Ltd., UK, 1983.

[101] G N Patchett, "Automatic Voltage Regulators and Stabilizers," Third Edition, Published by Pitman Press, Bath, UK, 1970.

[102] British Standard, "On-load tap-changers," BS4571, 1994.

[103] M A Laughton and M G Say, "Electrical Engineer's Reference Book," 15th edition, Published by Butterworth-Heinemann, 1993.

[104] M E Roberts and W G Ashman, "A thyristor assisted mechanical on-load tap-changer," Proceedings of IEE Conference on power thyristors and their applications, 1969, pp. 185 - 192.

[105] G H Cooke, K T Williams, "New thyristor assisted diverter switch for on load transformer tap changers," IEE proceedings-B, Vol. 139, No. 6, November 1992, pp. 507 - 511.

[106] J Arrillaga and R M Duke, "A static alternative to the transformer on-load tap-changer," IEEE Trans. on Power Apparatus and Systems, Vol. PAS-99, No. 1, Jan/Feb 1980, pp. 86 - 91.

[107] K A Krishnamurthy and R M Mathur, "Improvement in a thyristor controlled static on-load tap-changer for transformers," IEEE Trans. on Power Apparatus and Systems, Vol. PAS-101, No. 9, September 1982, pp. 3091 - 3096.

[108] F Q Yousaf-Zai and D O'Kelly, "Transformer Tap-changer using thyristor switching," proceedings of the 23rd UPEC, Trent Polytechnic, Nottingham, UK, September 1988.

[109] Do-Hyun Jang, Gyu-Ha Choe, "Step-Up/Down AC voltage regulator using transformer with tap-changer and PWM AC chopper," IEEE Trans. on Industrial Electronics, Vol. 45, No. 6, December 1998, pp. 905 - 911.

[110] R Shuttleworth, et al, "An improved on-load tap changing scheme," Proceedings of 29th Universities Power Engineering Conference, UPEC'94, Vol. 2, Galway, Ireland, September 1994, pp. 633 - 636.

[111] X Tian, et al, "Development of a novel snubber circuit for on-load GTO assisted tap changer," International Journal of Electronics, Vol. 81, No. 5, November 1996, pp. 617 - 627.

[112] R Shuttleworth, et al, "A novel thyristor-assisted tap changer scheme," Proceedings of the 14th CIRED International Conference on Electricity Distribution, Part 1, Birmingham, UK, June, 1997, pp. 1.28.1 - 1.28.5.

[113] R S Ramshaw, "Power electronics semiconductor switches," Second edition, Published by Chapman and Hall, London, 1993.

[114] C C Johnson, "Dynamics of wind generators on electricity utility systems," IEEE Transaction on Aerospace and Electric systems, Vol. AES-12, No. 4, July 1979, pp. 483 -493.

[115] O Wasunczuk, et al, "Dynamic behaviour of a class of wind turbine generators during random wind fluctuations," IEEE Transaction on power apparatus and systems, Vol. PAS-100, No. 6, June 1981, pp. 2837 - 2845.

[116] A I Estanqueiro, et al, "Modelling the integration of wind parks onto weak grids" Proceedings of the 17th BWEA wind energy conference, UK, July 1995, pp. 167-172.

[117] F A Reis, et al, "Including a wind energy conversion system model in electromagnetic transients program" Proceedings of IPST'95, International Conference on Power Systems Transients, Lisbon, September 1995, pp. 243 - 248.

[118] W Q Jeffries, et al, "Development of dynamic models for no storage wind/diesel systems," Proceedings of the 17th BWEA wind energy conference, UK, July 1995, pp. 111 - 116.

[119] M Papadopoulos, et al, "Simulation and analysis of small and medium size power systems containing wind turbines," IEEE Transaction on power systems, Vol. 6, No. 4, November 1991, pp. 1453 - 1458.

[120] A I Estanqueiro, et al, "The development and application of a model for power output fluctuations in a wind park," Proceedings of the European Community Wind Energy Conference, Lubeck, Germany, March 1993, pp. 798 - 801.

[121] J Pakkolainen, et al, "Simulation of a radial MV/LV electricity grid voltage associated with wind power induction generator," Proceedings of the 17th BWEA wind energy conference, UK, July 1995, pp. 155 - 160.

[122] P Gardner, "Network connection of large wind turbines," Proceedings of the 17th BWEA wind energy conference, UK, July 1995, pp. 161 - 166.

[123] R M G Castro and J M Ferreira de Jesus, "A wind park reduced-order model using singular pertubations theory," IEEE Trans. on energy conversion, Vol. 11, No 4, December 1996, pp. 735 - 741.

[124] S K Salman and I M Rida, "Investigating the electrical integration of wind power based embedded generation using ATP," Proceedings of the 33rd Universities Power Engineering Conference, UPEC'98, Edinburgh, UK, September 1998, pp. 407 - 410.

[125] S K Salman and I M Rida, "Impact of integration of wind farms into a utility network on relay settings of the utility feeders," Proceedings of the ERA Technology's International Conference "Quality and Security of Supply in Electrical Networks," London, UK, February 1999, pp. 2.3.1 - 2.3.8.

[126] S K Salman and I M Rida, "Investigating the electrical integration of wind power based embedded generation into utilities' networks," Proceedings of the IASTED

International conference of Power Energy Systems, Las Vegas, USA, November 1999, pp. 134 - 139.

[127] A E Efthymiadis, "Power system dynamics and transient stability calculations," MSc course notes on "Power system dynamics and control," University of Manchester Institute of Science and Technology (UMIST), Manchester, UK, 1996.

[128] M S Sarma, "Electric machines, steady-state theory and dynamic performance," West publishing company, USA, 1985.

[129] J Hertz, et al, "Introduction to the theory of neural computation," Published by Addison-Wesley publishing Co., Redwood City, California, USA, 1991.

[130] R Aggarwal and Y Song, "Artificial neural networks in power systems: Part 1, General introduction to neural computing," IEE Power Engineering Journal, June 1997, pp. 129 - 134.

[131] T Fukuda and T Shibata, "Theory and applications of neural networks for industrial control systems," IEEE Transactions on Industrial Electronics, Vol. 39, No. 6, December 1992, pp. 472 - 489.

[132] P Wasserman, "Neural computing: theory and practice," Published by Van Nostrand Reinhold, New York, USA, 1989.

[133] J Rogers, "Object-oriented neural networks in C++," Published by Academic Press Inc., USA, 1997.

[134] NeuralWare, "Neural Computing: A technology handbook for NeuralWorks Professional II/Plus and NeuralWorks Explorer," Published by Aspen Technology Inc., USA, 1998.

[135] G Orr and Klaus-Robert Muller, "Neural Networks: Tricks of the trade," Published by Springer-Verlag, Berlin Heidelberg, Germany, 1998.

[136] J McShane, "An introduction to neural nets," Hewlett-Packard Journal, February

1992, pp. 62 – 65.

[137] S Halpin and R Burch, "Applicability of neural networks to industrial and commercial power systems: a tutorial overview," IEEE Transactions on Industry Applications, Vol.33, No. 5, September/October 1997, pp. 1355 – 1361.

[138] R Aggarwal and Y Song, "Artificial neural networks in power systems, Part 3: examples of application in power systems," IEE Power Engineering Journal, December 1998, pp. 279 - 287.

[139] S K Salman and I M Rida, "Application of artificial neural networks for the voltage control of distribution networks," Proceedings of the 34th Universities Power Engineering Conference, UPEC'99, Leicester, UK, September 1999, pp. 529 – 532

[140] S K Salman and I M Rida, " ANN-based AVC relay for voltage control of distribution network with and without embedded generation," IEEE Proceedings of the DRPT'2000 Conference, City University, London, UK, April 2000, pp.263-267.

[141] M Daneshdoost, et al., "Neural network with Fuzzy srt-based classification for short-term load forecasting," IEEE Transaction on power systems, Vol. 13, No 4, November 98, pp 1386 - 1391.

[142] W B Su, et al, "A fault detection technique for composite transmission circuits using artificial neural networks," ," Proceedings of the 32nd Universities Power Engineering Conference, UPEC'97, Vol. 2, UK, September 1997, pp. 291 - 294.

[143] W Qi, et al, "Distance protection using an artificial neural network," Proceedings of the sixth international conference on "Developments in power system protection", Nottingham, UK, March 1997, pp. 286 - 290.

[144] T S Sidhu, H Singh, and M S Sachdev, "An artificial neural network for directional comparison relaying of transmission lines," Proceedings of the sixth international conference on "Developments in power system protection", Nottingham, UK, March 1997, pp. 282-285.

[145] P Ye, et al, "Inteligent phase comparison carrier protection," Proceedings of the sixth international conference on "Developments in power system protection", Nottingham, UK, March 1997, pp. 295- 298.

[146] D V Coury and D C Jorge, "Artificial neural network approach to distance protection," IEEE Transactions on Power Delivery, Vol. 13, No. 1, January 1998, pp. 102-108.

[147] Q Y Xuan, et al, "a neural network based protection technique for combined 275kV/400kV double circuit transmission lines," Neurocomputing, Volume 23, Issues 1-3, December 1998, Pages 59-70.

[148] Y H Song, "Genetic algorithm based neural networks applied to fault classification for EHV transmission lines with a UPFC," Proceedings of the sixth international conference on "Developments in power system protection", Nottingham, UK, March 1997, pp. 278 - 281.

[149] Z Q Bo, et al, "Non-communication protection of transmission line based on genetic evolved neural network," Proceedings of the sixth international conference on "Developments in power system protection", Nottingham, UK, March 1997, pp. 291- 294.

[150] D J Sobajic and Yoh-Han Pao, "Artificial neural-net based dynamic security assessment for electric power systems," IEEE Transactions on Power Systems, Vol. 4, No. 1, February 1989, pp. 220 - 228.

[151] M Aggoune, et al, "Preliminary results on using artificial neural networks for security assessment," IEEE Transaction on power systems, Vol. 6, No. 2, May 1991, pp. 890- 896.

[152] Feng-Chang Lu and Yuan-Yih Hsu, "Fuzzy dynamic programming approach to reactive power/voltage control in a distribution substation," IEEE Transaction on power systems, Vol. 12, No. 2, May 1997, pp. 681 - 688.

[153] H P Schmidt, "Application of artificial neural networks to the dynamic analysis of

the voltage stability problem," IEE Proceedings: Generation, Transmission, and Distribution, Vol. 144, No. 4, July 1997.

[154] D M Monro, "Fortran 77," Published by Edward Arnold (Publishers) Ltd., London, 1982.

[155] E Koffman and F Friedman, "Fortran with engineering applications," Fifth edition, Published by Addison-Wesley Publishing Company, Inc., USA, 1993.

Appendix A

The Newton-Raphson Method for Load Flow Calculation

The Newton-Raphson method is a well known iterative method for finding the roots of an equation such as $f(x) = 0$. The method can be illustrated assuming that after iteration k an estimated value of x^k for the solution of $f(x)$ is calculated and the associated error is equal to Δx^k. Thus, the exact solution will be $(x^k + \Delta x^k)$, so that:

$$f(x^k + \Delta x^k) = 0 \qquad \text{(a.1)}$$

Expanding the left had side of (a.1) into Taylor series at x^k yields:

$$f(x^k) + \Delta x^k \left(\frac{df}{dx}\right)^k + \frac{1}{2}(\Delta x^k)^2 \left(\frac{d^2 f}{dx^2}\right)^k + \ldots = 0$$

Provided that the error is relatively small, the terms containing (Δx^k) to the power 2 and higher can be ignored, so that:

$$f(x^k) + \Delta x^k \left(\frac{df}{dx}\right)^k \approx 0$$

Thus, the approximate value of the error will be:

$$\Delta x^k \approx - \frac{f(x^k)}{\left(\frac{df}{dx}\right)^k}$$

An improved approximation of the true solution ($x^k + \Delta x^k$) will then be given by:

$$x^{k+1} \approx x^k - \frac{f(x^k)}{\left(\frac{df}{dx}\right)^k} \qquad \text{(a.2)}$$

Equation (a.2) is the Newton-Raphson algorithm for the solution of a one-dimensional equation. To apply this algorithm to a multi-dimensional equation, assume that such an equation is given as:

$$\mathbf{f(X)} = 0 \qquad \text{(a.3)}$$

where **X** is the vector of variables [x_1, x_2, x_3, ..., x_n].

If $\mathbf{X^k}$ is the estimate for the solution at iteration k and $\Delta\mathbf{X^k}$ is the corresponding error, then the true solution is ($\mathbf{X^k}+\Delta\mathbf{X^k}$) and:

$$\mathbf{f(X^k}+\Delta\mathbf{X^k}) = 0 \qquad \text{(a.4)}$$

Expanding the left side of (a.4) as a Taylor series about $\mathbf{X^k}$ and neglecting the higher derivative terms, results the following:

$$\mathbf{f}_1(\mathbf{X^k}) + \Delta x_1 \frac{\partial \mathbf{f}_1}{\partial x_1} + \Delta x_2 \frac{\partial \mathbf{f}_1}{\partial x_2} + \ldots + \Delta x_n \frac{\partial \mathbf{f}_1}{\partial x_n} \approx 0$$

$$\mathbf{f}_2(\mathbf{X^k}) + \Delta x_1 \frac{\partial \mathbf{f}_2}{\partial x_1} + \Delta x_2 \frac{\partial \mathbf{f}_2}{\partial x_2} + \ldots + \Delta x_n \frac{\partial \mathbf{f}_2}{\partial x_n} \approx 0$$

.

$$\mathbf{f}_n(\mathbf{X^k}) + \Delta x_1 \frac{\partial \mathbf{f}_n}{\partial x_1} + \Delta x_2 \frac{\partial \mathbf{f}_n}{\partial x_2} + \ldots + \Delta x_n \frac{\partial \mathbf{f}_n}{\partial x_n} \approx 0$$

which can be written in the matrix form as:

$$[\mathbf{f(X^k)}] + [\mathbf{J^k}]\ [\Delta\mathbf{X^k}] \approx [\mathbf{0}] \qquad \text{(a.5)}$$

where **J** is a two dimensional matrix known as Jacobian matrix, which is given by:

$$[\mathbf{J}] = \begin{bmatrix} \frac{\partial f_1}{\partial x_1} & \frac{\partial f_1}{\partial x_2} & \frac{\partial f_1}{\partial x_3} & \cdot & \frac{\partial f_1}{\partial x_n} \\ \frac{\partial f_2}{\partial x_1} & \frac{\partial f_2}{\partial x_2} & \frac{\partial f_2}{\partial x_3} & \cdot & \frac{\partial f_2}{\partial x_n} \\ \cdot & \cdot & \cdot & \cdot & \cdot \\ \frac{\partial f_n}{\partial x_1} & \frac{\partial f_n}{\partial x_2} & \frac{\partial f_n}{\partial x_3} & \cdot & \frac{\partial f_n}{\partial x_n} \end{bmatrix}$$

Solving (a.5) for the error vector, results in:

$$[\Delta \mathbf{X}^k] \approx -[\mathbf{J}^k]^{-1} [\mathbf{f}(\mathbf{X}^k)]$$

The multi-dimensional form of the Newton-Raphson algorithm is therefore given by:

$$[\mathbf{X}^{k+1}] = [\mathbf{X}^k] - [\mathbf{J}^k]^{-1} [\mathbf{f}(\mathbf{X}^k)] \qquad \text{(a.6)}$$

To apply equation (a.6) to the load flow problem, it is first necessary to choose the variables to be contained within the vector **X** and then to write the load flow equations in a form similar to that of (a.3). In a power flow problem the following variables are to be calculated:

a) The magnitude of the voltage and its associated phase angle for each PQ busbar.

b) The phase angle of the bus voltage of each PV busbars.

The swing (slack) bus is omitted from the iterative solution as the amplitude and phase of the voltage of this bus is already defined and the injected power into this bus can be calculated afterwards.

Assuming that there are N_{PQ} PQ busbars and N_{PV} PV busbars, the total number of unknown variables will be $2N_{PQ} + N_{PV}$. Vector **X** can be partitioned into two vectors:

$$[\mathbf{X}] = \begin{bmatrix} \theta \\ \mathbf{V} \end{bmatrix}$$

where θ is the vector of voltage phase of PQ and PV buses and **V** is the voltage magnitude vector of PQ buses.

The function f(**X**) can be formulated from the real and reactive power mismatches, errors, at all nodes (buses) except the slack bus. The power mismatch can be found by summing all complex power that enters a bus. Assuming that $\mathbf{I_i}$ is the vector of injected currents at bus i, the complex power mismatch is given by [27,79,84]:

$$\Delta S_i = \Delta P_i + j\Delta Q_i = P_i^{sp} + jQ_i^{sp} - V_i\angle\theta_i \left[\sum_{j=1}^{n} Y_{ij}\, V_j\angle\theta_j\right]^* \qquad \text{(a.7)}$$

where :

ΔS_i is the mismatch in the total complex power of bus i,

ΔP_i is the mismatch in the active power of bus i,

ΔQ_i is the mismatch in the reactive power of bus i,

P_i^{sp} is the specified active power at bus i,

Q_i^{sp} is the specified reactive power at bus I,

Y_{ij} is the $(i,j)^{th}$ element of the nodal admittance matrix of the considered system,

$Y_{ij} = G_{ij} + jB_{ij}$,

V_i, V_j are the complex voltage of bus i and j respectively,

θ_i, θ_j are the phase of voltages at bus i and bus j respectively.

Expanding and decomposing equation (a.7) into real and imaginary parts yields the real and imaginary power mismatches:

$$\Delta P_i = P_i^{sp} - V_i \sum_{j=1}^{n} (G_{ij} \cos\theta_{ij} + B_{ij} \sin\theta_{ij}) V_j = 0 \qquad \text{(a.8)}$$

$$\Delta Q_i = Q_i^{sp} - V_i \sum_{j=1}^{n} (G_{ij} \sin\theta_{ij} - B_{ij} \cos\theta_{ij}) V_j = 0 \qquad \text{(a.9)}$$

where $\theta_{ij} = \theta_i - \theta_j$.

Equation (a.8) is applied for PQ and PV buses, whereas, (a.9) is applied for PQ buses only. Hence the number of equations in the set of $f(\mathbf{X}) = 0$ will be $2N_{PQ} + N_{PV}$, which is the same as the number of unknown variables.

From (a.8) and (a.9), it can be said that the load flow problem is about finding the magnitude and phase angle of bus voltages such that the power mismatch at all buses are minimised. The Newton-Raphson numerical method can be used to solve this problem. During an iterative solution of the system equations, the terms subtracted from P_i^{sp} and Q_i^{sp} in the right-hand side of (a.8) and (a.9) will be the estimated injected powers based on the currently estimated voltage and angle. Noting that when $i=j$, $\sin\theta_{ij} = 0$, and $\cos\theta_{ij} = 1$, the estimated power at iteration k can be written as:

$$P_i^k = G_{ii} V_i^2 + V_i \sum_{\substack{j=1 \\ j \neq i}}^{n} (G_{ij} \cos\theta_{ij} + B_{ij} \sin\theta_{ij}) V_j$$

$$Q_i^k = -B_{ii} V_i^2 + V_i \sum_{\substack{j=1 \\ j \neq i}}^{n} (G_{ij} \sin\theta_{ij} - B_{ij} \cos\theta_{ij}) V_j$$

Using the Newton-Raphson method, the change in power mismatches, which are produced by changes in the bus voltages and angles, are given by the Jacobian matrix equation:

$$\begin{bmatrix} \Delta \mathbf{P} \\ \Delta \mathbf{Q} \end{bmatrix} = [\mathbf{J}] \cdot \begin{bmatrix} \Delta \theta \\ \Delta \mathbf{V} \end{bmatrix} \qquad \text{(a.10)}$$

The Jacobian matrix, **J**, is obtained by differentiating the mismatch equations (a.8) and (a.9) with respect to θ and V. For more convenience, **J** is partitioned into four submatrices **H**, **N**, **M**, and **L** as follows:

$$\begin{bmatrix} \Delta \mathbf{P} \\ \Delta \mathbf{Q} \end{bmatrix} = \begin{bmatrix} \mathbf{H} & \mathbf{N} \\ \mathbf{M} & \mathbf{L} \end{bmatrix} \cdot \begin{bmatrix} \Delta \theta \\ \Delta \mathbf{V} \end{bmatrix}$$

where the elements of the submatrices **H**, **N**, **M**, and **L** are given by [84]:

$$H_{ii} = \frac{\partial \Delta P_i}{\partial \theta_i} = Q_i^k + B_{ii} V_i^2$$

$$H_{ij} = \frac{\partial \Delta P_i}{\partial \theta_j} = -V_i (G_{ij} \sin \theta_{ij} - B_{ij} \cos \theta_{ij}) V_j, \qquad i \neq j$$

$$M_{ii} = \frac{\partial \Delta Q_i}{\partial \theta_i} = -P_i^k + G_{ii} V_i^2$$

$$M_{ij} = \frac{\partial \Delta Q_i}{\partial \theta_j} = V_i (G_{ij} \cos \theta_{ij} + B_{ij} \sin \theta_{ij}) V_j, \qquad i \neq j$$

$$N_{ii} = V_i \frac{\partial \Delta P_i}{\partial V_i} = -P_i^k - G_{ii} V_i^2$$

$$N_{ij} = V_j \frac{\partial \Delta P_i}{\partial V_j} = -M_{ij}$$

$$L_{ii} = V_i \frac{\partial \Delta Q_i}{\partial V_i} = -Q_i^k + B_{ii} V_i^2$$

$$L_{ij} = V_j \frac{\partial \Delta Q_i}{\partial V_j} = H_{ij}$$

Assuming that for the k^{th} iterative all bus votages and angles are known, all the elements of the Jacobian matrix can be calculated. The power mismatch for the k^{th} iterative can also be calculated using (a.8) and (a.9). Then, the correction for the magnitude and angle of bus voltages is found rearranging (a.10) as follows:

$$\begin{bmatrix} \Delta\theta \\ \Delta V \end{bmatrix} = \left[J^{-1}\right] \cdot \begin{bmatrix} \Delta P \\ \Delta Q \end{bmatrix}$$

where J^{-1} is the inverse of the Jacobian.

Thus, voltage magnitude and angles for the k+1 iteration is given by:

$$V_i^{k+1} = V_i^k + \Delta V_i$$

$$\theta_i^{k+1} = \theta_i^k + \Delta\theta_i$$

As mentioned before, iteration is repeated until the power mismatches are reduced to acceptable values.

Appendix B

The Trapezoidal Rule for Numerical Integration

Numerical methods are usually used whenever analytical methods are either inconvenient or impossible to perform. Numerical integration and differentiation methods, in particular, are widely implemented for power system analysis. They are used for solving differential equations, which are formulated to describe the behaviour of power systems under transient and dynamic operating conditions. The problem of numerical integration is the numerical evaluation of integrals of the form:

$$J = \int_a^b f(x)\,dx \tag{b.1}$$

where a and b are given limits and f is a function given analytically by a formula or empirically by a table of values. Geometrically, J is the area under the curve f between a and b, as shown in Fig. (b.1).

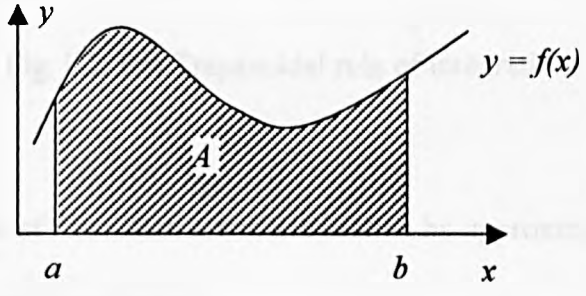

Fig. b.1 Geographical interpretation of a definite integral

When it is possible to find a differentiable function F whose derivative is f, i.e.

$F'(x) = f(x)$, then J can be evaluated using the following formula:

$$J = \int_a^b f(x)\,dx = F(b) - F(a) \qquad \text{(b.2)}$$

However, when the function is complicated and no analytical integration can be found, numerical methods of approximate integration are used, whereby the integrated function is approximated by functions that can be easily integrated. One of these methods, which is widely used is known as the "Trapezoidal Rule". Using the Trapezoidal rule of integration, the area under the integrated function f can be obtained by dividing the interval of integration $a \leq x \leq b$ into n subintervals of equal length each of which is h, such that $h = \frac{b-a}{n}$. The function is then approximated by a broken line of segments (cords), as shown in Fig. b.2.

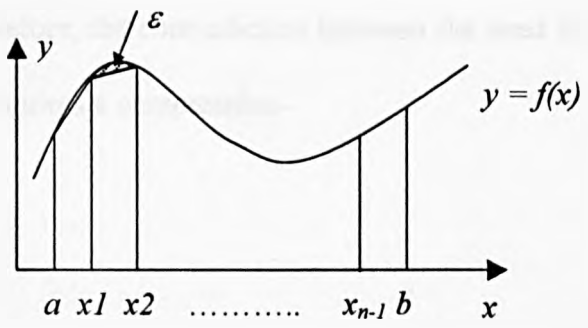

Fig. b.2 The Trapezoidal rule of integration

The area under the curve of f between a and b can then be approximated by the sum of n trapezoidal areas, which are given below:

$$\frac{1}{2}h[f(a)+f(x_1)],\quad \frac{1}{2}h[f(x_1)+f(x_2)],\quad \cdots\quad ,\quad \frac{1}{2}h[f(x_{n-1})+f(b)]$$

and the sum of these areas formulates the trapezoidal rule:

$$J = \int_a^b f(x)\,dx \approx h\left[\frac{1}{2}f(a) + f(x_1) + f(x_2) + \cdots + f(x_{n-1}) + \frac{1}{2}f(b)\right] \qquad \text{(b.3)}$$

Compared with analytical solution, the result obtain by the application of trapezoidal rule is associated with a certain amount of error. The error induced in single interval, say between x_1 and x_2 is given by [89]:

$$\varepsilon = -\frac{(x_2 - x_1)^3}{12} f''(\hat{x}) = -\frac{h^3}{12} f''(\hat{x}) \qquad x_1 \leq \hat{x} \leq x_2 \qquad \text{(b.4)}$$

where

$f''(\hat{x})$ is the second derivative of function f at point $\hat{x}$

It can be seen from (b.4) that as the width of the subintervals h decreases, i.e. the number of subintervals increases, the error of Trapezoidal integration reduces, hence, more precise results are obtained. However, increasing the number of intervals results in longer computational time. Therefore, the contradiction between the need for more precise results and faster computation requires a compromise.

Appendix C

Voltage Regulation Using Reactive Power Injection.

Voltage regulation based on the injection of reactive power is achieved indirectly. The idea behind this method is based on the direct relation between the voltage of a node and the flow of reactive power into that node. This relation can be explained using the simple distribution system shown in Fig. c1(a). A phasor diagram that represents the transfer of power through the system is shown in Fig c1(b). From this figure, the relation between the voltage at the sending end, E, and the voltage at the receiving end, V, is given by [26]:

$$E^2 = (V + \Delta V)^2 + \delta V^2$$

$$= (V + RI\cos\phi + XI\sin\phi)^2 + (XI\cos\phi - RI\sin\phi)^2$$

$$\therefore\ E^2 = \left(V + \frac{RP}{V} + \frac{XQ}{V}\right)^2 + \left(\frac{XP}{V} - \frac{RQ}{V}\right)^2 \qquad \text{(c.1)}$$

Hence,

$$\Delta V = \frac{RP + XQ}{V}$$

And

$$\delta V = \frac{XP - RQ}{V}$$

Since $\delta V << V + \Delta V$, Equation (c.1) can be approximated to:

$$E^2 \approx \left(V + \frac{RP}{V} + \frac{XQ}{V}\right)^2$$

Or

$$E - V = \Delta V \approx \frac{RP}{V} + \frac{XQ}{V} \qquad \text{(c.2)}$$

The arithmetic difference between the voltage at the sending end and that at the receiving end approximately equals the voltage drop in the distribution system. It can be seen from (c.2) that this voltage drop is related to the flow of active and reactive power.

The transfer of reactive power through a distribution system causes high power losses, I^2R. It also reduces the ability of the system to transfer active power due to thermal limitations of the system components. Therefore, instead of transferring reactive power through the system, means of reactive power injection, which are known as "reactive power compensation", are usually installed close to load centres. In general, three methods of reactive power injection are implemented in power systems, based on the use of:

a) Static shunt capacitors,

b) Synchronous compensators,

c) Static reactive power compensators

These methods are mainly used for reactive power compensation that alleviates the problem of transfer of reactive power through the distribution system. On the other hand, because of the relation between the reactive power flow into a node and the voltage of that node, they are also indirectly used for voltage control.

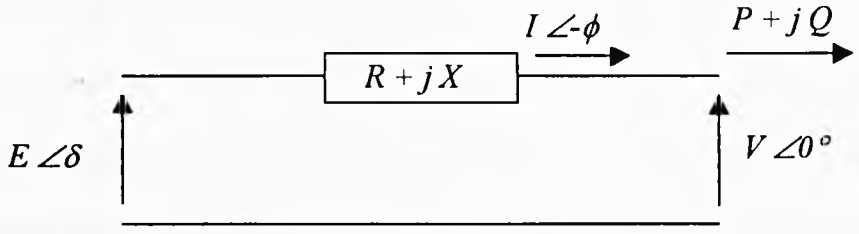

(a)

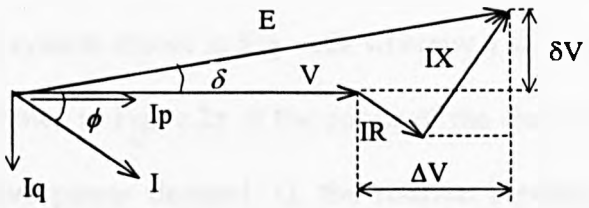

(b)

Fig. c.1 Power transfer through a transmission system

c.1 Voltage Control Using Static Shunt Capacitors

Static shunt capacitors consist of either fixed capacitor banks or switched capacitors. The selection of the amount of shunt capacitors is dependent on the required range of voltage control and the lagging reactive power (VAR) demand by the load. Using fixed capacitor banks is the simplest and less expensive way of VAR/Voltage control. However, in the case of widely fluctuating loads, fixed capacitors may lead to either over-compensation or under-compensation. The former may cause over-voltage problems, whereas the latter may cause under-voltage problems. Switched capacitors overcome the disadvantage of fixed capacitors. In this case a number of switched shunt-capacitors are connected to a node and a control algorithm is used to switch them in or out as required. The control algorithm of switched capacitors can be based on time

switches, temperature controls, voltage controls, current controls, active and reactive power controls or a combination of these methods [97]. One drawback of shunt capacitors is that the VARs produced by them are proportional to the square of the node's voltage, consequently, as the voltage falls, the VARs also fall reducing the effectiveness of shunt capacitors.

The effect of shunt capacitors on the voltage amplitude can be demonstrated using the simple distribution system shown in Fig. c.2a whereby a shunt capacitor is added at the receiving end, as shown in Fig. c.2a. If the power of the shunt capacitor, Q_c, is assumed equal to the reactive power demand, Q, the relation between the voltages E and V should then be as shown in the phasor diagram in Fig. c.2b. By comparing to the phasor diagram in Fig. c.1b with that in Fig. c.2b, it can be seen that, adding a shunt capacitor to the receiving end has increased the amplitude of the voltage V. This also resulted in a reduction in the voltage drop across the line.

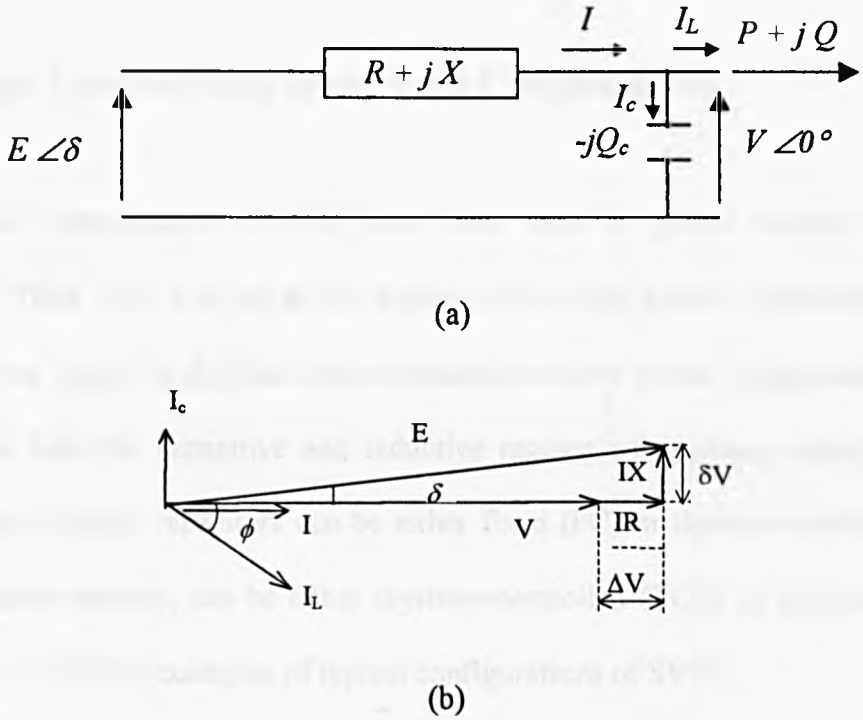

Fig. c.2 Power transfer through a transmission system with shunt capacitors

c.2 Voltage Control Using Synchronous Compensators

A synchronous compensator (SC) is a synchronous motor running without a mechanical load. Depending on the value of excitation, a SC can absorb or generate reactive power [98], which allows it to operate for all load conditions. The advantage of an SC over shunt capacitors is that when used with a voltage regulator, the compensator can automatically run over-excited at times of high loads and under-excited at times of light loads, consequently, providing a smooth VAR/voltage control. Synchronous compensators have some disadvantages compared with static shunt capacitors. Their losses are much higher than those of shunt capacitors and hence, their efficiency is lower. Because of the rotating parts of an SC, its failure rate is higher and maintenance is more difficult than the other types of compensators. The cost of SC installations is also relatively high. The use of SC is therefore justified only in particular circumstances when proper control can not be achieved with the application of other control methods.

c.3 Voltage Control Using Static VAR Compensators

Static VAR compensators (SVCs) have been used in power systems since the 1970s[76]. Their role is to adjust the amount of reactive power compensation to the actual system needs. A flexible and continuous reactive power compensation can be achieved in both the capacitive and inductive regions using shunt capacitors and/or shunt reactors. Shunt capacitors can be either fixed (FC) or thyristor-switched (TSC), whereas, shunt reactors, can be either thyristor-controlled (TCR) or thyristor-switched (TSR). Fig. c.3 shows examples of typical configurations of SVCs.

It is worth noting that thyristors generate high harmonics and therefore SVCs are

usually equipped with additional harmonic filters to smooth current waveforms.

The reactive current of an SVC can be regulated by controlling the firing angle of the thyristors. The thyristor firing circuit used in SVCs are usually controlled by a voltage regulator, which attempts to keep the node voltage constant by controlling the amount, and polarity, of the reactive power injected into the node.

The cost of SVCs is typically several times that of an uncontrolled bank of shunt reactors or fixed capacitors [76]. Consequently, they are only used in those parts of a system where heavy fluctuations of load occur and compensation in both inductive and capacitive VARs is required.

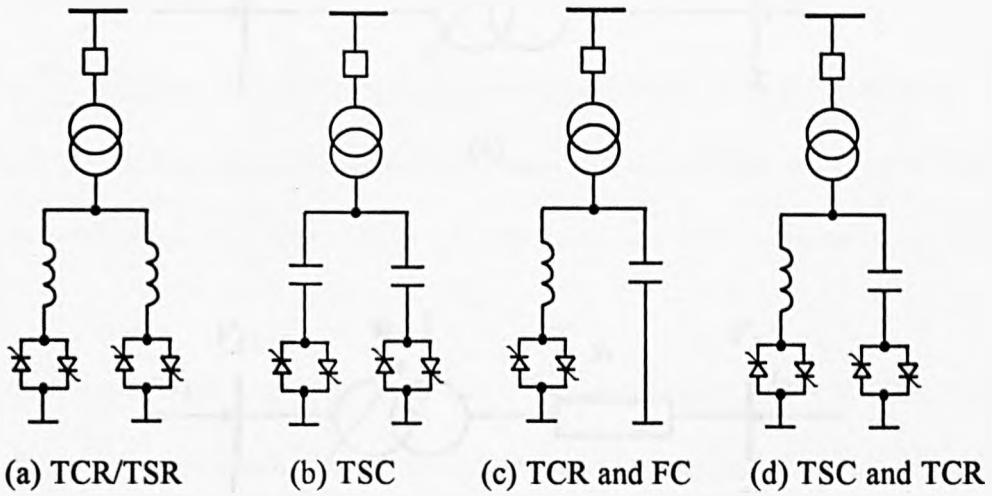

Fig. c.3 Typical configurations of SVCs

Appendix D

Representation of OLTCT in the Load Flow Program

A two-winding OLTCT, similar that shown in the schematic diagram of Fig. d.1(a), can be represented by an ideal transformer, which represents its transformation ratio, connected in series with the transformer's admittance y_t, as depicted in Fig. d.1(b).

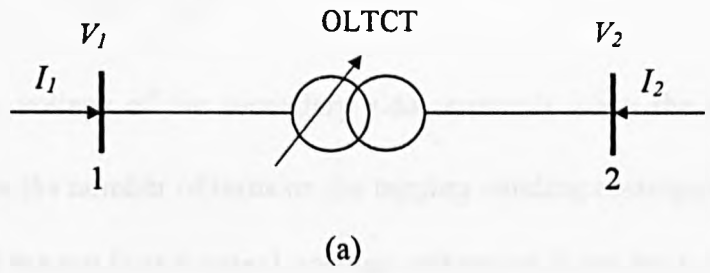

(a)

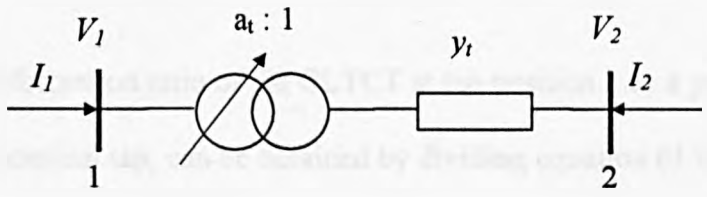

(b)

Fig. d.1 Schematic diagram of an OLTCT.

In Fig. d.1(b) a_t is the per unit value of the transformation ratio based on the transformer ratio at the nominal tap position.

The transformation ratio at the nominal tap can be expressed in terms of its turns ratio as follows:

$$\frac{V_1}{V_2} = \frac{N_1}{N_2} \tag{d.1}$$

where N_1 is the number of turns on the primary winding and N_2 is the number of turns on the secondary. V_1 and V_2 are the terminal voltages of transformer's primary and secondary windings. The transformation ratio at tap position k can be given by:

$$\frac{V_1}{V_2'} = \frac{N_1 + k\Delta N}{N_2}$$

$$= \frac{N_1}{N_2} + \frac{k\,\Delta N}{N_2} \tag{d.2}$$

where V_2' is the voltage of the secondary side terminals when the transformer is at tap position k, ΔN is the number of turns on the tapping winding corresponding to one tap step. k equals zero if the tap is at nominal position, otherwise it can be a positive or a negative number depending on position of the tap with reference to the nominal position.

Hence, the transformation ratio of the OLTCT at tap position k as a per unit value based on the ratio at the nominal tap, can be obtained by dividing equation (d.2) by equation (d.1):

$$a_t = \frac{\frac{N_1}{N_2} + \frac{k\,\Delta N}{N_2}}{\frac{N_1}{N_2}}$$

$$= 1 + k\frac{\Delta N}{N_1} \tag{d.3}$$

where $\frac{\Delta N}{N1}$ is the per unit change in the number of turns of the primary windings, or the per unit step voltage, due to one step change in the tap position.

To develop an equivalent circuit of an OLTCT that accounts for the operation of tap the changer, assume that the calculation of the parameters shown in Fig. d.1(b) is performed in per unit values. The injected current at bus 2 can then be expressed as follows:

$$I_2 = -\left(\frac{V_1}{a_t} - V_2\right) y_t$$

$$= -\frac{y_t}{a_t} V_1 + y_t V_2 \qquad \text{(d.4)}$$

The injected current at node 1, can also be determined by:

$$I_1 = -\frac{I_2}{a_t} \qquad \text{(d.5)}$$

and substituting (d.4) into (d.5), yields:

$$I_1 = \frac{y_t}{a_t^2} V_1 - \frac{y_t}{a_t} V_2 \qquad \text{(d.6)}$$

Equation (d.4) and Equation (d.6) can be arranged in a matrix form as follows:

$$\begin{bmatrix} I_1 \\ I_2 \end{bmatrix} = \begin{bmatrix} \frac{y_t}{a_t^2} & -\frac{y_t}{a_t} \\ -\frac{y_t}{a_t} & y_t \end{bmatrix} \begin{bmatrix} V_1 \\ V_2 \end{bmatrix} \qquad \text{(d.7)}$$

Equation (d.7) can be represented by a Π-circuit, as shown in Fig. d.2, which has the following general equation:

$$\begin{bmatrix} I_1 \\ I_2 \end{bmatrix} = \begin{bmatrix} y_{10} + y_{12} & -y_{12} \\ -y_{12} & y_{20} + y_{12} \end{bmatrix} \begin{bmatrix} V_1 \\ V_2 \end{bmatrix} \qquad \text{(d.8)}$$

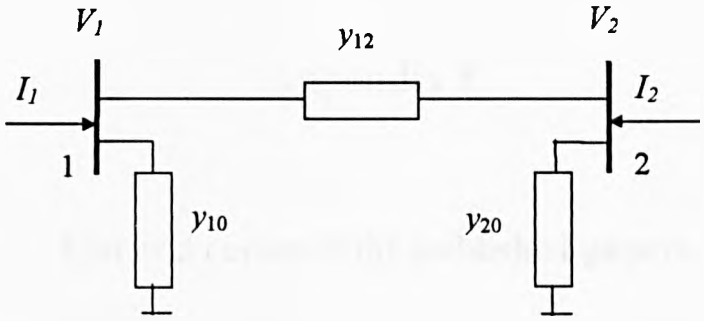

Fig. d.2 Equivalent circuit of an OLTCT.

From (d.7) and (d.8), it can be seen that :

$$y_{12} = \frac{y_t}{a_t} \tag{d.9}$$

$$y_{10} = \frac{y_t}{a_t^2} - y_{12}$$

$$= \frac{y_t(1-a_t)}{a_t^2} \tag{d.10}$$

$$y_{20} = y_t - y_{12}$$

$$= \frac{y_t(a_t-1)}{a_t} \tag{d.11}$$

As can be seen from Equations (d.9), (d.10), and (d.11), the admittance values of the equivalent circuit are proportional to the tap ratio a_t. This equivalent circuit is implemented in the load flow program to consider the effect of tap changing on the voltage control by including it in the general nodal admittance matrix.

Appendix E

List and copies of the published papers

Based on the results obtained during the course of this work, the papers listed below have been presented at different conferences, as indicated in the list and published in their proceedings. A copy of each of these papers is attached to this appendix.

(a) S K Salman and I M Rida, "Investigating the electrical integration of wind power based embedded generation using ATP," Proceedings of the 33rd Universities Power Engineering Conference, UPEC'98, Edinburgh, UK, September 1998, pp. 407 - 410.

(b) S K Salman and I M Rida, "Impact of integration of wind farms into a utility network on relay settings of the utility feeders," Proceedings of the ERA Technology's International Conference "Quality and Security of Supply in Electrical Networks," London, UK, February 1999, pp. 2.3.1 - 2.3.8.

(c) S K Salman and I M Rida, "Application of artificial neural networks for the voltage control of distribution networks," Proceedings of the 34th Universities Power Engineering Conference, UPEC'99, Leicester, UK, September 1999, pp. 529 – 532.

(d) S K Salman and I M Rida, "Investigating the electrical integration of wind power based embedded generation into utilities' networks," Proceedings of the IASTED International conference of Power Energy Systems, Las Vegas, USA, November 1999, pp. 134 - 139.

(e) S K Salman and I M Rida, " ANN-based AVC relay for voltage control of distribution network with and without embedded generation," IEEE Proceedings of the DRPT'2000 Conference, City University, London, UK, April 2000, pp.263-267.

(f) S K Salman and I Rida, "Investigating the impact of embedded generation on relay settings of utilities' electrical feeders,". This paper has been submitted for publication in the IEEE Transactions on Power Delivery, which at the time of writing this thesis is being considered.

INVESTIGATING THE ELECTRICAL INTEGRATION OF WIND POWER BASED EMBEDDED GENERATION USING ATP

Dr S K Salman and I M Rida

The Robert Gordon University, Aberdeen, UK.

ABSTRACT

In the recent years wind power based embedded generation (WPBEG) has received considerable attention world-wide. Generators of such power plants are usually connected to utilities' electrical networks at distribution levels. However, the integration of such power plants at distribution levels could create technical problems that require appropriate investigation both during steady-state and dynamic condition. Digital simulation programs are usually employed for such investigation. One of these programs is the Alternative Transient Program (ATP). In this paper the simulation of a distribution system that includes WPBED using the ATP is described. The model is employed to investigate effects of wind speed variation on generator output and also the behaviour of the system during different types of disturbances such as fault conditions.

INTRODUCTION

Wind energy is one of the most promising renewable energy resources. It has been estimated that generation of electricity using wind energy resource in Scotland can be as much as 7500 MW [1]. In Resent years this source of energy has become very attractive. The technology for the generation of electricity by wind turbines is even operationally proven. Wind turbines that convert wind energy into mechanical energy can now drive generators with capacities reaching 1500 kW [2]. Several wind turbines are usually installed at on site constituting what is known as wind farms. Generators of wind farms are commonly connected to electrical networks at distribution levels [3] and referred to as Embedded Generators (EGs). However, existing distribution systems are originally designed as supply networks and may not be tailored to collecting power from EGs [2]. Therefore, the integration of wind farms with utilities distribution networks may create safety as well as technical problems. Such problems include contribution to the fault currents, stability and reliability problems, introduction of harmonics, voltage fluctuations, and problems to the automatic voltage control (AVC) of distribution networks [4].

In order to address these problems, distribution systems that include wind power based EGs requires investigation during both steady-state and dynamic conditions. Digital simulation programs are usually employed for such investigation. One of these programs is the Alternative Transient Program(ATP).

In this paper the ATP is used to simulate a distribution network that includes a wind farm which used induction generators. The later are modelled using a Universal Machine (UM) model. Such model provide a linkage between the mechanical and electrical parts of a generator-turbine unit. Variation of wind speed is modelled using a facility in ATP called 'Transient Analysis of Control Systems (TACS)'. A control circuit that initiates the disconnection of wind turbines in cases when terminal voltages or rotor speed exceed their limits is also modelled using TACS facilities. The model is then utilised to investigate the behaviour of the system for different types of disturbances.

MODELLING ELECTRIC POWER SYSTEMS USING ATP

The ATP is one of the versions of the well-known ElectroMagnetic Transient Program (EMTP) which has been used for several years for power system analyses under transient and dynamic conditions. The theoretical basis of the solution method in ATP is based on a step-by-step procedure [5].

The existing facilities in ATP

The ATP is composed of a library of models of network components such as lines, transformers, generators, etc. that can be used to simulate electrical networks. One of these models is the Universal Machine (UM) proposed by Lauw and Meyer [6] in 1982. It is an electromechanical energy conversion device that can be used to simulate the electrical and mechanical components of electrical machines. The UM model can be used to represent 12 major types of electric machines, e.g. single-phase and multiple-phase synchronous or induction machines and dc machines [7]. The mechanical side of the machine

can be included by an equivalent electric network with lumped RLC elements, which is then solved as part of the complete electric network. For each mass connected to the shaft system, a node is created in the equivalent electric network, with a capacitor placed between the node and the ground to represent the moment of inertia of that mass. A mechanical torque on that mass can be simulated by a current source connected to that node [5]. The Transient Analysis of Control Systems, TACS, is another facility that is available in ATP software package which allows models of control and protection components to be included in the simulation. The control circuitry whose behaviour is to be simulated must first be described as a block diagram. Recognised block diagrams can be transfer functions, limiters, algebraic functions, logical operators, and other special-purpose devices [7]. Recently, a programming language known as "MODELS" has been added to the ATP. MODELS provides users of ATP even more flexibility. It is designed to simulate control systems as well as network components which are not available in the library of ATP. It also enables to link the ATP package with other programming software [8]. Electrical components such as transmission lines can be simulated using different types of models, as an example lumped series RLC model, distributed parameter line model and frequency dependant line model.

Modelling the network under consideration

The distribution system shown in Fig. 1. has been modelled in ATP. The system comprises a wind farm, a 33/11 kV substation, and an 11 kV feeder connecting the wind farm with the substation. The wind farm is assumed to have eight wind turbine-generator units each of 600 kW with a nominal voltage of 690V. The generating units are grouped and represented in the ATP package by three UM models. The first machine, shown in Fig. 1, represents a single 600 kW unit, the second machine represents two 600 kW units, and the third machine represents five 600 kW units. All units are assumed to be connected to a step-up transformer with a voltage ratio of 690/11000 V and a capacity of 7.5 MVA. The capacity of the transformer at the substation is assumed 10 MVA. Transformers are represented using a transformer model that consider their connection group and saturation of the magnetic core. The length of the line between the wind farm and the substation is assumed 10 km. A second feeder is assumed to be connected to the 11 kV bus-bar at the substation which supplies a group of loads at the end of the feeder via an 11kV/416V transformer. Feeders are simulated using lumped RLC model. Utility's network (Grid) is represented by a source behind the system equivalent impedance.

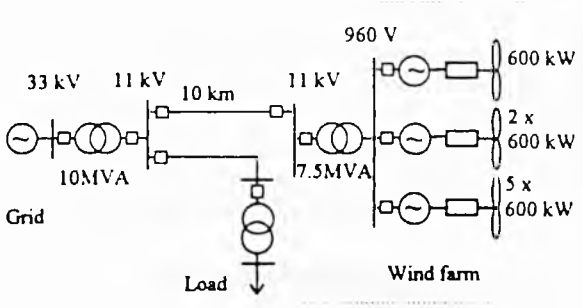

Fig. 1 Schematic diagram of the considered network.

SIMULATION CASES

Effects of faults within the network on EG

The aim of this particular investigation was to predict the dynamic behaviour of induction generators at a wind farm during and following a fault within the network. One of the investigated examples is a three phase to ground fault which was assumed to occur on a load feeder close to the substation. The fault was initially assumed to be cleared after 50ms. Fig. 2 shows the voltage at the terminals of induction generators at the wind farm, i.e. at the 690V bus-bar. As can be seen from this figure, the voltage has dropped to a value less than 30% of its nominal voltage. The electro-magnetic torque (T_e) developed inside an induction machine at any given speed is proportional to the square of the terminal voltage as follows[9]:

$$T_e = K\, s\, I^2 \qquad (1)$$

where K is a constant, s is the machine slip.

As a result, T_e was also reduced, as shown in Fig.3 This figure shows the Electro-magnetic torque in the air-gap of one generator. The swing equation for the rotor is given by[9]:

$$J\frac{d\omega}{dt} = T_m - T_e \qquad (2)$$

where J is the moment of inertia of the rotating mass, T_m is the mechanical torque on the rotor shaft and ω is the rotor speed.

From equation 2, for a constant mechanical torque, a reduction in the Electro-magnetic torque will cause the rotor to accelerate. This can be seen from the rotor speed curve in Fig.4.

As the fault was cleared and the voltage on the machine terminals was recovered, the magnetic field in the air-gap of the machine started to get established which caused inrush current to be drown from the network, as shown in Fig.5. Consequently, a proportional Electro-magnetic torque started to act on the rotor in a direction opposite to the applied

mechanical torque. If the energy stored in the rotating magnetic field is higher than the energy stored in the rotating rotor, speed would be reduced and the generator would return to its normal operating condition. As the exchange of power can not occur instantaneously due to the inductance of machine windings and the inertia of the rotating mass, currents, Electro-magnetic torque, and speed will have an oscillatory characteristic with an exponentially decaying envelope. This oscillatory behaviour can be seen in Figs 3,4 and 5.

It has been found that critical fault clearing time for the given case is 80 ms. When the fault was cleared in a time longer than 80 ms, rotor speed continued to increase until the wind farm was disconnected by a signal from a simulated over speed protection device. During this time induction generators continued to draw high inrush currents from the network which resulted in a sustained voltage sag on the network. Fig. 6 shows the voltage of the generator terminals when the fault was cleared after 90 ms.

Effects of power output fluctuation of wind farms on the network.

The mechanical torque developed by a wind turbine can be described using the following characteristic equation [10]:

$$T_{Mech}(\omega_m, v_o) = A(v_o)\,\omega_m + B(v_o) \qquad (3)$$

Where $A(v_o)$ and $B(v_o)$ are wind velocity dependant parameters, ω_m is the shaft's speed and v_o is the instantaneous wind's velocity.

In order to obtain mechanical torque using equation 3, the knowledge of the instantaneous wind velocity time series and the rotational speed characteristics of wind turbines, are essential. As such information is not available at the time of writing this paper, a signal representing a variable mechanical torque with a randomly generated wave form was used. The velocity of wind acting on individual wind turbines within the wind farm are not totally correlated, therefore, different signals were applied to different turbine-generators. Fig. 7 shows the speed of the shaft of one turbine when the mechanical torque was varied. Fig. 8 shows the electro-magnetic torque developed in the air-gap inside the generator due to the assumed variable mechanical power on the shaft. Fig. 9 shows the fluctuation in the total power output from the wind farm due to variation of wind speed.

CONCLUSION

The ATP package was used to simulate a distribution system that includes a wind farm. The universal machine, UM, model was used to represent wind turbine - generator units. Using this model enabled the mutual effects between the network and the wind to be examined. It was shown that the connection of wind farms to a distribution network can affect the critical clearing time of faults. Using the TACS facility has added more flexibility to the simulation.

ACKNOWLEDGEMENT

The authors would like to thank the Robert Gordon University for their technical and financial support.

REFERENCES

1. 'An assessment of the potential renewable energy resource in Scotland', The Scottish Hydro-Electric plc, Scottish Power plc, December, 1993.
2. P. Gardner, et al, 'Network connection of large wind turbines,' Wind Energy Conversion, 17th BWEA wind energy conf., July 1995.
3. S K Salman, F Jiang, W J S Rogers, 'Effects of wind power generators on the voltage control of utility distribution networks,' Renewable Energy, Conference Publication No. 385, IEE, 1993.
4. S K Salman, F Jiang, W J S Rogers, 'The effect of Private Generators on the voltage control of 11kV network and on operation of certain protective relays,' The NTUA/IEEE Int. Conference on Modern Power Systems, Athens, Greece, Sept. 1993.
5. H W Dommel, 'Electromagnetic transient program reference manual (EMTP theory book),' Bonneville Power Administration, Portland, USA, August 1986.
6. H K Lauw, W S Meyer, 'Universal Machine modelling for the presentation of electric machinery in an electromagnetic transient program,' IEE trans. Power App. Syst., Vol. PAS-101, June 1982.
7. K U Leuven EMTP Centre, 'Alternative Transient Program Rule Book,' Belgium, July 1987.
8. Laurent Dudè, 'Users guide to MODELS in ATP,' DEI, Oregon, USA, April 1996.
9. Mulukutla S. Sarma, 'Electric machines, steady-state theory and dynamic performance,' West publishing company, USA, 1985.
10. A I Estanquiro, et al, 'The use of stiff and flexible rotor models with regards to wind turbines power quality assessment,' 16th Wind Energy Conference "BWEA'16", Stirling, June 1994.

AUTHOR'S ADDRESS

The first author can be contacted at

School of Electronic and Electrical Engineering,
The Robert Gordon University, Schoolhill,
Aberdeen, UK, AB10 1FR.
email s.k.salman@eee.rgu.ac.uk

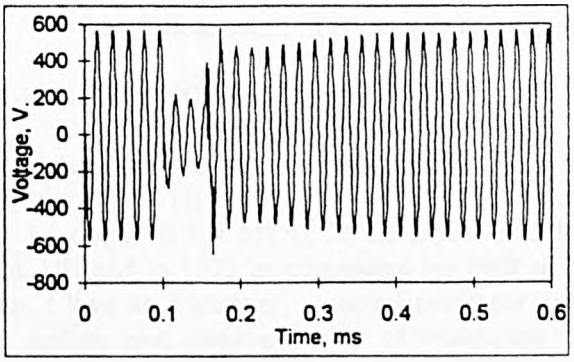

Fig. 2 Terminal Voltage of induction generators during a three phase to ground fault on the network.

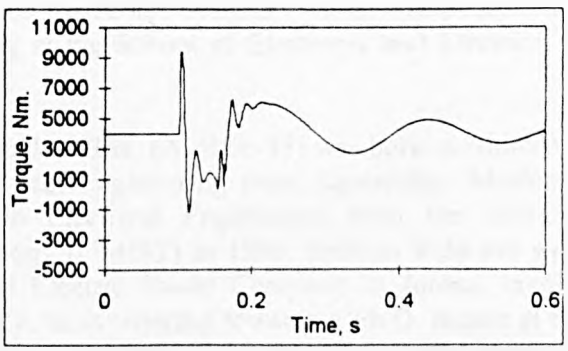

Fig. 3 Electro-magnetic torque in the air-gap of one generator during the fault.

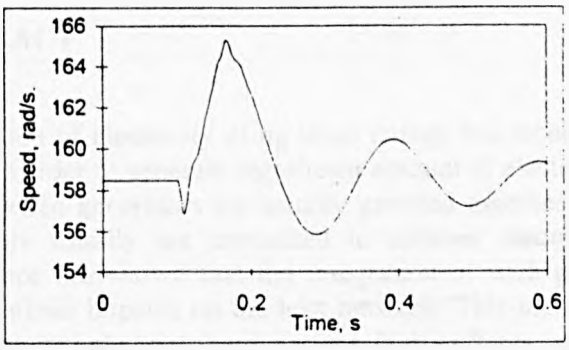

Fig.4 The rotor speed of the generator.

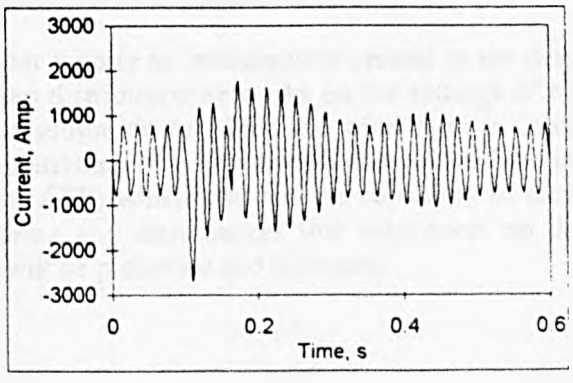

Fig. 5 Stator current of one generator.

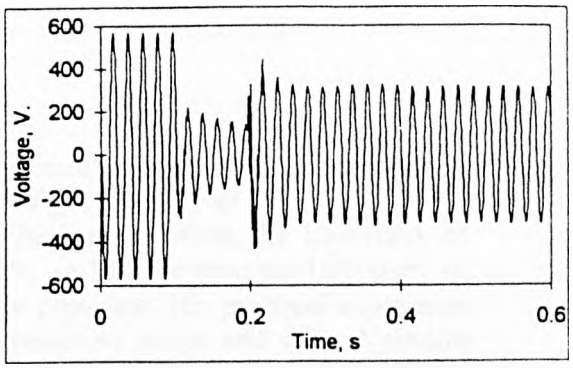

Fig. 6 Terminal Voltage of induction generators during a three phase to ground fault on the network.

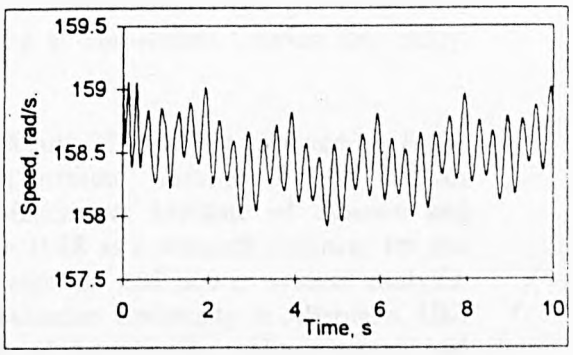

Fig. 7 Speed of the shaft of a wind turbine due to variation in mechanical torque.

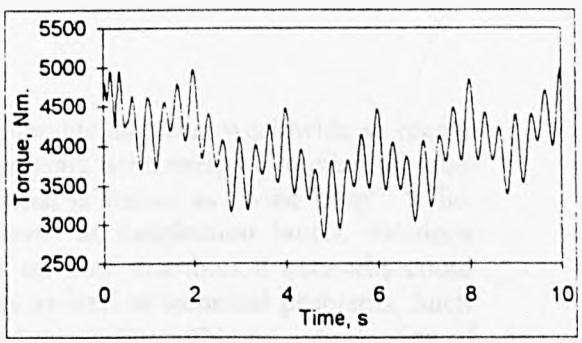

Fig. 8 Electro-magnetic torque developed in the air-gap of one generator.

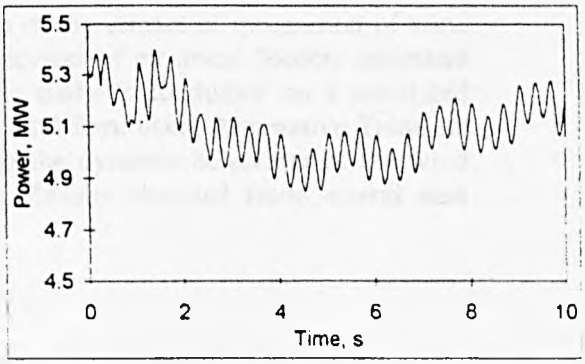

Fig. 9 Variation of the power output from the wind farm due to variation in wind speed.

Note: Figs. 1 through 5 are for fault duration of 50ms while Fig. 6 is for fault duration of 90ms.

IMPACT OF INTEGRATION OF WIND FARMS INTO A UTILITY NETWORK ON RELAY SETTINGS OF THE UTILITY FEEDERS

S K Salman and I M Rida, The Robert Gordon University, Aberdeen, U.K.

BIOGRAPHICAL NOTES

Salman K Salman: He is a member of the IEE and a senior member of the IEEE, was born in Basraha, Iraq, 1941. He graduated from the Faculty of Engineering, University of Baghdad in 1964. In 1972 he obtained his MEng in Electrical and Electronic Engineering from the University of Sheffield, UK and in 1975 he completed his PhD at UMIST, UK. In 1975 he joint the University of Benghazi, Libya as a lecturer, assistant professor and associate professor. His practical experience includes testing and commissioning of measuring devices, protection relays and control circuits related to 132 kV/33 kV/11 kV systems. He has published several papers on voltage control of distribution networks with embedded generation and on the protection of power systems at national and international conferences and scientific journals. He is also a co-author of a book titled "Digital Protection for Power Systems" which was published by the IEE in September 1995. Currently he is lecturing at the School of Electronic and Electrical Engineering at The Robert Gordon University, UK.

Ibrahim M. Rida (AMIEE-93) was born in Amman, Jordan on July 23 1960. He received his B.Sc. in Electrical Engineering from Zaporozhye Machine Building Institute, Ukraine, in 1985 and his M.Sc. in Electrical Engineering from the University of Manchester Institute of Science and Technology (UMIST) in 1996. Ibrahim Rida has worked since 1988 as a research engineer for the National Electric Power Company in Jordan, involved in protection and power system analysis. Currently, he is working towards a Ph.D. degree at the Robert Gordon University in Aberdeen, UK. His research interests are in the areas of wind power based embedded generation, voltage control and protection of distribution networks.

ABSTRACT

Generation of electricity using wind energy has received considerable attention worldwide in recent years. In order to generate significant amount of electrical power using wind energy a number of wind power based generators are usually grouped together to form what is known as "wind farm". Wind farms are usually are connected to utilities' electrical networks at distribution levels. Previous experience has shown that the integration of such plants into utilities' distribution networks could make various impacts on the host network. This includes safety as well as technical problems. Such problems include contribution to the fault currents, stability and reliability problems, introduction of harmonics, voltage fluctuation, interference with the process of automatic voltage control (AVC) of distribution networks, impact on network losses etc.

This paper reports an investigation related to the determination of the impact of integration of wind farms into distribution networks on the settings of protective devices of electrical feeders emanated from the substation to which the wind farm is connected. The study is conducted on a simulated system consisting of a distribution network with an integrated wind farm using Alternative Transient Program (ATP) which also has the capability of demonstrating the dynamic behaviour of the wind farm during any disturbances that may occur on the system. Results obtained from several case studies will be presented and discussed.

1 INTRODUCTION

It has recently been recognised that wind-power can be an effective way to counter global warming and under certain circumstances cost-competitive with other method of generation (1). Consequently, generation of electricity using wind-power has received considerable attention world wide in recent years. For example the total installed capacity worldwide has increased from its level of 6118 MW in 1996 to 7638 MW in 1997 which represents a growth of 25% in a span of one year (1). In order to generate significant amount of electricity using wind-power, a number of wind power based generators are usually grouped together to form what is known as "wind farm". Wind farms are usually connected to utilities' electrical networks at distribution voltage levels. Previous experience has shown that the integration of such plants into utilities' distribution networks could have various impacts on the host network. This includes safety as well as technical problems. Such problems include contribution to the fault currents, stability and reliability problems, introduction of harmonics, voltage fluctuation, interference with the process of automatic voltage control (AVC) of distribution networks, impact on network losses etc (2-5). It is therefore important that the operation of distribution systems that include wind farms should be investigated both during steady state and dynamic conditions.

This paper report an investigation to determine the impact of the integration of wind farms into distribution networks on the settings of protective devices of electrical feeders emanated from the substation to which the wind farm is connected. The study is conducted on a simulated system consisting of a distribution network with an integrated wind farm using Electromagnetic Transient Program (EMTP) which also has the capability of demonstrating the dynamic behaviour of the wind farm during any disturbances that may occur on the system. Results obtained from several case studies is presented and discussed.

2 REVIEW OF THE IMPACTS OF EMBEDDED GENERATION ON HOST DISTRIBUTION NETWORK

It is now well established that all forms of embedded generation (EG) including wind farms could affect the host distribution network (DN) in one way or the other. These include introducing safety problems to personnel and equipment. Technical impacts have also been reported extensively which cover aspects such as: (i) fault level can be increased to a degree that makes system reinforcement necessary, (ii) adaptation of new protection practices in order to provide adequate protection for EGs and associated network against any abnormal conditions including faults and islanding condition, (iii) limitation of harmonics introduction, (iv) stability and reliability related problems, (v) voltage fluctuations, (vi) interference with the control mechanism of voltage magnitude of distribution networks and (vii) minimisation of losses of distribution network (viii) the effect on relay settings of utilities feeders. The last point will be dealt with in some details in this paper.

3 SIMULATION OF A WIND FARM CONNECTED TO A DISTRIBUTION NETWORK USING EMTP

3.1 Advantages of using EMTP

Nowadays there are several commercial packages that can be used for power system studies but the experience have shown that most of them lack the flexibility to conduct fundamental research investigation. For this reason it has been decided to adopt the Electromagnetic Transient Program (EMTP) which has been used for several years for power system analyses under transient and dynamic conditions. Although this program is difficult to use and it takes rather long time to command it proved to be a very powerful and flexible tool. It consists of a library of models of network components such as electrical machines, transformers, lines, etc. that can be interconnected together to simulate any required electrical network.

The other reason for choosing EMTP for this work is that it offers an attractive way of modelling induction (or asynchronous) machines which are widely used in wind-farms using the concept of Universal Machine (UM) model that was proposed by Lauw and Meyer [5] in 1982. This model is found particularly attractive as the mechanical side of the machine can be conveniently represented using an equivalent electric network consisting of lumped RLC elements, which is then solved as part of the whole electric network. The mechanical torque on any mass connected to the shaft of the machine can be simulated by a current source [7].

3.2 The investigated system

The system considered in this investigation is shown in Fig. 1. It basically consists of a wind farm interconnected to a 33 kV distribution network through a 33 kV interfacing link. The distribution network in turn consists of the Grid represented by a voltage source behind its Thevenin's equivalent impedance and a substation represented by a 20 MVA, 132/33kV transformer with an impedance of 10%. The fault level of the Grid behind the 132kV busbar is assumed 1800MVA.

The wind-farm is assumed to have sixteen wind-turbine-generator units each rated at 600 kW and 690V. In order to simplify the simulation of the wind farm and at the same time to maintain the flexibility of having the ability to vary injected generation, generating units of the wind farm are represented by three UM models. The first machine, shown in Fig. 1, represents two 600 kW units, while the second machine represents four 600 kW units and the third machine represents ten 600 kW units. It is assumed that all units are connected to the common bus No 4. A 15 MVA, 690V/33kV step-up transformer with impedance of 10% is assumed between buses 3 and 4. All transformers are represented using EMTP transformer model that considers their connection group and the saturation effect of the magnetic core. The load connected to the substation is represented by a second feeder, which supplies two groups of loads connected at the middle and the end of the feeder via 33kV/416V transformers. Both the feeder and the interfacing link are simulated using EMTP lumped RLC and each of which is assumed to have an impedance (0.185 + j0.324) Ohm/km.

4 CASE STUDIES

The simulation developed for the system shown in Fig. 1 under EMTP is used to conduct a number of case studies, the results of which are presented in the following sections. It should be pointed out that although the number of wind turbine-generator units shown in Fig. 1 is sixteen distributed over three UM models as explained earlier. The necessity of varying power injection meant the actual number of units could be anything between 1 and 16 units distributed over one, two or three UM models depending on the magnitude of power injection under consideration.

4.1 Variation of wind-farm power output with wind speed variation

In order to simplify the analysis, it is assumed in this study, that the mechanical torque on the shaft of induction generators follows the same pattern of wind speed variation (8). Consequently the effect of wind speed variation is taken into account by using a randomly generated mechanical torque signal such as that shown in Fig 2a.

This signal is then applied to the shaft of the generator G1, shown in Fig. 1, which in this part of the study represents a single 600 kW unit. The corresponding electrical power output of generator G1 is shown in Fig. 2b. In this figure the 1 pu power output represents the rated power output of the unit, i.e. 600 kW. It can be seen from this figure that the power output follows the pattern of applied mechanical torque shown in Fig 2a.

Obviously this can be a very useful tool that may be used by industry for predicting the variation of a wind-farm power output at a specific site whereby the wind speed variation versus time is known either from forecasting or measurement.

4.2 Dynamic behaviour of wind farm induction generators following a fault within utility's network

The dynamic behaviour of wind-farm induction generators following a fault condition within utility's network has been considered. A three-phase fault is applied at the load feeder connected to bus No. 2. It is cleared after 70 msec. The resulting voltage variation at the wind-farm, i.e., bus No 4, versus time is shown in Fig 3a. It is evident form this figure that the voltage is gradually recovered its pre-fault value after the fault is being cleared off the system. It has also been observed that while each of the wind turbines at the wind-farm has accelerated to a speed equivalent to 108% of its per-fault speed, it regained its original speed after removing the fault from the system as shown in Fig 3(b).

In order to examine the effect of fault duration of on the dynamic behaviour of wind-farm induction generators, the study was repeated for the same fault condition described above but with longer duration. It was found that as the fault duration is increased, it reaches to a critical value beyond which the wind-farm can neither regain its pre-fault terminal voltage nor its pre-fault speed. Voltage magnitude settles at a value much less than its nominal value as shown in Fig 4(a) which would eventually prompt the operation of the under voltage relay as specified in G59/1 document (9). On the other hand if the wind turbine allowed to operate, its speed continues to grow, as shown in Fig 4(b), to a value which prompt the operation of over speed protection device normally installed on wind turbines. The time beyond which wind-farm induction generators behave in this way will be termed as "critical clearing time (CCT)". Such time will also be considered as the onset of the instability of induction generator. It should be pointed out that the concept of stability as applied to an induction generator is defined along the basis outlined above and not along the principles traditionally applied to synchronous machines.

For the system under consideration it has been found the CCT is 80 msec. This is obviously very small compared with the time settings of relays usually installed on feeders which can be in the region of 1 sec or above (10).

4.3 Comparison between CCTs due to voltage levels

The effect of connection voltage level on the CCT can be seen with reference to Fig 5. This figure shows the variation of terminal voltage of a 4.8 MW wind-farm with time once connected at 33 kV and then at 11 kV voltage levels. The fault duration in both cases corresponds to that related to the 33 kV CCT, i.e., 80 msec. It can be seen from Figure 5 that while the wind-farm regained its stability in the case when it is connected at 33 kV voltage level, it became unstable for the same fault duration when it is connected at 11 kV voltage level. The recovery of the wind-farm terminal voltage in first case and the collapse of the voltage in the second case indicate this.

4.4 Effect of power injection level by wind farm on the CCT

The effect of the magnitude of power injection from the wind-farm on the CCT has been examined. The result is demonstrated in Fig 6 which shows wind-farm terminal voltage variation with time due to minimum and maximum power injections of 600 kW and 9.6 MW respectively based on the assumption that the fault is cleared at their corresponding CCT of 105 msec. and 65 msec. It is evident from this figure that the CCT is effected by the magnitude of power injected to the network from the wind-farm. The CCT decreases with the injected power.

4.5 Effect of fault location at the 33kV utility's radial feeder on the CCT

The effect of fault location along the 33 kV load feeder (see Fig. 1) on the CCT is illustrated in Fig 7. This figure shows the variation of the CCT with the power injected from the wind-farm for three

different fault locations; namely at the feeder end connected to bus No 2, at a points 5 km and 10 km from bus 2. This figure demonstrates that the closer the fault to bus No 2, the smaller the CCT is. This suggests that if a co-ordination is to be achieved between the protection relays of utilities feeder and those at the wind-farm it should be based on the worse condition, i.e., on faults at the feeder end connected to bus No 2.

5 CONCLUSION

The EMTP has been successfully used to simulate a distribution system with a wind-farm integrated at 33 and 11 kV voltage levels. The developed simulated system is then used to demonstrate its capability of determining wind-farm power output due to a given wind-farm input torque variation (resulted from a certain wind speed variation). This can be a very useful tool both at planning and operating stages.

The simulated system is then extensively used to determine the effect of wind-farm on the CCT for faults on utilities' feeders. It has been concluded from this investigation that the integration of wind-farm into distribution network could greatly effect the magnitude of CCT of electrical feeder of the network. It has also been found that the magnitude of the CCT depends on factors such as the magnitude of injected generation, fault location and the voltage level at which a wind-farm is connected to the network.

6 ACKNOWLEDGEMENT

The authors would like to thank the Robert Gordon University for provision of facilities. Ibrahim Rida is grateful to the Robert Gordon University and the ORS in UK for their financial support to undertake this research

7 REFERENCES

1. K. Dodman, "Public opinion warms to windpower", International power generation, October 1999, pp. 16-17.

2. Soderholm, L H, "Interfacing small wind systems to rural power distribution systems", IEEE Trans on Ind. Appl., Vol IA-20, No 2, 1984, pp 439-442.

3. Kirkham, H and Das, R "Effect of voltage control in utility interactive dispersed storage and generation systems", IEEE Trans. Power Appar. & Syst., Vol PAS-103, 1984, pp 2277-82.

4. Salman, S K, Jiang, F and Rogers, W J S, "The effect of private generators on the voltage control of 11 kV networks and on the operation of certain protective relays", Athens Power Tech: IEEE/NTUA Inter. Conf. On Modern Power Systems, Athens, 5 – 8 September 1993, pp 591-595.

5. Salman, S K, "Optimising system losses by effective communication between embedded generators and distribution networks", ERA conf. - Protecting electrical networks and quality of supply. London, 22 -23 January 1997.

6. H K Lauw, W S Meyer, 'Universal Machine modelling for the presentation of electric machinery in an electromagnetic transient program,' IEE trans. Power App. Syst., Vol. PAS-101, June 1982.

7. K U Leuven EMTP Centre, 'Alternative Transient Program Rule Book,' Belgium, July 1987.

8. O. Wasynczuk and D. T. Man, 'Dynamic Behaviour of a class of wind turbine generators during random wind fluctuations,' IEEE Trans. on PAS, Vol. PAS-100, No. 6 June 1981, pp.

2837 - 2845.

9. Engineering Recommendation G59/1, "Recommendation for the connection of embedded generating plant to the public electricity suppliers' distribution system", Electricity Association, London, 1991.

10. W. J. S. Rogers, 'The Parallel operation of generating plant within a regional electricity company's distribution network,' IEE Colloquium on 'The parallel operation of generating plant within a public electricity network,' IEE, Chester, UK, Feb. 1991, pp 1.1 – 1.9

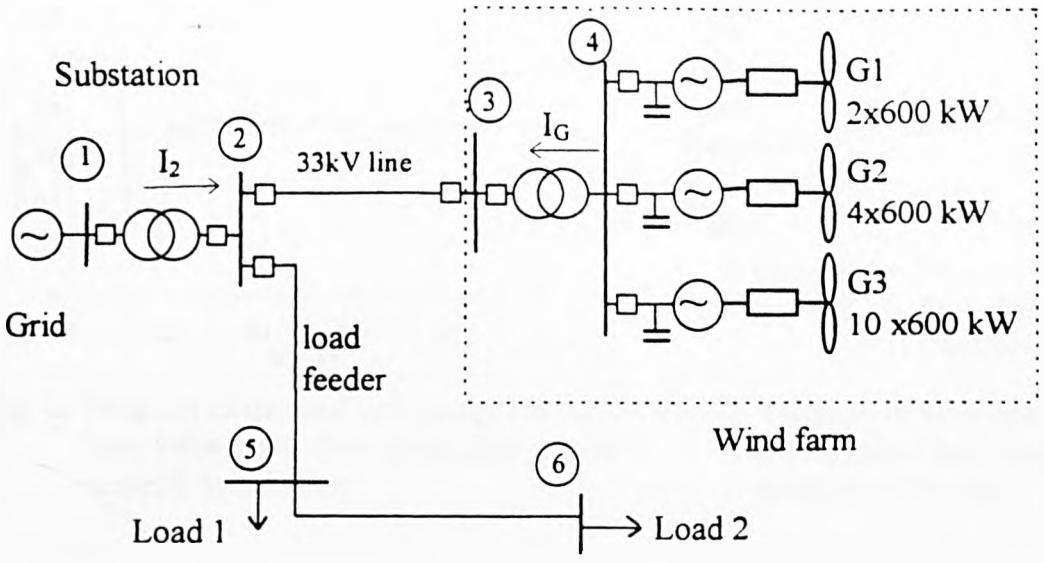

Fig. 1 Schematic diagram of the considered network.

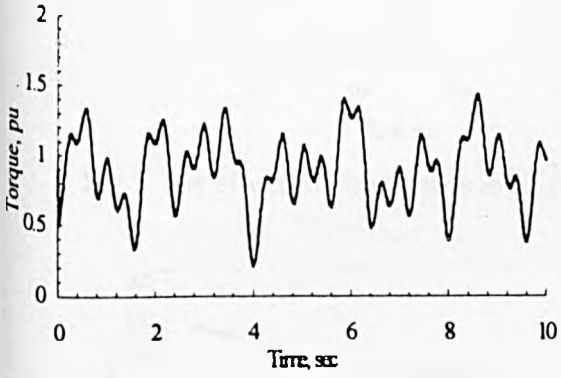

Fig. 2a Variable mechanical torque applied to the shaft of G1.

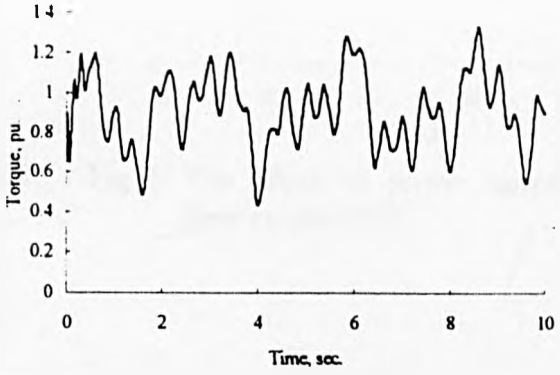

Fig. 2b Variation of output power of G1 due to input torque shown in Fig. 2a.

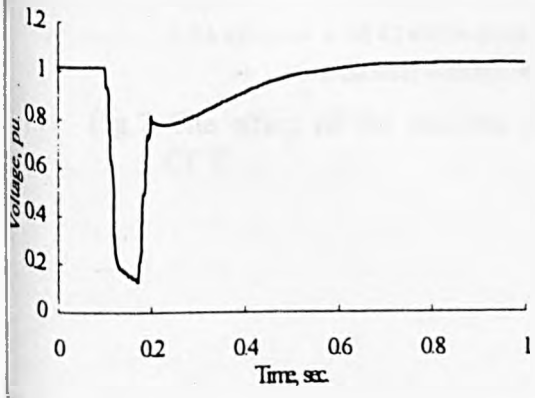

Fig. 3a Variation of terminal voltages of IGs at wind farm following a three phase fault on the network with a duration of 70 msec.

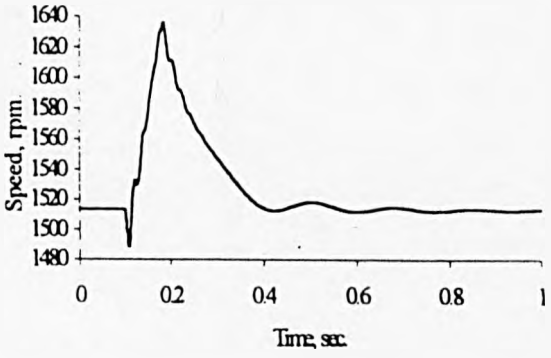

Fig 3b Variation of rotor speed of G1 following a three phase fault on the network with a duration of 70 msec.

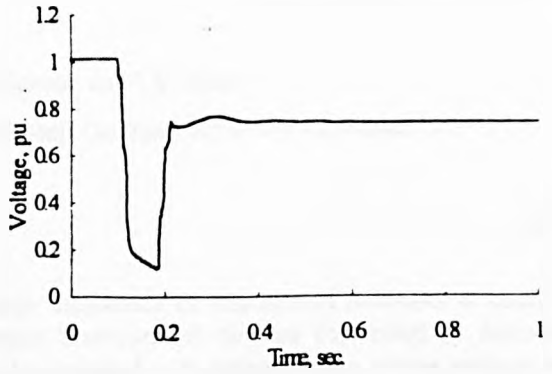

Fig.4a Variation of terminal voltages of the wind farm following a three phase fault on the network for 85 msec.

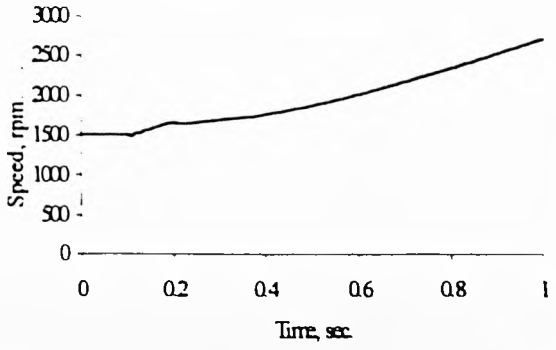

Fig. 4b Variation of rotor speed of G1 following a three phase fault on the network with a duration of 85 msec.

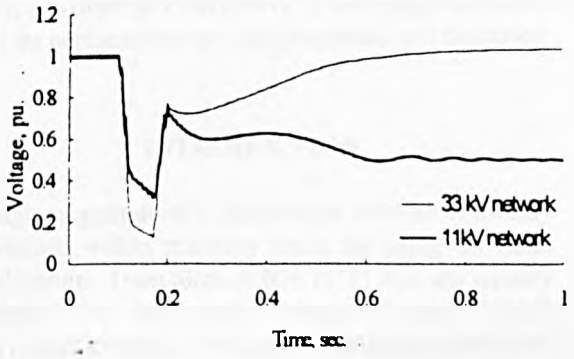

Fig.5 The effect of connection level on the CCT.

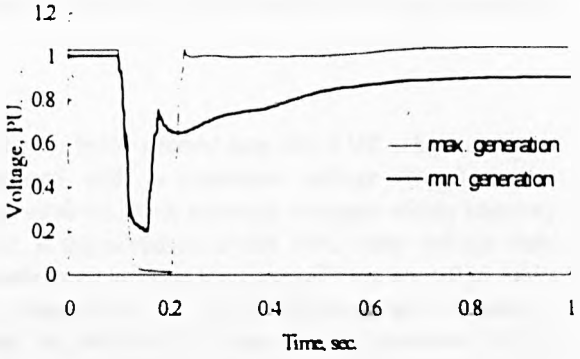

Fig. 6 The effect of power injected by wind farm on the CCT.

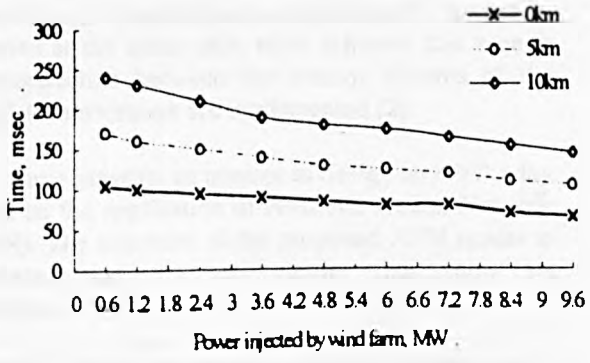

Fig.7 The effect of the location of fault on the CCT.

APPLICATION OF ARTIFICIAL NEURAL NETWORKS FOR THE VOLTAGE CONTROL OF DISTRIBUTION NETWORKS

S K Salman and I M Rida

The Robert Gordon University, Aberdeen, UK

ABSTRACT

Voltage magnitude of distribution networks is usually maintained within statutory limits by using On Load Tap Changer Transformers that are controlled by Automatic Voltage Control (AVC) relays. Traditional AVC relay usually equipped with compounding whose settings are chosen in such away to compensate for the voltage drop along the feeder(s) emanating from source substation. Compounding should also insure satisfactory operation of parallel-connected transformers. When these two requirements can not be satisfied at the same time, other schemes that require interconnection between the control systems of the parallel-transformers are implemented. This paper presents an attempt to design an AVC relay based on the application of Artificial Neural Network (ANN). The input data file used for the training of the proposed AVC relay model is prepared using a power system load flow program, which is written in FORTRAN. In this paper the structure of the proposed model is presented and the test results that show its performance are also presented and discussed.

INTRODUCTION

Voltage magnitude of a distribution network is usually maintained within statutory limits by using On Load Tap Changer Transformers (OLTCT) that are usually controlled by Automatic Voltage Control (AVC) relays. Conventional AVC relays are usually equipped with compounding to compensate for the voltage drop in the distribution network [1]. Compounding should also insure satisfactory operation of parallel-connected transformers. When these two requirements can not be satisfied at the same time, other schemes that require interconnection between the control systems of the parallel-transformers are implemented [2].

This paper presents an attempt to design an AVC relay based on the application of Artificial Neural Network (ANN). The structure of the proposed ANN model is presented and the test results that show its performance are also presented and discussed.

OPERATING PRINCIPLES OF AVC RELAYS

The operation of an AVC relay incorporates two main steps. The first step involves the calculation of the voltage of AVC relay using current and voltage values measured at the low voltage side of OLTCT. This voltage is given by the following expression [1]:

$$V_{AVC} = V - I_T (R_{AVC} \pm j X_{AVC}) \quad (1)$$

Where, V is the voltage of the terminals of the transformer on the secondary side, I_T is the transformer current, and $(R_{AVC} \pm j X_{AVC})$ is the relay compounding settings. Depending on the application, it consists of resistance and either positive or negative reactance. In the second step, the AVC relay voltage is compared with a reference voltage (V_{REF}) that is required to maintain network voltages within statutory limits. If the deviation of the AVC relay voltage from the reference voltage V_{REF} exceeds the specified limits of a bandwidth, say $\pm$2%, the relay then initiates a signal to operate the tap-changing device of the transformer.

BASIC PRINCIPLES OF ANN

Application of ANNs to electric power systems has received considerable attention in the recent years [3,4], especially in the field of control and protection where fast, accurate and on-line decisions are required to insure that power system stability and reliability are maintained. Different types of ANNs are described in literature. However, Multilayer Perceptrons type is the most popular for power system applications [5]. It is used in more than 80% of such applications. This type can be explained using a three layer neural network as shown in Fig. 1. As can be seen from this figure, the network comprises a number of interconnected processing elements (PE), known as artificial neurons [6]. The neurons are arranged in layers, including an input layer, followed by a hidden layer(s), and finally an output layer. Neurons in the input layer receive signals from external source and transmit them to the next hidden layer. Each neuron in the hidden layers or in the output layer receives a number of inputs (x_{ij}) equals to number of neurons in the previous layer. Each of these inputs is given by [6] :

$$x_{ij} = Y_i * w_{ij} \quad (2)$$

Where Y_i is the output of i_{th} neuron in the preceding layer and w_{ji} is the weight of the connection between i-th and j-th neurones of successive layers,

Hence, the total input to a neuron is given by [6,7]:

$$\mathbf{X}_j = \Sigma\, x_{ij} = \Sigma\, w_{ji}\, Y_i \qquad (3)$$

Where $\mathbf{X}_j$ is the total input to the j-th neuron in the hidden or output layer.

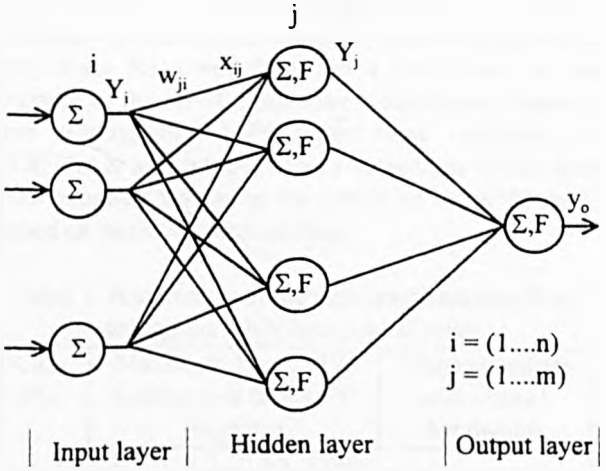

Fig. 1. A three layer neural network system

The output of jth neuron, Y_j, in the hidden or output layer is a function of the total input [6,7], i.e. :

$$Y_j = F(\mathbf{X}_j) \qquad (4)$$

Function F(x) can be any continuous differentiable non-linear function like the log-sigmoid, which is given by[6,7]:

$$F(x) = 1/(1+e^{-xi}) \qquad (5)$$

ANN must be first trained to work properly. In the training process a special training algorithm is used for adjusting the weights so that the network output for given inputs will be as close as possible to the desired output values. Training methods can be divided into supervised and unsupervised. In the supervised training method, the desired output is given in the data file. Supervised algorithms require longer learning time than the unsupervised, but they can be more accurate [5]. One of the most popular supervised learning algorithms is the Backpropagation method. It is based on a gradient-search optimisation method applied to an error function. The error function is calculated as the sum-of-squared errors, given by [6]:

$$e = \sum_i \left\{ y_{ik\ \text{calculated}} - y_{ikdesired} \right\}^2 . \qquad (6)$$

Where y_{ik} is the output of i_{th} neuron in the k_{th} layer.

The error in the outputs for a given input pattern is propagated back through the network to adjust the weights. A recursive algorithm is usually used to adjust the weights such that the error is minimised.

As mentioned above, the learning process requires a data file that contains pairs of input-output patterns. To be effective, the data file must include sufficient amount of training patterns that cover most possible conditions. Such a file can be made from historical records, computer simulation, or measured data [4].

The result of a successful training process is a set of weights that is assigned to the ANN. Using these weights, the network calculates an output very close to the desired values for each pattern in the training file. The network can then be considered ready for application.

THE PROPOSED ANN FOR CALCULATING THE VOLTAGE OF AVC RELAY

An ANN was designed to calculate the voltage of an AVC relay. The ANN model is similar to that shown in Fig.1. It comprises three layers, e.g. an input layer with three processing elements (PE), a hidden layer and an output layer with one PE. The inputs are derived from system voltage (V) and the real (I_r) and imaginary (I_{im}) components of the transformer current. The output is the calculated AVC relay voltage (V_{avc}). A training data file was obtained from a load flow (LF) program that was written in FORTRAN by simulating different steady-state operating conditions for the network shown in Fig.2.

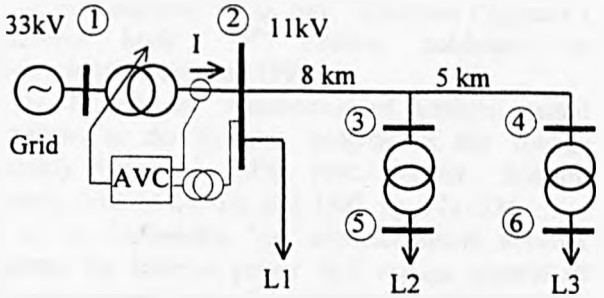

Figure 2. Single line diagram of the considered distribution network

The distribution network comprises a 33/11kV substation, a radial load feeder connected with two groups of variable loads via 11/0.415 kV transformers. One group is represented by the load L2 with a total power of 1MW and the second group is represented by the load L3 with a total of 2MW. L2 is assumed connected at a distance of 8 km from the substation and load L3 is assumed connected at a distance of 13 km. In order to simplify the model, a bulk load, L1, with a total power of 9MW, is assumed connected to the substation to represent other load feeders. Voltage control was achieved by a conventional AVC relay

with a positive compounding. The reference voltage for control is assumed equal to 1pu and the calculated voltage was allowed to vary by ± 2%. The three loads are allowed to change from zero to maximum and to zero again in incremental steps simultaneously. When the calculated AVC voltage exceeded the ± 2% limits, the AVC relay initiates a signal to adjust the tap-changer. The calculated results at every step were saved in a training data file. Several load flow cases with different combinations of the system loads were simulated and the results were saved in separate files and used in the ANN testing stage. Table 1 shows a summary of the simulated cases. From all these cases, only Case No 1 and Case No 4 were used for the training of the ANN. Following a satisfactory training and testing, the ANN model was converted to FORTRAN and integrated as a subroutine in the load flow program instead of the model of the AVC relay based on positive compounding.

Table 1. A summary of the simulated cases used for testing the ANN based AVC relay.

Case No	Maximum Load, MW Load power factor, PF (lagging)				Voltage setting and control bandwidth
	L1	L2	L3	PF	
1	**9**	**1**	**2**	**.98**	**1 + 2 %**
2	3	1	2	.98	1 + 2 %
3	3	0	2	.98	1 + 2 %
4	**9**	**1**	**2**	**1.0**	**1 + 2 %**
5	3	1	2	1.0	1 + 2 %
6	3	0	2	1.0	1 + 2 %
7	9	1	2	.98	0.98 + 2 %
8	3	1	2	.98	0.98 + 2 %
9	3	0	2	.98	0.98 + 2 %

TESTING THE PERFORMANCE OF THE ANN MODEL

The performance of the proposed ANN for calculating the voltage of AVC relay was tested by running the ANN model in the test mode. Two examples of the test results are shown in Fig. 3 and 4. These figures show a comparison between the AVC voltage as calculated using conventional method and ANN based method. The voltage curves in Fig. 3 correspond to case No. 2 of Table 1 and the curves in Fig. 4 correspond to case No. 3. It can be seen from these results that the ANN based AVC relay is able to calculate the relay voltage with a negligible error.

The ANN based relay when integrated in the load flow program was also tested and its performance was compared with the performance of the relay based on the conventional method. Figures 5 to 10 show pairs of examples of the test results for both the ANN and conventional based AVC relays. These figures show the variation of the voltages of the network shown in Fig. 2 as the connected loads change from zero to their maximum value and back to zero. It can be seen from these results that, although it was trained using only two cases, the ANN based AVC relay could provide a voltage control of the network similar to that provided using conventional AVC relay based on positive compounding.

CONCLUSION.

The use of an ANN in calculating the voltage of AVC relay was investigated in this paper. The results obtained were found very encouraging. The proposed ANN based AVC relay could provide proper voltage control of a distribution network as loads changed with different patterns. It was shown that the performance of the relay was not affected when the reference voltage of the relay was changed. Further investigation should focus on the application of the proposed method in the voltage control of a network that includes parallel connected transformers and embedded generation.

ACKNOWLEDGEMENT

The authors would like to thank the Robert Gordon University for provision of facilities. Ibrahim M. Rida is grateful to the Robert Gordon University and the Committee of Vice-Chancllors and Principals of UK for their financial support to undertake this research

REFERENCES.

1. S K Salman, W J Rogers, 'Effects of wind power generators on the voltage control of utility distribution networks,' Renewable Energy, IEE, 1993.
2. M, A, Laughton, M, G, Say, 'Electrical Enginner's reference book', 15th Edition, published by Butterworth-Heinmann, 1993.
3. H. P. Schmidt, 'Application of artificial neural networks to the dynamic analysis of the voltage stability problem,' IEEE Proc.- Gener. Transm. Distrib., Vol. 144, No.4, July 1997, pp. 371- 376.
4. A. A. El-Samahy, 'An artificial neural network scheme for reactive power and voltage control of power systems,' Proc. of the fifth international Middle East Power Conference MEPCON'97, Alexandria, Egypt, Jan 1997, pp. 62 - 65.
5. S M Halpin, R F Burch, 'Applicability of neural networks to industrial and commercial power systems: A tutorial overview,' IEEE Trans. on Industry Applications, Vol. 33, No. 5, September/October 1997.
6. Philip D. Wasserman, 'Neural computing, Theory and practice,' VAN NOSTRAND REINHOLD, New York, 1989.
7. R Beale, T Jackson, 'Neural computing, an introduction,' Adam Hilger, Bristol, 1990.

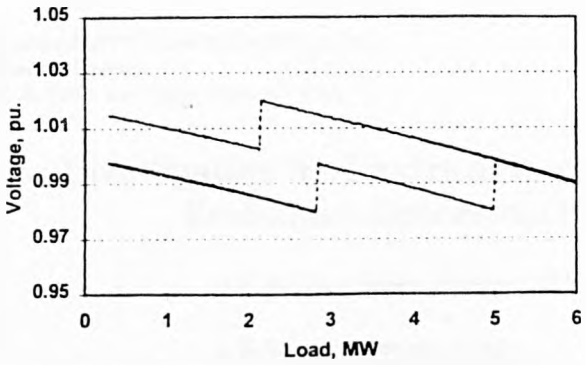

Fig.3 AVC relay voltage as calculated using conventional method and ANN.(Case 2).
Conventional ANN

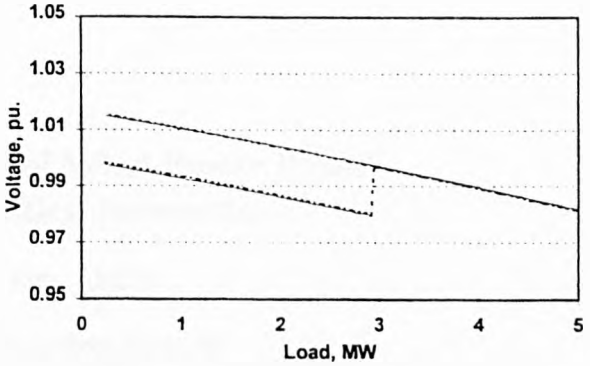

Fig.4 The AVC relay voltage as calculated using conventional method and ANN. (Case 3).
Conventional ANN

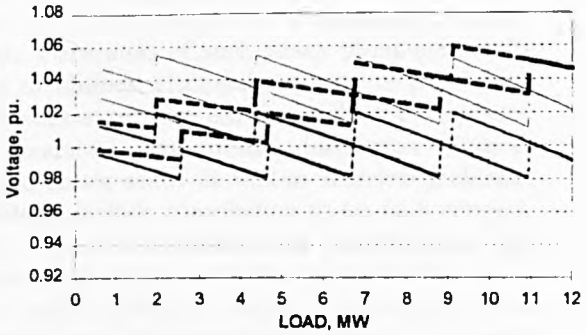

Fig. 5 Network voltages for Case No 1 when AVC relay was based on positive compounding.
V2 V4 V6 Vavc

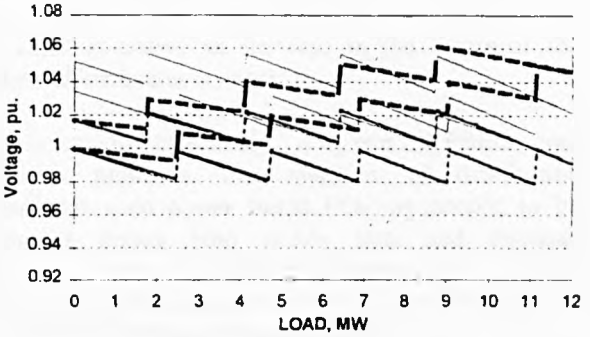

Fig. 6 Network voltages for Case No 1 when AVC relay was based on ANN.
V2 V4 V6 Vavc

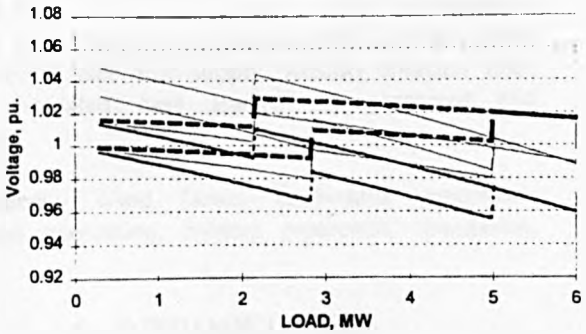

Fig. 7 Network voltages for Case No 2 when AVC relay was based on positive compounding.
V2 V4 V6 Vavc

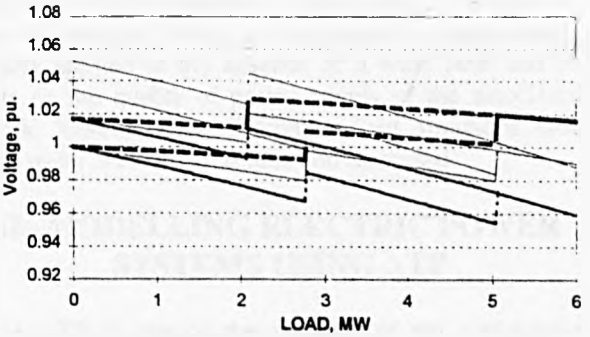

Fig. 8 Network voltages for Case No 2 when AVC relay was based on ANN.
V2 V4 V6 Vavc

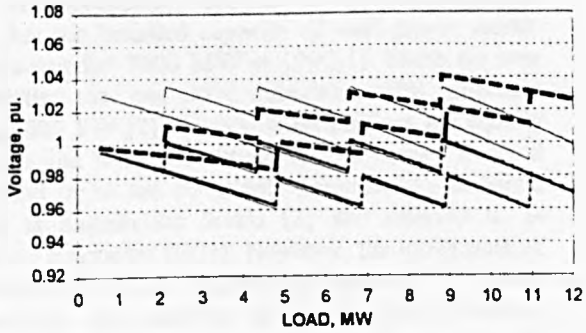

Fig. 9 Network voltages for Case No 7 when AVC relay was based on positive compounding.
V2 V4 V6 Vavc

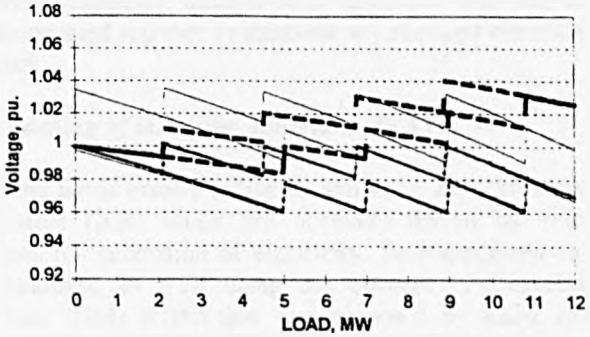

Fig. 10 Network voltages for Case No 7 when AVC relay was based on ANN.
V2 V4 V6 Vavc

Proceedings of the IASTED International Conference
Power and Energy Systems
November 8-10, 1999, Las Vegas, Nevada - USA

Investigating the Electrical Integration of Wind Power Based Embedded Generation into Utilities' Networks

S K Salman, Senior Member, IEEE I M Rida, AMIEE

S.K.Salman@eee.rgu.ac.uk I.M.Rida@eee.rgu.ac.uk
School of Electronic and Electrical engineering,
The Robert Gordon University,
Aberdeen, AB10 1FR, UK

Abstract: Recently wind power based embedded generation (WPBEG) has received considerable attention world-wide. Generators of such power plants are usually connected to utilities' electrical networks at distribution levels. Previous experience has shown that the integration of such generators into utilities' distribution networks (DNs) could create safety as well as technical problems. Such problems include contribution to the fault currents, stability, voltage fluctuation, and problems to the automatic voltage control, etc. Therefore, the operation of DNs that include WPBEG requires investigation both during steady state and dynamic conditions. This paper reports an investigation conducted on a simulated system consisting of a wind farm integrated into a DN using Alternative Transient Program (ATP). The investigation covers two main aspects; the effect of the integration of the wind farm into a DN on the settings of protective relays of electrical feeders and its effect on the power quality of the electrical supply. Results obtained from various simulated case studies are presented and discussed.

Keywords: Wind farms, Embedded generators, Distributed generation, System protection, Simulation, ATP.

I. INTRODUCTION

Recently wind energy has been considered as one of the most attractive renewable energy resources. The technology for the generation of electricity using wind turbines is operationally proven. It has been reported recently that the installed capacity of wind power world-wide has exceeded 7600 MW in 1997[1]. There are now wind turbines that can drive generators with capacities reaching 1500 kW [2]. Several wind turbines are usually installed at one site constituting what is known as wind farms. Wind farms are commonly connected to electrical networks at distribution levels [3] and referred to as Embedded Generators (EGs). However, the integration of wind farms with utilities distribution networks may create safety as well as technical problems. Such problems include contribution to the fault currents, stability and reliability problems, introduction of harmonics, voltage fluctuations, interfering with the process of automatic voltage control (AVC) of distribution networks [4] and in some cases it causes an increase in the losses of the associated distribution network.

In order to effectively integrate WPBEG into distribution networks, the operation of distribution systems with wind power based EGs are needed to be investigated during both steady state and dynamic conditions. Digital simulation programs are usually utilised for such investigation. One of these programs is the Alternative Transient Program (ATP).

In this paper the ATP is used to simulate a wind farm integrated into a distribution network. The model is then used to investigate the effects of the integration of the wind farm into the network on the setting of protective relays of electrical feeders as compared with those settings normally applied in the absence of a wind farm and its effects on the quality of power supply of the associated network. Results obtained from various simulated case studies using ATP are presented and discussed.

II. MODELLING ELECTRIC POWER SYSTEMS USING ATP

The ATP is one of the versions of the well-known Electro-Magnetic Transient Program (EMTP) which has been used for several years for power system analyses under transient and dynamic conditions. It consists of a library of models of network components such as electrical machines, transformers, lines, etc. that can be interconnected together to simulate any required electrical network.

A. Modelling of induction generators in ATP

Wind farms usually utilise induction (or asynchronous) generators (IGs) which are normally driven by wind turbines for generation of electricity. Such machines can be simulated in ATP using the concept of Universal Machine (UM) model that was proposed by Lauw and Meyer [5] in 1982. The UM is considered as an electromechanical energy conversion device that can be

used to simulate the electrical and mechanical components of electrical machines. The UM model embedded in the ATP library can be used to represent 12 major types of electric machines, e.g. single-phase and multiple-phase synchronous or induction machines and dc machines [6]. This model is found particularly attractive because the mechanical side of the machine can be conveniently represented using an equivalent electric network consisting of lumped RLC elements, which is then solved as part of the whole electric network. For example each mass connected to the shaft system can be represented by creating a node in the equivalent electric network whereby a capacitor is placed between the node and the ground to represent the moment of inertia of that mass. The mechanical torque on that mass can be simulated by a current source connected between the same node and the ground [7].

B. Modelling the network under consideration

The considered distribution system shown in Fig. 1 has been modelled using ATP. As the figure shows, it comprises a wind farm, a substation represented by a 10 MVA, 33/11 kV transformer with an impedance of 10%, and an 11 kV interfacing feeder connecting the wind farm with the substation. The wind farm is assumed to have eight wind-turbine-generator units each of 600 kW with a nominal voltage of 690V. In order to simplify the simulation of the wind farm and at the same time maintain the flexibility of having the ability of varying the injected generation, generating units of the wind farm are represented using the ATP package by three UM models. The first machine, shown in Fig. 1, represents a single 600 kW unit, while the second machine represents two 600 kW units, and the third machine represents five 600 kW units. It is assumed that all units are connected at the same bus No 4. A 7.5 MVA, 690/11000 V step-up transformer with an impedance of 7.5% is assumed between buses 3 and 4. All transformers are represented using the ATP transformer model that considers their connection group and the saturation effect of the magnetic core.

The load connected to the substation is represented by a second feeder which supplies two groups of loads connected at the middle and the remote end of the feeder via 11kV/416V transformers. The feeders are simulated using the ATP lumped RLC model. Both the interfacing and load feeders have an impedance of (0.185+j324) ohm/km. The utility's network (Grid) is represented by a source behind the system equivalent impedance. The fault level of the Grid behind the 33kV busbar is assumed 600MVA.

III. INVESTIGATED CASES

A. Dynamic behaviour of WPBE following a fault within the network.

The dynamic behaviour of induction generators in the wind farm following a fault on the network is investigated. One of the considered cases was a three phase to ground fault which is assumed to occur at the end of the load feeder connected to the substation. The fault was initially assumed to be cleared after 60ms. Fig. 2a shows the variation of the terminal voltage of induction generators at the wind farm, i.e. at the 690V bus-bar No. 4. It can be seen from this figure that the voltage magnitude has dropped to a value less than 35% of its nominal value.

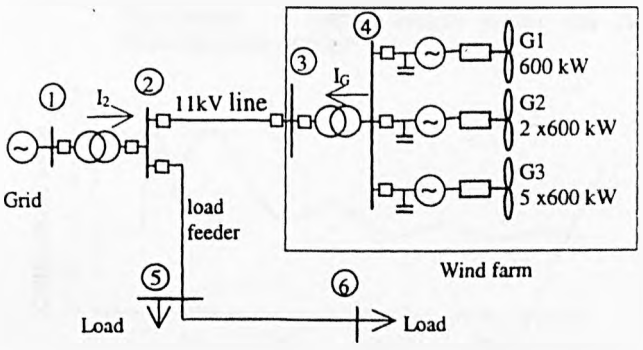

FIG. 1 SCHEMATIC DIAGRAM OF THE CONSIDERED NETWORK.

Since the electro-magnetic torque (T_e) developed inside an induction machine at any given speed is proportional to the square of the terminal voltage as follows[8]:

$$T_e = K\, s\, V^2 \qquad (1)$$

where K is a constant, s is the machine slip.

T_e is bound to reduce following a fault condition, as shown in Fig.2b. This figure shows the Electro-magnetic torque inside the air-gap of the first generator. On the other hand, the dynamic behaviour of the rotor is governed by the swing equation given below [8]:

$$J\frac{d\omega}{dt} = T_m - T_e \qquad (2)$$

where J is the moment of inertia of the rotating mass, T_m is the mechanical torque on the rotor and ω is the rotor speed.

From (2), it can be concluded that if the mechanical torque is kept constant, then any reduction in the electro-magnetic torque will cause the rotor to accelerate. This is demonstrated for the case under consideration by the rotor speed variation curve shown in Fig.2c. When the fault is cleared, the magnetic field inside the air-gap of the

machine starts to recover as a consequence of an inrush current which is drown from the network, as shown in Fig.2d. The resulting electro-magnetic torque would act on the rotor in a direction opposite to that of the applied mechanical torque. If the newly established stored energy in the rotating magnetic field becomes higher than the energy stored in the rotating mass, rotor speed would be reduced and the generator would eventually return to its normal operating condition, otherwise, its speed continue to increase until it is tripped by appropriate protection devices. As the exchange of power can not occur instantaneously due to the inductance of machine windings and the inertia of the rotating mass, electro-magnetic torque, speed and current will vary in oscillatory fashion with an exponentially decaying envelope versus time as can be seen in Figs 2b,2c and 2d respectively. This investigation was repeated for different fault clearing time values. It was found that for the system under consideration IGs can not retain its speed for a clearing time greater than 65 msec.

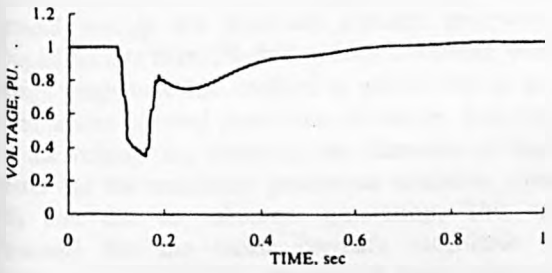

FIG. 2A. VARIATION OF TERMINAL VOLTAGES OF EGS AT WIND FARM FOLLOWING A THREE PHASE FAULT ON THE NETWORK FOR 60MSEC.

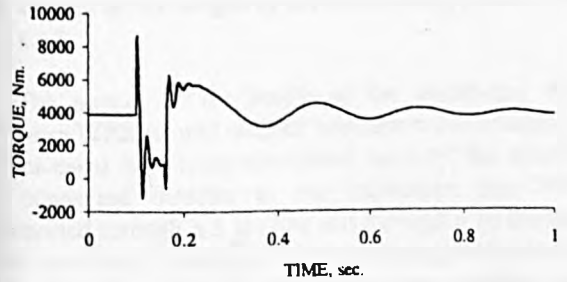

FIG. 2B. VARIATION OF ELECTROMAGNETIC TORQUE INSIDE THE AIR GAP OF THE 600 KW IG FOLLOWING A THREE PHASE FAULT ON THE NETWORK FOR 60MSEC.

Such time will be thereafter known as the critical clearing time (CCT). This time is therefore considered as the time beyond which induction generator(s) losses its(their) stability. This investigation has shown that when the fault is cleared at time greater than the CCT, the rotating speed of IGs continued to increase and induction generators continued to draw high inrush currents from the network until these generators are disconnected from the network by over speed protection devices which are usually installed on IG in such application. The high inrush currents resulted in a sustained voltage sag at the generator terminals when the fault is cleared beyond the CCT. Fig. 3a shows such voltage for a CCT of 70 msec. The corresponding total current drawn by the wind farm is shown in Fig.3b.

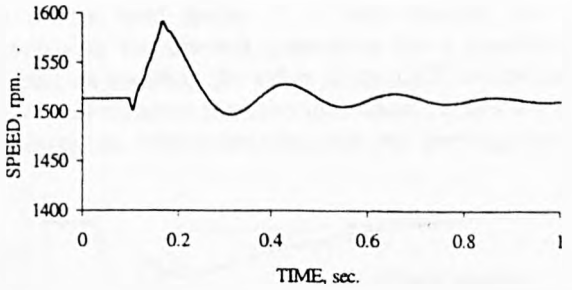

FIG. 2C. VARIATION OF ROTOR SPEED OF THE 600 KW IG FOLLOWING A THREE PHASE FAULT ON THE NETWORK FOR 60MSEC.

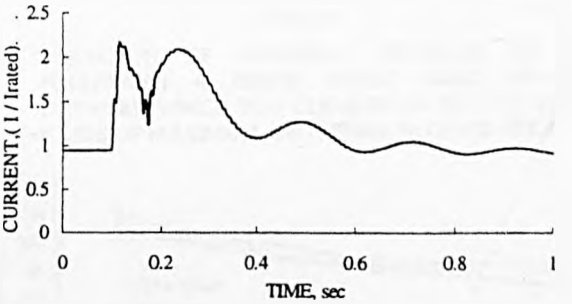

FIG. 2D. VARIATION OF THE TOTAL CURRENT OF WIND FARM FOLLOWING A THREE PHASE FAULT ON THE NETWORK FOR 60MSEC.

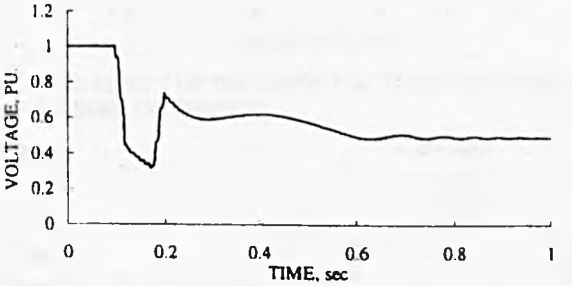

FIG. 3A. VARIATION OF TERMINAL VOLTAGES OF EGS AT WIDFARM FOLLOWING A THREE PHASE FAULT ON THE NETWORK FOR 70MSEC.

B. Impact of the magnitude of injected generation by WPBEG on the CCT

The impact of the magnitude of injected generation by WPBEG on the CCT has also been investigated. Two extreme cases are considered; the first case corresponds to operating the wind farm with only one turbine-generator, i.e., the injected generation is 600 kW.

The other extreme corresponds to the operation of the

wind farm at its full capacity, i.e. the injected generation8x600 kW. The end of the load feeder

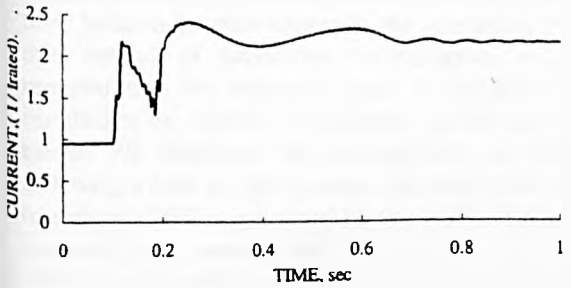

FIG. 3B. VARIATION OF THE TOTAL CURRENT OF WIND FARM FOLLOWING A THREE PHASE FAULT ON THE NETWORK FOR 70MSEC.

connected to the substation is subjected to a three phase fault for the two cases and the CCT was then examined. It was found that the CCT for the first case is 105 msec, whereas, the CCT for the second case is 65 msec. Fig. 4 shows a comparison between the generator terminal voltage for both cases. This figure also shows that the terminal voltage for minimum injected generation has dropped to less than 5% during fault condition, while the voltage magnitude has dropped to about 35% in the case of maximum injected generation. However, it is observed that the voltage sag following the clearance of fault was greater for the maximum generation condition compared with that due to minimum generation. This can be explained that the inrush current's magnitude during maximum generation is due to all units while during minimum generation condition is due to only one unit.

C. *Impact of the length of the interfacing feeder on the CCT.*

The impact of the length of the interfacing feeder between WPBEG and utilities' substation was examined. Three cases have been considered, namely, the wind farm is connected directly to the substation bus No. 2, connected through a 5 km line and through a 10 km line. It was found that the length of the interfacing feeder has only a small effect on the CCT. For the network under consideration, it was found that the direct connection of the wind farm to the substation give rise to a lower CCT compared with the connection through a 5 km or a 10 km feeders. It is also found that the difference between the values of the CCT due to direct connection and through a 10 km feeder does not exceed 15 msec, as shown in Fig.5. This figure also shows the corresponding variation of the CCT versus the injected power by the wind farm due to the three considered cases.

D. *Effect of the location of faults on the CCT*

In order to determine the effect of fault location within the utility on the CCT, a three phase to ground fault was assumed to occur at three different locations on the load feeder including its end which is close to bus 2, bus 5 and bus 6. The study was repeated for different generation injection from the wind farm for each of these locations. It is observed that the CCT, which decides the stability of IGs at the wind farm, is greatly affected by the location of fault on the load feeder. It is also observed that the magnitude of the injected generation has a considerable influence on deciding the value of the CCT for the faults which occur far away from the substation, i.e. bus 6. Fig. 6 summarises the results obtained from this investigation.

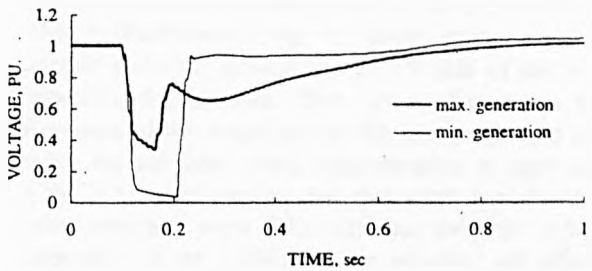

FIG.4. VARIATION OF TERMINAL VOLTAGES OF EGS FOLLOWING A THREE PHASE FAULT ON THE NETWORK WHICH WAS CLEARED AT THE CCT IN THE CASES OF MAXIMUM AND MINIMUM GENERATION

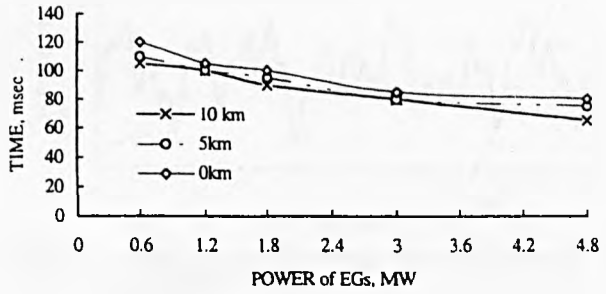

FIG. 5 THE EFFECT OF THE LENGTH OF THE INTERFACING FEEDER ON THE CCT

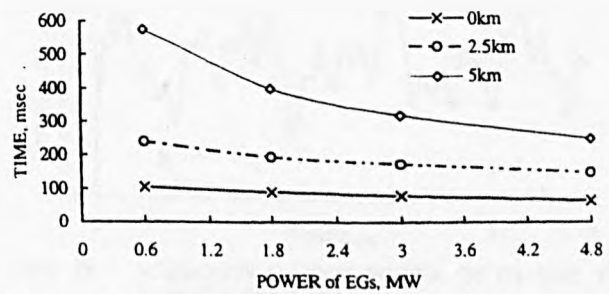

FIG. 6 THE EFFECT OF THE LOCATION OF FAULT ON THE CCT

E. *Impact of EG on protection co-ordination of the network.*

In the absence of EG the normal practise to achieve proper protection co-ordination in distribution network is to insure that the operating time of protective devices

located at the far end of a feeder be minimum. The operating time of other protective devices along the feeder, on the other hand, are progressively increased as their location become nearer to the substation. Following this method of protection co-ordination it has been reported that the operating time of protective devices installed at the source of the feeder can be as high as 1.5 second [9]. However this investigation has shown that following a fault on the network, the restoration of normal operation of EG is governed by the fault clearing time. It has also been shown that the maximum clearing time which is acceptable for normal operation of EG may vary depending on the magnitude of injected generation, the length of the interfacing link between the wind farm and the network, and the location of the fault within the associated network. For the network under consideration, it is found that the maximum CCT for a three phase fault does not exceed 600ms (see Fig. 5 and Fig. 6). It is therefore important that the protection co-ordination should be carefully looked at when the integration of EG into a distribution network is considered.

F. Effect of wind velocity variation on power quality

It is well known that wind speed variation can affect the generated electrical power output of WPBEG [10-12]. In order to examine the effect of wind speed variation on the power quality and other electrical parameters such as the current through substation transformer which is usually used in the process of automatic voltage control, the dynamic behaviour of the network under consideration during wind fluctuations using the ATP program has been considered.

In order to simplify the analysis, it is assumed in this study, that the mechanical torque on the shaft of induction generators follows the same pattern of wind speed variation [11]. Consequently the effect of wind speed variation is taken into account by using a randomly generated mechanical torque signal such as that shown in Fig 7a. This signal is then applied to the shaft of generator G1, shown in Fig. 1. The corresponding electrical power output of generator G1 is shown in Fig. 7b. In this figure the 1 pu power output represents the rated power output of the unit, i.e. 600 kW. It can be seen from this figure that the power output follows almost the same pattern of the applied mechanical torque shown in Fig 7a.

Since not all individual wind turbines within a wind farm are usually subjected to the same wind speed variation, different signals are required to be applied to the three generating units of Fig 1. Fig. 7c shows the assumed resulting speed variation of the shaft of the three induction generators. Fig. 7d shows the corresponding total power output from the wind farm. The 1 pu power in this figure represents the total capacity of wind farm, i.e. 4.8 MW. By comparing Figs. 7b with Fig. 7d, it can be concluded that the variation of the total power output of the wind farm is smoother than that of individual units. As stated earlier, this is due to the fact that not all wind turbines in a wind farm are subjected to the same wind speed variations.

The relative deviation of the power output of the wind farm with respect to its mean value may affect the quality of the power supplied to local loads. It may also cause fluctuation to other electrical parameters, such as the current through the substation transformer, which is normally used in controlling the quality of system voltage. This is illustrated in Fig. 7e, which shows a plot of the current variation through the 11 kV side of the 10 MVA substation transformer. This figure also shows that the deviation of the magnitude of this current around its mean value for the case under consideration is approximately 12%. It is worth noting that this work has shown, as in other reported work [11], that the terminal voltages of generators at the wind farm are virtually not affected by wind variation.

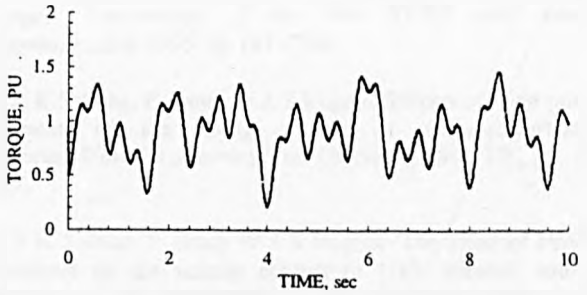

FIG 7A VARIABLE MECHANICAL TORQUE APPLIED TO THE SHAFT OF G1

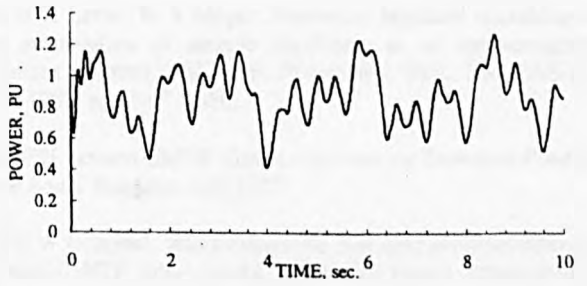

FIG. 7B VARIATION OF OUT POWER OF G1 DUE TO RANDOM INPUT TORQUE

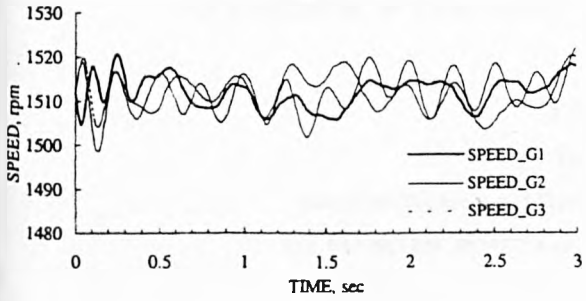

FIG. 7C ROTOR SPEED OF THREE GENERATORS DUE TO RANDOM INPUT TORQUES

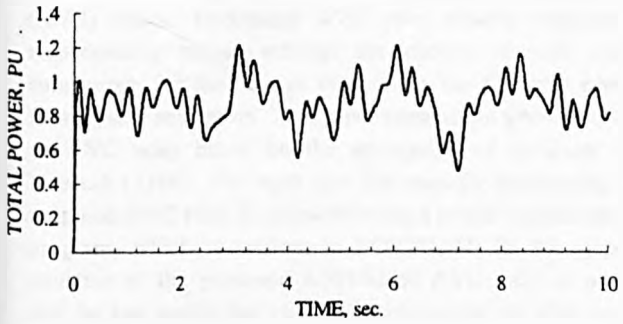

FIG. 7D VARIATION OF THE TOTAL WIND FARM POWER OUTPUT DUE TO RANDOM INPUT TORQUES

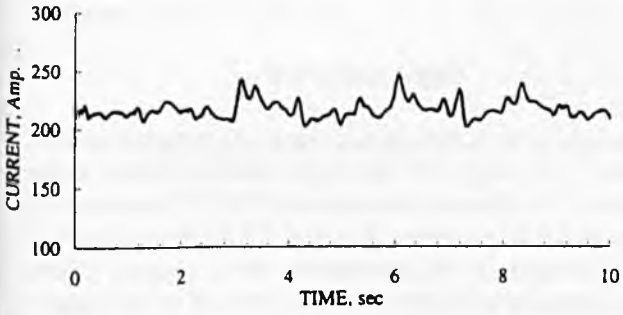

FIG.7E VARIATION OF THE CURRENT THROUGH TRANSFORMER AT SUBSTATION DUE TO RANDOM INPUT TORQUES AT THE WIND FARM

IV. CONCLUSION

The ATP package has successfully been used to simulate a distribution system with a wind farm integrated at 11 kV voltage level. The simulated system is then used to investigate certain aspects related to the integration of WPBEG into distribution networks. The conclusion drawn from this investigation is that the presence of WPBEG greatly affects the value of the CCT of electrical feeders of the network. It is found that the integration of WPBEG requires much smaller CCT compared with that normally used in the absence of such EG. It has also concluded that such CCT depends on factors such as the magnitude of injected generation, fault location and the length of the interfacing feeder between the wind farm and the distribution farm. This investigation also covers the effect of wind speed variation on the power quality of electrical supply whereby it is found that wind speed variation can cause power fluctuation at the output of the wind farm. It is also found that such power fluctuation could introduce variation in other electrical parameters such as the current through the substation transformer which in turn could affect the process of maintaining the quality of network voltage.

V. ACKNOWLEDGEMENT

The authors would like to thank the Robert Gordon University for provision of facilities. Ibrahim M. Rida is grateful to the Robert Gordon University and the Committee of Vice-Chancllors and Principals of UK for their financial support to undertake this research

VI. REFERENCES

[1] Kevin Dodman, 'Public opinion warms to windpower,' *IPG international power generation,* Vol. 21, No. 6, October 1998, pp. 16-17.

[2] P. Gardner, et al, 'Network connection of large wind turbines,' *Proceedings of the 17th BWEA wind energy conference.,* July 1995. pp 161 - 166.

[3] S K Salman, F Jiang, W J S Rogers, 'Effects of wind power generators on the voltage control of utility distribution networks,' *Wind Engineering,* Vol. 18, No. 4, 1994, UK, pp. 181 - 187.

[4] S K Salman, F Jiang, W J S Rogers, 'The effect of Private Generators on the voltage control of 11kV network and on operation of certain protective relays,' *Proceedings of the NTUA/IEEE Int. Conference on Modern Power Systems,* Athens, Greece, Sept. 1993.pp 591-595.

[5] H K Lauw, W S Meyer, 'Universal Machine modelling for the presentation of electric machinery in an electromagnetic transient program,' *IEE trans. Power App. Syst.*, Vol. PAS-101, June 1982. pp 1342 -1350.

[6] K U Leuven EMTP Centre, *'Alternative Transient Program Rule Book,'* Belgium, July 1987.

[7] H W Dommel, *'Electromagnetic transient program reference manual (EMTP theory book),'* Bonneville Power Administration, Portland, USA, August 1986.

[8] Mulukutla S. Sarma, *'Electric machines, steady-state theory and dynamic performance,'* West publishing company, USA, 1985.

[9] W. J. S. Rogers, 'The Parallel operation of generating plant within a regional electricity company's distribution network,' *IEE Colloquium on 'The parallel operation of generating plant within a public electricity network,'* Chester, UK, Feb. 1991, pp

ANN-BASED AVC RELAY FOR VOLTAGE CONTROL OF DISTRIBUTION NETWORK WITH AND WITHOUT EMBEDDED GENERATION

S K Salman and I M Rida

The Robert Gordon University

School of Electronic and Electrical Engineering , Schoolhill, Aberdeen AB10 1FR, UK

Tel: +44 (0)1224 262448, Fax: +44 (0)1224 262424, E_mail: s.k.salman@eee.rgu.ac.uk

Abstract: Voltage magnitude of distribution networks is usually maintained within statutory limits by using On Load Tap Changer Transformers that are controlled by Automatic Voltage Control (AVC) relays. Traditional AVC relay usually equipped with compounding whose settings are chosen in such away to compensate for the voltage drop along the feeder(s) emanating from source substation. This paper presents an attempt to design an AVC relay based on the application of Artificial Neural Network (ANN). The input data file used for the training of the proposed AVC relay is prepared using a power system load flow program, which is written in FORTRAN. In this paper the structure of the proposed ANN-based AVC relay is presented and the test results that show its performance are also presented and discussed.

Keywords: Voltage control, Distribution network, Embedded generation, Distributed generation, Artificial Neural Network

I. INTRODUCTION

Voltage magnitude of a distribution network is usually maintained within statutory limits by using On Load Tap Changer Transformers (OLTCT) that are usually controlled by Automatic Voltage Control (AVC) relays. Conventional AVC relays are usually equipped with compounding to compensate for the voltage drop in the distribution network]. Compounding should also insure satisfactory operation of parallel-connected transformers. It has been reported [1-3] that the integration of dispersed or embedded generators (EGs) into utilities' distribution networks could introduce problems to the performance of these relays. It has been found that the voltage measured by a conventional AVC relay is shifted up or down compared with that obtained in the absence of EG(s) depending on the power factor of the current through OLTCT. The latter in turns depends on the power factor of embedded generators and system loads. As a result, a proper voltage control of the distribution network can not be achieved

This paper presents an attempt to design an AVC relay based on the application of Artificial Neural Network (ANN). The structure of the proposed ANN model is presented. The test results which show its performance are also presented and discussed.

II. DEFINITION OF THE PROBLEM

Prior to the deregulation and restructuring of electric utilities in recent years, voltage control of distribution networks is achieved using on-load tap changer transformers that are controlled by automatic voltage control (AVC) relays. The operating principles of such relays are outlined in [2]. They are based on the assumption that the role of distribution networks is confined to transferring electric power from transmission systems to load centres. However the deregulation process which led to the integration of embedded generation in large number into network at distribution levels makes the above assumption no longer valid. This in turn has led to the deterioration of the performance of existing AVC relays due to their inability to accommodate EG. Consequently it has becoming increasingly important to develop new principles for AVC relay which enable them to properly regulate voltage magnitudes of distribution networks whether EG(s) integrated into them or not.

III. SIMULATION OF DISTRIBUTION NETWORK

Figure 1 shows a single line diagram of a distribution network with embedded generation and the typical application of the AVC relay in such a network. This network consists of a substation represented by a transformer, T1, connected between buses 1 and 2 which is equipped by on-load tap changer. The substation is connected from one side to the Grid, which is represented by a generator connected to bus No 1. The other side of the substation its associated distribution network which is represented by a radial feeder consists of a 5 km O/H line between buses 2 and 4, transformer T2 between buses 4 and 5 and a variable load connected to bus 5. It is also assumed that the substation is supplied with electric power from an integrated EG connected to the substation via transformer T3 and a 10 km O/H line between buses 2 and 3.

Fig 1 also shows the installation of AVC relay, which is used to control voltage magnitude along radial feeder. The

Paper accepted for presentation at the International Conference on Electric Utility Deregulation and Restructuring and Power Technologies 2000, City University, London, 4-7 April 2000.

0-7803-5919-4/00/$10.00 ©2000 IEEE.

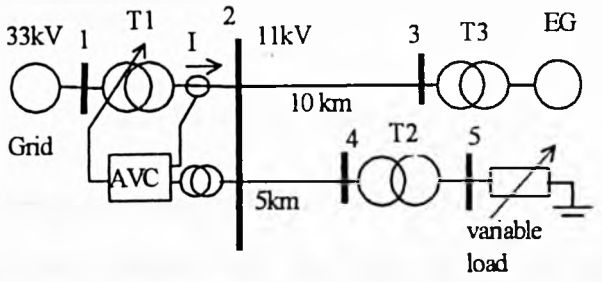

Fig. 1. Single line diagram of a distribution network with embedded generation

relay could be of conventional type with a positive compounding. The reference voltage for control is assumed equal to 1pu and the calculated voltage is allowed to vary between the limits of ± 2% of the nominal voltage. Consequently when the calculated AVC voltage exceeds these limits, the AVC relay initiates a signal for operating the tap-changer to bring the controlled voltage back within the specified limits.

IV. OPERATING PRINCIPLES OF AVC RELAYS

A detailed discussion of the operating principles of AVC relays can be found elsewhere [2,3]. However for the completeness of the presentation of this paper a brief review will be given. The operation of an AVC relay involves two main actions. The first action deals with the calculation of the voltage of AVC relay using current and voltage values measured at the low voltage side of OLTCT. This voltage is given by the following expression [2,3]:

$$V_{AVC} = V - I_T (R_{AVC} \pm j X_{AVC}) \quad (1)$$

Where, V is the voltage of at the terminals of the secondary side of OLTCT, I_T is the transformer current, and $(R_{AVC} \pm j X_{AVC})$ is the relay compounding settings. Depending on the application, the relay compounding consists of resistance and either positive or negative reactance. The second action involves comparing the AVC relay voltage with a reference voltage (V_{REF}). The aim is to maintain the controlled network voltage within specified limits. If the deviation of the AVC relay voltage from the reference voltage V_{REF} exceeds the specified limits of a bandwidth, say ±2% the relay initiates a signal to operate the tap-changing device of the transformer in a direction which brings it back within the bandwidth.

V. BASIC PRINCIPLES OF ANN

Application of ANNs to electrical power systems has received considerable attention in the recent years [4-6]. Different types of ANNs are described in literature [7,8]. However, Multilayer Perceptrons type is the most popular for power system applications [6]. It is used in more than 80% of such applications. This type can be explained using a three layer neural network as shown in Fig. 2. It can be seen from this figure that the network comprises a number of interconnected processing elements (PE), known as artificial neurons [7,8]. The neurons are arranged in layers, including an input layer, followed by a hidden layer(s), and finally an output layer. Neurons in the input layer receive signals from external source and transmit them to the next hidden layer. Each neuron in the hidden layers or in the output layer receives a number of inputs (x_{ij}) equals to number of neurons in the previous layer. Each of these inputs is given by [7,8]:

$$x_{ij} = Y_i * w_{ij} \quad (2)$$

Where Y_i is the output of i_{th} neuron in the preceding layer and w_{ji} is the weight of the connection between i-th and j-th neurones of successive layers,

Hence, the total input to a neuron is given by [7,8]:

$$\mathbf{X_j} = \Sigma x_{ij} = \Sigma w_{ji} Y_i \quad (3)$$

Where $\mathbf{X_j}$ is the total input to the j-th neuron in the hidden or output layer.

The output of jth neuron, Y_j, in the hidden or output layer is a function of the total input [6,7], i.e. :

$$Y_j = F(\mathbf{X_j}) \quad (4)$$

Function F(x) can be any continuous differentiable non-linear function like the log-sigmoid, which is given by[6,7]:

$$F(x) = 1/(1+e^{-x}) \quad (5)$$

ANN must be first trained to work properly. In the training process a special training algorithm is used for adjusting the weights so that the network output for given inputs will be as close as possible to the desired output values. Training methods can be divided into supervised and unsupervised. In the supervised training method, the

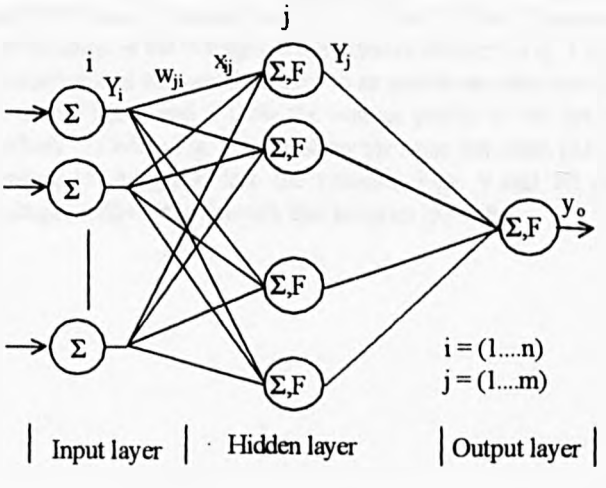

Fig. 2. A three layer neural network system

desired output is given in the data file. Supervised algorithms require longer learning time than the unsupervised, but they can be more accurate [4]. One of the most popular supervised learning algorithms is the Backpropagation method. It is based on a gradient-search optimisation method applied to an error function.

The error function is calculated as the sum-of-squared errors, given by [7,8]:

$$e = \sum_{i} \left\{ y_{ik\ calculated} - y_{ik\ desired} \right\}^2 \qquad (6)$$

Where y_{ik} is the output of i^{th} neuron in the k^{th} layer.

The error in the outputs for a given input pattern is propagated back through the network to adjust the weights. A recursive algorithm is usually used to adjust the weights such that the error is minimised.

As mentioned above, the learning process requires a data file that contains pairs of input-output patterns. To be effective, the data file must include sufficient amount of training patterns that cover most possible conditions. Such a file can be prepared from historical records, computer simulation, or measured data.

The result of a successful training process is a set of weights that is assigned to the ANN. Using these weights, the network calculates an output very close to the desired values for each pattern in the training file. The network can then be considered ready for application.

VI. DESIGN OF ANN-BASED AVC RELAY

An ANN is designed so that its performance mimics that of automatic voltage control relay. The designed structure of the proposed ANN-based AVC relay is similar to that shown in Fig.2. The input layer has four processing elements. The input to this layer consists of system voltage, V, the power factor angle of the current through OLTCT and the real and imaginary components of the transformer current I_r and I_{im} respectively. The output of the ANN-based AVC relay is the calculated relay voltage, V_{avc}.

A. Training of the ANN-based AVC relay

The proposed ANN-based AVC has been trained using specially prepared training data file. Such file is obtained from a load flow study, which was conducted using the distribution network shown in Fig. 1 by simulating different steady-state operating conditions. This is achieved using a specifically dedicated load flow program written in FORTRAN.

The effect of EGs on the performance of the AVC relay was simulated by considering cases whereby the network is assumed operating with and without EG. It is also assumed that EG operating with lagging and leading power factor. It has been found that the compounding impedance is case-study dependent and accordingly for each case a compounding impedance is chosen to suit that particular case. The reference voltage is assumed equal 1 pu but the calculated voltage is allowed to vary the limits of $\pm$ 2% of reference voltage. The load is assumed to change from zero to maximum and back to zero in incremental steps. When the calculated AVC voltage exceeds the $\pm$ 2% limits, the AVC relay initiates signal to adjust the tap-changer of OLTCT to bring back the voltage within the specified limits. The calculated results at every step are then saved into an output file to represent a particular pattern that corresponds to a specific operating condition. Some of the output files are stacked together in one data file which is then used in the training stage of the proposed ANN-based AVC relay. The rest of files are used during the testing stage of the relay. Following a satisfactory training and testing, the designed ANN-based AVC relay model was converted to FORTRAN and integrated into the load flow program, as a subroutine, to substitute the algorithm that calculates the voltage of the AVC relay based on conventional approach.

B. Performance of the proposed relay

The performance of the proposed ANN-based AVC relay, in terms of calculating its voltage V_{avc}, has been tested by presenting test data to it. The obtained voltage profile is then compared with that of conventional AVC relay. Two examples of the test results are shown in Figs. 3 and 4. These figures show a comparison between the AVC voltage calculated using conventional method and ANN-based approach. The voltage profile curves in Fig. 3 corresponds to a network without EG and the curves in Fig. 4 correspond to a network with EG. It can be seen from these results that the ANN based AVC relay is able to calculate the relay voltage with a maximum error not exceeding 0.002 pu.

The performance of the proposed ANN-based relay has also been tested after it has been integrated into the load flow program. The program is used to simulate different operating conditions related to the system shown in Fig. 1 whereby the voltage profile of the system as controlled by the proposed relay is determined and compared with that obtained from conventional relay. Several load flow cases have been simulated including the distribution network operating with and without EG. Table 1 shows a summary of the simulated cases.

Figures 5 to 10 show pairs of examples of the test results for both the ANN and conventional based AVC relays. These figures show the variation of the voltages of the network shown in Fig. 1 as the connected load changes from zero to its maximum value and back to zero. Figs. 5 and 6 show the voltage profile of the network without EG while Fig. 7 and 8 show the same but when EG with leading PF integrated into the network. Figs. 9 and 10 show voltage profile of the network that includes EG with

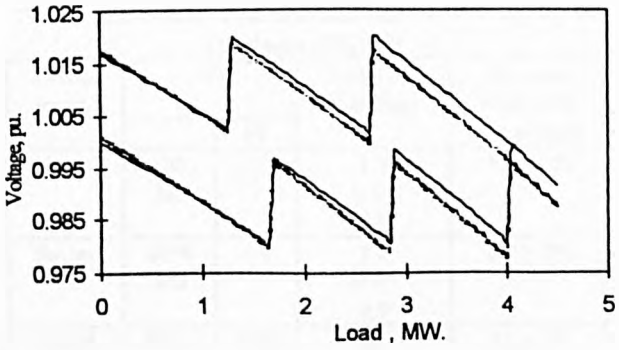

Fig.3 AVC relay voltage of a network without EG as calculated using conventional method and ANN.

—— Conventional —— ANN

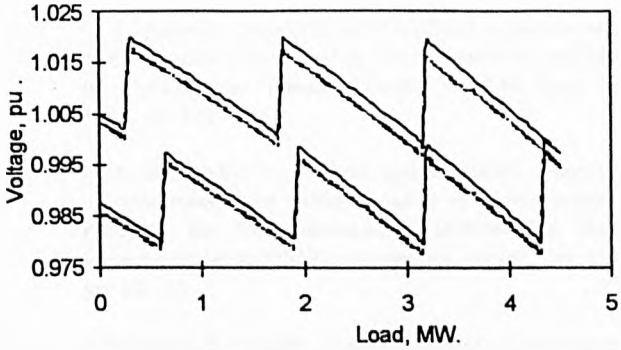

Fig.4 AVC relay voltage of a network with EG as calculated using conventional method and ANN.

—— Conventional —— ANN

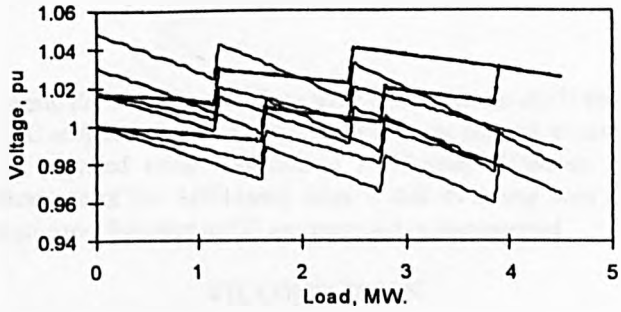

Fig. 5 Performance of the ANN based AVC relay, network without EG and PF of load = 0.95 (Lag.)

—V2 —— V3 —— V4 —— V5 —— V_{AVC}

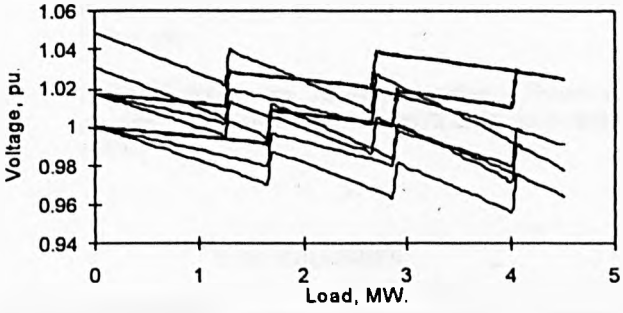

Fig. 6 Performance of conventional AVC relay, network without EG and PF of load = 0.95 (Lag.)

—V2 —— V3 —— V4 —— V5 —— V_{AVC}

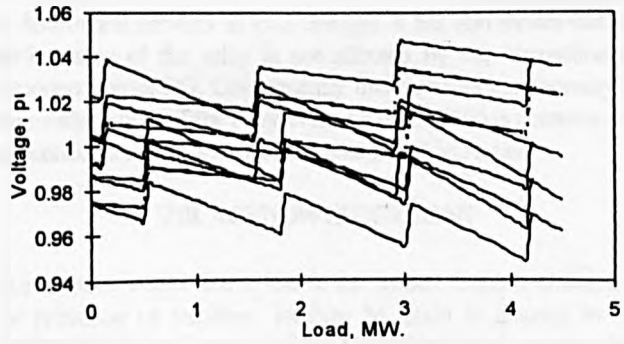

Fig. 7 Performance of the ANN based AVC relay, PF of EG = 0.95 (lead) and PF of load = 0.95 (Lag.).

—V2 —— V3 —— V4 —— V5 —— V_{AVC}

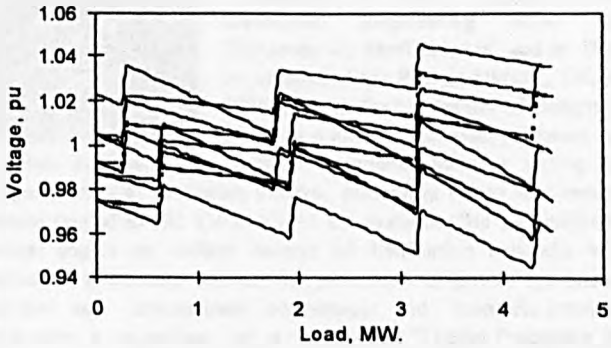

Fig. 8 Performance of conventional AVC relay, PF of EG = 0.95 (lead) and PF of load = 0.95 (Lag.).

—V2 —— V3 —— V4 —— V5 —— V_{AVC}

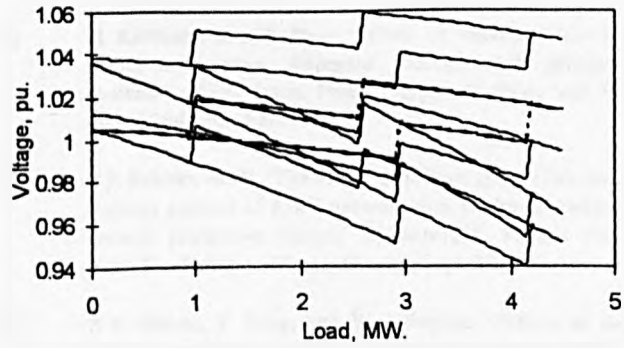

Fig. 9 Performance of the ANN based AVC relay, PF of EG = 0.95 (lag.) and PF of load = 0.95 (lag.).

—V2 —— V3 —— V4 —— V5 —— V_{AVC}

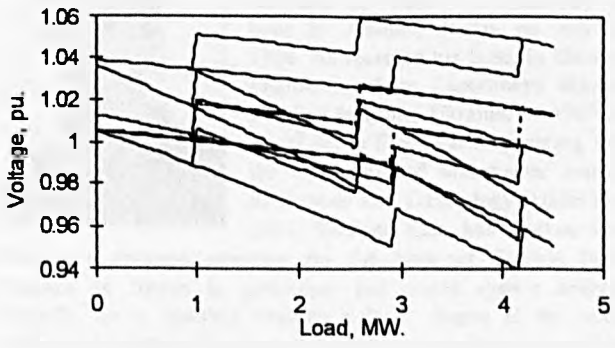

Fig. 10 Performance of conventional AVC relay, PF of EG = 0.95 (lag.) and PF of load = 0.95 (lag.).

—V2 —— V3 —— V4 —— V5 —— V_{AVC}

Table 1. A summary of the simulated cases used for testing the ANN based AVC relay.

Group cases	EG		Load PF (Lagging)	V_{REF} and band width limitations
		PF		
First	NO EG	—	1.0 0.95 0.9	1.0 ± 2%
Second	With EG	1.0	1.0 0.95 0.9	1.0 ± 2%
Third	With EG	0.95 lead	1.0 0.95 0.9	1.0 ± 2%
Forth	With EG	0.95 lag	1.0 0.95	1.0 ± 2%
Fifth	With EG	0.9 lead	1.0 0.95	1.0 ± 2%

lagging PF. It can be seen from these results that the ANN-based AVC relay can provide a voltage control of the network similar to that provided using conventional AVC relay. However, the advantage of the ANN-based relay is that its setting does not require re-adjustment as EG are connected or disconnected.

VII. CONCLUSION

The use of an ANN in calculating the voltage of AVC relay was investigated in this paper. The results obtained were found very encouraging. It has been found that the proposed ANN-based AVC relay has the ability to properly control voltage magnitude of distribution network as load changes. It has also shown that the performance of the relay is not affected by the connection or disconnection of EG. Consequently this removes the necessity to the re-adjustment of the relay every time an EG(s) is connected or disconnected as the case with conventional AVC relays.

VIII. ACKNOWLEDGEMENT

The authors would like to thank the Robert Gordon University for provision of facilities. Ibrahim M. Rida is grateful to the Robert Gordon University and the Committee of vice-chancellors and Principals of UK for their financial support to undertake this research

IX. REFERENCES.

[1] H Kirkham, R and Das, "Effect of voltage control in utility interactive dispersed storage and generation systems", IEEE Trans. Power Appar. & Syst., Vol PAS 103, 1984, pp. 2277-82.

[2] S K Salman, et all, 'The effect of private generators on the voltage control of 11kV network and on the operation of certain protective relays,' IEEE/NTUA Athens Power Tech Conference, Athens, Greece, Sept. 1993

[3] S K Salman, F Jiang, and W J Rogers, "Effects of wind power generators on the voltage control of utility distribution networks", Inter. conf. on renewable energy - Clean power 2001, London, 17 - 19 November 1993, IEE Publication No 385, pp 196-201.

[4] H. P. Schmidt, "Application of artificial neural networks to the dynamic analysis of the voltage stability problem", IEE Proc.- Gener. Transm. Distrib., Vol. 144, No.4, July 1997, pp. 371- 376.

[5] A. A. El-Samahy, 'An artificial neural network scheme for reactive power and voltage control of power systems,' Proc. of the fifth international Middle East Power Conference MEPCON'97, Alexandria, Egypt, Jan 1997, pp. 62 - 65.

[6] S M Halpin, R F Burch, "Applicability of neural networks to industrial and commercial power systems: A tutorial overview", IEEE Trans. on Industry Applications, Vol. 33, No. 5, September/October 1997.

[7] R Beale and T Jackson, Neural computing – an introduction, Bristol, phladephia and New york: Adam Hilger, 1991.

[8] Philip D Wasserman, Neural computing - Theory and practice, New York: VAN NOSTRAND REINHOLD, 1989.

X. BIOGRAPHIES

Salman K Salman: He is a member of the IEE and a senior member of the IEEE, was born in Basraha, Iraq, 1941. He graduated from the Faculty of Engineering, University of Baghdad in 1964. In 1972 he obtained his MEng in Electrical and Electronic Engineering from the University of Sheffield, UK and in 1975 he completed his PhD at UMIST, UK. In 1975 he joint the University of Benghazi, Libya as a lecturer, assistant professor and associate professor. His practical experience includes testing and commissioning of measuring devices, protection relays and control circuits related to 132 kV/33 kV/11 kV systems. He has published several papers on voltage control of distribution networks with embedded generation and on the protection of power systems at national and international conferences and scientific journals. He is also a co-author of a book titled "Digital Protection for Power Systems" which was published by the IEE in September 1995. Currently he is a Reader at the School of Electronic and Electrical Engineering at The Robert Gordon University, UK.

Ibrahim M. Rida (AMIEE-93) was born in Amman, Jordan on July 23, 1960. He received his B.Sc. in Electrical Engineering from Zaporozhye Machine Building Institute, Ukraine, in 1985 and his M.Sc. in Electrical Engineering from the University of Manchester Institute of Science and Technology (UMIST) in 1996. Ibrahim Rida has worked since 1988 as a research engineer for the National Electric Power Company in Jordan in protection and power system analysis. Currently, he is studying towards a Ph.D. degree at the Robert Gordon University in Aberdeen, UK. His research interests are in the areas of wind power based embedded generation, voltage control and protection of distribution networks.

INVESTIGATING THE IMPACT OF EMBEDDED GENERATION ON RELAY SETTINGS OF UTILITIES' ELECTRICAL FEEDERS

S K Salman, Senior Member, IEEE I Rida, AMIEE

School of Electronic and Electrical Engineering,
The Robert Gordon University,
Schoolhill, Aberdeen, AB10 1FR,
Scotland, U.K.

Abstract: Since the late 70s intensive efforts have been made to utilise renewable energy sources to generate electric power. On the other hand economical pressure experienced in recent years has led to the development of high efficiency combined heat and power schemes to use the normally wasted heat to generate electric power. Generators used under both schemes can be either synchronous or asynchronous types and when they are integrated into utilities' distribution networks (DNs) they are commonly known as "embedded generators (EGs)". Previous experience has shown that the integration of EGs into DNs could create safety and technical problems. They may contribute to fault currents, cause voltage flickers, interfere with the process of voltage control, etc.

This paper reports an investigation to determine the impact of the integration of EGs on the settings of protective devices of electrical feeders emanated from the substation to which EGs are connected. This study also covers the dynamic behaviour of EG caused by disturbances on the host network. Results obtained from several case studies presented and discussed.

Keywords: Embedded generation, Distribution networks, Critical clearing time, Protection, Simulation, EMTP.

I. INTRODUCTION

Since the late 70s and after what is now known as the "energy crisis", intensive efforts have been made to utilise renewable energy sources, such as wind, hydro, tidal, etc, to generate electric power. On the other hand economical pressure experienced in recent years has led to high-energy efficiency commitment. This in turn has led to developing high efficiency combined heat and power (CHP) schemes [1] to use the normally wasted heat to generate electric power. Generators used under both schemes can be either synchronous or asynchronous types and when they are integrated into utilities' networks at distribution voltage levels they are commonly known as "embedded generators (EGs)". Various investigations conducted by both industry and academia have revealed that EGs could affect the host distribution network in number of ways [2-8]. They may contribute significantly to the fault current, cause voltage flickers, interfere with the process of voltage control, affect the losses of the network etc.

This paper reports an investigation related to the determination of the impact of the integration of embedded generators into distribution networks on the settings of protective devices of electrical feeders emanated from the substation to which EGs are connected. It particularly focused on determining the critical clearing time (CCT) of integrated EG(s) when a disturbance occurred on the associated network. Such CCT is determined by the onset of an EG becoming unstable. The concept of stability is well defined for the case of synchronous machines but it is not so for asynchronous machines. Therefore, an attempt has been made in this paper to introduce a definition of the CCT which can be applied to asynchronous generator. The study is conducted on a simulated system consisting of a distribution network with integrated EG(s) using Electromagnetic Transient Program (EMTP). This study also covers the dynamic behaviour of EG(s) caused by disturbances on the host network. Results obtained from several case studies are presented and discussed. In the first instance a definition of the stability criteria as far as asynchronous generator is concerned will be introduced followed by presenting a comparison between the dynamic behaviour of synchronous and asynchronous EGs.

II. DEFFINITION OF THE PROBLEM.

Prior to the introduction of embedded generation into distribution networks in large scale, such networks are considered passive, i.e., their role confined to transferring the electrical energy received from the transmission systems to consumers. Consequently the design and protection of DNs are based on the basis that such networks are passive. For example protection schemes of distribution feeders are usually designed on the assumption of unidirectional power flow and are based on two basic principles; (i) they must insure minimum disruption supply, i. e., the removal of a fault from the system should be achieved with minimum tripping of equipment. (ii) they must be fast enough to minimise damage to system components [9]. The first principle is achieved by a

proper co-ordination in the operating time of protective devices. This, however, may lead the operation time of protective devices at the up-stream of a distribution network to be as high as 1.5 second [10]. When EG is connected into a DN, the operating time of protective devices installed on load feeders may exceed the CCT limit required to maintain the stability of EG which this paper tries to establish.

III. MODELLING ELECTRIC POWER SYSTEMS USING EMTP.

The Electro-Magnetic Transient Program (EMTP) has been used for several years for power system analyses under transient and dynamic conditions. It consists of a library of models of network components such as electrical machines, transformers, lines, etc. that can be interconnected together to simulate any required electrical network [11].

A. Modelling of Embedded Generators in EMTP

Embedded generator(s) can be of synchronous and/or asynchronous types depending on the energy source used. For example Wind Farms usually utilise induction generators (IGs) which are normally driven by wind turbines for generation of electricity. Such machines can be simulated in EMTP using the concept of Universal Machine (UM) model that was proposed by Lauw and Meyer [12] in 1982. The UM is considered as an electromechanical energy conversion device that can be used to simulate the electrical and mechanical components of electrical machines [11]. This model is found particularly attractive because the mechanical side of the machine can be conveniently represented using an equivalent electric network consisting of lumped RLC elements, which is then solved as part of the whole electric network. For example each mass connected to the shaft system can be represented by creating a node in the equivalent electric network whereby a capacitor is placed between the node and the ground to represent the moment of inertia of that mass. The mechanical torque on that mass is then simulated by a current source connected between the same node and the ground [11]. Synchronous generators (SGs) can also be simulated by a UM model, however, another machine model which is known as Type95 model is found more suitable for this work. It is a three phase dynamic synchronous machine model which represents the details of the electrical part of a generator as well as the mechanical part of the generator and its associated turbine [11]. Using Type59 model allows the dynamics of the prime mover (e.g. governor and turbine) to be included in the simulation. This is achieved using Transient Analysis of Control Systems (TACS) specially developed in the EMTP, which can be interfaced with the control circuitry of the SG Type95 model. Voltage applied to the field winding can also be controlled using TACS. The required control machine variables (e.g. rotor speed and field voltage) can be directly obtained from the Type59 model. In this paper both IGs and SGs have been considered.

B. Modelling the network under consideration

The system considered in this investigation is shown in Fig.1. Basically it consists of a distribution network with embedded generator(s). The latter can be either a wind farm, represented by asynchronous generator(s) or a gas-turbine synchronous generator unit. In either cases the generator(s) is integrated into the distribution network at 33 kV voltage level through a 33 kV interfacing link. The distribution network in turn consists of the Grid represented by a voltage source behind its Thevenin's equivalent impedance and a substation represented by a 20 MVA, 132/33kV transformer with an impedance of 10%. The fault level of the Grid behind the 132kV busbar is assumed 1800MVA. The wind farm considered in this investigation is assumed to have sixteen wind-turbine-generator units each of 600 kW with a nominal voltage of 690V see Fig. 1. In order to simplify the simulation of the wind farm and at the same time maintain the flexibility of having the ability of varying the injected generation, generating units of the wind farm are represented using the ATP package by three UM models. The first machine, as can be seen in Fig. 1a, represents two 600 kW units, while the second machine represents four 600 kW units, and the third machine represents ten 600 kW units. All units are assumed connected at the same bus No. 4. A 10 MVA, 690/33000 V step-up transformer with an impedance of 10% is assumed between buses 3 and 4. All transformers are represented using the ATP transformer model that considers their connection group and the saturation effect of the magnetic core. The load connected to the substation is represented by a second feeder which supplies a load connected at the remote end of the feeder via 33kV/416V transformers. The feeders are simulated using the ATP lumped RLC model. Both the interfacing and load feeders have an impedance of (0.185+j324) ohm/km. Fig. 2 shows the same network shown in Fig 1 but this time the wind farm is replaced by a gas-turbine synchronous generator unit. It is assumed that the SG is rated at 10 MVA and 11 kV. It is also assumed that the generator is interfaced with the 33 kV network through a 10 MVA, 11/33 kV step-up transformer with an impedance of 10%. The rest of the network in Fig. 2 is assumed similar to that shown in Fig. 1.

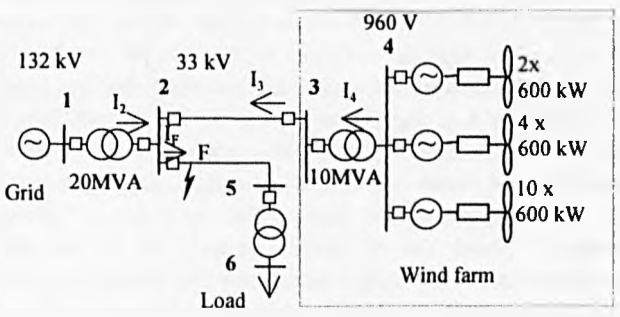

Fig. 1 Schematic diagram of the investigated network with embedded induction generators

IV. THE CONCEPT OF CRITICAL CLREARING TIME

A. Synchronous generators.

During normal operating condition a synchronous generator embedded into a distribution network usually run at synchronous speed with a rotor angle of δ_0 corresponding to an electrical output power P_e and mechanical input power P_m. The output power P_e which is transferred from the generator to the network is approximately proportional to the square of generator terminal voltage [13]. When a fault occurs on the network, P_e suddenly reduces due to the sudden change in network voltage. This leads to the acceleration of SG to account for the difference between P_m and P_e according to the well known following swing equation [13]:

$$\frac{d^2\delta}{dt^2} = \frac{\omega_s}{2H}(P_m - P_e) \qquad (1)$$

Where ω_s is angular frequency, t time, and H is the inertia constant of the rotating mass.

This in turn causes the SG to gain kinetic energy which is normally stored in the rotating mass. When this happened the rotor angle increases with time as shown below [13]:

$$\delta = \frac{\omega_s (P_m - P_e)}{4H} t^2 + \delta_0 \qquad (2)$$

When the fault is cleared at time t_c which corresponds to a rotor angle δ_c, the power demand by the network re-establishes and the generator find itself generating power greater than P_e due to the new rotor angle. Assuming that the input mechanical power remains unchanged the extra power is supplied from the kinetic energy of the rotating mass. However due to the moment of inertia the rotor angle continues to increase, but because the input power this time is less than the output power the generator begins to decelerate passing its synchronous speed. The oscillation of the speed (and consequently the rotor angle δ) continues for a while, but eventually they settle to a new steady-state condition and the system is considered stable. Otherwise, δ continue to increase further and generator losses synchronism with the network. The system in this case is considered unstable.

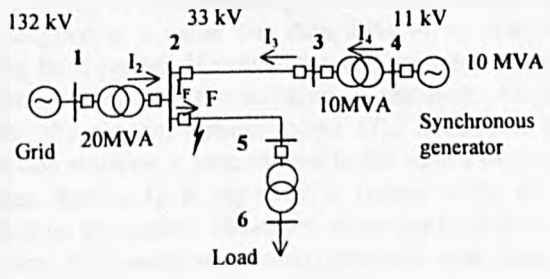

Fig. 2 Schematic diagram of the investigated network with embedded synchronous generator.

There is a maximum rotor angle below which SG can retain a stable operation. This position is known as critical clearing angle. The corresponding maximum clearing time is known as critical clearing time.

B. Induction generators.

Unlike SGs, induction generators do not have field windings to develop the required electro-magnetic field in the machine's air-gap. Therefore, IGs can not work with out external power supply. The electro-magnetic torque (T_e) developed inside an induction machine at any given speed is proportional to the square of the terminal voltage as follows[14]:

$$T_e = K s V^2 \qquad (3)$$

where K is constant value depends on the parameters of the machine, s is the machine slip.

T_e is, therefore, bound to reduce following a fault condition. On the other hand, the dynamic behaviour of the rotor is governed by the swing equation given below [12]:

$$J\frac{d\omega}{dt} = T_m - T_e \qquad (4)$$

where J is the moment of inertia of the rotating mass, T_m is the mechanical torque applied on the rotor of the associated wind turbine and ω is the rotor speed.

It can be concluded from (4) that assuming the mechanical torque is kept constant, then any reduction in the electro-magnetic torque, for instance due to fault condition, causes the rotor to accelerate. This in turn leads to an increase in the kinetic energy of the rotating mass. When the fault is cleared and consequently system voltage recovers, the magnetic field inside the air-gap of the machine starts to build up. This causes high inrush current to be drown by the machine from the network which in turn causes a voltage drop across the interfacing link between the induction generator (in this case the wind farm) and the substation leading to a reduction in the voltage at the generator (wind farm) terminals. The resulting electro-magnetic torque acts on the rotor in a direction opposite to that of mechanical torque applied by wind turbine(s). If the energy stored in the newly established rotating magnetic field becomes higher than that stored in the rotating mass, rotor speed is forced to slow down and the generator eventually retains its normal operating condition following few oscillations, otherwise, its speed continues to increase until it is tripped by appropriate protection devices. When this happened generator terminals usually experience

sustained voltage dip. This investigation has shown (see Section V-B.1) that there is a maximum time for the fault to be cleared, otherwise induction generator(s) losses its(their) stability. Such time will thereafter be referred to as the CCT for induction (or asynchronous) generator.

V. INVESTIGATED CASES

A. *Behaviour of embedded SGs and IGs during fault conditions*

Contribution of embedded generators to fault currents could increase the short-circuit capacity throughout distribution network which may lead network "make and break" fault levels to exceed the permitted ratings of network equipment [7]. It can also disrupt the co-ordination of protective devices [8]. The objective of this part of the work is to investigate the behaviour of embedded SGs and IGs during fault conditions and compare the two with each other. A three phase fault with a duration of 200 ms is assumed on the load feeder terminals at location F (see Figs 1 and 2). The results obtained are displayed in Figs 3 and 4. The former shows the waveforms of the total fault current and that contributed from embedded SG while Fig.4 shows the same but this time SG is replaced by IGs. These figures show that while the current supplied by SG is sustaining during the fault period, the current from IGs tends to decay after few cycles from the fault incident.

B. *Behaviour of embedded SGs and embedded IGs during post-fault period*

The aim of this part of the study is to investigate the behaviour of embedded generators, whether SGs or IGs, following the clearance of a fault. Similar to the previous case the system is subjected to a three-phase fault at point F. However in order to determine the critical clearing time of SGs and IGs, the simulation was run for different fault durations.

B.1. *Embedded Induction Generators*

One of the cases considered is the examination of the behaviour of embedded IG following a three-phase to ground fault with a duration of 60 ms on the load feeder at location F. Fig. 5a shows the variation of terminal voltage of induction generators at the wind farm, i.e. at the 690V bus-bar shown in Fig. 1. It can be seen from Fig. 5a that the voltage magnitude has dropped to a value less than 25% of its nominal value during fault period. However the voltage retained its normal operation level after the isolation of the fault. As explained earlier, the electromagnetic torque (T_e) developed inside an induction machine is proportional to the square of the terminal voltage, hence, T_e is expected to reduce while the fault is applied on the system. However, when the fault is cleared, T_e recovers its operational value provided that the machine remain stable after the removal of the fault. Fig.5b. shows the variation of the electromagnetic torque inside the air gap of the 2x600 kW IG. Such variation leads to a variation in the generator's rotor speed, as illustrated in Fig. 5c (see (2)). The recovery of electromagnetic torque normally requires high current drawn from the network. Fig. 5d shows the variation of the total current of the wind farm following the fault. As the exchange of power can not occur instantaneously due to the inductance of machine windings and the inertia of the rotating mass, therefore electromagnetic torque, speed and current have varied in oscillatory fashion with an exponentially decaying envelope versus time as can be seen in Figs 5b,5c and 5d respectively. This investigation was repeated for different fault clearing time values. It was found that for the system under consideration, IGs can not retain normal operation when the clearing time is greater than 65 ms. Consequantly this time is considered the CCT for the case under consideration. This investigation has also shown that if the fault is cleared at time greater than the CCT, the rotating speed of IGs continue to increase and induction generators continue to draw high inrush currents from the network until they are disconnected from the network

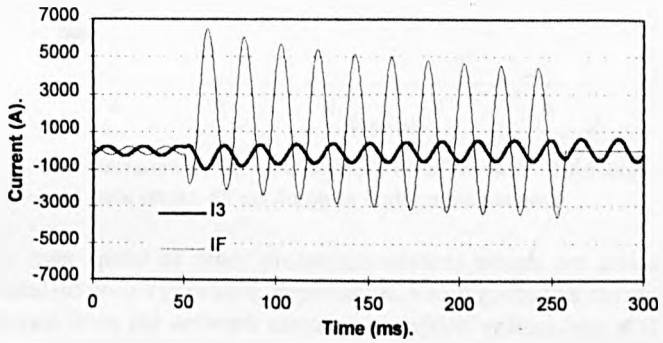

Fig. 3 Current waveforms for a three-phase fault on the load feeder,
I3 - Contribution of synchronous generator to the fault,
IF - Total fault current.

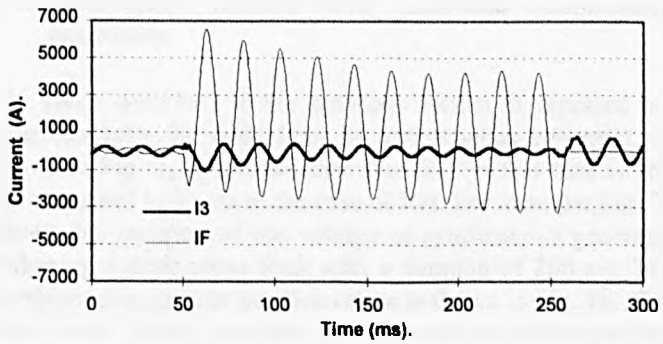

Fig. 4 Current waveforms for a three-phase fault on the load feeder,
I3 - Contribution of induction generators.
IF - Total fault current.

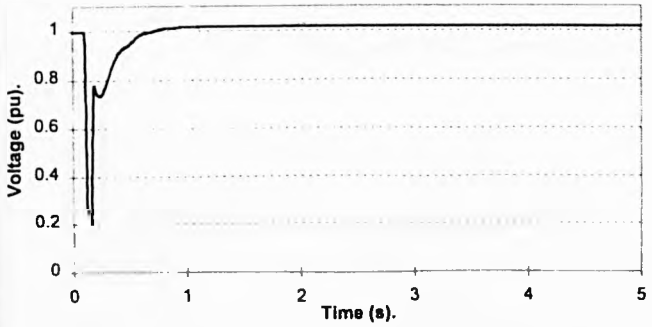

Fig. 5a Variation of terminal voltage of IGs at wind farm following a three phase, 60 ms duration fault on the network.

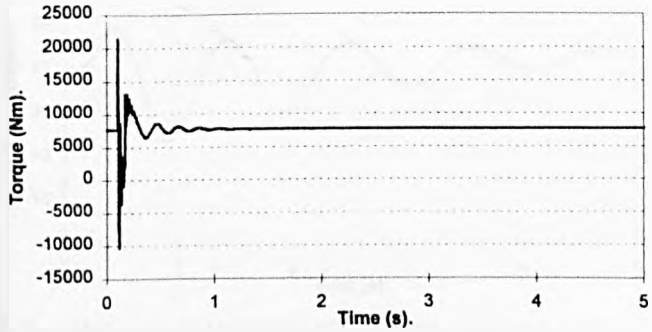

Fig. 5b Variation of electromagnetic torque inside the air gap of 2x600 kW IG following a three phase, 60 ms duration fault on the network.

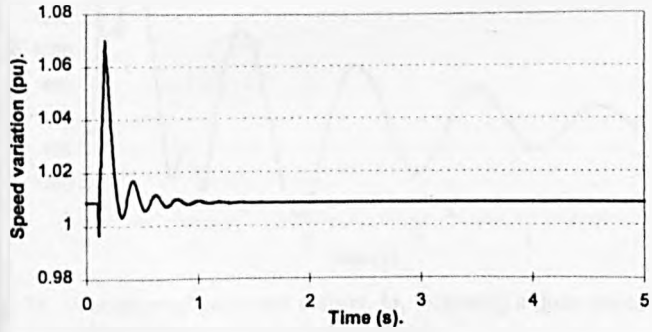

Fig. 5c. Variation of rotor speed of the 2 x 600 kW IG following a three phase, 60 ms duration fault on the network.

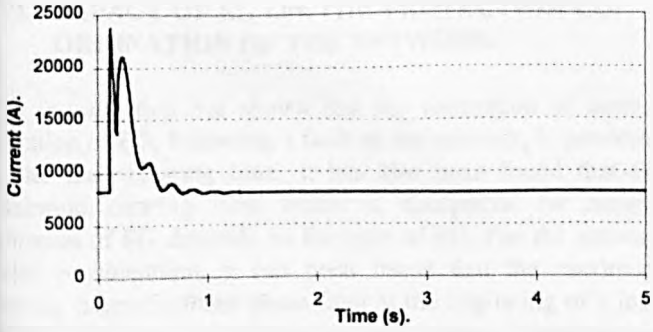

Fig. 5d. Variation of the total current of the wind farm following a three phase, 60 ms duration fault on the network.

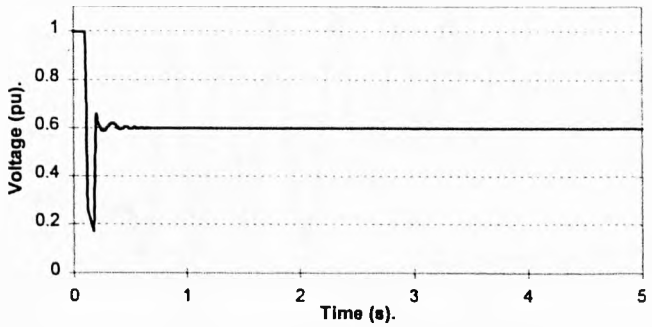

Fig. 6a. Variation of terminal voltages of IGs at wind farm following a three phase, 80 ms duration fault on the network.

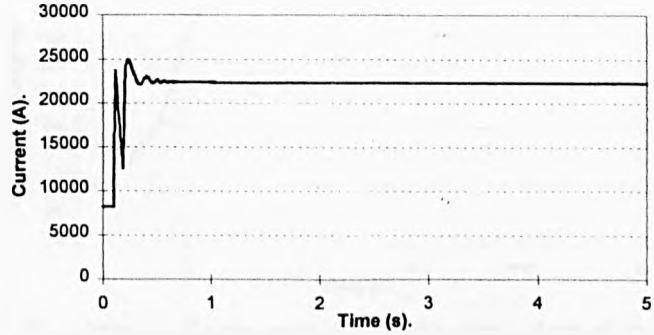

Fig. 6b. Variation of the total current of wind farm following a three phase, 80 ms duration fault on the network.

by over speed or other protection devices which are usually installed on IG(s) in such application. The high inrush currents drown from the network causes a sustained voltage sag at the generator terminals. Fig. 6a shows such voltage for a clearing time of 80 ms. The corresponding total current drawn by the wind farm is shown in Fig. 6b.

B.2. Distribution network with embedded synchronous generators

The study described in the previous section is repeated but after replacing the wind farm by synchronous generator, as shown in Fig. 2. It is found that, the CCT in this case is 360 ms compared to 65 ms in the case of IGs. For example Fig. 7a shows the variation of the voltage of synchronous generator following a three-phase fault with a duration of 200 ms. The corresponding angular position of the is shown in Fig. 7b. This figure also shows that the rotor assumes a stable position following few oscillations after the removal of the fault. The corresponding variation of the stator current is shown in Fig.7c. On the other hand Fig. 8a and 8b show the variation of generator terminal's voltage and its rotor angle respectively following a three-phase fault with a duration of 400 ms. It can be seen from Fig 8b that the rotor angle continues to grow, i.e, the generator continues to accelerate until it loses its synchronism with the network.

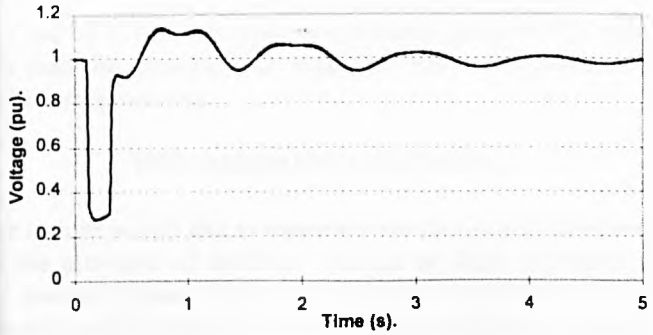

Fig. 7a Variation of terminal voltages of SG following a three phase, 200 ms duration fault on the network.

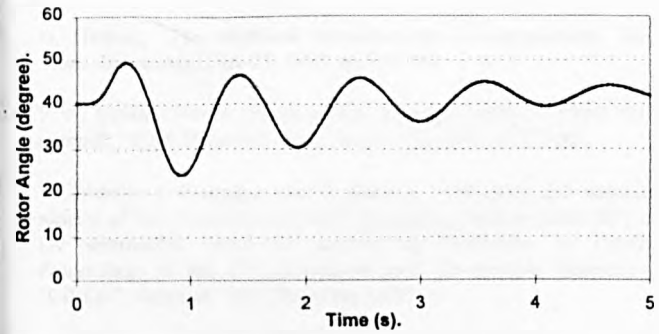

Fig. 7b. Variation of rotor angle of synchronous generator following a three phase, 200 ms duration fault on the network.

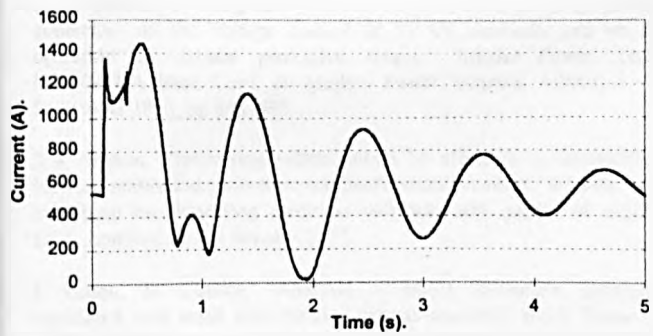

Fig. 7c. Variation of generator current, I_4, following a three phase, 200 ms duration fault on the network.

VI. IMPACT OF EG ON THE PROTECTION CO-ORDINATION OF THE NETWORK.

This investigation has shown that the restoration of normal operation of EG, following a fault on the network, is governed by the fault clearing time. It has also been found that the maximum clearing time which is acceptable for normal operation of EG depends on the type of EG. For the network under consideration, it has been found that the maximum clearing time of a three phase fault at the beginning of a load feeder can be as high as 360 ms in the case of synchronous generator compared to only 65 ms in the case of induction generator. It has also been observed that clearing of fault

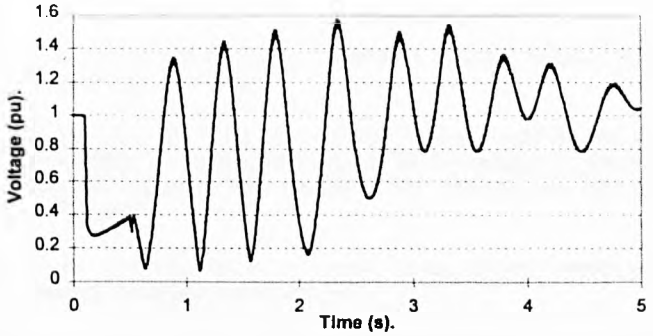

Fig. 8a Variation of terminal voltages of SG following a three phase, 400 ms duration fault on the network.

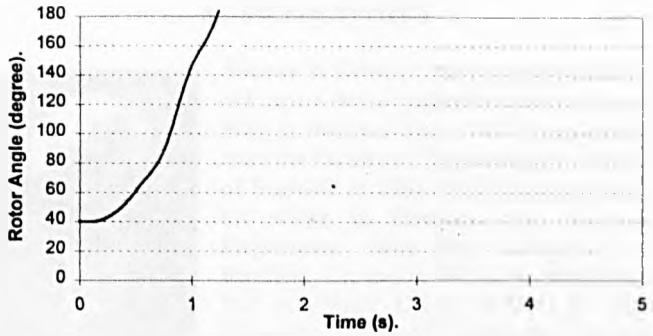

Fig. 8b. Variation of rotor angle of SG following a three phase, 400 ms duration fault on the network.

beyond the CCT causes synchronous generators to run out of synchronism with respect to the network, whereas, it causes a sustained voltage drop at the point of connection to the network in case of induction generators. This investigation has also revealed that, immaterial of the type of embedded generator used, the maximum clearing time can be much lower than the expected operating time of a time graded protective relay usually applied for distribution feeders. It is, therefore, important that protection co-ordination should be carefully be looked at when integration of EG into a distribution network is considered.

VII. CONCLUSION

The EMTP package has successfully been used in this work to simulate a distribution system with embedded induction generators and/or embedded synchronous generator. The simulation is then used to investigate the impact of the integration of embedded SG(s) and embedded IG(s) on the settings of protective devices normally installed on the distribution feeders. Several case studies have been conducted to determine the effect of the clearing time of a fault on the network on the stability of embedded generator(s) includingsynchronous and induction types. It has been concluded that the presence of EG greatly affects the clearing time of protective devices installed at the up stream distribution feeders. It has also been found that although the CTT of embedded SGs is much high than that of embedded

IGs, the CCT for both types of embedded generators is much less than the clearing time normally used in the absence of embedded generation.

VIII. ACKNOWLEDGEMENT

The authors would like to thank the Robert Gordon University for the provision of facilities. Ibrahim M. Rida is grateful to the Robert Gordon University and the Committee of Vice-chancellors and Principals of UK for their financial support to undertake this research

IX. REFERENCES

[1] N. Nichols, 'The electrical considerations in cogeneration,' IEEE Trans. Indus. Appl., IA-21, 1985, pp 754-761.

[2] P. A. Nobile, 'Power system studies for cogeneration: What's really needed?,' IEEE Trans Ind. Appl., Vol IA-23, 1987 pp 777-85.

[3] Y. Pourcin, J. Fourgous and B. Battalia, "Technical and economic aspects of the connection of small generating plant to public MV and LV distribution networks operated by Electricite de France", Proceedings of the 7th International conf. On Electric Distribution, "CIRED", Belgium, 1983, Paper No a.02.

[4] H. Kirkham and R. Das, 'Effect of voltage control in utility interactive dispersed storage and generation systems,' IEEE Trans. Power Appar. & Syst., Vol PAS-103, 1984, pp 2277-82.

[5] S. K. Salman, F. Jiang and W. J. S. Rogers, 'The effect of private generators on the voltage control of 11 kV networks and on the operation of certain protective relays,' Athens Power Tech: IEEE/NTUA Inter. Conf. on Modern Power Systems, Athens, 5 - 8 September 1993, pp 591-595.

[6] S K Salman, 'Optimising system losses by effective communication between embedded generators and distribution networks,' Int.conf. and exhibition on Protecting electrical networks and quality of supply, ERA, London, 22 -23 January 1997.

[7] J. Patton, D. Curtice, 'Analysis of utility protection problems associated with small wind turbine interconnections,' IEEE Trans. on Power Applications and Systems, Vol. PAS-101, No 10, October 1982, pp 3957-3966.

[8] R. Dugan, D. Rizy, 'Electric distribution problems associated with the interconnection of small , dispersed generation devices,' IEEE Trans. on Power Applications and Systems, Vol. PAS-103, No 6, June 1984, pp. 1121-1127.

[9] E. Lakervi, E. J. Holmes, 'Electricity deistribution network design,' IEE Power Engineering series 21, Peter Peregrinus Ltd., on behalf of the IEE, London, UK, 1995.

[10] W. J. S. Rogers, 'The Parallel operation of generating plant within a regional electricity company's distribution network,' IEE Colloquium on 'The parallel operation of generating plant within a public electricity network,' Chester, UK, Feb.1991, pp 1-9.

[11] K U. Leuven EMTP Centre, 'Alternative Transient Program Rule Book,' Belgium, July 1987.

[12] H. K. Lauw, W S Meyer, 'Universal Machine modelling for the presentation of electric machinery in an electromagnetic transient program,' IEE trans. Power App. Syst., Vol. PAS-101, June 1982. pp 1342 -1350.

[13] P. M. Anderson and A. A. Fouad, 'Power System Control and stability,' Iowa University Press, 1977.

[14] Mulukutla S. Sarma, 'Electric machines, steady-state theory and dynamic performance,' West publishing company, USA, 1985.

X. BIOGRAPHIES

Salman K Salman: He is a member of the IEE and a senior member of the IEEE, was born in Basraha, Iraq, 1941. He graduated from the Faculty of Engineering, University of Baghdad in 1964. In 1972 he obtained his MEng in Electrical and Electronic Engineering from the University of Sheffield, UK and in 1975 he completed his PhD at UMIST, UK. In 1975 he joint the University of Benghazi, Libya as a lecturer, assistant professor and associate professor. His practical experience includes testing and commissioning of measuring devices, protection relays and control circuits related to 132 kV/33 kV/11 kV systems. He has published several papers on voltage control of distribution networks with embedded generation and on the protection of power systems at national and international conferences and scientific journals. He is also a co-author of a book titled "Digital Protection for Power Systems" which was published by the IEE in September 1995. Currently he is a Reader at the School of Electronic and Electrical Engineering at The Robert Gordon University, UK.

Ibrahim M. Rida (AMIEE-93) was born in Amman, Jordan on July 23, 1960. He received his B.Sc. in Electrical Engineering from Zaporozhye Machine Building Institute, Ukraine, in 1985 and his M.Sc. in Electrical Engineering from the University of Manchester Institute of Science and Technology (UMIST) in 1996. Ibrahim Rida has worked since 1988 as a research engineer for the National Electric Power Company in Jordan in protection and power system analysis. Currently, he is studying towards a Ph.D. degree at the Robert Gordon University in Aberdeen, UK. His research interests are in the areas of wind power based embedded generation, voltage control and protection of distribution networks.